



HAL
open science

The Beam Energy Scan under the scope of EPOS 4

Johannes Jahan

► **To cite this version:**

Johannes Jahan. The Beam Energy Scan under the scope of EPOS 4: Studying the impact of hadronic cascades on the 2nd order cumulants of conserved net-charges in heavy-ion collisions. High Energy Physics - Theory [hep-th]. Nantes Université, 2022. English. NNT : . tel-04051507

HAL Id: tel-04051507

<https://theses.hal.science/tel-04051507>

Submitted on 30 Mar 2023

HAL is a multi-disciplinary open access archive for the deposit and dissemination of scientific research documents, whether they are published or not. The documents may come from teaching and research institutions in France or abroad, or from public or private research centers.

L'archive ouverte pluridisciplinaire **HAL**, est destinée au dépôt et à la diffusion de documents scientifiques de niveau recherche, publiés ou non, émanant des établissements d'enseignement et de recherche français ou étrangers, des laboratoires publics ou privés.

THESE DE DOCTORAT DE

NANTES UNIVERSITE

ECOLE DOCTORALE N° 596

Matière, Molécules, Matériaux

Spécialité : Physique Théorique

Par

Johannès JAHAN

The Beam Energy Scan under the scope of EPOS 4

Studying the impact of hadronic cascades on the 2nd order cumulants of conserved net-charges in heavy-ion collisions

Thèse présentée et soutenue à Nantes, le 30 septembre 2022

Unité de recherche : SUBATECH UMR6457

Rapporteurs avant soutenance :

Boris TOMÁŠIK Professor, Univerzita Mateja Bela & České vysoké učení technické v Praze
Magdalena DJORDJEVIC Professor, University of Belgrade & Institute of Physics Belgrade

Composition du Jury :

Président : Boris TOMÁŠIK Professor, Univerzita Mateja Bela & České vysoké učení technické v Praze

Examineurs : Boris TOMÁŠIK Professor, Univerzita Mateja Bela & České vysoké učení technické v Praze
Magdalena DJORDJEVIC Professor, University of Belgrade & Institute of Physics Belgrade
Jean-Yves OLLITRAULT Directeur de Recherche, Institut de Physique Théorique & CNRS
Marlene NAHRGANG Maître assistante, IMT Atlantique & Subatech
Sarah PORTEBOEUF-HOUSSAIS Maître de conférences, Université Clermont Auvergne & Laboratoire de Physique de Clermont

Dir. de thèse : Klaus WERNER Professeur d'Université, Nantes Université & Subatech

Invitée

Claudia RATTI Professor, University of Houston

TABLE OF CONTENTS

Acknowledgements / Remerciements	1
Introduction	7
1 Particle physics: from theory to experiments	11
1.1 The Standard Model of particle physics	13
1.1.1 General description	13
1.1.2 Limitations of the Standard Model	14
1.1.3 Beyond the Standard Model	16
1.2 Hadronic physics and Quantum ChromoDynamics	16
1.2.1 The foundation of QCD	17
1.2.2 How to deal with QCD: methods & phenomenological approaches	20
2 The hottest matter of the Universe	21
2.1 On a theoretical level: from first predictions to current models	22
2.1.1 The theoretical genesis behind the discovery of the QGP	22
2.1.2 The phase diagram of nuclear matter	25
2.2 Studying the QGP at the experimental level	27
2.2.1 Kinematics of high-energy collisions	27
2.2.2 The experimental apparatus	29
2.2.3 Methods to study the QGP	32
2.3 Focus on: criticality in the nuclear phase diagram	34
2.3.1 Thermodynamic susceptibilities and net-charge cumulants	35
2.3.2 Limits and shortcomings of experimental and theoretical observables	39
2.3.3 STAR results & enhanced proxies for 2 nd order cumulants	41
3 The EPOS event generator	47
3.1 Generalities on event generators	48
3.1.1 Event generators & high-energy physics	48
3.1.2 Event generators for heavy-ion collisions	49
3.2 A little history of EPOS and related projects	51
3.2.1 From VENUS to EPOS 4	51
3.2.2 Side projects with EPOS	52
3.3 Theoretical frame of EPOS	53
3.3.1 Parton Model	54
3.3.2 Gribov-Regge Theory	54
3.3.3 Parton-Based Gribov-Regge Theory	55
3.3.4 String Model	58
3.4 Generation of an event in EPOS	59

3.5	Objectives of the thesis	63
3.5.1	Towards the release of EPOS 4	63
3.5.2	Towards the study of net-charge cumulants	64
4	Technical developments for EPOS 4	67
4.1	RIVET	68
4.1.1	General presentation	68
4.1.2	The benefits for EPOS	71
4.2	How EPOS works in practice	72
4.2.1	Structure of the repository	72
4.2.2	Running simulations	73
4.2.3	Using on-the-run analyses	75
4.3	Integration of RIVET into EPOS analysis framework	77
4.3.1	Producing HEPMC files	77
4.3.2	Automating the usage of RIVET	83
4.3.3	Dealing with centrality calibration	86
4.4	Summary of the technical work	86
5	Beam Energy Scan & study of cumulants with EPOS	89
5.1	Basic spectra for the BES energies	91
5.1.1	Pseudorapidity densities of charged hadrons	91
5.1.2	Transverse momentum spectra of identified hadrons	93
5.2	Study of the 2 nd order cumulants of conserved charges	99
5.2.1	Results for STAR proxies: variances, covariances and their ratios	99
5.2.2	Comparison with enhanced proxies and conserved charges cumulants	102
5.2.3	Impact of hadronic cascades on the 2 nd order cumulants	106
5.3	Summary of results on 2 nd order cumulants study	111
	Conclusion & Outlook	113
	A Transverse momentum spectra for identified hadrons	117
	B Centrality-Bin Width Correction	125
	C Net-multiplicity cumulants analysis in EPOS	129
	C.1 Technical implementation of the analysis	129
	C.2 Structure of the analysis routine	130
	C.3 Writing a net-multiplicity cumulant analysis	132
	D Cumulants of conserved charges before & after hadronic cascades	135
	E Résumé français de la thèse	137
	E.1 Contexte et motivations	137
	E.2 Motivations et objectifs de la thèse	141
	E.3 Développements techniques pour EPOS 4	143
	E.4 Résultats sur l'étude des cumulants de charges conservées	145
	Acronyms	151
	List of Figures	159
	List of Tables	161
	Bibliography	183

ACKNOWLEDGEMENTS / REMERCIEMENTS

Ayant toujours été quelqu'un de très curieux, les sciences naturelles me sont rapidement apparues comme une discipline de choix au cours de ma scolarité. En particulier, les sciences physiques ont été un déclic dès la fin du collège, à la mention de l'existence des atomes et de la structure microscopique de la matière. Les quelques cours de physique nucléaire et de relativité restreinte que j'ai pu suivre au lycée ont alors été une vraie révélation, et m'ont permis d'entrer à l'Université en ayant pour objectif de réaliser un jour, si possible, un doctorat en physique des particules. Ce manuscrit attestant ainsi de cet accomplissement, je tiens avant toute chose à remercier en quelques pages toutes les personnes qui m'ont permis d'aller au bout de cette aventure. Je ne vais bien évidemment pas pouvoir nommer une par une toutes ces personnes, et j'espère donc que celles et ceux que j'aurais omis de citer nominativement ne m'en tiendront pas rigueur. Je ne vous oublie pas ! À noter que, certaines personnes que je tiens à remercier ne parlant pas français, je rédigerai les passages les concernant en anglais.

Je souhaiterais tout d'abord commencer par remercier les différents membres de mon jury. For accepting to be reviewers of my thesis manuscript, I would like to thank Boris Tomášik and Magdalena Djordjevic, especially when considering the struggle I had to respect the deadlines. Thanks for your patience and comprehension, as well as for all the useful feedbacks you have given to me; I truly appreciated and valued them. De la même façon, je tiens à remercier Jean-Yves Ollitrault, pour les longues conversations très intéressantes à propos de mon travail, et Marlène Nahrgang pour m'avoir également donné de nombreuses pistes de réflexion, en plus d'avoir été une excellente professeure durant mon Master. J'adresse des remerciements tout particuliers à Sarah Porteboeuf-Houssais, qui est en quelque sorte ma "marraine" de profession, la personne qui m'a initié à la recherche en physique des hautes énergies. Merci pour toute l'inspiration que tu m'as donnée au travers des discussions que nous avons pu avoir, mais aussi simplement de par ton parcours. I also owe unspeakable thanks to Claudia Ratti, who did not only manage to find the time to attend my defense despite the distance and the time shift, but also accepted earlier in my PhD to be part of my follow-up committee. Most of all, thank you for offering me a postdoctoral position with you in such a great environment like Houston, and for being such a nice and inspiring advisor, collaborator and friend. Grazie mille per tutto ! Despite not being part of my jury, I also wanted to thank Ludmila Malinina for being the other member of my follow-up committee, and having shown interest in my work.

Il est évident que cette expérience n'aurait jamais pu avoir lieu sans la confiance que m'a accordée Klaus, en me proposant cette thèse sous sa direction avant même que je n'entame ma deuxième année de Master. Merci pour ta constante bonne humeur, et pour ta réactivité. Cette thèse ayant été marquée par la pandémie de Covid-19, il m'a été d'une grande aide de pouvoir compter sur nos échanges malgré les confinements successifs. Je

te suis également reconnaissant pour toute la liberté que tu m'as accordée durant ces trois années et demi, en me laissant enseigner et participer à de nombreuses conférences notamment, tout en sachant me guider avec sagesse dans mon projet de recherche. Ce savant mélange m'a apporté énormément en tant que chercheur, et a très certainement été décisif pour le début de ma carrière. Je n'aurais honnêtement pas pu imaginer de meilleur encadrement pour réaliser mon doctorat. Merci d'avoir partagé avec moi une partie de ton incroyable expertise et de tes connaissances dans le domaine de la physique des ions lourds, et j'espère que notre collaboration continuera aussi fructueusement que possible !

L'environnement de travail est également un élément clé pour le bon déroulé d'un doctorat, et j'ai pu compter pour cela sur le cadre idéal du laboratoire Subatech. Je remercie pour commencer l'ensemble du groupe du Théorie dans lequel j'ai effectué cette thèse. Ce fut un réel plaisir de côtoyer, en tant que désormais collègues, celles et ceux qui furent pour la plupart mes professeur.e.s auparavant. Merci à Thierry, pour avoir assuré un rôle essentiel à la tête du groupe durant la quasi-totalité de mon doctorat, en plus d'avoir été un interlocuteur privilégié de part sa position de responsable du Master PFA. Une autre pensée particulière à Guy, pour avoir été un excellent encadrant lors de mon tout premier stage de recherche, ainsi qu'un professeur passionné et passionnant. Je retiens également les bons moments passés à Saint-Jacut-de-la-Mer en compagnie de Stéphane P. et François, ce qui a notamment permis d'amener la pétanque à la Chantrerie. Enfin, je tiens à remercier Pol-Bernard pour avoir appuyé avec autant de sympathie mes candidatures de postdoc à l'étranger, et pour m'avoir soutenu et rassuré quant à l'idée de vivre une telle expérience aussi loin de ma ville natale. En tant que résident temporaire du couloir H200, j'ai eu la chance de côtoyer quotidiennement la direction ainsi que toute l'équipe administrative du laboratoire. Merci donc à Ginés, Pol-Bernard (à nouveau), Isabelle et Jean-Luc pour avoir formé une équipe de direction de choc, du moins de mon point de vue. Un grand merci à Véro, Séverine, Merryl, Stéphanie, Sandrine, Pascaline, Anne, Tanja, Andreas et Nadège pour votre travail indispensable au bon fonctionnement du laboratoire, et pour les bonjours souriants du matin ! J'ai bien sûr volontairement omis de citer Sophie et Farah, de par la place spéciale qu'elles occupent dans ce groupe. Merci à vous deux pour avoir été des partenaires de badminton infatigables (ou presque), pour toutes les discussions, pauses cafés et autres activités extra-professionnelles en votre compagnie. Je remercie bien sûr tout l'ensemble du laboratoire pour avoir contribué à me faire sentir comme chez moi sur mon lieu de travail, et avoir contribué à en faire un environnement si stimulant. Merci particulièrement à Damien, Gilles, Marcus, Jacopo, Jean-Michel, Khalil, Pierrick, Erwan M., Maxime G., Marie, Guillaume B., Arnaud, Richard et Lilian entre autres (et je dois abrégé ici la liste des noms si je ne veux pas me retrouver à citer l'ensemble du personnel...).

Ce qui a rendu cette expérience si unique, c'est aussi bien sûr la compagnie es autres doctorant.e.s avec qui j'ai partagé ces années à Subatech. Merci tout d'abord aux "ancien.ne.s", à commencer par le duo de choc Gabriel (ATER!) et David Fazou, Roland, Ophé et Chardmou, mais aussi Manu, David H., Chloé, Anthony et Erwann, pour avoir su nous accueillir et nous intégrer aussi facilement dans ce groupe. Marysia, thank you very much for having been a wonderful supervisor during my first months there, and for becoming a wonderful friend too. Bien évidemment, mes camarades de promotions sont les premières personnes qui me viennent à l'esprit, ce "cru" ayant été si spécial pour moi de part la bonne ambiance qui régnait entre nous. Merci énormément à Arthur notre parisien préféré, Vincent (malgré son arrivée tardive), Rita ma camarade de karaoké, ma sista Claudia et Goiregré l'homme en chaussettes qui m'a accompagné dans mon exil

américain. Mention spéciale à Michael, notre British guy who "does not talk like this!", mon partenaire de bureau depuis notre arrivée à Subatech, pour les nombreuses discussions sur tant de sujets plus intéressants les uns que les autres, et toutes les fois où tu as pris le temps de m'aider avec tant de persévérance. Le coeur de ce groupe, ceux avec qui j'aimais désigner le quatuor que nous formions sous le nom de "4 fantastiques", ce sont mes camarades de Master Thomas, Maxime et Victor. Un immense merci pour tout: les "Hello sunshine", les fameuses pauses thé dans le salon, tous les délires et bons moments partagés ensemble. C'est cette alchimie si particulière entre nous qui nous a permis de traverser toutes ces épreuves pourtant pas si évidentes ensemble, et je suis heureux d'avoir pu le faire en compagnie de personnes aussi incroyables que vous. Merci aussi à mes autres collègues de bureau Denys et Mahbobeh, pour avoir partagé mon quotidien et toutes ces petites choses qui ont créé ce lien particulier avec vous. De même, je remercie mes voisins de bureau Stéphane, Nathan et Eamonn, avec qui j'ai passé beaucoup de temps à discuter, bien que rarement à propos du travail. Je n'oublie pas non plus Nadiya et Hanna ; merci d'être venues apporter un peu de sang nouveau, de joie et de bonne humeur dans notre groupe après ces interminables confinements. Merci enfin à tous ceux qui sont venus compléter les rangs plus tardivement, notamment Léonard, Nico, Johan, Alexander, Victor V., Tobie et Félix.

Je tenais à remercier également toutes les personnes de passage, comme Antoine P., Guillaume F., notre hôte de bureau pendant quelques mois avec qui j'ai apprécié d'avoir eu autant de discussions sur nos projets futurs, ou bien encore tous les stagiaires que j'ai pu côtoyer. Bien sûr, je remercie en particulier les stagiaires que j'ai personnellement encadrés, pour tout ce qu'ils et elles m'ont apporté en échange de ce que j'ai pu leur apprendre. Merci donc à Gabriel P., Xavier, Émilie M., Mme la présidente Émilie B. et Chloé qui a visiblement tellement apprécié de travailler sur EPOS qu'elle est revenue une deuxième fois ! Un énorme merci à Axel, car je n'aurais pas pu espérer mieux finir ma thèse qu'en encadrant en stage un étudiant aussi autonome, perspicace, et par-dessus tout un ami.

J'ai adoré l'expérience de pouvoir enseigner à l'Université durant les deux premières années ma thèse, et c'est en grande partie grâce aux très bons contacts que j'ai pu avoir avec les étudiant.e.s, que je remercie donc à leur tour. J'espère avoir été à la hauteur, en vous rendant l'apprentissage de la physique un peu plus facile, et en y ayant donné du sens, en particulier durant les périodes de cours à distance dues aux différents confinements. Parce que j'ai aussi été un étudiant avant d'en arriver là, j'ai une pensée pour tous les enseignant.e.s qui m'ont permis d'appréhender la physique au travers de mon parcours universitaire. Je remercie notamment Thierry et Julien, les responsables du Master PFA et du parcours RPS à cette époque, mais aussi toute l'équipe pédagogique pour avoir assuré un enseignement que j'ai grandement apprécié. Enfin, je remercie spécialement Olivier Ravel, directeur du département de Physique, pour m'avoir fait confiance en me proposant des tâches d'enseignement, pour avoir été un professeur de physique de particule et d'astroparticules aussi passionnant. Merci de nous avoir motivé.e.s et soutenu.e.s dans la création de L'Association des Etudiant.e.s de Physique de Nantes (LAEPtoN), qui, je l'espère, assurera aussi longtemps que possible sa mission au sein de l'Université de Nantes. J'en profite ainsi pour remercier de même toutes les personnes qui ont pris part et contribué à la vie de cette association.

Ces années passées à l'Université de Nantes m'ont permises, au-delà d'évoluer dans un milieu qui m'a tant apporté, de faire de superbes rencontres. Les premières personnes que je souhaite remercier sont évidemment Margot, Elie, Teddy R., Quentin Lenouvel et

Victor, pour avoir été aussi présents, ce encore aujourd'hui malgré la distance, et pour être des amis aussi géniaux et fidèles. Merci particulièrement à Victor, pour avoir été mon infatigable compagnon de route durant ces 10 dernières années, avec qui j'ai pu tant partager et sur qui j'ai toujours pu compter. J'ai le sentiment que vous avez tou.te.s contribué à faire de moi la personne que je suis aujourd'hui, et j'espère pouvoir continuer à vous compter dans mes plus proches ami.e.s aussi longtemps que possible. Bien sûr, je remercie aussi toute ma promotion de Master, et notamment Quentin Lesigne, Mathilde, Teddy D., ainsi que Pierre le Pipou dont la venue à ma soutenance m'a sincèrement touché. Un grand merci également aux "Faux Nantais", pour avoir rempli notre dernière année de Licence d'autant de si bons moments, ainsi qu'à Ugo et Arsène durant notre année de Licence 2. Merci enfin à tous les autres camarades qui ont contribué à rendre ces années de Licence aussi agréables à vivre.

Bien qu'il soit difficile d'y mettre de simples mots, je tiens à exprimer l'immense gratitude que je ressens pour la personne qui a occupé une place si spéciale durant les 7 dernières années et demi de ma vie. Merci infiniment d'avoir agrémenté toutes ces années passées ensemble de moments de joie et de bonheur. Merci pour le soutien que tu m'as apporté au quotidien, dans tous les projets que j'ai entrepris, et pour l'influence considérablement positive que tu as eue dans ma vie. Merci d'avoir été à l'écoute, d'avoir été présente dans les moments difficiles, et d'avoir su trouver les mots justes pour me pousser vers l'avant lorsque c'était nécessaire, tout en m'empêchant de me noyer dans le travail lorsque je me sentais dépassé. Je ne serais sûrement pas sorti aussi grandi de toutes ces expériences sans toi à mes côtés, et je te serai toujours reconnaissant pour cela. Je remercie de même sincèrement ma belle-famille d'alors pour avoir cru en moi, et pour m'avoir offert tant de parenthèses de bonne humeur et de bons moments.

Pour finir, je remercie avant tout mes parents, du fond du coeur, pour m'avoir toujours poussé à donner le meilleur de moi-même, et surtout pour m'avoir toujours laissé la liberté de suivre la voie que je désirais emprunter, sans jamais avoir douté de moi. Merci d'avoir fait tout votre possible pour que je puisse réaliser ce que je souhaitais faire dans la vie, d'avoir considéré que le bien-être et le bonheur de vos enfants était une priorité, et que cela passait avant tout par les aider à accomplir leurs rêves, quand bien même cela signifiait nous voir prendre des voies qui vous étaient complètement inconnues. Merci à ma petite soeur de m'avoir supporté depuis toujours, dans le sens positif comme négatif du terme, il faut l'admettre. Merci aussi et surtout pour avoir été, bien que ma cadette, une réelle source d'inspiration pour ton courage et ta détermination. Merci à mon petit frère pour m'avoir aidé à sortir de si nombreuses fois de ma bulle, et pour tout ce qu'on a pu partager ensemble malgré notre différence d'âge. Je remercie aussi l'ensemble de ma grande famille pour m'avoir toujours énormément soutenu, pour avoir été motivants et bienveillants, mais aussi compréhensifs lorsque mon travail m'obligeait malheureusement à manquer des célébrations avec vous. Je suis heureux et fier d'être le premier Dr. de cette famille, et c'est en grande partie grâce à vous tous que j'ai pu accomplir cela. Une mention spéciale à mon oncle et ma tante qui ont accepté de se charger de la préparation de mon pot de thèse : je n'aurais pas pu espérer mieux finir ma thèse autrement, merci beaucoup. Enfin, un énorme merci à mes grands-parents pour tout ce qu'ils m'ont apporté dans la vie, toutes les valeurs qu'ils m'ont transmises, et en particulier à mes grands-parents maternels pour avoir été présents le jour de ma soutenance, bien qu'ignorant tout de mon travail et ne parlant pas un mot d'anglais. Je termine ces remerciements avec quelques mots pour mon grand-père paternel, Henri, qui nous a malheureusement quitté avant de me voir accomplir tout cela. Parce que tu as été un modèle de sagesse toute ma vie, je te dédie cette thèse Papi.

How does matter take form? What are we, the world surrounding us, and even the whole Universe, fundamentally made of? These questions, which anyone might have asked themselves at some point, are the ultimate reasons motivating the work presented in this thesis. Thanks to the incredible knowledge acquired from centuries of progress in science and technology, we know that ordinary matter of which we are composed is made of atoms, whose properties and behaviours are now studied in atomic physics and chemistry. Even more fundamentally, particle physics focuses on how the atom's components, *i.e.* electrons, nucleons and the quarks and gluons inside them, interact at such tiny scales. My research takes place in this context, and is more particularly related to the theory used to describe the strong interaction: the quantum chromodynamics (QCD). A first important property of this theory is the colour confinement, the fact that quarks and gluons, which carry a colour charge proper to this interaction, are always confined in composite particles called hadrons. One direct consequence is that they can only be probed, below the femtometer scale, in high-energy collisions performed in powerful accelerators such as, among others, the giants LHC or RHIC.

Almost half a century ago, while QCD was just established, some physicists suggested that there might exist a state of matter where quarks and gluons are deconfined, called the quark-gluon plasma (QGP). The observation of this new state of matter, expected to compose the core of neutron stars and formerly the early Universe, has been formally announced in the first half of the 2000's decade by several experimental collaborations, after having gathered several pieces of evidence. The study of the QGP is achieved via relativistic heavy-ion collisions, which allows to reach the high temperature and density required for its formation. However, collecting information about it is challenging: because of its very short lifetime ($\sim 10^{-23}$ s), the QGP droplet created in such collisions cools down and returns to the hadronic phase before reaching the detectors. Hence, it is only possible to access its properties indirectly, via the signatures imprinted in the final-state hadrons originating from its freeze-out.

A specific topic of interest in that field is the characterisation of the phase diagram of nuclear matter, *i.e.* determining under which conditions precisely a QGP can be created, where are the phase transitions to a hadronic gas, and what is the nature of these transitions. Nowadays, the thermodynamics of this fundamental matter cannot be determined completely from the first principles of the theory, though. This is due to another important property of QCD, the fact that its coupling constant depends on the energy scale, and so the strength of the strong interaction between quarks. Hence, perturbative calculations can only be achieved at high energy, and it is impossible to describe the tran-

sition from a QGP to a hadron phase analytically. There exists however one approach, consisting of discretising space-time in a lattice and called lattice quantum chromodynamics (lQCD), which allow to resolve it non-perturbatively via numerical simulations, but only at zero or limited baryonic density. These simulations enabled to predict a crossover transition between the QGP and the hadron gas in this region, which is the only part of the phase diagram known with certitude so far. Nonetheless, several other models predict the existence of a 1st order phase transition at finite baryonic density, that involves the existence of a critical endpoint (CEP) due to the crossover transition at low density.

My work will focus on the search for this CEP via the study of fluctuations of conserved charges (baryonic number, strangeness and electric charge), which are expected to diverge in its vicinity, and so indicate its location. They are quantified theoretically by the so-called susceptibilities, calculated with lQCD or the statistical thermal Hadron Resonance Gas (HRG) model, and evaluated experimentally through moments of the net-multiplicity distributions of hadrons carrying the charges of interest. These measurements are notably achieved by the STAR experiment in the frame of the *Beam Energy Scan* (BES) program, whose goal is to search for experimental signatures of the CEP by achieving Au-Au collisions at many energies. By doing so, they create different systems describing several trajectories which probe a large region of the phase diagram, hoping to see any clue hinting for the presence of a CEP. Considering, however, the fundamental differences between a theoretical idealised system at equilibrium, and the highly dynamical system created in heavy-ion collisions, it is primordial to understand the experimental limitations toward these fluctuation observables to relate them properly to the theory. Such investigations are only possible by using phenomenological approaches to simulate collisions, in particular thanks to event generators, which are the most realistic tools developed for this purpose. Hence, the first objective of my study is to quantify the impact of hadronic cascades, the successive re-interactions between formed hadrons at the late stage of the collisions, on the 2nd order cumulants of net-pions, net-kaons and net-protons, by using such simulations. The underlying motivation is to see how these proxies measured by STAR, supposedly related to the fluctuations of conserved charges, are impacted by processes which are not related to any critical behaviour of the nuclear matter. Another objective is to compare these observables to some "enhanced" proxies, expected to better reproduce the theoretical susceptibilities as proposed after a study using HRG model calculations. Both of them could finally be compared to the cumulants of the exact corresponding conserved charges, as event generators enable to access all the hadrons created in the simulated events, to see how effective proxies they are truly.

To this end, I used the EPOS event generator, which is based on a unique theory for initial interactions mixing multiple scattering approach and perturbative QCD, and which features a relativistic viscous hydrodynamic evolution of the bulk matter created in the simulated collisions. My study was led during the preparation of a new version, EPOS 4, to be publicly released soon. Thus, in order to improve the usability of EPOS, I adapted it in parallel to make it compatible with the RIVET software. To go even further, I even integrated this tool which offers an automatisation of the comparison between event generator simulations and experimental data, into the EPOS analysis framework, so that developers could also benefit from it. For the energy range of the BES program, I also wrote many analyses in the EPOS framework itself, for the ones not available in RIVET, to compare its results to experimental data. Thus, it allows testing the parametrisation validity before the public release, and ensures that the simulated events used for my main study exhibit a good description of what we observe experimentally.

In the following manuscript, I will therefore introduce briefly in Chapter 1 the general context of the Standard Model, with a specific focus on QCD. Chapter 2 will be dedicated to the physics of heavy-ion collisions and the study of the QGP, to introduce the search of the critical point in the phase diagram of nuclear matter as well as the tools to used to achieve it. I will end it with a presentation of the two main publications which inspired my work, followed by the detailed motivations of my study. In the Chapter 3, I will present EPOS and outline the main objectives of my thesis as a conclusion. Finally, Chapter 4 will contain the description of the technical work related to EPOS and RIVET, and Chapter 5 the results of my study on the 2nd order cumulants of net-charges.

CHAPTER 1

PARTICLE PHYSICS: FROM THEORY TO EXPERIMENTS

Contents

1.1	The Standard Model of particle physics	13
1.1.1	General description	13
1.1.2	Limitations of the Standard Model	14
1.1.3	Beyond the Standard Model	16
1.2	Hadronic physics and Quantum ChromoDynamics	16
1.2.1	The foundation of QCD	17
1.2.2	How to deal with QCD: methods & phenomenological approaches	20

Since Antiquity, scientists have elaborated theories and experiments to explain what matter is made of. The concept of atoms, as tiny indivisible elementary pieces composing everything, has been proposed by Ancient Greek philosophers Democritus and Leucippus during the 6th century BC. However, the idea was only largely accepted in the scientific community by the end of the 19th century, thanks to the work of *e.g.* John Dalton, Amedeo Avogadro or James Clerk Maxwell. At the dawn of the 20th century, the discovery of electrons by Joseph J. Thomson [1], quickly followed by the one of the atomic nucleus by Ernest Rutherford, Hans Geiger and Ernest Marsden [2, 3], proved that atoms were finally not the most elementary pieces of matter. After the pioneering work of Max Planck and Albert Einstein towards the interaction between light and atoms [4, 5], Niels Bohr developed a quantum atomic model published in 1913 [6–8]. This progress led, during what is considered to be the golden age of modern physics, to the development of quantum mechanics, a fundamental theory used to describe how particles behave and interact with each others below the nanometre scale. The main principles of this theory, as well as the proper formalism to describe it, were mainly established during the 1920s by numerous physicists like Louis de Broglie, Werner Heisenberg, Max Born, Erwin Schrödinger or Paul Dirac, to name just a few famous ones.

The 1930s decade saw further progress on the understanding of the fundamental interactions. In an attempt to explain radioactive β -decay, the bases of weak interaction were set by Wolfgang Pauli who postulated the existence of the neutrino [9], and by Enrico Fermi, who incorporated this new particle into a formulation of a contact interaction to describe the process responsible for this decay [10]. James Chadwick also brought to light the existence of the neutron [11], which eventually led to the discovery of the neutron-induced nuclear fission by Otto Hahn, Fritz Strassmann and Lise Meitner [12, 13]. It opened a gate to a powerful new source of energy, which was at first sadly famous for its military application, but was also exploited afterwards for civil purposes and therefore providing electricity for millions of people.

The politico-economical context of the post-World War II era pushed many countries to invest in fundamental research. Thus, many American laboratories quickly developed large experimental complexes thanks to the legacy of the Manhattan Project, while the *European Organization for Nuclear Research*, or "*Conseil Européen pour la Recherche Nucléaire*" (CERN) was created in 1954 in Geneva. In particular, the important progress on accelerator physics and technologies allowed to achieve particle collisions at greater and greater energies, probing thus smaller and smaller length scales.

From there was born the field of modern particle physics, which has developed until now into a community of several thousands of active researchers all around the world. Despite the significant advances in our knowledge of matter and fundamental interactions, our motivations remain the same: to understand the laws that govern our universe at a microscopical level. Since the work presented in this thesis is part of that dynamic, I will introduce in section 1.1 of this chapter the broad lines of the Standard Model of particle physics, the most complete and advanced theory describing matter at such scale up to date, although known to be limited. I will then describe with a little bit more details in section 1.2 the history and principal aspects of QCD, the theory describing strong interaction, which is the main background of my work. This will open the way to chapter 2, where I will depict more precisely the context of the research presented in this thesis: the study of quark-gluon plasma in relativistic heavy-ion collisions.

1.1 The Standard Model of particle physics

The Standard Model of particles physics, often simply referred to as the Standard Model (SM), describes how elementary particles interact with each other via electromagnetic, weak and strong interactions, in the framework of quantum field theory (QFT) based on $SU(3) \otimes SU(2) \otimes U(1)$ gauge symmetry [14]. It offers a solid theoretical description of those three fundamental forces, from which several predictions have been validated by posterior measurements and none ever formally refuted so far. Nevertheless, the fact that the SM has never been formally contradicted experimentally does not mean it is flawless. Hence, after giving a short description of its key ingredients, I will briefly discuss its limits, and mention some theories established to describe physics beyond the Standard Model (BSM).

1.1.1 General description

The different elementary particles composing the SM are listed in Figure 1.1. The twelve particles composing matter, on the left panel, are the so-called fermions, generally classified in three generations after their mass hierarchy (their antiparticles, which just have opposite electric charge, are not displayed here). These fermions, carrying a spin value of $1/2$, are themselves divided into two groups called quarks and leptons. On the right panel are shown the bosons, particles carrying an integer spin value, among which the four gauge bosons are vectors of the fundamental interactions.

		FERMIONS			BOSONS		
		I	II	III			
QUARKS		$\begin{matrix} 2/3 & 1/2 \\ u \\ 2,2 \text{ MeV}/c^2 \end{matrix}$	$\begin{matrix} 2/3 & 1/2 \\ c \\ 1,3 \text{ GeV}/c^2 \end{matrix}$	$\begin{matrix} 2/3 & 1/2 \\ t \\ 173 \text{ GeV}/c^2 \end{matrix}$	$\begin{matrix} 0 & 1 \\ g \\ 0 \end{matrix}$	$\begin{matrix} 0 & 0 \\ H^0 \\ 125,3 \text{ GeV}/c^2 \end{matrix}$	HIGGS
		$\begin{matrix} -1/3 & 1/2 \\ d \\ 4,8 \text{ MeV}/c^2 \end{matrix}$	$\begin{matrix} -1/3 & 1/2 \\ s \\ 93 \text{ MeV}/c^2 \end{matrix}$	$\begin{matrix} -1/3 & 1/2 \\ b \\ 4,2 \text{ GeV}/c^2 \end{matrix}$	$\begin{matrix} 0 & 1 \\ \gamma \\ 0 \end{matrix}$		GAUGE BOSONS
LEPTONS		$\begin{matrix} -1 & 1/2 \\ e \\ 0,511 \text{ MeV}/c^2 \end{matrix}$	$\begin{matrix} -1 & 1/2 \\ \mu \\ 106 \text{ MeV}/c^2 \end{matrix}$	$\begin{matrix} -1 & 1/2 \\ \tau \\ 1777 \text{ MeV}/c^2 \end{matrix}$	$\begin{matrix} 0 & 1 \\ Z^0 \\ 91,2 \text{ GeV}/c^2 \end{matrix}$		GAUGE BOSONS
		$\begin{matrix} 0 & 1/2 \\ \nu_e \\ < 2 \text{ eV}/c^2 \end{matrix}$	$\begin{matrix} 0 & 1/2 \\ \nu_\mu \\ < 0,19 \text{ MeV}/c^2 \end{matrix}$	$\begin{matrix} 0 & 1/2 \\ \nu_\tau \\ < 18,2 \text{ MeV}/c^2 \end{matrix}$	$\begin{matrix} \pm 1 & 1 \\ W^\pm \\ 80,4 \text{ GeV}/c^2 \end{matrix}$	$\begin{matrix} \text{charge} & \text{spin} \\ X \\ \text{masse} \end{matrix}$	

Figure 1.1: Components of the Standard Model listed with their main properties (mass, spin and electric charge) [15] taken from the *Particle Data Group 2022* [14].

The electromagnetic (EM) interaction, the elderly known of the three described by the SM, is described in this framework by the so-called quantum electrodynamics (QED). It rules how all electrically charged particles interact with photons, pictured by the γ symbol. The Z^0 and W^\pm bosons are vectors of the weak interaction, respectively responsible for the elastic interaction of neutrinos with other fermions via neutral currents [16], and for flavour-changing reactions. The charged W bosons couple with the two different leptonic species of same generation (*e.g.* electron e and electronic neutrino ν_e),

as well as quarks of different flavours, being therefore responsible for radioactive β -decay and decay of heavy-flavoured hadrons (*i.e.* containing quarks of 2nd and 3rd generation). For instance, in the β -decay of a radioactive nucleus which sees one of his neutrons n transformed into a proton p , the actual underlying process involving the flavour change of a quark is:

$$\underbrace{ud d}_n \xrightarrow{W^- \rightarrow e^- + \bar{\nu}_e} \underbrace{ud u}_p + e^- + \bar{\nu}_e . \quad (1.1.1)$$

The mixing parameters between quarks flavours are given in a unitary matrix called Cabibbo-Kobayashi-Maskawa (CKM) matrix, named after the scientists who elaborated it [17, 18]. From this matrix, one can deduce the transition probability from one quark of flavour i to another of flavour j , by squaring the corresponding element V_{ij} ; hence, the unitarity of the CKM matrix can be easily tested by checking if $\sum_j |V_{ij}|^2 = 1$ for any given i . The parameters of the matrix have been experimentally determined with the following up-to-date values [14]:

$$V_{\text{CKM}} = \begin{pmatrix} V_{ud} & V_{us} & V_{ub} \\ V_{cd} & V_{cs} & V_{cb} \\ V_{td} & V_{ts} & V_{tb} \end{pmatrix} = \begin{pmatrix} 0.97435 & 0.22500 & 0.00369 \\ 0.22486 & 0.97349 & 0.04182 \\ 0.00857 & 0.04110 & 0.999118 \end{pmatrix} \quad (1.1.2)$$

The EM and weak interactions are in fact two faces of the same interaction, the electroweak (EW) interaction [19–21]. Below a given energy scale, they dissociate from each other due to the Englert–Brout–Higgs–Guralnik–Hagen–Kibble mechanism [22–24]. To make it simple, due to the breaking of weak isospin symmetry, this mechanism provides a mass to the W and Z bosons via interaction with the so-called Higgs field, interaction mediated by the associated Higgs boson. Although with a different mechanism, fermions also acquire a mass by interacting with the Higgs field, while photons remain massless.

The last element of Figure 1.1 yet not discussed is the gluon, vector of the strong interaction, which is the third fundamental interaction included in the SM description. Carrying a specific charge called "colour", the gluon only interacts with itself and with quarks, which have in addition the specificity to be the only particles to carry a fractional electric charge. The theory used to describe this interaction, the QCD, will be presented in detail in section 1.2.

1.1.2 Limitations of the Standard Model

Despite being so far the most elaborated and successful theory in particle physics, the Standard Model is still limited in its description of the universal laws of physics. First of all, it does not include any description of the gravitational interaction, only focusing on three of the four fundamental interactions in physics. It can consequently not be the ultimate theory in physics, if at least there were to be one. It is however rarely an issue in itself as, in particle physics, gravitational interaction is completely negligible compared to the other ones (approximately 40 times less intense than the EM interaction between a proton and an electron in the atom). In fact, very few physical contexts require a rigorous treatment of both QFT and general relativity: the study of the Big-Bang, black holes or even neutron stars, which are way out of the scope of the present work. Another important feature of contemporary research not described by the SM is the existence of dark matter [25]. Several astrophysical and cosmological observations, made since the middle of the last centuries [26–29], have shown that approximately 95% of the mass content of the Universe is not visible, thus not made of ordinary matter nor interacting via processes described by the SM.

Considering the SM itself, many elements of the theory are fundamentally not understood. Additionally to the usual discussions on the "elegance" of this theory (see for instance [30]), which depends on 26 parameters to be determined experimentally in its contemporary form, it exhibits a completely irregular and unexplained mass hierarchy between the different fermion generations.

Beyond these rather aesthetic considerations, which could perhaps just be how nature is made, the SM cannot explain the matter-antimatter asymmetry observed in our Universe [31]. Indeed, all interaction it describes conserve both baryonic number B and leptonic number L , so it cannot be responsible for the clear asymmetry observed nowadays, if the Universe was created without any imbalance in the original quantities of matter and antimatter as expected. Moreover, the SM suffered initially from incompleteness regarding the topic of neutrinos. Predicted originally as massless leptons, it was discovered in 1998 that they have the unique property to oscillate while propagating [32]. To be explicit, a neutrino created with a flavour i and a mass m_a , has a non-zero probability to be detected with a different flavour j and with a different mass m_b . The amplitude of these oscillations depends on the elements of a matrix relating the 3 flavour eigenstates to the 3 mass eigenstates (called the Pontecorvo-Maki-Nakagawa-Sakata (PMNS) matrix), on the difference between the mass eigenstate values, on the distance traveled by the neutrino and its energy [33]. Hence, such a particular feature requires that neutrinos have a mass. Although their oscillating behaviour can be added to the SM *ad hoc* without raising any inconsistency, it is not an original prediction of the theory and comes at the price of implementing 7 additional free parameters in it, plus additional features discussed in the next subsection.

Finally, several recent experimental measurements show appearing tensions with SM predictions. The first one concerns the anomalous contribution to the magnetic moment of the muon $(g - 2)_\mu$, a quantum mechanical correction to the value coming from the Dirac equation [34], originally predicted by Julian Schwinger for the electron [35]. As a matter of fact, results of measurements from the Muon $g - 2$ Experiment in 2021 [36], combined with previous measurements achieved by the E821 experiment [37], revealed a discrepancy of 4.2σ (standard deviations) compared to SM predictions. Another essential property of the theory, lepton flavour universality, says that all leptons couple the same way to gauge bosons, or in other words that an interaction should occur at equal rates for all leptonic flavours, aside from mass condition. To test this property, it is usual to study decays of hadrons into a pair of leptons plus another hadron, and to make the ratio of decay rates into a certain leptonic flavour l , over the rate of the same decay into other flavour(s), which is then expected to be equal to 1. However, several experimental measurements of such ratios have shown significant deviations from unity in the past 10 years. The $\bar{B} \rightarrow D^{(*)}l^-\bar{\nu}_l$ decays measured by the BaBar collaboration, as well as the $B \rightarrow K^{(*)}l^+l^-$ measured by the LHCb collaboration have pointed out deviations of respectively 3.4σ and 3.1σ from the universality hypothesis [38, 39]. The authors of [40] even claimed that, by performing an analysis over data from several experiments of some hadronic decays implying the $b \rightarrow sl^+l^-$ underlying process, they observe a deviation from SM predictions by 5σ . At last, a recent precise measurement of the W boson's mass by the CDF experiment revealed a difference from SM expectation with a significance level of 7σ [41].

1.1.3 Beyond the Standard Model

The different shortcomings of the Standard Model, added to the increasing number of measurements yielding tensions with its predictions, tend to clearly indicate that there are processes we do not understand yet which are out of its reach. Hence, this subsection will give a glimpse of the research led nowadays on beyond the Standard Model (BSM) physics.

The search for a quantum gravity theory, which aims at describing gravitational interaction in the frame of a QFT, would offer a scheme including the whole 4 fundamental interactions of physics, even though far from being a trivial problem to solve [30]. It has been an active research field since the famous physicist Stephen W. Hawking formulated the black hole information paradox in the middle of the 1970s decade [42, 43]. One of the numerous intents to marry quantum mechanics with general relativity is the string theory [44], not to be confused with the string model I will describe in subsection 3.3.4.

Another path widely explored concerns the existence of Supersymmetry (SUSY). Such theories postulates the existence of additional global symmetries, which would imply that each existing particle of the SM has a so-called "superpartner", heavier and from different nature (fermions have bosonic superpartners, and vice-versa) [45]. Among the huge diversity of possible SUSY theories, one can find a large diversity of explanations to the appearing tensions mentioned in the previous subsection, *e.g.* the lepton flavour universality violation or the anomaly of the $(g - 2)_\mu$ [46]. The experimental search for new massive particles, which would hint for the existence of SUSY and also discriminate some of those theories in the myriad of existing ones, is an active field for the ATLAS and CMS collaborations at CERN [47] as well as for the CDF and D0 collaboration at Fermilab [48].

The aforementioned search for new particles in high-energy collisions also aims at looking for the potential sign of dark matter candidates [49], in addition to the numerous experiments entirely dedicated to this hunt [50]. Another avenue that could potentially solve the dark matter puzzle would be the existence of the sterile neutrino, an additional (if not many) flavour of the neutrino which would not interact with any gauge boson of the SM, hence being not directly detectable [14]. It emerges naturally when including the oscillation mechanism and masses to neutrinos in the extended SM, with this inclusion being in some sense already BSM physics in itself. In addition, its existence has been hinted experimentally by anomalies in the measured flux of neutrinos, compared to predicted values, observed in different kinds of experiments. Consequently, a wealth of new experiments dedicated to neutrino physics plans to have a look at potential signs of sterile neutrinos in their results, whether being a major or only a secondary research focus [51].

1.2 Hadronic physics and Quantum ChromoDynamics

The last section has set the scene for this thesis, focusing however more on the electroweak side of the Standard Model. In this section, I will introduce the other side of it, which is the main context of my work: the quantum chromodynamics (QCD). Just like the other parts of the SM, QCD, and even more broadly hadronic physics, still has many shadow areas and is even probably the part of the SM which still has the most elements to unveil. After portraying QCD and its main characteristics in a historical manner, I will present several approaches and phenomenological models which have been developed to circumvent the difficulties encountered when intending to use it.

1.2.1 The foundation of QCD

The identification of elementary particles which compose the ordinary matter, *i.e.* protons, pions and electrons, as discussed in the introduction of this chapter, was of course not the end of the story. First using cosmic rays, and taking then advantage of the development of modern particle accelerators, a bunch of new particles were discovered during the 1940's and 1950's decades [52]. The lightest ones, with a mass inferior to the proton's one, were called mesons (from the Greek *mésos*, "middle") after Hideki Yukawa's prediction of bosonic particles carrying the strong interaction between nucleons in the atomic nucleus (lately identified as pions) [53]. The particles heavier than the protons were called baryons (from the Greek *barýs*, "heavy") by Abraham Pais, in his work on the description of the interaction of the newly discovered strange particles [54]. Besides, this same physicist was the first to propose that the decay of some of those new particles, called initially V-particles because of the pattern formed by their decay, was due to a different process than the strong interaction [55]. It led to the concept of strangeness as a property and new quantum number of those particles, which were actually kaons, Λ and Σ^\pm baryons [56, 57].

In order to organise this so-called zoo of particles, a successful model has been proposed independently by Yuval Ne'eman and Murray Gell-Mann in 1961, the famous "Eightfold Way" [58, 59]. They realised that, by sorting mesons (of spin $J = 0$, as bosons) and baryons (of spin $J = 1/2$, as fermions) into two distinct groups, they could organise them as a function of their respective hypercharge Y and isospin projection I_3 . They obtained in this way two representations of the symmetry group $SU(3)$ called octets, which are portrayed in Figure 1.2, based on the Lie algebra of group representation theory. This scheme predicted the existence of the η meson which would be discovered soon after [60], and could also be repeated for other groups of identical spin particles, which led to the prediction of the Ω^- baryon for the $J = 3/2$ decuplet of baryons for instance.

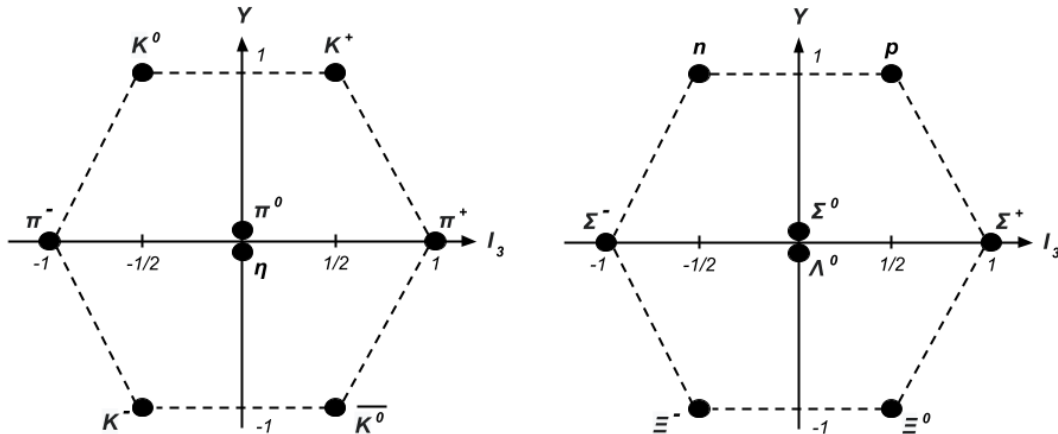


Figure 1.2: Illustration of the $J = 0$ and $J = 1/2$ octets as representations of the $SU(3)$ group.

Once in the path of the $SU(3)$ group, it was realised independently in 1964 by Murray Gell-Mann [61] and Georges Zweig [62] that a more fundamental symmetry of this group could be flavours, at the number of 3 in its fundamental representation. The u , d and s flavour quarks thus introduced were supposed to have fractional electric charge $+2/3$ and $-1/3$. When bound together, they produce the previously shown representations of the two hadronic families: $q\bar{q}$ pairs form mesons, and qqq trios form baryons. These elementary particles were called "quarks" by Gell-Mann, a name which stuck to them until now (unlike the "aces" discussed by Zweig), even though the author didn't believe

in their existence as real physical objects at that time. Few months later, Oscar Wallace Greenberg [63] and then Moo-Young Han and Yoichiro Nambu [64] proposed the introduction of another quantum number for quarks, following an additional and distinct SU(3) symmetry group. This new charge, which is now known as the "colour", could explain how baryons like Δ^{++} (uuu) and Ω^- (sss) could exist in the frame of the quark model without violating Pauli's exclusion principle.

It was not until 1969 that quarks were finally experimentally discovered. James Björken and Emmanuel Paschos interpreted the existence of point-like particles composing hadrons from the results of deep inelastic scattering (DIS) at the *Stanford Linear Accelerator Center* (SLAC). Basically, it was noticed that the cross-section of this inelastic reaction can be expressed with the dependence of only one variable x (sometimes written x_B) like in elastic cross-sections, that is often referred to as the Björken scaling [65]. It translates the fact that, when the energy of the electron is increased, the resolution wavelength of the virtual photon exchanged becomes smaller and the electron scatters a smaller constituent of the proton.

Richard P. Feynman introduced then the parton model [66], giving hence a theoretical explanation to the observations of Björken and Paschos, calling these proton's constituents "partons". The framework of the parton model is an inclusive approach, formulated to make calculations for only one exit process, with all other ways out being integrated. For example, in a $A + B \Rightarrow u + X$ event, the u quark for which one makes calculation is isolated from the rest of the system, and all other processes occurring in parallel are integrated in the X . Then, each parton takes a fraction x , of the momentum p and energy of the hadron it is composing, defined by [67]:

$$x = \frac{Q^2}{2p \cdot q} = \frac{Q^2}{2M \cdot \nu}, \quad (1.2.1)$$

when using $\nu = p \cdot q/M = E - E'$ the total energy exchanged during the interaction, where M is the mass of the proton, q the exchanged photon's energy and $Q^2 = -q^2$ the so-called virtuality of the process considered. Obviously, the sum of those variables x is equal to 1, and summing over all the partons i with $f_i(x) = \frac{dP_i}{dx}$ their parton distribution function, we obtain:

$$\sum_i \int x f_i(x) \cdot dx = 1. \quad (1.2.2)$$

Another important assumption of the parton model is the fact that partons are expected to be almost free. As will be discussed in subsection 3.3.1, this assumption puts limits on its application. Afterwards, Feynman identified partons with the quarks proposed by Gell-Mann and Zweig [68]. However, the results of equation 1.2.2 applied to DIS on protons and neutrons indicated that only a third of their total momentum was carried by quarks, when assuming their structures as predicted by the quark model. Consequently, there had to be some electrically neutral partons in the nucleons then, which were thought to be the gluons [68].

The last piece of the puzzle was brought by David Gross, Franck Wilczek and David Politzer in 1973, who proposed to describe strong interaction with a non-Abelian theory of the group SU(3), using color as a local symmetry [69, 70]. From this theory emerged one significant property of QCD: the coupling constant α_s is actually not a constant, but tends asymptotically to 0 when increasing the energy scale of the interaction, or when quarks are getting closer to each other as an equivalent picture. It can be expressed, in

the specific case of a $SU(3)$ group:

$$\alpha_s(Q) = \frac{12\pi}{(33 - 2N_f) \ln\left(\frac{Q^2}{\Lambda_{QCD}^2}\right)}, \quad (1.2.3)$$

with N_f the number of quark flavours, and Λ_{QCD} an infrared cut-off [67]. This property, called asymptotic freedom as quarks become free with the asymptotic diminution of the strong interaction strength, has been verified by many measurements as shown in figure 1.3.

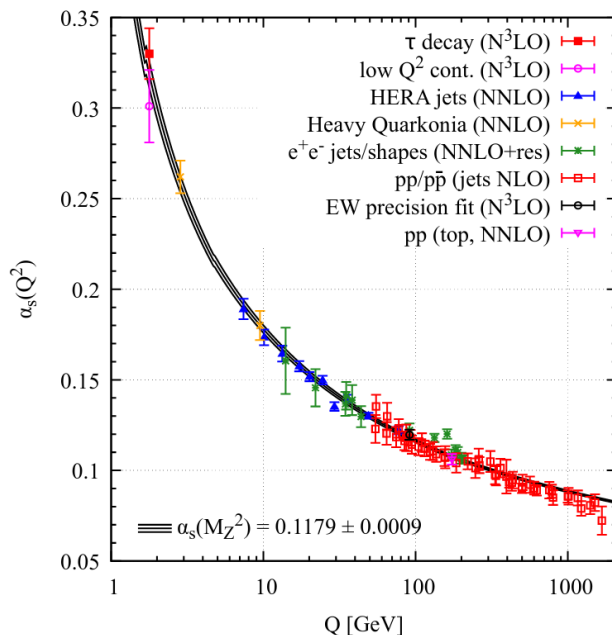


Figure 1.3: The intensity of the running coupling constant α_s as a function of the virtuality Q of the process considered. Analytical prediction based on the renormalisation scale of the order of M_Z , and values extracted from different processes are also displayed [14].

This same year, Gell-Mann again, with Harald Fritzsch and Heinrich Leutwyler, gathered all the pieces to complete the puzzle of QCD [71]. They demonstrate that the $SU(3)$ non-Abelian gauge theory describes perfectly the strong interaction, in agreement with all previous predictions of the quark model and Björken scaling, and integrates perfectly colour as a charge of this interaction. They went even further by assuming, in agreement with observations, that all interactions and physical particles observed have to be colour singlet (or, as usually said, "colour neutral"). It translates the fact that quarks and gluons can never be observed as free particles beyond the reach of the interaction, of the order of ~ 1 fm, and thus are always confined into hadrons.

The experimental confirmation came from the observation of two jets events at SLAC in 1975, in e^+e^- collisions at a center-of-mass energy $\sqrt{s} = 7.4$ GeV [72, 73]. Jets are collimated bunches of hadrons which were predicted to emerge from the fragmentation of quarks, produced in such collisions via the annihilation process $e^+e^- \rightarrow \gamma \rightarrow q\bar{q}$ [74, 75]. With the same idea that gluons eventually materialise as a $q\bar{q}$ pair resulting in a jet, their existence was deduced from the observation of three jets in e^+e^- collisions by the PLUTO experiment in 1979, in the decay of $\Upsilon(1S) (c\bar{c}) \rightarrow ggg$ [76].

1.2.2 How to deal with QCD: methods & phenomenological approaches

Even though being well established as the theory describing strong interaction, the nature of the QCD makes it hard to employ. I will hence present in this subsection some of the methods and approaches which are used nowadays to make calculations, predictions and simulations, and are closely or remotely based on QCD first principles. The aim is indeed not to make an exhaustive listing, but to introduce the ones which will be further mentioned and discussed in this thesis.

The running character of the QCD coupling constant restrains for instance the use of perturbative theory. In QED, the coupling remains approximately constant around a value $\alpha = 1/137$ (it increases slightly to higher values at high energies, but still close to this value for the energies reached nowadays), which allows perturbative calculations whatever the energy scale implied. On the contrary, the value of α_s in QCD only enables to perform perturbative calculation starting from few GeV, as can be seen in Figure 1.3. Processes at such energies are often referred to as "hard processes". Thus, Λ_{QCD} from equation 1.2.3 can be interpreted as a scale below which perturbative calculations can not be performed reasonably.

Nevertheless, an approach initiated very soon after the establishment of QCD as a SU(3) gauge field theory, called lattice quantum chromodynamics (lQCD), allows to perform non-perturbative calculations [77]. It consists of discretising the field theory on a lattice in Euclidean space-time, where quarks and antiquarks are on sites of the lattice and edges represent the colour field. The main limitations of lQCD are of course its non-dynamical nature, the related assumption of thermal equilibrium, and the fact that the lattice spacing has to be extrapolated to the continuum to render physical results, which requires huge computing resources [14]. Even though this formulation of QCD is non-covariant due to the space-time discretisation, it opened the gate for predictions of low-energy processes, and made confinement of quarks appear naturally as a first successful application. It allowed since to predict the masses of several hadrons [78], of bare quark masses [79, 80] or to study the behaviour of quarkonia (mesons made up of the same heavy flavoured $q\bar{q}$ pair) in medium [81]. In the study of the phase diagram of nuclear matter, lQCD is also widely used, as will be discussed in chapter 2. In particular, it can be used to calculate susceptibilities, which are directly related to the cumulants of conserved charges, the observables at the heart of the study exposed in chapter 5.

However, none of the two previous QCD-based methods enables to make prediction about the dynamical process of hadronisation occurring in high-energy collisions, which has not been proven analytically so far. Following the concept of confinement and the fact that the potential of the strong interaction increases linearly with distance, as proven in [77], phenomenological approaches were developed to treat such important question. One of them in particular, the string model, based on $q\bar{q}$ pair creation when strong interaction potential energy increases (also called vacuum fragmentation), will be presented in subsection 3.3.4.

CHAPTER 2

THE HOTTEST MATTER OF THE UNIVERSE

Contents

2.1	On a theoretical level: from first predictions to current models	22
2.1.1	The theoretical genesis behind the discovery of the QGP	22
2.1.2	The phase diagram of nuclear matter	25
2.2	Studying the QGP at the experimental level	27
2.2.1	Kinematics of high-energy collisions	27
2.2.2	The experimental apparatus	29
	The BES program at RHIC	29
	Heavy-ions at CERN	31
	Future facilities	32
2.2.3	Methods to study the QGP	32
	Soft probes	32
	Hard probes	34
2.3	Focus on: criticality in the nuclear phase diagram	34
2.3.1	Thermodynamic susceptibilities and net-charge cumulants	35
2.3.2	Limits and shortcomings of experimental and theoretical observables	39
2.3.3	STAR results & enhanced proxies for 2 nd order cumulants	41
	Variances and covariances of net- Q , net- p and net- K multiplicity distributions	41
	New proxies for the ratios of 2 nd order susceptibilities	44

While chapter 1 was devoted to depict the main background of my work, this second chapter will focus on the field it addresses in particular: the study of the quark-gluon plasma (QGP). This extremely hot and dense form of matter is expected to have composed our Universe around a microsecond after the Big-Bang [82, 83]. In order to learn more about its properties, we can produce it in heavy-ion collisions (HICs), recreating for very short time lapses the behaviour of the early expanding Universe [84].

In the following section 2.1, I will thus present the theoretical knowledge developed around the QGP, through another few paragraphs of history. This will lead me to introduce the phase diagram of nuclear matter, whose study combines both QCD and statistical physics, leading since recent years to even make a link with neutron star studies [85]. I will then move on to the experimental side in section 2.2, where I will introduce some basic kinematics variables used to study particle production in heavy-ion collisions (HICs), some of which being compared in the first part of chapter 5 to the results of simulations from EPOS. This event generator, designed to bridge the gap between theory and experiment in the study of QGP in HICs, will be presented in detail later on in chapter 3. Thereupon, I will portray some of the past, current and future experimental programs dedicated to HICs, and describe shortly the experiments from which results will be shown in this thesis. I will end up this section by mentioning several soft and hard key observables studied to display signatures, or extract properties of the QGP. At last, in order to contextualise the major study that I have led, exposed in chapter 5, section 2.3 will deal with the search for a critical endpoint in the phase diagram of nuclear matter. I will introduce the susceptibilities of conserved charges, theoretical tools used to probe the criticality, and their experimental counterparts, the moments of net-particle multiplicity distributions. Notably, I will focus on their 2nd order cumulants and their ratios, and relate the limitations and mismatches between these homologues. I will eventually discuss the results of the two publications on which my study is based. I will take this opportunity to start drawing the lines of my strategy to make a connection between theoretical developments and experimental measurements, preparing the ground for the list of my objectives exposed in section 3.5.

2.1 On a theoretical level: from first predictions to current models

This first section will shed light on the motivations that lead to investigate the new form of matter created in HICs. I will notably discuss the underlying thermodynamics via the study of the phase diagram of hadronic matter, and highlight the part of interest for this thesis, *i.e.* the prediction of a 1st order phase transition and a critical endpoint (CEP) between hadronic gas and QGP.

2.1.1 The theoretical genesis behind the discovery of the QGP

During, and even before the tales told about QCD in subsection 1.2.1 happened, some physicists were already working on phenomenological models to describe the behaviour of hadronic matter. A pioneering work has notably been achieved by Rolf Hagedorn, who introduced his so-called Statistical Bootstrap Model (SBM) in 1965, based on statistical physics considerations [86]. The main conjecture was that all heavy hadronic resonances are composed of lighter resonances, themselves composed of lighter resonances... and so forth until the lightest possible hadrons (*e.g.* pions), like Matryoshka dolls. Hence, pouring energy into such a system will lead to create new light hadrons, forming thus an even heavier resonance, rather than increasing the kinetic energy of the pre-existent

particles. As the temperature of a medium is precisely related to the motion, or mean kinetic energy, of its constituents, this idea led naturally to the concept of a maximum possible temperature for hadronic matter, the Hagedorn temperature $T_H \approx 158$ MeV. The SBM predicted thus an exponentially rising slope for the cumulative mass spectrum of hadron resonances, which is related to the decreasing exponential slope of particle's momentum spectra [87]. Indeed, as they originate from the decay of heavier resonances, the underlying mechanism is the same that led to form those heavy resonances from lighter ones [88]. It is worth noticing, nevertheless, that a precursor work in that sense had already been published in 1951 by Isaac Pomeranchuk (the same man who helped at developing the S -matrix theory and inspired the name of the Pomeron, both discussed later in section 3.3). He postulated that, if one assumes that pions have a finite size, they could not exist beyond a certain critical density. When considering an ideal gas of pions with a radius of 1fm, it would result in a similar maximum temperature of the order of T_H [89]. However, such an hypothesis was not given credit, as it was commonly agreed that pions were point-like particles, at such early times before the idea of hadrons as composite particles emerged [90].

Taking back the history where I left it in the end of subsection 1.2.1, the quark model has been eventually widely accepted by physicists once fitted in a rigorous theoretical formulation of QCD. Just after the completion of the theory, Tsung-Dao Lee and Gian-Carlo Wick suggested in 1974 that there might exist a new state of strongly interacting matter made of a continuum of quarks, antiquarks and gluons [91]. They have been followed by some other authors, among which John Collins and Malcolm Perry who went further with the concept of a quark matter phase at the beginning of the Universe [82]. A lot of discussions were then triggered about how to study such state of matter, and the idea of using relativistic HICs appeared naturally, with the experiments already ongoing at the Bevalac of the *Lawrence Berkeley National Laboratory* (LBNL) and at the CERN *Intersecting Storage Rings* (ISR) [92–95]. In the meantime, the theoretical developments on the modeling of HICs kept going on. Eventually, Hagedorn realised that the T_H of his SBM could in fact be re-interpreted as a transition temperature between hadron gas and QGP phases, when considering hadrons with finite volume and composed of quarks [96]. Some approaches pretty similar to the SBM, predicting an exponential slope of hadrons based on transition temperature, and integrating the notions of quarks and gluons as elementary constituents of matter, had also been developed in parallel [97, 98].

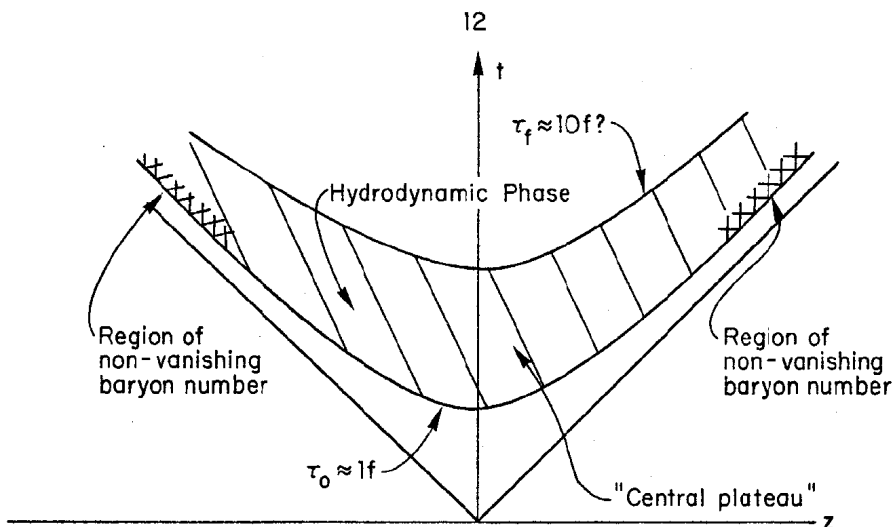


Figure 2.1: Description of the evolution of the system created in HICs, in a space-time diagram, following the Björken scenario. The t and z coordinates are in Euclidean space-time, while the $\tau = \sqrt{t^2 - z^2}$ is in Milne coordinate [99].

James Björken proposed, in 1983, a scenario to describe the expected space-time evolution of a symmetric system in HICs at ultra-relativistic energies [99]. Based on some experimental results of that time, he depicted that the system should quickly reach thermal equilibrium, due to the high energy density and temperature (≥ 200 MeV) reached at the beginning of the collision. After undergoing a phase transition to a quark-gluon plasma, the system can be described as a fluid, expanding following the longitudinal collision axis (usually denoted z) but also then radially, using hydrodynamic equations. The entropy density decreases there as t^{-1} , implying that it remains constant per rapidity unit¹ in the central region, which will result into a constant particle production per rapidity unit in the final-state. In this same central region, the net-baryon number is supposed to be null, as its initial value is carried by the remnants of the colliding nuclei, located at high forward and backward rapidities. After around a dozen of fm/c units of time ($\sim 10^{-22}$ s), the system temperature has decreased due to its expansion, leading to another transition from QGP to hadron gas (referred to as hadronisation). This description, sketched in figure 2.1, has now become a basis for the standard picture in the phenomenology of HICs, as we will see in subsection 3.1.2. Following this idea, one can see some similarities between HICs and the early epochs of the Big-Bang: a quickly expanding system, cooling down from very hot and dense matter to dilute small clusters, in which initial anisotropies are inscribed in final-state observables through a chemical freeze-out [84]. Even though the size and time magnitudes involved are very different, as well as the theoretical framework used to describe each of these two processes (general relativity against strong and electromagnetic interactions), it is common to call HICs as "Little Bangs".

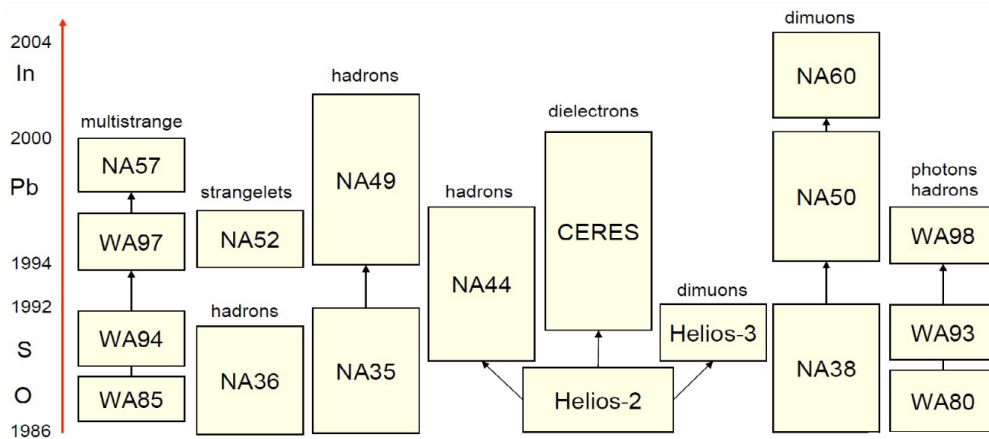


Figure 2.2: Timeline of the different experiments which took place at the CERN *Super Proton Synchrotron* (SPS), with the different ion beams used to collide on various targets, with the main topics of interest specified on top of the corresponding boxes [100].

Under the impulsion of a community motivated by the hunt of this QGP, new programs dedicated to ever more energetic ion beams were proposed in the early 1980's [101]. New experiments were thus proposed at the CERN SPS [102, 103], while it was even decided to build a new accelerator at *Brookhaven National Laboratory* (BNL), the RHIC [104]. Finally, the accumulation of different results from the SPS experiments shed light on the evidence that QGP droplets had been formed in collisions involving lead ions at CERN [105]. The list of experiments involved in the HIC program at SPS, which led to this discovery, are shown in figure 2.2. The year of this announcement, in 2000, the RHIC started its operation which led to the confirmation, 5 years later, of the formation

¹Space-time rapidity, defined as $\varsigma = \frac{1}{2} \ln [(t+z)/(t-z)]$

of this new state of matter in higher-energy Au-Au collisions [106–109], although the formal confirmation came in 2010 in [110]. Some details about the involved experiments, colliders and physical signatures leading to this conclusion will be provided in section 2.2.

2.1.2 The phase diagram of nuclear matter

Nowadays, two decades have passed since the discovery of the deconfined state of nuclear matter. The center of the related research is of course to learn more about its behaviour and properties of this new form of matter. In particular, physicists are interested in mapping the phase diagram of nuclear matter, which displays the relation between thermodynamic quantities of the system in a thermal equilibrium. For the case of matter described by QCD, it is usual to represent this phase diagram as a function of the temperature T , and of the baryonic chemical potential μ_B , which quantifies the imbalance between matter and antimatter (quarks and antiquarks in this case). Such phase diagram can be seen in figure 2.3, where the $(0, 0)$ coordinates describe vacuum. Standard nuclear matter as we know it is located at $T \approx 0$ MeV and $\mu_B \approx 935$ MeV, which simply corresponds to the rest mass of a nucleon that represents a surplus of matter over antimatter. In addition, we know that in the low T/μ_B region, quarks are confined into hadrons so we talk about a hadron gas phase, while at high T and/or high μ_B , we expect to see them in the QGP phase (discussed in the previous subsection). But where is, or are, the phase transition(s), and what are their nature ?

In order to answer this question, one needs to determine the equation of state (EoS) of nuclear matter, an equation which relates at least two thermodynamic variables of the system, and from which can be derived all the other quantities. However, because of the difficulties discussed in subsection 1.2.2, it is impossible to establish a complete (T, μ_B) map from the pure QCD theory. In the early 1980's, the phase transition was first thought to be of 1st order [87]. Such phase transition implies discontinuities in the densities of some conserved thermodynamics quantities, meaning that the system changes in a discontinuous way and experiences a heterogeneous coexistence of two phases, like the liquid/gas transition (or boiling) of water [111]. However, the Statistical Bootstrap Model for instance, as already introduced, could not give any clue on its true nature, as the model diverges at the transition temperature T_H . Moreover, applying the description of an ideal quantum Fermi gas to quarks and gluons was not possible either around this temperature. Following a naive train of thoughts: by using Fermi-Dirac statistical distribution to describe such a system [111], partons would have a mean energy of $\langle \varepsilon \rangle \approx 0.02$ GeV at T_H . This would roughly correspond, for collisions caused by thermal agitation, to a typical $Q^2 \sim 0.04$ GeV involved, and thus still a very high coupling (looking at figure 1.3). This makes clearly impossible, around these temperatures, the use of such formalism which is supposed to describe a gas of weakly interacting particles.

Nevertheless, some first-principle-based models predicted a 1st order phase transition at finite μ_B and low T , some of them even hinting for the existence a 2nd order phase transition at higher T , separated by a critical point [112, 113]. On the other side, a major step was taken when first calculations from lQCD indicated a crossover (so not a real phase transition) at zero μ_B , when considering u, d and s quarks with their physical masses [114]. This means that the change from hadron gas phase to a QGP phase happens, although quite rapidly, in a continuous way and homogeneously. This seems to be confirmed by experimental data from LHC so far [115]. The most up-to-date lQCD results for the crossover transition temperature predicts $T_c = 158 \pm 0.6$ MeV [116], in remarkable agreement with the predicted Hagedorn temperature T_H .

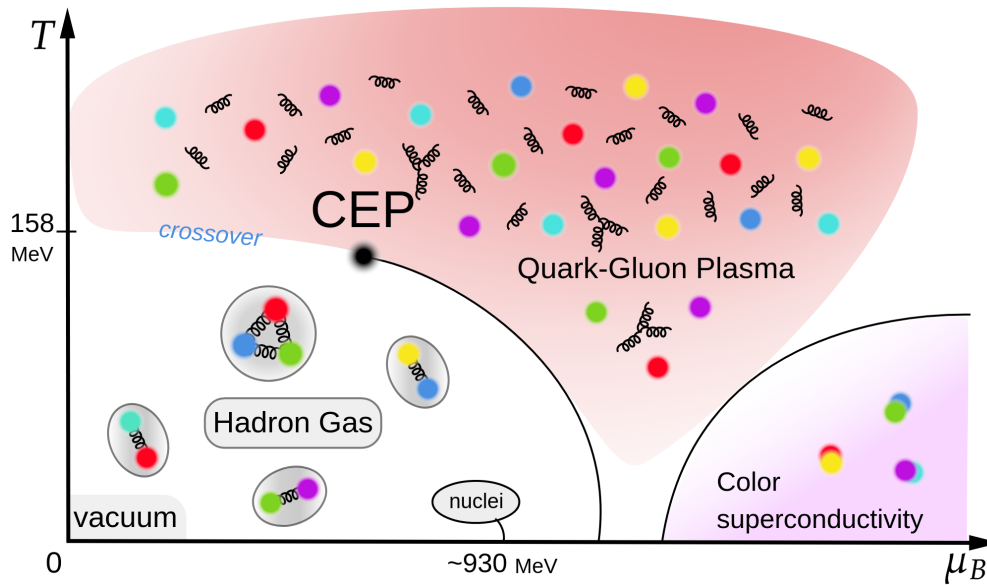


Figure 2.3: The semi-hypothetical phase diagram of nuclear matter sketched as a function of temperature T and baryonic chemical potential μ_B . Exact position of phase transitions and critical point are approximate, just displayed to illustrate roughly the main structures [117].

Putting everything together, we know that the transition from hadron gas to QGP happens via a crossover at low baryonic density thanks to lQCD, and numerous models indicate the existence of a 1st order transition at $T = 0$ and finite μ_B . This tends to indicate the existence of a 2nd order CEP somewhere in the phase diagram, as indicated in figure 2.3. The search for the location of this CEP has become a major objective today, and many other approaches have been used since to predict its location, such as the Dyson-Schwinger equation [118], the PNJL model [119] or the functional renormalisation group method [120]. Simulations with lQCD could not initially provide any prediction at $\mu_B > 0$ because of the sign problem, a numerical issue appearing when integrating complex exponential functions, encountered when running Monte Carlo (MC) simulations to evaluate path integrals for fermionic systems at finite density [121]. Despite these difficulties, a lot of progress in the last decade have brought several methods to extend the predictive power of lQCD to finite density, using for instance analytic continuation from imaginary μ [122] or Taylor expansions [123]. While it is still impossible to predict any CEP with such methods, they can at least indicate curvature of the crossover transition in the low μ_B region. This search for the CEP is a major goal of the BES program, presented in subsection 2.2.2, and a specific motivation for the work I will present in chapter 5. The objectives of this work will be exposed at the end of chapter 3 after having introduced the tool to achieve it, and the specific observables studied, discussed in section 2.3.

The last region of the phase diagram not discussed so far is the region of cold and dense nuclear matter, at high μ_B and low T , found in neutron stars [124]. There, a 1st order phase transition has been predicted, leading to a phase of so-called colour superconductivity [125, 126]. This state, analogous to the electrical superconductivity but for the colour charge, is notably expected to be present in the core of neutron stars. There has been a revival of interest in this area lately, thanks to the detection of gravitational waves from a binary neutron star merger [127]. It opened the gate to infer the properties of the nuclear matter composing them, and to identify a 1st order hadron to quark phase transition [128], confirming the existence of quark matter in their core

[129]. Since, numerous studies are intending to explore this region of the phase diagram using information obtained from neutron star mergers and astrophysical observations, completing little by little the great puzzle of the QCD phase diagram [130–132]. In a recent study, a connection has even been made between neutron star mergers and HICs, by simulating both of them using relativistic hydrodynamics with a single EoS [133]. It shows that the dynamics of neutron star mergers can be studied via HICs performed at $\sqrt{s_{NN}} \approx 0.5$ GeV. In that respect, it builds a bridge with HICs, and adds a new motivation to study them in the laboratory.

2.2 Studying the QGP at the experimental level

Before coming back to the study of the QCD phase diagram in section 2.3, I will review the experimental side of the study of the QGP in the present section, beginning with the definitions of basic kinematic variables which will be useful afterward. I will then present the main experimental apparatus (colliders and detectors) used to perform and analyse HICs, focusing especially on the ones whose measurements will be compared to the results of EPOS simulations in chapter 5. I will end up with a discussion of the observables used to probe the existence of the QGP and to evaluate its properties.

2.2.1 Kinematics of high-energy collisions

Primordial kinematics variables used in hadronic collisions are, in any reaction of the type $X_1 + X_2 \rightarrow Y_1 + Y_2$, the Mandelstam variables:

$$s = (P_{X_1} + P_{X_2})^2 = (P_{Y_1} + P_{Y_2})^2, \quad (2.2.1)$$

$$t = (P_{X_1} - P_{Y_1})^2 = (P_{X_2} - P_{Y_2})^2, \quad (2.2.2)$$

with P the 4-momentum vectors of the corresponding particles here [134]. As can be seen from the formula, \sqrt{t} represents the energy transfer for an elastic collision, while \sqrt{s} is the center-of-mass energy for an inelastic collision. When dealing with HICs, it is also usual to talk about the center-of-mass energy in a nucleon pair frame, either by indicating $\sqrt{s_{NN}}$ or by using the GeV/A unity as $\sqrt{s_{NN}} = \sqrt{s}/A$.

When characterising the spatial parameters of particles produced in a collision, the common reference frame takes its origin at the interaction point, with the z axis defined as the beam axis, also called longitudinal axis. Hence, one usually calls transverse plane the (x, y) plane, which leads to define the transverse momentum $p_T = \sqrt{p_x^2 + p_y^2}$, and by extension the longitudinal momentum $p_L = p_z$. In order to study the spatial distribution of particles, one can use the momentum rapidity y which measures the relativistic velocity of a particle with respect to the frame of observation, *i.e.* the laboratory. However, the pseudorapidity η is generally simpler to handle in the experiment, because it is defined as a function of the angle relative to the beam axis, θ . The advantages of such variable are that it can be easily defined geometrically, without having to know the mass of the particle considered, and that it tends towards y as the particle's speed tends to the speed of light:

$$\eta = -\ln\left(\tan\frac{\theta}{2}\right) = \frac{1}{2}\ln\left(\frac{|\vec{p}| + p_z}{|\vec{p}| - p_z}\right) \xrightarrow{\beta \rightarrow 1} y = \frac{1}{2}\ln\left(\frac{E + p_z}{E - p_z}\right). \quad (2.2.3)$$

Both variables are null for $\theta = 90^\circ$, in other words when the considered particle goes only in the transverse direction, and tend to infinity when the particles gets closer to the beam axis [14].

Another extremely important notion, when dealing with HICs, is the centrality. Because heavy-ions have an important transverse dimension compared to protons, the total energy involved in inelastic interactions will vary, depending on how much centrally they collide with each other, or how much of their nucleons have interacted. Thus, the number of particles produced (the so-called multiplicity) will not be the same for head-on collisions, referred to as central collisions, compared to the peripheral ones, when only a small fraction of each ion is involved. However, it is not possible experimentally to infer directly the value of the impact parameter b of a collision, which gives the geometry of the collision. One assumes then that the produced particle multiplicity, detected whether at mid or forward rapidity, is proportional to the number of participants of the collision, and by extension to b [135]. Hence, to determine the centrality, experiments exploit the distribution of inelastic cross-section as a function of the charged particles multiplicity (or any related detector parameter), measured in a specific kinematic region. For instance, STAR generally uses the charged multiplicity within $|\eta| < 0.5$ in all azimuths [136], while ALICE uses the charged multiplicity distribution in forward ($2.8 < \eta < 5.1$) and backward ($-3.7 < \eta < -1.7$) pseudorapidity regions [137]. Once obtained, this distribution of events is divided into several centrality groups, as a function of the size of integrated areas under the curve, as shown in figure 2.4. The events contained in the highest 0-5% multiplicity part of the distribution are indeed the most central events, and the higher the percentage of the class, the more peripheral are the events, by convention.

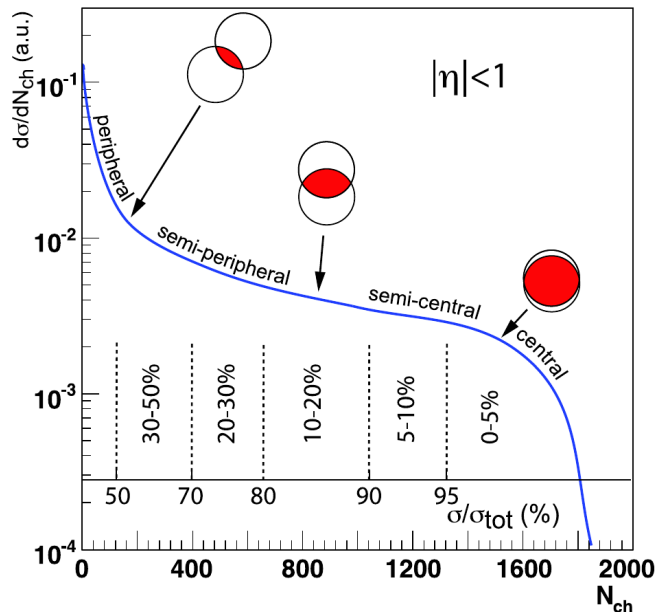


Figure 2.4: Distribution of the total inelastic cross-section as a function of the number of charged particles N_{ch} produced by a collision within the $|\eta| < 1$ region. A correspondence with the integrated percentage of the total cross-section, used to determine the centrality percentage, is added. Values used on both axes are arbitrary and purely indicative [138].

Then, one can use the Monte Carlo Glauber model, based on a quantum mechanical approach of diffraction [139], to evaluate simple geometrical quantities of the collisions. By simulating collisions with this simple model, one can reproduce the differential distribution of the cross-section cited earlier, and evaluate for each centrality class the corresponding mean values of impact parameter $\langle b \rangle$, number of participants $\langle N_{part} \rangle$ or number of nucleon-nucleon collisions $\langle N_{coll} \rangle$ [138]. However, it is only suitable to study such simple parameters related to the early stages of a collision, and not really relevant for looking at particle production.

2.2.2 The experimental apparatus

In this subsection are briefly reviewed the different facilities currently used to accelerate heavy ions at relativistic energies, as well as the different experiments studying the collisions of those heavy-ion beams. The emphasis will be put on the RHIC and the *Beam Energy Scan* (BES) program carried out there, of which the work presented in chapter 5 is a part. It will be followed by a quick presentation of the CERN complex and engagement in the exploration of the QCD phase diagram, and by few information provided on the future planned accelerators for heavy ions.

The BES program at RHIC

The *Relativistic Heavy Ion Collider* (RHIC), the second most powerful particle accelerator in the world after the LHC (discussed afterwards), has been operating since 2000. It is part of the BNL, located in the hamlet of Upton in Long Island, New York (USA). As the last part of an accelerating complex, it is composed of two storage rings of 3.83 km intersecting at 6 different interaction points, using superconducting magnets to both focus and deflect the beams [140]. A total of four experiments have taken place in some of the RHIC interacting points, from which data will be shown in the last chapters of the thesis. All of them were conceived with the same global objective to make a general study of the collisions in which the creation of QGP was expected, but each of them with a specific design proper to their specific physics goal, taking into account the cost limitations.

The smallest experiment, *Broad RAnge Hadron Magnetic Spectrometers* (BRAHMS), was conducted from 2000 to 2006. It was composed of two spectrometers at forward and mid rapidity, complementary and versatile, covering a rapidity range of $0 < y \lesssim 4$ with a limited azimuthal angular acceptance, and a p_T range from ~ 0 to ~ 25 GeV for π , K and p hadrons. The two main parts of the BRAHMS experiment were completed with three other sub-detectors, among which two *Zero Degree Calorimeters* (ZDCs) common to all experiments at RHIC [141]. These three additional detectors were used to characterise general properties of recorded collisions, such as luminosity, charged multiplicity and centrality [142]. The PHOBOS experiment, which took data from 2000 to 2005, offered a full azimuthal coverage for a pseudorapidity range of $|\eta| < 5.4$ with its multiplicity array. It had the particularity to get along with 2 forward spectrometers covering $0 \leq \eta \leq 2$ and only 10° of azimuthal angle (opposite to each other), dedicated to particle identification at $0.03 < p_T \leq 1$ GeV with an excellent resolution. One of the spectrometer arms was completed by time-of-flight detector, to extend the p_T range for particle identification [143].

The second most important experiment, by the size of the collaboration involved and its data-taking duration, is the *Pioneering High Energy Nuclear Interaction eXperiment* (PHENIX). It is made of two central multilayer detector arms, with a typical structure of a multi-purpose experiment dedicated to hadronic physics, involving many detector with different applications [144]. Because of the peculiar structure of the central magnet, each of the two central arms cover only 90° azimuthal angle, with a very limited rapidity acceptance of $|y| < 0.35$. Along the beam axis, and perpendicular to it, are located two muon spectrometer, one on each side of the interaction point, covering $-2.2 < \eta < -1.1$ and $1.1 < \eta < 2.4$ respectively. Decommissioned since 2016, PHENIX has cleared the way for its successor: the sPHENIX experiment. It will inherit from the cylindrical superconducting magnetic solenoid of the BaBar experiment, enabling a full 2π azimuthal coverage and an improved pseudorapidity coverage of $|\eta| < 1$ [145].

The *Solenoidal Tracker At RHIC* (STAR) is finally the most complete RHIC experiment, with the largest collaboration, and is the only one still in operation since the first collisions achieved in the accelerator. Built as a multi-purpose experiment, it is also composed of a multilayer ensemble of detectors, and offers an excellent reconstruction and identification of charged particles in an acceptance of $|\eta| < 1$ and for $0.1 < p_T$ GeV. The pseudorapidity coverage is even larger for some of the sub-detectors, and it can especially be extended to the forward direction, to $2.5 < \eta < 4$, by using a dedicated forward time projection chamber [146].

The RHIC has been used to collide a wide variety of heavy nuclei, like ^{64}Cu [147] or ^{238}U [148] to cite just a few, but the ones which have been used the most often are ^{197}Au ions [149]. As the heaviest stable nuclei accelerated there, they have been the main protagonists of the BES program, started in 2010. This program, which consists of exploring the phase diagram of QCD by varying the collision energy, involves both STAR and PHENIX experiments (until the latter was stopped). The goals are to study the onset of deconfinement, by determining at which energy the signatures of QGP formation appear, to search for the predicted 1st order phase transition and CEP, and for the chiral symmetry restoration [150].

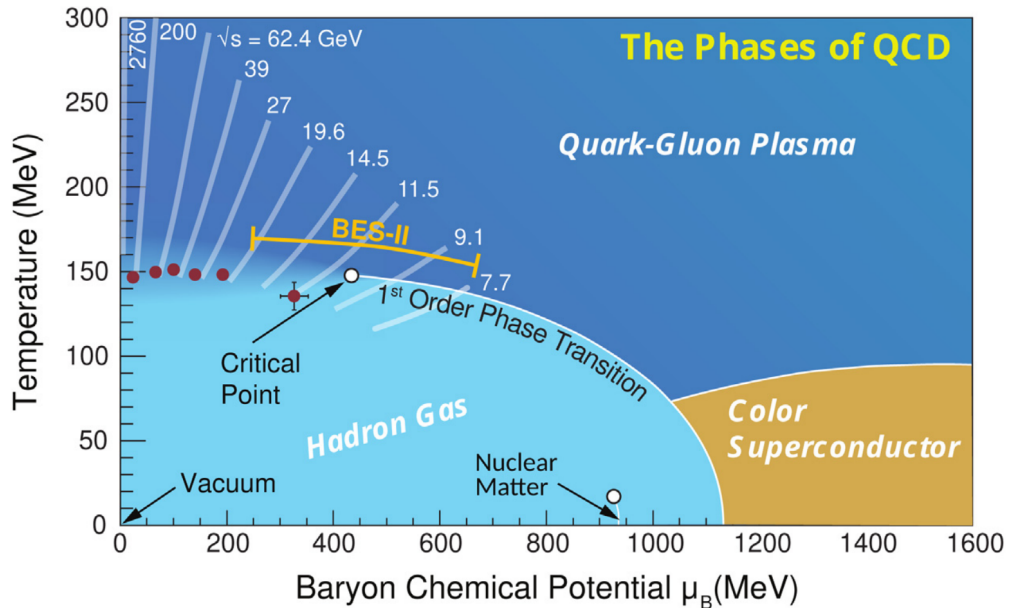


Figure 2.5: Phase diagram of nuclear matter, with representations of the trajectories described by several collisions systems of the BES program.

Positions of phase transitions and critical point are purely illustrative [151].

To do so, Au-Au collisions have been performed at $\sqrt{s_{NN}} = 7.7, 11.5, 14.5, 19.6, 27, 39, 54.4, 62.4$ and 200 GeV in the first phase of the program. The systems thus created are supposed to span a range $25 \lesssim \mu_B \lesssim 420$ MeV, as decreasing the beam energy increases the baryon chemical potential [151]. In a second phase, named BES-II, the effort have been focused on the lowest beam energies (< 20 GeV/A), as numerous results point out intriguing behaviours of the system created in such collisions [151]. Figure 2.5 illustrates the scan of the phase diagram made possible by the BES program, in a schematic fashion. The red dots indicate values of freeze-out parameters extracted from Au-Au collisions data at the corresponding energy. To extend even further this prospection, fixed-target Au-Au collisions were achieved down to 3.0 GeV/A in the last few years, by the STAR experiment, in order to better characterise the onset of deconfinement [152].

One of the main results of the HICs achieved at RHIC, is the observation that the QGP droplets behave like an almost-perfect fluid which is, in fact, strongly coupled, although this statement might sound counter-intuitive as quarks and partons are deconfined in this state of matter [151]. This can be understood pretty well when considering the simple arguments exposed previously in subsection 2.1.2, about the typical value of the coupling constant for thermal interactions of partons around the transition temperature. When looking at figure 2.5, one clearly sees that for most of the systems created at RHIC energies, the temperature reached is too low to attain a small enough coupling needed to obtain a gas of quarks and gluons which is weakly interacting. Another important signal of the BES results so far, is the fact that several studied observables show a non-monotonic behaviour below $\sqrt{s_{NN}} \sim 20$ GeV. This could hint that some important changes in the EoS of nuclear matter happen in the created system, which may be caused by the existence of the long-sought 1st order transition and CEP [151].

Heavy-ions at CERN

Although the work presented in this thesis focuses on the BES program, it must be mentioned that CERN is also well involved in the study of HICs. At low beam energies, the NA61/*SPS Heavy Ion and Neutrino Experiment* (SHINE) has taken over the NA49 experiment [153], which was involved in the discovery of the onset of deconfinement at SPS, discussed by the end of subsection 2.1.1 [154]. Among the different guidelines of the SHINE physics program, an energy scan is achieved, to search for the predicted 1st order phase transition and CEP, and the onset of deconfinement [155]. To do so, the SHINE collaborations measures the spectra of many hadronic species, in fixed-target collisions involving protons and several ions like ^8Be , ^{40}Ar , ^{45}Sc , ^{129}Xe , ^{139}La or ^{208}Pb , in an center-of-mass energy range of $\sqrt{s_{NN}} \approx 5$ to 17.3 GeV [156]. In this way, the research conducted by this collaboration is complementary to the BES program.

The study of QGP at CERN is also achieved at very high energy, thanks to the most powerful accelerator ever built, the *Large Hadron Collider* (LHC). With a length of 26.7km, this ring uses the SPS as an injector, to accelerate protons up to a recent record energy of 6.8 TeV, thus producing collisions at $\sqrt{s} = 13.6$ TeV [157]. Despite of dedicating most of its beam time to proton's physics, the LHC also accelerates heavy ions such as ^{129}Xe at 2.72 TeV/A [158, 159], or ^{208}Pb up to 2.51 TeV/A [160, 161], reaching hence energies greater than the PeV for Pb-Pb collisions. The LHC recreates in this way the closest conditions possible to the early stage of the Universe, reaching very high temperature at zero baryonic density, offering the perfect conditions to search for the origin of matter-antimatter asymmetry. It also allows to study the so-called cold nuclear matter effects in asymmetric systems, by performing *p-A* collisions [162]. A *Large Ion Collider Experiment* (ALICE) is the only experiment entirely dedicated to the study of heavy-ion collisions, thanks to a full azimuthal covering ensemble of detectors at mid-rapidity region (for $|\eta| < 1$), and a forward muon spectrometer (at $-4 < \eta < -2.4$) mainly designed to study quarkonia production [163]. Even though being principally focused on the physics of *p-p* collisions (*e.g.* measurements of SM parameters, jet production or search for new physics), A *Toroidal LHC Apparatus* (ATLAS) and *Compact Muon Solenoid* (CMS) experiments of the LHC also conduct heavy-ion programs [164, 165]. In addition, the last main experiment located along the gigantic accelerator, *Large Hadron Collider beauty* (LHCb), has just started its heavy-ion program with the recent beginning of the Run 3, thanks to a new device to perform collisions on gaseous targets [166].

Future facilities

To close this section on the experimental efforts deployed to study the QGP, a quick overview of the future facilities dedicated to heavy-ion study is done here. In a near future, the *Facility for Antiproton and Ion Research* (FAIR) is expected to start operating in 2025, at the GSI center in Darmstadt (GER) [167]. Delivering beams of protons, antiprotons and ions in the energy range of few GeV/A, it will allow exploring the very high μ_B region of the phase diagram of nuclear matter, as the main research purpose of the *Compact Baryonic Matter* (CBM) experiment [168]. Another facility intending to explore the high baryonic density region in the same period is the *Nuclotron-based Ion Collider fAcility* (NICA) [169], at JINR in Dubna (RUS). It should perform ^{197}Au beam collisions, covering a range of $4 \leq \sqrt{s_{NN}} \leq 11$ GeV in collider mode, with a *Multi-Purpose Detector* (MPD) dedicated to characterise the matter formed in such events [170]. A third project, supposed to start in the second half of 2020's decade at the *Japanese Proton Accelerator Research Complex* (J-PARC), is expected to probe the same region of the phase diagram. It is expected to accelerate heavy-ions up to ^{238}U in the GeV/A energy range [171]. In a more distant future, a successor to the LHC, named so far the *Future Circular Collider* (FCC), is planned to be built as a 100km collider ring [172]. Even though the question of the nature of particles accelerated by such collider has not been definitely resolved so far, it would allow to achieve Pb-Pb collisions at $\sqrt{s_{NN}} = 39.4$ TeV or p - p collisions at $\sqrt{s} = 100$ TeV, if conceived for such beams. For HICs, it represents eight times the current energies at LHC: such facility would then fulfil a mission opposite to the two previously discussed one, by exploring the extremely high T region of QCD phase diagram.

2.2.3 Methods to study the QGP

The last part of this section is devoted to introduce the most commonly studied observables, assimilated to be signatures of the formation of QGP, as well as observables used to extract its properties. They are based on different probes, which can be classified into two groups.

Soft probes

Soft probes generally refers to particles produced thermally at rather late stages of the collisions, with a $p_T < 2 \sim 3$ GeV by convention, which reflects via their formation the dynamics and properties of the QGP. As we are discussing a very hot bulk matter, the first straightforward probes to study are the photons. At low p_T , thermal photons are indeed expected to be created by the partonic interactions or thermal radiations either as real photons, or as virtual ones which materialise mainly via e^+e^- pairs [173, 174]. The measurement of such direct photons, which need to be identified clearly among the background majority of photons created by hadronic decays, gives access to the temperature of the matter from which they originate [175, 176].

The measurement of light hadrons spectrum (π^\pm , K^\pm and p/\bar{p}) allows in turn to get access to the kinetic and chemical freeze-out parameters such as T and μ_B [177]. Such procedure is achieved by fitting the p_T spectra, yields and ratios of the hadrons in question with different models. The chemical freeze-out is the moment at which the yields of all hadronic species are fixed: the related parameters can thus be extracted from statistical models based on the concept of the SBM [178], introduced in subsection 2.1.1. The kinetic freeze-out parameters, *i.e.* when all interactions between hadrons cease, can be extracted by using the so-called Blast Wave Model [179].

Another signature of the formation of the QGP is the strangeness enhancement, the fact that an overproduction of multi-strange (anti)baryons (Ξ^- , Ξ^+ , Ω^- , Ω^+) is expected when a QGP is created. This is due to an enhanced production of strange $q\bar{q}$ pairs via $q\bar{q} \rightarrow s\bar{s}$ and $gg \rightarrow s\bar{s}$ processes, energetically favoured in a hot thermalised medium compared to the creation of a strange hadrons pair in a hadron gas [180]. Even more importantly, one should observe a lower production of strange hadron species compared to their corresponding anti-hadron partner, due to phase-space considerations [181]. This effect has been one of the first key observable to be seen, and has been observed by all HIC-dedicated experiments [182–185], with an example displayed in figure 2.6. One clearly sees on this figure the rise of the $K^+(u\bar{s})/\pi^+(u\bar{d})$ ratio compared to the $K^-(s\bar{u})/\pi^-(d\bar{u})$ one at RHIC energies, illustrating the overpopulation of \bar{s} antiquarks compared to s quarks.

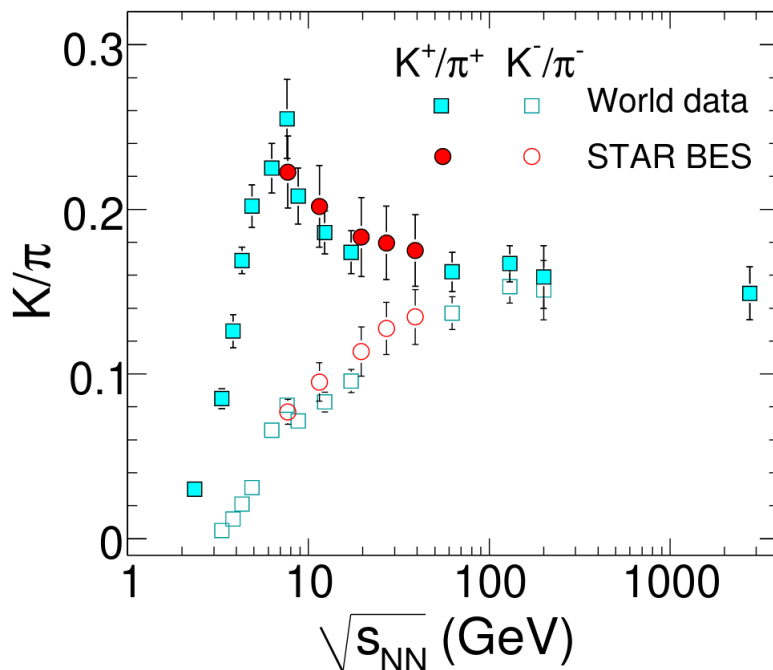


Figure 2.6: K/π ratios measured within $|y| < 1$ in 0-5% Au-Au collisions as a function of the collision energy [177].

Last but not least, an important observable to study the collective behaviour of matter created in HICs is the anisotropic flow. Because of the pressure gradient between the extremely hot matter created by the collision and the surrounding vacuum, the medium will expand and flow due to the multiple interactions between its constituents. The spatial asymmetries of the original geometry of the collision will then be transferred into a non-uniform azimuthal distribution of final-state particles in the momentum space [186, 187]. Anisotropic flow refers to the Fourier coefficient of the azimuthal distribution of momenta, denoted v_n , with n the order of the coefficient. Hence, v_2 is called for instance elliptic flow as it measures the elliptic asymmetries, v_3 is the triangular flow as it measures the triangular asymmetry, and so on. The magnitude of the flow provides information on the level of thermalisation of the medium created, and comparing the flow harmonics measurements with simulations of viscous hydrodynamics enables to better constrain the EoS of nuclear matter. Consequently, flow coefficients have been extensively studied since the QGP have been first observed (see for example [188, 189]). It has notably allowed to determine that QGP is the most perfect fluid ever observed, with the lowest shear viscosity over entropy ratio ever measured of the order of $\eta/s \sim 0.1$ [190].

Hard probes

The hard probes, resulting from hard scatterings happening at the early stages of the collisions, carry usually a large energy as a consequence. The jets are a perfect definition of a hard probes, being collimated cones of hadrons coming from the fragmentation of a high- p_T parton (with a p_T superior to several GeV) produced in a hard scattering. As the partons initiating the jets, are created at the very beginning of the collision, they will endure the full evolution of the medium. In particular, in the case of QGP formation, the partons will lose energy through elastic collisions and medium-induced gluon radiation which will result in a less important and/or energetic hadron shower: this is the so-called jet quenching [191]. Because the creation of a hard parton pair can happen anywhere, it is usual that one among the two partons has to travel a larger distance through the medium than the other, and thus lose more energy, leading to asymmetric dijet emissions. This is experimentally visible via the unbalance of high- p_T dihadron azimuthal correlation, or simply by the suppression of high- p_T hadrons when compared to scaled p - p collisions [192]. The effects of jet quenching has been observed both at RHIC [193, 194] and LHC [195, 196]. Moreover, jet quenching can be exploited to extract properties of the medium, such as the gluon density or the transport coefficient \hat{q} , which characterises the mean energy loss per unit length when travelling through the medium [192].

Heavy quarks are also very good hard probes of the QGP, as they can only be created via the initial hard scatterings. In particular, quarkonia (unflavoured mesons made of $c\bar{c}$ or $b\bar{b}$ pairs, like J/Ψ or Υ for instance) are studied because, when travelling through the deconfined medium, they can be dissociated due to colour screening. This process, called quarkonia suppression, is thus expected to indicate without any ambiguity the presence of QGP, by comparing their yields from HICs with scaled p - p collisions [197]. Quarkonia turn out to then be usable as a thermometer of the hot medium in which it evolves, as knowing their binding energies enables an estimation of the temperature reached by the QGP when looking at their sequential suppression. However, some effects of recombination are also possible at LHC energies, as heavy quarks pairs initially produced incoherently can bind to each other while roaming through the medium [198, 199]. Quarkonia suppression has therefore been observed at RHIC [200] and LHC [201], but less pronounced in the latter case. Although having discussed solely quarkonia physics, the study of heavy flavours in general is of interest as heavy quarks can, like jets, provide information on the transport properties of the QGP [202].

Finally, questioning results about the aforementioned signatures of the QGP in small systems should be addressed. Since a decade, analyses of high-multiplicity events for p - p and p -Pb collisions at LHC unveil trends such as strangeness enhancement of angular correlations, which are commonly interpreted as signatures of collective behaviour of the system [203–206]. Claiming that QGP is formed in such systems could be too premature, as understanding the processes leading to these measurements is still under investigation, requiring a reconsideration of many concepts that were thought to be clearly established.

2.3 Focus on: criticality in the nuclear phase diagram

Beyond learning about its very own properties, one of the important aspects of the study of QGP lies in the knowledge of the conditions in which it is formed. As already explained in subsection 2.1.2, an important effort of today’s research is devoted to searching for the predicted 1st order phase transition and the associated CEP. It is the heart of the *Beam Energy Scan* program, introduced in the subsection 2.2.2, and the motivation for the main study of this thesis. But how would the existence of a critical point manifest

itself? What kind of observables could be used to search for its existence?

The CEP marks the separation between the 1st order phase transition, where both hadronic and QGP phases coexist, and the crossover transition where the whole system is under the same phase. Hence the correlation length of the system, representing the typical length for which the elements of the system are correlated (or, in other words, in a homogeneous state), diverges at that point. As the event-by-event fluctuations of conserved charges, measured via the cumulants of net-charge multiplicity distribution, are related to the correlation length, it has been suggested that they could serve as a good probe for the existence of the CEP [207–209]. The thermodynamic susceptibilities, linked to these two variables, are also used as they can be calculated in the frame of lQCD [210]. The first part of this section will then be dedicated to the introduction of those quantities. During the past few years, many measurements of proxies for the aforementioned cumulants have been made [211–215], some of those results being part of the clues hinting for the interesting physics happening in HICs below 20 GeV/A (as mentioned in subsection 2.2.2). But those observables are also subjects to shortcomings, in their relation with their thermodynamic counterparts as well as in their experimental evaluation ; I will expose these flaws in the second part of this section. It is extremely important to ascertain and understand properly the difference between these observables and the theoretical variables to which they are related. Therefore, I will present, in the last part of the section, some results from STAR on the experimental cumulants used as proxies, and a theoretical study which resulted into proposing the use of "enhanced" proxies to measure fluctuations of the conserved charges in the experiment. I will explain how this conclusion motivated my work, which goals will be outlined later on in section 3.5.

2.3.1 Thermodynamic susceptibilities and net-charge cumulants

The theoretical quantities widely used nowadays to study criticality in the phase diagram with lQCD are the so-called thermodynamic susceptibilities. In order to introduce them, let's start with basic notions of statistical physics.

The grand-canonical (GC) ensemble, used to describe the systems simulated in lQCD, gives a description of the states of a system in thermodynamic equilibrium with a reservoir, with which it can exchange energy and particles. Such an ensemble is characterised by its temperature T , its volume V and one or several chemical potential(s) μ . The partition function of the system contains the information on how the probabilities to find the system in a given microstate are distributed, a microstate being a specific microscopic configuration of the system. It is expressed in the GC (or macrocanonical) ensemble, for the simplified case of a single particle specie, as:

$$\mathcal{Z}(T, V, \mu) = \sum_i e^{-\beta(E_i - \mu N_i)} , \quad (2.3.1)$$

with i a given microstate, E_i its energy, N_i the number of particles which compose it and $\beta = 1/k_B T$ [111]. It defines the grand-potential Φ_G , which is the generator function of the GC ensemble, via the relation:

$$\Phi_G = -k_B T \times \ln(\mathcal{Z}(T, V, \mu)) . \quad (2.3.2)$$

One can then obtain the pressure via the derivation of this grand-potential with respect to the volume, at constant μ and T :

$$P(T, V, \mu) = - \left[\frac{\partial \Phi_G}{\partial V} \right]_{T, \mu} = \frac{T}{V} \ln(\mathcal{Z}(T, V, \mu)) \quad (2.3.3)$$

(note that from here, k_B is not explicitly written anymore and taken as 1, using natural units).

In the framework of phenomenology, one considers generally three chemical potentials for electric charge Q , baryonic number B and strangeness S , what leads to define the chemical potential vector $\vec{\mu} = (\mu_B, \mu_Q, \mu_S)$. The thermodynamic susceptibilities of the conserved charges (B, Q, S) are defined as the derivatives of the dimensionless pressure P/T^4 with respect to the chemical potentials of these charges [216]:

$$\chi_{ijk}^{BQS} = \frac{\partial^{i+j+k}(P/T^4)}{(\partial\hat{\mu}_B)^i(\partial\hat{\mu}_Q)^j(\partial\hat{\mu}_S)^k}, \quad (2.3.4)$$

with the reduced chemical potential $\hat{\mu}_X$ defined as $\hat{\mu}_X = \mu_X/T$. In this thesis I will only focus on the 2nd order susceptibilities, explicitly given, when using equation (2.3.4), by:

$$\chi_2^X = \frac{\partial^2(P/T^4)}{\partial\hat{\mu}_X^2}, \quad \chi_{11}^{XY} = \frac{\partial^2(P/T^4)}{\partial\hat{\mu}_X\partial\hat{\mu}_Y}, \quad (2.3.5)$$

with $X, Y = B, Q, S$. Otherwise known as diagonal and off-diagonal correlators respectively, the six corresponding quantities can easily be expressed as linear combinations of the quark number susceptibilities, which are the quantities directly accessible via IQCD [210]:

$$\begin{aligned} \chi_2^B &= \frac{1}{9}(2\chi_2^u + \chi_2^s + 4\chi_{11}^{us} + 2\chi_{11}^{ud}), & \chi_{11}^{BQ} &= \frac{1}{9}(\chi_2^u - \chi_2^s + \chi_{11}^{ud} - \chi_{11}^{us}), \\ \chi_2^Q &= \frac{1}{9}(5\chi_2^u + \chi_2^s - 4\chi_{11}^{ud} - 2\chi_{11}^{us}), & \chi_{11}^{BS} &= -\frac{1}{3}(\chi_2^s + 2\chi_{11}^{us}), \\ \chi_2^S &= \chi_2^s, & \chi_{11}^{QS} &= \frac{1}{3}(\chi_2^s - \chi_{11}^{us}). \end{aligned} \quad (2.3.6)$$

One can link these susceptibilities to the cumulants of net-charges, starting back from the definition of the grand-potential in equation (2.3.2). Following statistical mechanics, its differential can be expressed as $d\Phi_G = -P dV - S dT - N d\mu$, with S the entropy and N a conserved number of charges or particles associated to μ [111]. Comes then straight-forwardly that the expectation value (or mean) $\langle N_X \rangle$ of a conserved charge X is given by the derivative of Φ_G with respect to μ_X :

$$\langle N_X \rangle = \frac{\partial}{\partial\mu_X}\Phi_G = T \frac{\partial}{\partial\mu_X} \ln(\mathcal{Z}(T, V, \vec{\mu})) = \frac{\partial}{\partial\hat{\mu}_X} \ln(\mathcal{Z}(T, V, \vec{\mu})), \quad (2.3.7)$$

recalling the definition of the reduced chemical potential. Using equation (2.3.3) to replace the grand-potential logarithm,

$$\langle N_X \rangle = \frac{\partial}{\partial\hat{\mu}_X} \left(P(T, V, \vec{\mu}) \frac{V}{T} \right) = \frac{\partial}{\partial\hat{\mu}_X} \left(\frac{P(T, V, \vec{\mu})}{T^4} \right) \times VT^3, \quad (2.3.8)$$

one eventually finds the relation between the 1st order cumulant C_1^X of conserved charge X and the corresponding 1st order susceptibility χ_1^X as defined in equation (2.3.4) [217]:

$$\chi_1^X = \frac{\langle N_X \rangle}{VT^3} = \frac{1}{VT^3} C_1^X. \quad (2.3.9)$$

In the same way, one can derive the variation of the mean conserved charge X due to the fluctuations of any conserved charge Y [216]:

$$\frac{\partial\langle N_X \rangle}{\partial\mu_Y} = T \frac{\partial^2}{\partial\mu_Y\partial\mu_X} \ln(\mathcal{Z}(T, V, \vec{\mu})) = \frac{1}{T} \frac{\partial^2}{\partial\hat{\mu}_Y\partial\hat{\mu}_X} \left(\frac{P(T, V, \vec{\mu})}{T^4} \right) \times VT^3. \quad (2.3.10)$$

leading again to the relation between the 2nd order cumulant C_{11}^{XY} and the corresponding 2nd order susceptibility χ_{11}^{XY} , still based on equation (2.3.4) [217]:

$$\chi_{11}^{XY} = \frac{\langle N_X N_Y \rangle - \langle N_X \rangle \langle N_Y \rangle}{VT^3} = \frac{1}{VT^3} C_{11}^{XY} \quad (2.3.11)$$

This result enables to write explicitly the expression of both 2nd order susceptibilities χ_2^X and χ_{11}^{XY} , and their relation to diagonal and off-diagonal cumulants C_2^X and C_{11}^{XY} , also usually referred to as variances σ_X^2 and covariances σ_{XY}^{11} [217]:

$$\chi_2^X = \frac{\partial^2 \ln(\mathcal{Z}(T, V, \vec{\mu}))}{\partial \hat{\mu}_X^2} = \frac{\langle N_X^2 \rangle - \langle N_X \rangle^2}{VT^3} \equiv \frac{1}{VT^3} \sigma_X^2, \quad (2.3.12)$$

$$\chi_{11}^{XY} = \frac{\partial^2 \ln(\mathcal{Z}(T, V, \vec{\mu}))}{\partial \hat{\mu}_X \partial \hat{\mu}_Y} = \frac{\langle N_X N_Y \rangle - \langle N_X \rangle \langle N_Y \rangle}{VT^3} \equiv \frac{1}{VT^3} \sigma_{XY}^{11}, \quad (2.3.13)$$

by using equations (2.3.11), and equation (2.3.5) with (2.3.3).

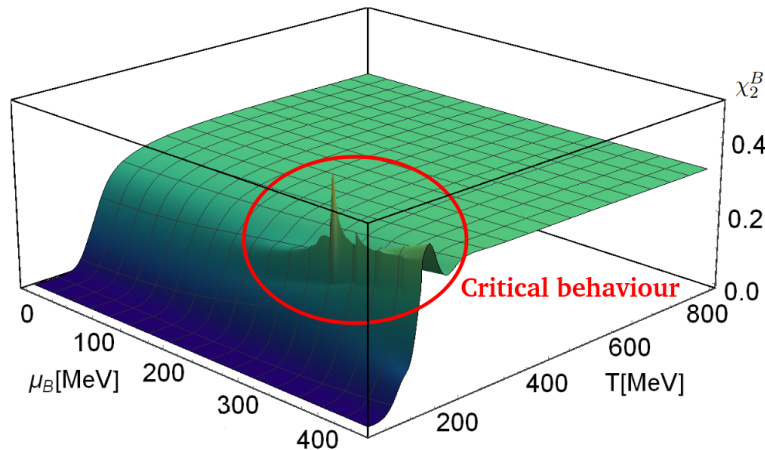


Figure 2.7: 3D representation of the behaviour of χ_2^B as a function of T and μ_B , for an equation of state containing a CEP at coordinates $T_{CEP} = 143$ MeV and $\mu_B^{CEP} = 350$ MeV. The divergence of χ_2^B around this location is indicated [218].

But why are those quantities interesting to search for the CEP? First of all because they are proportional to the correlation length ξ of the system, which diverges at the CEP; in particular, $\chi_2 \propto \sigma^2 \propto \xi^2$ [151]. The cumulants and related susceptibilities of conserved charges are then expected to diverge around the critical point, as shown for χ_2^B in the figure 2.7. Note that higher order cumulants are even more sensitive to critical fluctuations, as they diverge with ξ like $C_3 \propto \xi^{4.5}$ and $C_4 \propto \xi^7$ [151], although they won't be studied in this manuscript. Secondly, on a more fundamental level, one can understand from equations (2.3.12) and (2.3.13) that susceptibilities quantify how the partition function \mathcal{Z} of the system changes when varying the values of chemical potentials. As this function carries information on the possible microscopic configurations of the system, it shall change drastically at the vicinity of the CEP, as the system goes from a 1st order phase transition where it is made of two heterogeneous phases, to a crossover transition where it is composed of only one homogeneous phase. Hence, the susceptibilities quantifying these variations should diverge when \mathcal{Z} endures such dramatic modification.

On the experimental side, it is obviously impossible to measure directly the susceptibilities in HICs, as the volume of the system and the temperature cannot be determined

on an event-by-event basis. Nevertheless, one can have access to the cumulants of conserved charges, via the measurement of the hadronic species which carry them in a given phase space. Even though all hadrons cannot be measured, in particular the neutral or short-lived ones requiring to be reconstructed, what can induce important uncertainties, one uses then the most frequent hadrons formed which carry the charges of interest. For instance, one can use pions as proxies for Q [219], as they represent the majority of charged particles produced in HICs; using in addition protons and kaons, one gets more than 95% of the total number of charged particles. However, Q can also be measured directly without the requirement to identify the particles themselves, into a certain limit though, as I will explain in subsection 2.3.3 when presenting the results of STAR used in my study. With similar arguments, experimental collaborations such as STAR use kaons as proxies for strangeness S [220], and protons as proxies for baryonic number B [214]. In fact, the choice of such proxies will be a central part of my work, as I will describe in subsection 2.3.3.

In order to compare experimental results to theoretical values of susceptibilities, it is usual then to compare ratios of net-multiplicity distributions cumulants for proxies, to ratios of susceptibilities [217]. The use of such ratios has been proposed as they allow to cancel the trivial dependence of V and T , as can be seen from equations (2.3.12) and (2.3.13). The 2nd order cumulants of net-multiplicity distribution of the hadrons that I will study, called (co)variances of net-hadrons from now on, are explicitly calculated using the formulae:

$$\sigma_\alpha^2 (= C_2^\alpha) = \langle \delta N_\alpha^2 \rangle - \langle \delta N_\alpha \rangle^2, \quad (2.3.14)$$

$$\sigma_{\alpha,\beta}^{11} (= C_{11}^{\alpha\beta}) = \langle \delta N_\alpha \delta N_\beta \rangle - \langle \delta N_\alpha \rangle \langle \delta N_\beta \rangle. \quad (2.3.15)$$

Here, α and β indices refer to any hadronic specie, and δN_α is the net-number of those particles, *i.e.* the number of such particles n_α minus the number of corresponding antiparticles $n_{\bar{\alpha}}$: $\delta N_\alpha = n_\alpha - n_{\bar{\alpha}}$. Note consequently that δN_α in these equations are the equivalent of the net-numbers of conserved charges N_X used previously, but for the particles (to use STAR notation). Finally, $\langle \dots \rangle$ denotes the average over the number of events used for the calculation.

The global strategy of experimental collaborations to scan the phase diagram consists then of creating systems which will describe different trajectories when evolving, via the already discussed BES program, by varying the collision energy. The objective is to detect any potential critical behaviour of the fluctuations of conserved charges via the measure of their proxies, which could be due to a passage through a 1st order phase transition or CEP [217]. As mentioned several times, some results of the BES program show interesting non-monotonic behaviour for collisions with $\sqrt{s_{NN}} \leq 20$ GeV, in particular in the case of net-protons cumulants. The ratio $\kappa\sigma^2 = C_4/C_2$ for net-protons in particular, displayed in figure 2.8 (left), deviates from the Poisson baseline in central Au-Au collisions, which is expected if p and \bar{p} multiplicity distributions are independent from each other. This behaviour and the specific shape it describes was predicted in [221] for $\omega_4 = C_4/C_1$ in the case of a freeze-out line crossing the critical region at the vicinity of the CEP, see figure 2.8 (right). Despite the fact that $\kappa\sigma^2$ and ω_4 are slightly different, this results remains intriguing and justifies the fact to perform the same measurements at lower energy, to see if the characteristic shape is confirmed. However, many experimental effects and biases on the measured quantities has to be investigated and taken into account before drawing hasty conclusions, compared to the prediction based on pure statistical fluctuations coming from the CEP [151, 217]. These subtleties will be the topic of the next subsection.

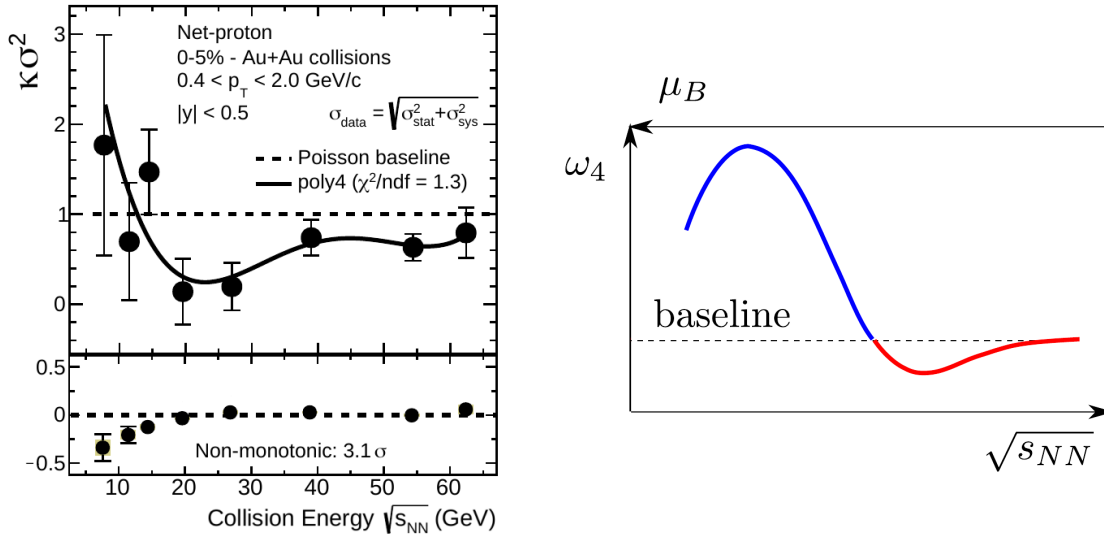


Figure 2.8: Left: cumulant ratio $C_4/C_2(= \kappa\sigma^2)$ for net-protons, measured by STAR as a function of energy for central (0-5%) Au-Au collisions, compared to the linear Poisson baseline in the lower panel [214]. Right: expected behaviour of $C_4/C_1(= \omega_4)$ for net-protons, in the case of a freeze-out line passing through the critical region near the CEP (modified from [151]).

2.3.2 Limits and shortcomings of experimental and theoretical observables

There are indeed many caveats to keep in mind when comparing results from any theoretical prediction with measurements made in HICs, and even simply when dealing with fluctuations at the experimental level. It is thus important to address them in this thesis, dedicated to the study of such cumulants with the phenomenological tool that is an event generator, in order to understand my motivations. For this reason, I will discuss in this subsection the most important ones, but might omit some of them (which should be less relevant for the work I will present). I refer hence the reader to the following exhaustive reviews [151, 217, 222] to have a more complete overview on the topic.

The most important point to tackle is the clear conceptual gap between many theoretical studies achieved in the GC frame, like IQCD calculations, and what happens in a HIC. In the former case, the system is considered at fixed volume in the infinite limit, in thermal equilibrium with a heat bath with which it can exchange particles, and only global conservation is ensured. In the latter case of HICs however, the system is highly dynamical, temperature and volume fluctuates from event to event, but temperature is also inhomogeneous among the whole system in each event, and both global and local conservation laws apply.

Those discrepancies between theory and the experimental ways to probe critical fluctuations points at several effects which has to be kept in mind when measuring net-particle cumulants in HICs:

- Several kinds of fluctuations emerge from the event-by-event analysis of net-multiplicity distributions [222]. In addition to the thermal fluctuations of conserved charges, which are sought as they should diverge near the critical point, the initial geometry of the collision will vary from events to events and cause additional fluctuations. Moreover, hadronisation of the fluid being a quantum mechanical process, it results in intrinsic fluctuations both in the kinematic distribution and in the chemistry of hadrons created.

- The use of ratios might cancel the trivial dependence of cumulants on the volume, but it does not prevent from volume fluctuations, which are a source of unwanted dynamical fluctuations. The cumulants are generally measured in centrality classes, determined generally via the Glauber model (introduced in subsection 2.2.1). But the geometry of the system within a given centrality class varies, and naturally enhances the measured fluctuations in what is called the centrality bin-width effect (CBWE) [223]. These volume fluctuations can be minimised though, *e.g.* by using centrality classes as small as possible, and/or by using a correction method, the centrality bin-width corrections (CBWC). It consists of calculating the value of a cumulant C_i for a given centrality class by averaging its value C_i^m through all bins m of the multiplicity distribution in the class considered, weighted by the normalised number of events ω_m in the associated multiplicity bin [224]:

$$C_i = \sum_m \omega_m \times C_i^m = \sum_m \frac{n_m}{\sum_m n_m} \times C_i^m \quad (2.3.16)$$

- The amplitude of the critical fluctuations which would be seen if the system created in a HIC reached the CEP has to be estimated properly, taking into account critical slowing-down and finite-size effect of the system. The correlation length ξ (and thus the related cumulants) are expected to diverge to infinity at the vicinity of the CEP, when performing IQCD simulations of an infinite size system during an infinite time. However, in a HIC, the system has a finite size, what will limit the growth of ξ as it can logically not be larger than the system itself [225]. This finite-size effect is even more strengthened by the fact that, as the system is inhomogeneous, only a part of the whole system would approach the CEP. In addition, the system would reach the conditions of criticality only for a finite time as it cools down and cannot thus stay in equilibrium in this region, what would slow down the growth of ξ . Taking into account those two effects, the amplitude of ξ would then be limited to the order of $2 \sim 3$ fm [226].

Other shortcomings, more related to the experimental measurement of the net-particle cumulants, will also have an impact on the search for critical fluctuations. The first one is the fact of measuring the cumulants in the momentum phase space, while it is generally integrated out in theoretical studies [227]. In order to take the momentum cuts into account in theoretical calculations, one can use for instance the Hadron Resonance Gass model, which will be presented in subsection 2.3.3. The subensemble acceptance method (SAM), taking into account exact charge conservation, has also been developed recently to improve the comparison method between cumulants measured in HICs and susceptibilities calculated from theory [228]. Besides, the detectors used in experiment cover only a restricted phase space of the kinematic region. This can turn out to be problematic if the accessible rapidity window is too narrow, as the critical fluctuations are expected to have a correlation range of the order of $\Delta y \sim 1$ [229]. Nevertheless, measuring fluctuations in a rapidity window smaller than the whole system has the advantage to reproduce approximately the GC limit, as the sub-system can exchange particles with the rest of the system considered as a heat bath [230]. Furthermore, one has to be careful not to mix the set of particles used to determine centrality with the particles used to measure cumulants, what would lead to auto-correlations effects and decrease the signal [217]. A simple solution is to use particles from a different kinematic region to determine the centrality of the collision, than the particles of interest.

Finally, remains the important question of the impact of the hadronic cascades on the fluctuations carried by hadronic species after hadronisation. Several studies suggested

that the inelastic collisions and annihilation of hadrons in this last stage, and the resulting change in the hadronic chemistry and kinematics, impact significantly the signal from potential fluctuations [208, 231]. This argument is the main motivation which led me to study firstly the quantitative impact of hadronic cascades on the experimental cumulants measured by STAR, presented in the next subsection. I will then elaborate further on the method in section 3.5, once having presented the event generator used to perform this work.

Even beyond these considerations though, the choice of proxies to measure conserved net-charges has to be considered carefully. Whereas cumulants for net- Q can be reproduced almost perfectly experimentally (up to detector uncertainties), B and S require proxies as a non-negligible part of the particles carrying these charges are not directly measurable. For B , an important process happening in the hadronic phase is the isospin randomisation, caused by reactions $p + \pi^{0/-} \leftrightarrow \Delta^{+/0} \leftrightarrow n + \pi^{+/0}$. Such processes completely blur the original isospin distribution of nucleons [232]. On one hand, authors of [232] pretend that such process enable to reconstruct cumulants of net- B via net- p cumulants, which contains then the information for the whole nucleon contribution. Nonetheless, it is claimed on the other hand, in a recent work using a microscopic transport approach, that isospin randomisation prevent from the possibility to reconstruct the proper net- B cumulants from proton distribution [233]. Off-diagonal correlator, *i.e.* cumulants involving different conserved charges, are also studied. In particular, the baryon-strangeness correlations in particular have been proposed as a potential probe for deconfinement via the measurement of the σ_{pK} covariance [209]. The importance of choosing a good proxy to evaluate correctly the fluctuations emerging from critical behaviour motivated a recent study, on their effectiveness to reconstruct theoretical quantities [234]. Presented with more details in the following subsection, this work incited me to investigate the impact of the choice of proxies, compared to conserved charges cumulants. The objectives and global method will also be synthetically presented in section 3.5.

2.3.3 STAR results & enhanced proxies for 2nd order cumulants

Variations and covariances of net- Q , net- p and net- K multiplicity distributions

The first publication which motivates the research outlined in section 3.5, and exposed thereafter in chapter 5, deals with the systematic measurement of variances and covariances proxies for B, Q, S by the STAR experiment [211]. They present, for Au-Au collisions at $\sqrt{s_{NN}} = 7.7, 11.5, 14.5, 19.6, 27, 39, 62.4$ and 200 GeV, the following (co)variances of net-multiplicity distributions for identified charged p, π and K :

$$\begin{pmatrix} \sigma_{\pi}^2 & \sigma_{\pi p}^{11} & \sigma_{\pi K}^{11} \\ " & \sigma_p^2 & \sigma_{pK}^{11} \\ " & " & \sigma_K^2 \end{pmatrix}. \quad (2.3.17)$$

By convention, the net-multiplicity distributions are determined as the difference between the positively charged hadron distribution and the negative one ($\delta N_{\alpha} = n_{\alpha+} - n_{\alpha-}$), to follow the particle-antiparticle scheme of protons. They have been measured as a function of the pseudorapidity window $|\Delta\eta| < 0.1 - 0.5$ used for the measurement, and of the collision centrality within $|\Delta\eta| < 0.5$, in both cases for particles with $0.4 < p_T < 1.6$ GeV. In the latter case, which will interest me in particular, the values of the (co)variances have been calculated for 0-5%, 5-10% and each of the 10% centrality classes for 10% to 80%,

using the CBWC method introduced in the previous subsection. They are displayed as a function of the $\langle N_{part} \rangle$ value estimated for each centrality class with the Glauber model (see subsection 2.2.1). The reason is that it allows to verify if (co)variances show a linear dependence to N_{part} , as expected according to the Central Limit Theorem (CLT), what can be seen on figure 2.9 for covariances [211]. To avoid auto-correlation effects (discussed in subsection 2.3.2), the centrality is determined using charged particles within $0.4 < p_T < 1.6$ GeV, but in the $0.5 < |\eta| < 1$ region.

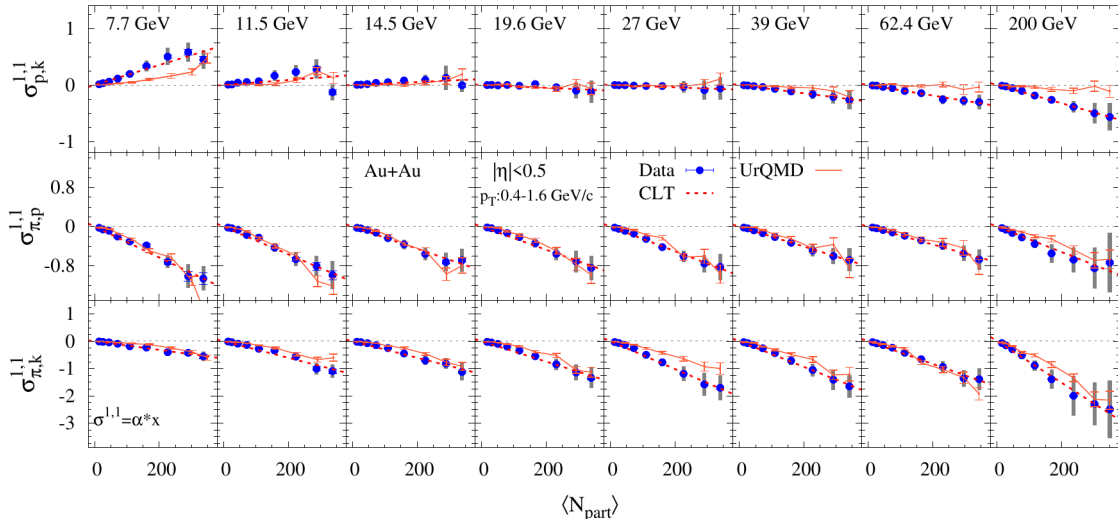


Figure 2.9: Centrality dependence of the covariances of p , K and π net-multiplicity distributions, for Au-Au collisions at several indicated energies of the BES program, within $|\eta| < 0.5$ and $0.4 < p_T < 1.6$ GeV. Results from STAR, with systematic errors indicated by the boxes, are compared to CLT expectations and UrQMD simulations results [211].

Based on these measurements, the following ratios $C_{\alpha\beta}$ ² have been calculated:

$$C_{Qp} = \frac{\sigma_{Qp}^{11}}{\sigma_p^2} \left(\cong \frac{\chi_{11}^{QB}}{\chi_2^B} \right), \quad C_{QK} = \frac{\sigma_{QK}^{11}}{\sigma_K^2} \left(\cong \frac{\chi_{11}^{QS}}{\chi_2^S} \right), \quad C_{pK} = \frac{\sigma_{pK}^{11}}{\sigma_K^2} \left(\cong \frac{\chi_{11}^{BS}}{\chi_2^S} \right), \quad (2.3.18)$$

with β always referring to the particle considered for the denominator's variance. They are displayed as a function of $\langle N_{part} \rangle$ too, and also as a function of the collisions energy for central (0-5%) and peripheral (70-80%) events, as shown in figure 2.10.

Note that I refer to the " Q^{PID} " of the STAR publication directly by " Q " here. STAR precises " PID " for "*identified particles*", because of an erratum addressed on the initial publication. In this erratum, new measurements of (co)variances implying net- π are used in addition to net- p and net- K to determine the (co)variances implying net- Q^{PID} , meanwhile the raw net- Q distribution was used directly in the original paper. The reason for this change is that in the original work, net- Q distribution was determined with unidentified particles tracks in the kinematic region of interest, and net- p/K distributions from the subsequently identified particles. In such case, the fact that p and K distributions are not independent from the charged one requires a specific treatment in the calculations of covariances, when correcting from the detection efficiency of particles. As STAR was initially using a covariance calculation formula which assumes independence of the two

²Note that, following the convention from the STAR paper, $C_{\alpha\beta}$ refers here to ratios of cumulants and not to cumulants themselves, as it was the case in subsection 2.3.1. As from now on we will only discuss 2nd order cumulants, *i.e.* (co)variances $\sigma^{2/11}$, we will keep this convention of $C_{\alpha\beta}$ designating cumulants ratios for the whole manuscript.

particles set, it resulted in auto-correlation effects, and hence an overestimation of the real correlation from σ_{Qp}^{11} and σ_{QK}^{11} . This issue was pointed out in [235] and led to the publication of these corrected measurements, which cured the important discrepancies observed with model predictions in the original version.

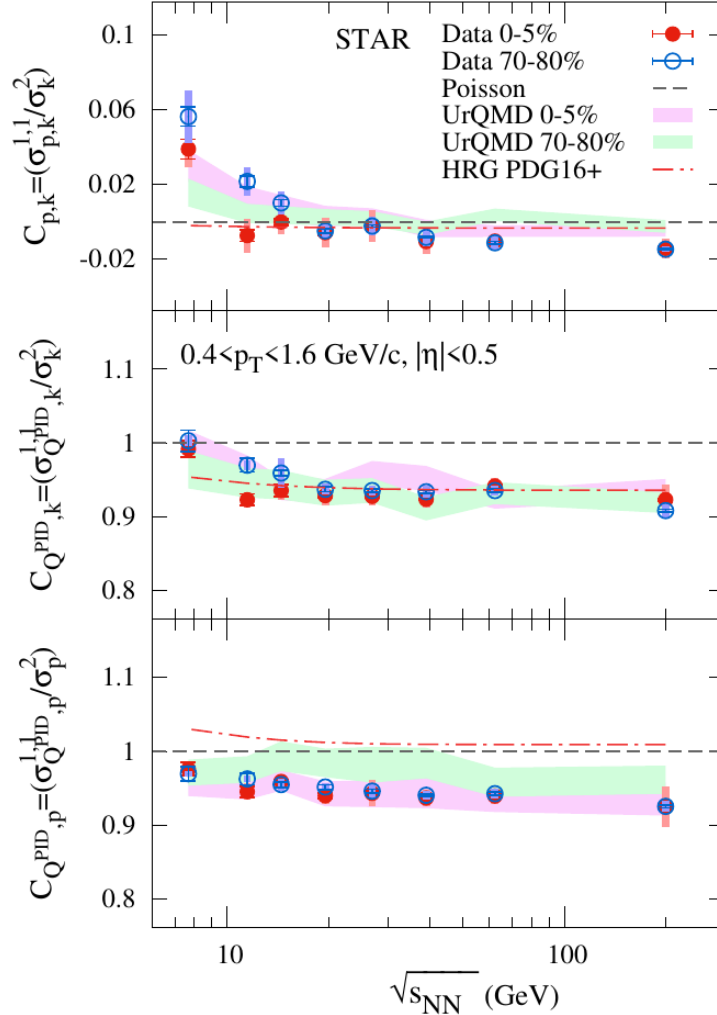


Figure 2.10: Energy dependence of the cumulants ratios C_{pK} , C_{QK} for central (0-5%) and peripheral (70-80%) Au-Au collisions, within $|\eta| < 0.5$ and $0.4 < p_T < 1.6$ GeV. Results from STAR have systematic errors indicated by the boxes and statistical ones by bars. Poisson baseline, UrQMD simulations results and calculations using HRG model including the PDG16+ [236] particles set are displayed for comparison [211].

Looking at the updated data of [211], the most notable result of this study is the fact that the ratio C_{pK} , which shows no centrality dependence at high energy, changes its sign below 19.6 GeV/A, and is not centrality independent anymore. It is more exactly caused by the underlying sign change of σ_{pK}^{11} (see figure 2.9), a phenomenon expected to be related to the change of the phase (hadronic gas or QGP) from which the correlations arise, as pointed out in [209]. Such results motivated me to study the impact of the hadronic cascades in HICs on these observables, in order to disentangle how much of the signal effectively comes from each of the two phases, as such theoretical work is even explicitly requested in the conclusion of the paper in question. To do so, I will employ the event generator EPOS, which I will introduce in the next chapter.

New proxies for the ratios of 2nd order susceptibilities

The second main aspect of my research work has been inspired by a theoretical study on the choice of the proxies used to probe the fluctuations of B, Q, S [234]. The authors estimated the values of 2nd order susceptibilities of the conserved charges, using two different methods to extend lattice quantum chromodynamics predictions at finite nuclear density: the Taylor extension method, and the sector method. Then, in order to relate them to net-particle cumulants measured in experiments, they investigated the breakdown of contributions to these susceptibilities from each of the most commonly reconstructed hadronic species with the HRG model.

The HRG model is a thermal model, using Fermi-Dirac and Bose-Einstein statistics, and taking its origins in the ideas of the SBM presented in subsection 2.1.1. The main assumption of this model is that a gas of interacting hadrons in their ground states can be described by a gas of non-interacting hadrons and resonances [237]. Thus, the partition function of such system can be expressed as the sum of ideal gas contributions from each known hadronic resonance R :

$$\ln(\mathcal{Z}_R) = \eta_R \frac{V d_R}{2\pi^2 T^3} \int_0^\infty p^2 dp \times \ln \left(1 - \eta_R e^{-\frac{1}{T}(E_R - \mu_R)} \right), \quad (2.3.19)$$

with $E_R = \sqrt{p^2 + m_R^2}$ being the energy of a resonance R , and the chemical potential associated to each resonance R being $\mu_R = \mu_B \cdot B_R + \mu_Q \cdot Q_R + \mu_S \cdot S_R$ (B_R, Q_R and S_R are the value of conserved charges associated to each resonance). Finally, d_R and m_R are respectively the spin degeneracy and the mass of each resonance, and $\eta_R = (-1)^{1+B_R}$ will be +1 for (anti)baryons and -1 for mesons [234]. This way, the pressure can then be seen as a sum of pressures from the different resonance gases, and one can re-write the grand-potential:

$$\frac{P}{T^4} = \frac{1}{T^4} \sum_R P_R = \frac{1}{VT^3} \sum_R \ln(\mathcal{Z}_R(T, \vec{\mu})). \quad (2.3.20)$$

In the frame of this model, the susceptibilities can be written :

$$\chi_{ijk}^{BQS}(T, \vec{\mu}) = \sum_R B_R^i Q_R^j S_R^k \times I_l^R(T, \vec{\mu}) \quad (2.3.21)$$

with $l = i + j + k$ ($= 2$ in the study in question) and the phase space integral I_l^R defined as:

$$I_l^R(T, \vec{\mu}) = \frac{\partial^l P_R / T^4}{\partial \hat{\mu}_R^l} \quad (2.3.22)$$

Considering those definitions, one can easily take into account kinematic cuts on transverse momentum and rapidity in the phase space integration, which is of great interest when comparing theoretical predictions to experimental data. To do so, one has to modify from (2.3.19):

$$\frac{1}{2\pi^2} \int_0^\infty p^2 dp \rightarrow \frac{1}{4\pi^2} \int_{y^1}^{y^2} dy \int_{p_T^1}^{p_T^2} p_T \cosh(y) \sqrt{p_T^2 + m^2} dp_T, \quad (2.3.23)$$

as well as, for pseudorapidity:

$$\frac{1}{2\pi^2} \int_0^\infty p^2 dp \rightarrow \frac{1}{4\pi^2} \int_{\eta^1}^{\eta^2} d\eta \int_{p_T^1}^{p_T^2} p_T^2 \cosh(\eta) dp_T. \quad (2.3.24)$$

The main result of the study in [234] is to propose ratios of proxies (denoted $\tilde{C}_{\alpha\beta}$) which are enhanced versions of the ones used by experimental collaborations (see equation (2.3.18)). To do so, the authors used the equation (2.3.21), from which they could estimate the breakdown contribution of each hadronic specie to the total diagonal and off diagonal 2nd order susceptibilities of B , Q and S . For instance, the breakdown contribution of different hadronic species to χ_{11}^{QS} and χ_2^S are displayed in figure 2.11, compared with the corresponding total susceptibilities.

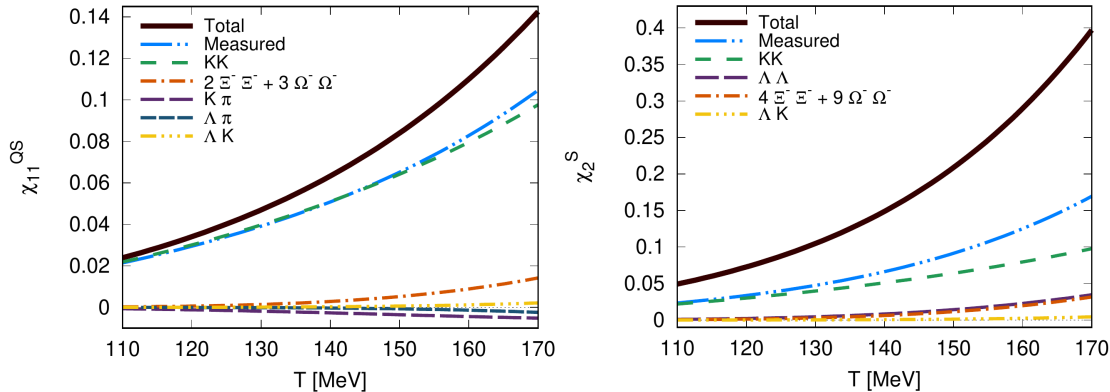


Figure 2.11: Breakdown of hadronic contribution to χ_{11}^{QS} and χ_2^S as a function of T , obtained with HRG model calculations [234].

They tried then to construct several good proxy ratios, following the argument that to do so, it is important to use in both numerator and denominator (co)variance proxies that are equally good to reconstruct their respective related susceptibilities. For the strangeness related ratios, whose comparison to exact susceptibility ratios is shown in figure 2.12, the proposed best enhanced proxy ratios are the following:

$$\tilde{C}_{QS} = \frac{1}{2} \cdot \frac{\sigma_K^2}{\sigma_K^2 + \sigma_\Lambda^2} \left(\cong \frac{\chi_{11}^{QS}}{\chi_2^S} \right), \quad (2.3.25)$$

$$\tilde{C}_{BS} = \frac{\sigma_\Lambda^2}{\sigma_K^2 + \sigma_\Lambda^2}, \quad \tilde{C}'_{BS} = \frac{\sigma_\Lambda^2 + 2\sigma_\Xi^2 + 3\sigma_\Omega^2}{\sigma_\Lambda^2 + 4\sigma_\Xi^2 + 9\sigma_\Omega^2 + \sigma_K^2} \left(\cong \frac{-\chi_{11}^{BS}}{\chi_2^S} \right), \quad (2.3.26)$$

still with the same convention that the second index corresponds to the charge of the ratio denominator's variance. The choice of these enhanced proxy ratios is based on the fact that they have to be close to the exact susceptibility ratios, but should exhibit as well a similar behaviour over the whole temperature range. It is worth noticing that these enhanced proxies are only made up of variances, and not any covariance, based on the simple fact that the hadronic species employed carry several of the conserved charges. Note also that the negative sign in the relation of χ_{11}^{BS} to its proxies is simply due to the fact that strange baryons carry $B = 1$ and $S < 0$, as s quarks associated to negative strangeness by convention. In particular, two proxy ratios are proposed to evaluate the baryon-strangeness correlation: one using only K and Λ , named here \tilde{C}_{BS} , and another using in addition multi-strange baryons Ξ and Ω (which are however more difficult to measure experimentally with reduced uncertainty), \tilde{C}'_{BS} .

Added to the idea of studying the impact of hadronic cascades on the proxies employed to probe the fluctuations of conserved charges, the results of this theoretical work motivated me to go even further. That is to say, to test the proposed enhanced proxy ratios against the experimental one, by comparing in addition both of them to the fluctuations of exact conserved charges, in order to see how much the reconstruction of these

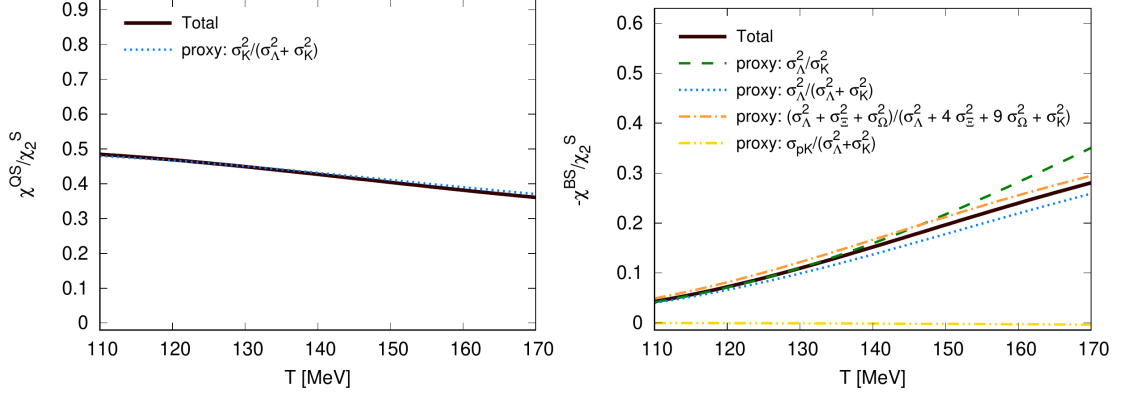


Figure 2.12: Comparison of several proxy ratios for QS and BS correlations obtained via HRG model calculations. Both are plotted as a function of T , with their related ratio of exact susceptibilities calculated with lQCD [234].

fluctuations would improve. Then, following up on from my first idea, I can also study the impact of hadronic cascades on the enhanced proxies and on the cumulants of exact conserved charges themselves. Such research work requires realistic dynamical simulations of HICs to relate properly the two experimental and theoretical studies presented previously, what is again possible thanks to an event generator like EPOS, presented in the following chapter.

CHAPTER 3

THE EPOS EVENT GENERATOR

Contents

3.1	Generalities on event generators	48
3.1.1	Event generators & high-energy physics	48
3.1.2	Event generators for heavy-ion collisions	49
3.2	A little history of EPOS and related projects	51
3.2.1	From VENUS to EPOS 4	51
3.2.2	Side projects with EPOS	52
3.3	Theoretical frame of EPOS	53
3.3.1	Parton Model	54
3.3.2	Gribov-Regge Theory	54
3.3.3	Parton-Based Gribov-Regge Theory	55
3.3.4	String Model	58
3.4	Generation of an event in EPOS	59
3.5	Objectives of the thesis	63
3.5.1	Towards the release of EPOS 4	63
3.5.2	Towards the study of net-charge cumulants	64

After having dedicated the chapters 1 and 2 to introduce the physical context of my Ph.D. thesis, namely hadronic physics and more particularly the study of the QGP, I will introduce in this third chapter the *Energy conserving quantum mechanical approach based on Partons, parton ladders, strings, Off-shell remnants and Saturation of parton ladders* (EPOS) event generator. It has been the heart of all the work I have achieved during this thesis, both because my main objective was to contribute to its development in view of a public release, and because I used it to conduct the studies I have led.

Starting with a short presentation of what is an event generator (EG) in section 3.1 and a little glimpse of the role of such tool, I will then relate quickly in section 3.2 the chronology of the different developments and projects that have led to make what EPOS is now. section 3.3 will contain the description of the theoretical foundations on which EPOS relies, especially the ones that are exclusive to this EG, leading to the section 3.4 in which I will explain how events are generated with EPOS. Finally, I will present the main goals of my thesis in section 3.5, relative to the new technical developments I implemented in EPOS, and to the study I have carried out on the cumulants of net-charges and net-particles used for the search of criticality in the phase diagram of nuclear matter.

3.1 Generalities on event generators

The major developments achieved on modern physics and on new technologies in the early twentieth century has inevitably led to intertwine the history of physics and informatics since then. Numerous progresses in both fields were due to discoveries or motivated by requirements from the other discipline. A famous example is the *World Wide Web*, which was developed by scientists of the CERN in order to facilitate the exchange of information between collaborators via computer networks, eventually used in the Internet. The other way around, the limits of computing technology have often been pushed to satisfy physicists requirements: some elements of the first computers were created for the need of nuclear physics.

Nowadays, high-energy physics (HEP) requires enormous computing resources. As always, both experimental and theoretical communities are concerned: the data flux collected from detectors are constantly growing upgrade after upgrade, with the continuous increase of colliders luminosity (*e.g.* in the context of the *High-Luminosity Large Hadron Collider* (HL-LHC)), and on the other hand one necessitates ever greater precision in calculations to evaluate model parameters extracted from these data. Simulation tools are also of primary interest, because of their central role in the comprehension of experimental observations, whether to understand and quantify detector effects, or to confront results with theoretical predictions. This last point is the purpose of EGs, which will be discussed in this section.

3.1.1 Event generators & high-energy physics

Event generators are computer code which aims to reproduce particle production by simulating the dynamics of a collision step by step. In the context of HEP, an event refers to everything that happens between the interaction of the colliding particles and the list of final-state particles, in a similar sense of an event reconstructed in an experiment.

However, such events are very complicated to compute due to the complexity and diversity of underlying processes at different stages of the collision. They imply at the same time perturbative calculations which are sometimes directly computable (up to a certain precision order though), but also modelling of non-perturbative processes which cannot be derived from first principles, and which require parametrisation, like the problem of confinement which is responsible for hadronisation. Moreover, handling such problem requires to deal with very large and varying number of particles, thus with phase-space of a very large number of dimensions, and the quantum nature of those particles necessitate a probabilistic approach of their interactions.

Fortunately, such aforementioned problems offer a perfect playground to apply Monte Carlo (MC) techniques, in particular thanks to the possibility to factorise many different processes according to their energy scale regime. MC methods rely on the generation of random numbers that are used to reproduce stochastically known distribution of given processes, by using function inversion and/or *hit-or-miss* method. They can also be used to evaluate numerically highly multi-dimensional phase space integrals and solve integro-differential equations, that are commonly met in HEP as previously explained [238].

As a consequence, EGs are fully suited tools to do phenomenology. They enable physicists to compute models and theories in order to confront them with experimental data and therefore validate them, or extract model parameters, but also to help at discovering and interpreting newly observed phenomena. They are employed to design future experiments and facilities like the ones discussed in subsection 2.2.2, or to estimate systematic uncertainties in the reconstruction of events with detectors, when combined with simulation tool kits of particle-matter interaction like GEANT4 [239]. Definitely, EGs are the cornerstone of modern particle physics, the heart of the interplay between theoretical and experimental communities. However, they also come with some flaws, because of their phenomenological nature: they generally necessitate a parametrisation, and one has to be careful about their limited applicability.

There exists a myriad of EGs, due to the numerous fields of interest in HEP: neutrino physics, cosmic-ray showers, testing the SM or, as it is indeed the main focus of this thesis, heavy-ion physics. Nevertheless, many physics elements can be common across these topics despite this diversity, often leading to a "modular" conception of the dedicated simulation tools, which parts can be used in different fields. Furthermore, EGs can be more or less elaborated, in other word offering a more or less complete description of the events studied, depending on the purpose for which they are developed. Hence, there is a specific class of EGs, called general-purpose event generators, which aim is to reproduce a rather exhaustive range of processes and observables of interest.

Even though primarily dedicated to heavy-ion physics, EPOS is considered to be a general-purpose EG, as its goal is to offer a complete and unified description of different systems such as e^+e^- annihilation, $e-p$ scattering and from $p-p$ to $A-A$ collisions, thanks to the rich legacy inherited from its predecessor which I will introduce in section 3.2. It also takes advantage of a "modular" design, what is partly due to its targeted scope of application though, as I will discuss in the next subsection.

3.1.2 Event generators for heavy-ion collisions

When simulating particle collisions for small systems in the context of colliders physics, *i.e.* $p-p$ collisions in the LHC, EGs usually generate at first the hardest subprocess of the event, before completing the evolution of the event with other subprocesses

by decreasing order of energy scale involved. This is mainly due to the fact that in this field, the focus is generally put on hard interactions, whether to study SM parameters via exclusive production of gauge bosons for instance, or to investigate the "rest", *i.e.* the underlying event (secondary scatterings that are independent of the primary hard processes) [238]. On the contrary, EGs used for the simulation of HICs generate events in a more traditional time-ordered way, following the Björken scenario described in subsection 2.1.1, because the aim is generally to study the properties and signatures of QGP.

They start with the modeling of initial-state interaction implying multiple scatterings, which can be as simple as the Glauber model [139] introduced in subsection 2.2.1, that allows total cross-section calculations in the optical limit [138]. For instance, HIC event generators HIJING [240] and PYTHIA 8/Angantyr [241] use enhanced versions of MC-Glauber model to generate their initial-state interaction. Some other approaches include Color-Glass Condensate effective field theory (EFT), which describes the dynamics of colliding nuclei as saturated gluon fields [242]. The second common step in EGs of HICs is to simulate the evolution of the system, generally by using transport theories which can be either macroscopic or microscopic. In the macroscopic case, the partonic degrees of freedom are supplanted by an energy-momentum tensor in order to make the system evolve using relativistic hydrodynamics, assuming local thermal equilibrium [243]. In the microscopic case, kinetic theories are used in order to keep partons or quasi-particles as degrees of freedom, such as in PHSD [244] or AMPT [245]. In order to come back to hadronic degrees of freedom, hadronisation has to be achieved then, whatever the nature of the medium evolution chosen. Eventually, models such as UrQMD [246, 247] or SMASH [248] can be used as afterburners to model interaction between remaining hadrons, until the system reaches kinetic freeze-out. It is this stage of the collision when hadronic interactions occur, or more precisely its impact on fluctuation observables, that will be the heart of my study in chapter 5.

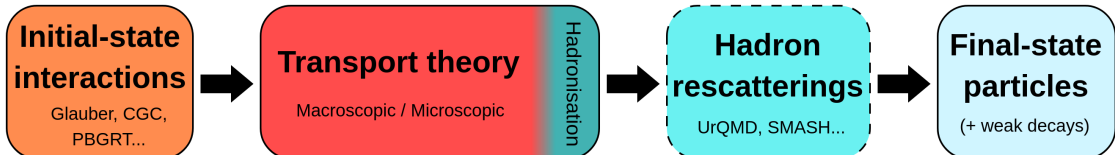


Figure 3.1: Schematised general structure of an event simulated with HIC event generators.

In the previous description, I intentionally didn't discuss the inclusion of jet-quenching effects (how jets are modified by the presence of a hot and dense medium, and vice-versa), neither how to treat the transport of heavy-flavours through the QGP, in order to describe at first a simple picture. This is also because such treatments are not systematically basic ingredients of HIC event generators, which are generally primarily focused on the study of "soft" physics. But the implementation of such effects exists, and many works are still ongoing on these very active research topics. About jet-quenching, one can see for instance *Heavy Ion Jet Interaction Generator* (HIJING) [240], *Jet Evolution With Energy Loss* (JEWEL) [249], *Dynamical Radiative and Elastic ENergy loss Approach* (DREENA) [250] or even *Jet Energy-loss Tomography with a Statistically and Computationally Advanced Program Envelope* (JETSCAPE) [251], a framework including packages of different models, giving to the user the choice of a desired modular conception to generate the events. Even though no actual EG dedicated to HICs simulation include a proper description of transport heavy-flavours through the QGP, several approaches under development or already well advanced are available [252–255], and could (or are already on their way to) be coupled with EGs.

EPOS follows in some way this classical picture of EGs for HICs, as will be depicted with more details in section 3.4. Nevertheless, it is based on a treatment of initial conditions which is different from the ones previously described, what makes it a unique approach. Besides, EPOS also served as a basis for the application of some jet+fluid and heavy-quarks+fluid interaction models, which are shortly presented in section 3.2.

3.2 A little history of EPOS and related projects

This section aims at giving a brief overview of the development history of EPOS in the first place, before describing shortly the different extension and projects derived from it.

3.2.1 From VENUS to EPOS 4

The very first ancestor of EPOS was the *Very Energetic Nuclear Scattering* (VENUS) model [256]. It is an event generator based on a multiple interactions model, the Gribov-Regge theory (GRT) [257] (see explanations in subsection 3.3.2), coupled to the string fragmentation model *Artru-Mennessier Off-shell Resonance* (AMOR) inspired by [258], described in subsection 3.3.4. It was developed in the late 80's/early 90's to describe soft processes occurring in HICs achieved at the SPS and *Alternating Gradient Synchrotron* (AGS) accelerators, and was one of the first event generators for HICs.

In order to include hard processes to the scheme, VENUS was later merged with *Quark-Gluon String Jet* (QGSJet) [259], a parton model-based EG, giving birth to the so-called NEXUS event generator [260]. It relied on the Parton-Based Gribov-Regge Theory (PBGRT), a marriage of the initial-state models from both initial EGs (more details given in subsection 3.3.3). However, non-linear effects needed to be taken into account, either by re-summing diagrams up to all-orders, at the cost of violating energy conservation, or by implementing an effective saturation cut-off in to order to keep conserving energy. As a consequence, the NEXUS project splitted into two new event generators: QGSJet-II followed the first path with the main objective to be applied mostly to ultra-high energy cosmic-rays (UHECRs) physics [261], while EPOS was conceived to study more particularly colliders physics, thus following the second path ensuring energy conservation [262].

Further major developments led to a new version called EPOS 2 [263]. A core-corona procedure has been introduced, consisting of separating at an early time of the collision the core part (area of high string density) from the corona part (area of low string density) [264], strings being phenomenological objects representing partonic chains. The core part has then been set to evolve following perfect 3+1D relativistic hydrodynamics, using a cross-over transition EoS which matches lattice calculations and conserves B , Q and S [265]. At last, the fluid is hadronised using a Cooper-Frye procedure [266] when cooling down to a specific temperature $T_{Had} = 166$ MeV, and the formed hadrons can re-scatter through hadronic cascades modelled with UrQMD [247], also freshly implemented as an afterburner.

The advent of EPOS 3 brought an upgrade of the core-corona separation procedure, no longer static but allowing high- p_T string segments to escape (see section 3.4), and a new viscous hydrodynamical evolution of the core [267]. On the level of primary interactions, a huge work had also been done to treat properly the production of heavy-flavours,

and the saturation scale had been changed from a constant to a value depending on the number of participants of the collision (N_{part}) and on the energy shared by each partonic ladder (or Pomeron, in the PBGR formalism).

Since then, several improvements has been achieved, leading too a new version now publicly available, called EPOS 4 [268]. The work has been continued on the treatment of saturation, and the related questions of factorization and binary scaling [269]. A new EoS including a critical point and a 1st order phase transition from [218] has been implemented for the hydrodynamical evolution of the core, in order to improve the description of low-energy collision from the RHIC [270]. In addition to the GC Cooper-Frye approach for hadronisation, a new microcanonical approach have been implemented, giving a better description of results from small systems (namely p - p and p - A collisions), where energy and flavour conservation play an important role [271]. The hadronisation condition of the core, which was so far triggered when temperature cooled down to a value $T_{Had} = 166$ MeV, has been replaced by a criterion on energy density, being now triggered when $\epsilon < 0.57$ GeV/fm³ [270].

A substantial and no less important work has also been undertaken on the usability of the code, its maintainability and the interface with other tools such as RIVET, for what I dedicated a consequent amount of time and efforts during my PhD. I will introduce my contributions to this work in the last part of this chapter, and dedicate chapter 4 to give an in-depth description of it.

3.2.2 Side projects with EPOS

In parallel of the developments carried out on EPOS itself, several alternative projects based on EPOS are born over the years, among which EPOS-LHC [272] is probably the most famous one, as being publicly available. It is an extended version of EPOS 1.99 [262], tuned to reproduce data of several experiments from the first LHC run. It benefits from a parametrised flow of the core (using the same core-corona procedure than in EPOS 2), achieved by enforcing radial and longitudinal expansion of core clusters depending on their mass, and imposing an azimuthal anisotropy. This allows in particular to perform simulations much more faster than when using complete hydrodynamics calculations. Despite a resultant predictive power that is reduced, this advanced parametrisation has been made with the particular objective of implementing EPOS-LHC into the extensive air-shower (EAS) simulation framework *COsmic Ray Simulations for KAscade* (CORSIKA) [273]. It establishes this way a bridge between collider physics and UHECRs physics, and it has the technical asset of being way faster to generate events than EPOS 2 and more recent versions, which use a complete event-by-event hydrodynamical simulation of the bulk matter.

The EPOS *Heavy Quarks* (EPOS-HQ) project [274] has emerged from the marriage of EPOS and the MC@_sHQ energy loss model [275], with the aim of studying the correlations between light hadrons and heavy flavours. The latter model is based on a MC treatment of the Boltzmann equation for heavy quarks (HQs), with an energy loss modelled by a collisional part (including inelastic and elastic scatterings) and a radiative part (including coherent and incoherent gluon radiation). Time-dependent temperature and velocity fields of the hydrodynamical evolution of the core simulated by EPOS are thus used to sample thermal scattering partners for the HQs, which hadronise then via fragmentation or coalescence process. In the first version of this approach [276], EPOS 2 was solely used for its hydrodynamics modeling as a background. The HQs were inserted "by hand" at the position of initial NN scatterings, with their initial p_T -distribution ob-

tained from FONLL calculations [277]. The latest version of EPOS-HQ took advantage of the production of HQs properly implemented in the PBGR formalism of EPOS 3 (as described in the previous subsection), as well as the viscous hydrodynamics and the final re-scatterings of heavy-flavoured hadrons through UrQMD [278]. In parallel, a similar approach has been developed, also using initial conditions from FONLL and EPOS 2 hydrodynamics, but employing then Wigner densities based on the Remler formalism to study J/Ψ production in A - A collisions at LHC energy [254, 279].

EPOS3-Jet is a framework built using EPOS 3 as a baseline, coupled with a MC algorithm of the Dokshitzer-Gribov-Lipatov-Altarelli-Parisi (DGLAP) equation [280] to simulate the evolution of the parton cascade leading to a jet within the QGP in HICs. The parton shower will be modified by the medium in which it evolves via an effective increase of off-shell partons' virtuality dependent of the local temperature, and also via temperature- and momentum-dependent collisional terms. The other way around, the energy lost by the shower will be added via a source term to the energy-momentum tensor of the local fluid cells to translate the impact of the jet on the medium [281]. This framework has been used to study the interactions between jets and the hydrodynamically expanding medium [281], and to study the overlapping of jets in this context [282].

The last major project involving EPOS, called EPOSi+PHSDe [283], is an hybrid event generator mixing initial conditions from EPOS [284] and the non-equilibrium transport evolution of the matter from PHSD [244]. It has been developed in order to disentangle initial and evolution effects on several final-state "bulk" observables (rapidity density of hadrons, flow, etc.), via a systematic comparison of the results obtained from both EPOS, EPOSi+PHSDe and PHSD.

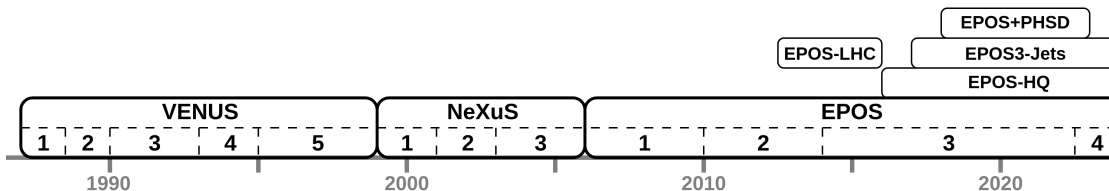


Figure 3.2: Timeline of the different versions of VENUS, NEXUS, EPOS and side-projects, based on the publication date of the first papers mentioning them.

(*N.B.* : EPOS-LHC [272] was released as a stable version, no longer developed after then)

To sum up this section, a chronological timeline of the different versions of EPOS, ancestors and side projects is displayed in Figure 3.2, based on the publication date of the corresponding reference papers.

3.3 Theoretical frame of EPOS

Before to describe how events are generated in EPOS, this section will be used to introduce briefly the main theoretical concepts behind some key ingredients of EPOS. Showing some limits and inconsistencies of the parton model and the GRT will lead to explain how the PBGR marry both approaches by curing their respective problems. It will be followed by a short presentation of the string model used to simulate the evolution and manage the hadronisation of parton chains in a phenomenological way.

3.3.1 Parton Model

The approach of the partons model, introduced in Chapter 1, consists of factorising the inclusive cross-section of two hard partons production from a hadronic collision, as a product of the sum of all parton distribution functions (PDFs) times the elementary partonic cross-section $d\hat{\sigma}/dp_T^2$ of the process [67]:

$$\sigma_{incl.}^{h_1 h_2 \rightarrow q_3 q_4} = \sum_{i,j}^{partons} \int dp_T^2 \iint f_{p_1}^i(x_1, p_T^2) f_{p_2}^j(x_2, p_T^2) \frac{d\hat{\sigma}^{q_i q_j \rightarrow q_3 q_4}}{dp_T^2} \theta(p_T^2 - Q_0^2) dx_1 dx_2. \quad (3.3.1)$$

Here, $f_{p_{1/2}}^{i,j}(x_{1/2}, p_T^2)$ are the fore-mentioned PDFs, which represent the probability density that the parton i/j of the hadron $h_{1/2}$ has a Björken variable equal to $x_{1/2}$ for a process happening at a given p_T^2 . While the PDFs necessitate to be extracted from data, the elementary partonic cross-section can be calculated directly with Feynman diagrams. The factorisation is made possible thanks to the Abramovsky-Gribov-Kancheli (AGK) cancellations [285], and can be interpreted as an increase in the resolution of the investigated problem from the hadronic scale to the partonic scale.

Remember, from its introduction in chapter 1, subsection 1.2.1, that one of the main assumption of this model is that the partons are considered as almost free. Consequently, the main limitation of the parton model comes obviously from the fact that it can only be applied to inclusive cross-section calculations, involving a hard process, *i.e.* implying a large Q transferred. This is clearly visible in the equation 3.3.1, with the Heaviside function $\theta(\dots)$ that introduces explicitly a virtuality cut-off Q_0 , but also hidden in the calculations of elementary partonic cross-sections via Feynman diagrams, which are only achievable in a perturbative regime. In addition, its inclusive approach nature allows to calculate cross-sections for one process in the collision, but there are no indications on how to proceed for the other processes, like how to share energy between the different processes in case of multiple parton interactions (MPI). An illustration of this problem is the fact that beyond $\sqrt{s} \approx 2$ TeV, the inclusive jet cross-section exceeds the total cross-section of the hadronic interaction [286]. Even if one can avoid this problem in hadron-hadron collisions with the so-called eikonalisation, the problem remains when treating nucleus-nucleus collision, as one cannot simply assume the total cross-section there to be a sum of individual nucleon-nucleon interaction cross-sections [284].

3.3.2 Gribov-Regge Theory

The main formalism on which the Gribov-Regge theory (GRT) is based is the S -matrix theory, derived from quantum mechanics by Werner Heisenberg [287]. It relies on the assumption that the elastic amplitude is in fact the projection of the transition matrix T_{fi} , the interaction term of the scattering matrix. This matrix, \hat{S} , relates initial and final states of a scattering process. It is expressed as [287]:

$$\hat{S} = \mathbf{1} + \hat{T} \quad \Longrightarrow \quad \langle f | \hat{S} | i \rangle = S_{fi} = \delta_{fi} + i(2\pi)^4 \delta(p_f - p_i) T_{fi} \quad (3.3.2)$$

and is linked to the total cross-section of the considered process by the optical theorem, through the relation [284]:

$$\sigma_{tot}(s) = \frac{1}{2s} \times 2 \times \text{Im}[T_{fi}(s, t = 0)] \quad (3.3.3)$$

Contrary to the parton model, the Gribov-Regge theory has been established in 1968 [257] to describe soft processes in the frame of MPI, in marge of the development of the quark model presented in subsection 1.2.1. There, interactions happen via the

exchange of "Pomerons", hypothetical mathematical objects that represent elementary interactions. Consequently, these objects can simply be parametrised, and the elastic amplitude $T_{\mathbb{P}}(s, t)$ for a unique Pomeron exchange is given by [284]:

$$T_{\mathbb{P}}(s, t) = i s^{\alpha_0 + \alpha' t} \quad (3.3.4)$$

with α_0 and α' experimental parameters, s and t the Mandelstam variables.

In hadron-hadron collisions, many Pomerons are exchanged in parallel, and the total cross-section can be rewritten as [284]:

$$\sigma_{tot}^{h_1 h_2}(s) = \int G_{fi}(s, b) d^2 b \quad (3.3.5)$$

where b is the impact parameter between the two colliding particles considered. Here $G(s, b)$ is the so-called profile function representing the Pomerons, and can be interpreted as the probability density to have an interaction at a given b . It is defined as the imaginary part of the Fourier transform of $T(s, t)$, divided by the initial parton flux $2s$:

$$G_{fi}(s, b) = \frac{1}{2s} \times 2 \times \text{Im} \left[\frac{1}{4\pi^2} \int e^{-iq\vec{T}\cdot\vec{b}} T_{fi}(s, t) d^2 q_T \right] \quad (3.3.6)$$

with considering $t = -q_T^2$ [284].

The main problem of this approach, pointed out in [288], is that each Pomeron takes the entire energy of the hadron in cross-section calculations, which will ineluctably lead to violate the energy conservation, as several Pomerons are exchanged in one reaction. In addition, the theory is even more inconsistent that the energy is however still conserved for the particle production calculations in all the approaches based on the GRT [284].

3.3.3 Parton-Based Gribov-Regge Theory

The Parton-Based Gribov-Regge Theory (PBGRT) have been introduced to merge the two previous approaches by treating consistently both particle production and cross-section calculations, while conserving strictly the energy. The main motivation was to be able to account for soft processes as well as hard processes in the same global formalism, to have a complete description of any type of hadronic collision. The PBGRT is a theory exclusive to EPOS, hence one of the key ingredients which make this EG one of its kind.

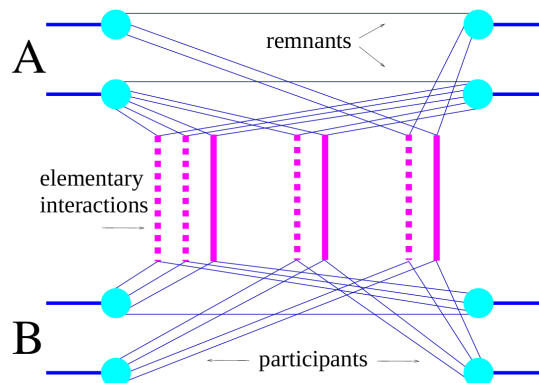


Figure 3.3: Diagram of a A-A collision viewed by the PBGRT formalism (original figure from [284])

One can see in Figure 3.3 a diagrammatic representation of a A - A collision in the PBGRT. In this diagram, the thick blue lines and blue circles represent nucleons of each colliding ion A and B , in the initial state on the left and in the final state on the right. All the tiny blue lines starting from the nucleons represent partons, that either participate to the collision via the exchange of Pomerons (drawn with vertical magenta lines), or are simply remnants. Note that in this framework, the Pomerons are different objects than in the GRT introduced in the last subsection, where the nucleon is not assumed to have any internal structure. This diagram gives a clear picture of the MPI nature of the PBGRT, where all the interaction represented are considered to happen instantaneously. The energy conservation is taken into account by ensuring that the sum of energy fractions carried out by all partons from each nucleon is equal to one : $\sum x_i + x_{remn} = 1$, for both nuclei.

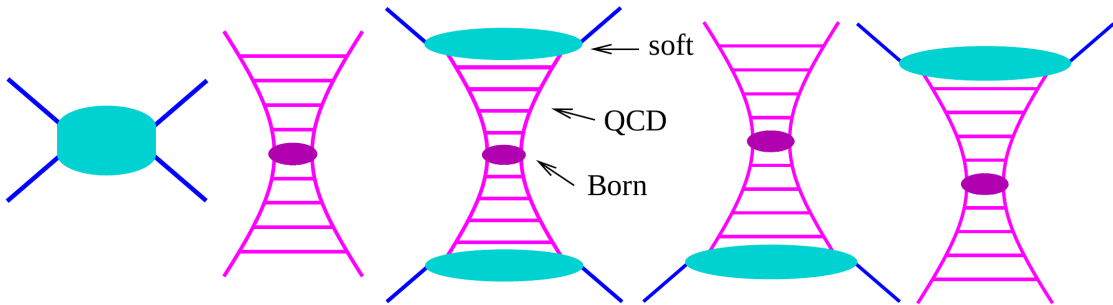


Figure 3.4: The five different structures of Pomerons considered in the PBGRT, corresponding respectively to (from left to right): G_{soft} , $G_{val-val}$, $G_{sea-sea}$, $G_{val-sea}$ and $G_{sea-val}$ [284].

In the frame of the PBGRT, the Pomerons are treated differently depending on the virtuality scale of the partons involved in the underlying scattering it represents phenomenologically. There are consequently five different kinds of Pomerons, represented schematically in Figure 3.4, based on three different types of contributions:

- **Soft contributions:** they correspond to low-energy scatterings, where the partons involved have a virtuality $Q^2 < Q_0^2$, taking $Q_0^2 \approx 1$ GeV. Being non-perturbative, the corresponding profile function G_{soft} cannot be calculated from first principles and has to be parametrised, done here in a similar way as in the GRT.
- **Hard contributions:** they correspond to high-energy processes, *i.e.* processes involving partons with virtualities $Q^2 > Q_0^2$; hence, it only applies to interaction between valence quarks. Here, the initial partons will go through successive perturbative radiations by increasing their virtuality, until reaching the $2 \rightarrow 2$ parton scattering (the so-called Born process) at the center of the parton ladder, where the virtuality is the highest. The corresponding profile function $G_{val-val}$ can then be calculated from perturbative quantum chromodynamics (pQCD), using the DGLAP equation [289] to model the virtuality evolution of the partons:

$$\frac{d}{dQ^2} \begin{pmatrix} q(x, Q^2) \\ G(x, Q^2) \end{pmatrix} = \frac{\alpha_s(Q^2)}{2\pi} \int_x^1 \frac{dz}{z} \begin{bmatrix} P_{qq}(\frac{x}{z}) & P_{qg}(\frac{x}{z}) \\ P_{gq}(\frac{x}{z}) & P_{gg}(\frac{x}{z}) \end{bmatrix} \begin{pmatrix} q(z, Q^2) \\ G(z, Q^2) \end{pmatrix}, \quad (3.3.7)$$

with colour indices not shown here. The functions $q(x, Q^2)$ and $G(x, Q^2)$ are respectively quark and gluons PDFs, which are not inputs but calculated within the theory. $P_{ij}(z)$ are the splitting functions, *i.e.* probability that a quark/gluon i with initial momentum fraction x splits into a quark/gluon j with final momentum fraction z plus another quark/gluon carrying a momentum fraction $x - z$.

- **Semi-hard contributions:** they correspond to all processes initiated by at least one sea quark or gluon, thus with virtuality $Q^2 < Q_0^2$, but with a virtuality which evolves to values high enough to enable perturbative calculation leading to a central Born process. Such contributions are represented by the profiles functions $G_{sea-sea}$, $G_{sea-val}$ and $G_{val-sea}$, and contain therefore both soft and hard parts.

In a hadron-hadron scattering, the total profile function $G_{1\mathbb{P}}^{h_1 h_2}$ is then a sum of all the contributions from each one-Pomeron-exchange partonic scattering.

In addition to the different possible structures of Pomerons, non-explicit in Figure 3.3, the latter ones can be either uncut or cut, as respectively represented by full and dashed magenta lines. The cut Pomerons represent the inelastic scatterings and can be assimilated to open parton ladders, as shown in Figure 3.5. They are used for particle production, and contribute to the total cross-section formula (3.3.8) with positive value of their corresponding profile functions. The uncut Pomerons, which represent the inelastic scatterings, or virtual parton emissions, are very important in the framework because they bring interference term in the cross-section calculation as they contribute with negative values of their corresponding profile functions.

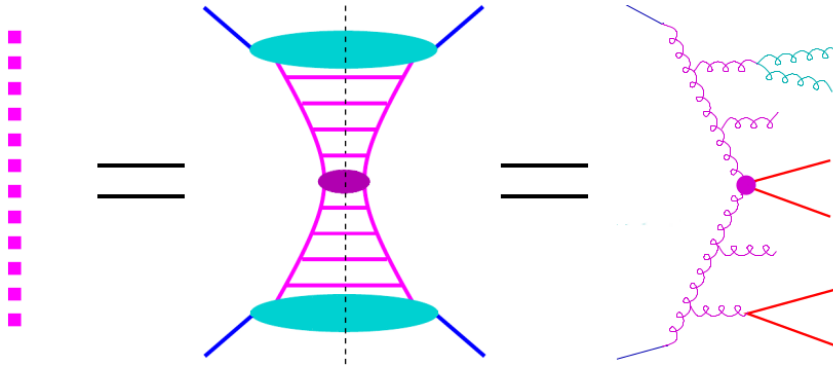


Figure 3.5: Schematic view of a cut Pomeron as a cut parton ladder, used to model particle production in the PBGRT. The blue lines are the initial interacting partons, the curly lines are gluons and straight lines quarks [290, 291]

In the case of A - A collision between two nuclei A and B , the total cross-section σ_{tot}^{AB} of the process given by the PBGRT is proportional to a sum over the nucleons of terms identical to the following simplified formula, integrated then over d^2b , based on equations (2.65) and (2.66) in [284]:

$$\begin{aligned} \sigma_{tot}^{AB}(s) \propto & \sum_c \int \prod_{i=1}^c d^2b_i \int \prod_{i=1}^c dx_i^+ . dx_i^- \times \left\{ \frac{1}{c!} \prod_{i=1}^c G(x_i^+, x_i^-, s, b_i) \right\} \\ & \times \sum_u \int \prod_{j=1}^u d^2b_j \int \prod_{j=1}^u dx_j^+ . dx_j^- \times \left\{ \frac{1}{u!} \prod_{j=1}^u -G(x_j^+, x_j^-, s, b_j) \right\}. \end{aligned} \quad (3.3.8)$$

In this equation, b refer to the impact parameter between two interacting partons, $x^\pm = (x^0 \pm x^3)/\sqrt{2}$ are the light cone momentum fraction of partons from projectile (+) and target(-), s the Mandelstam variable referring to the total energy of the collision, and c (respectively u) is the total number of cut (respectively uncut) Pomerons involved in the considered configuration. This important formula enables to calculate easily inelastic, elastic or inclusive cross-sections, by considering specific configuration of Pomerons, what is one of the strongest points of the PBGRT.

This subsection have exposed the main ingredients of the PBGRT, a successful MPI approach which treats energy sharing and particle production in a consistent way, by including both soft and hard scattering treated with pQCD calculations. It can also be applied to e^+e^- annihilation, using the string model inherited from VENUS [256], allowing then to test the hadronisation procedure (which will be introduced in the next subsection), and to $e-p$ scattering, in order to test the semi-hard Pomeron structure. All the details about the developments of the formulae presented in this section, the demonstrations of the AGK cancellations leading to cross-section factorisation for the different types of collisions and more can be found in [284].

The PBGRT suffers nonetheless from limitations, the most obvious one being due to the assumption of instantaneous interactions. It is by consequence only applicable for high-energy collisions, when the longitudinal size of the colliding hadrons is contracted enough so that all interactions do happen at the same time. As a simple illustration, making the reasonable conjecture that initial partons could interact more than once if the colliding hadrons were thicker than 0.5 fm, one can estimate that the relevance of the model starts to be questionable around energies down to ~ 25 GeV/A for HICs, or ~ 5 GeV for $p-p$ collisions. This result is obtained using simple relations from special relativity, *i.e.* $E = \gamma m_0 c^2$ and $\gamma = 2R/0.5\text{fm}$, with the liquid drop model formula $R = 1.2\text{fm} \times A^{1/3}$ to calculate the radius of a heavy ion with $A = 200$.

3.3.4 String Model

Another very important feature of the EPOS event generator is the string model, a phenomenological approach developed to treat hadronisation procedure. As already mentioned in subsection 1.2.2, the colour confinement cannot be treated dynamically with QCD-based methods ; one needs nevertheless to make a link between the partons discussed so far, and the hadrons observed in detectors.

This problem has been first treated in [292, 293], by assuming that the strong colour field between quarks can be modeled by a relativistic string. Such string is a one-dimensional object, which trajectory representing a surface in Minkowski space can be described by a four-vector x with two parameters σ and τ , representing respectively spatial coordinate along the string and proper time. Hence, requiring Lorentz invariance and gauge invariance on the dynamics of this string, one gets the following Lagrangian from which all the dynamics can be derived using the Euler-Lagrange equation:

$$\mathcal{L} = -\kappa \sqrt{(x' \dot{x})^2 - x'^2 \dot{x}^2}, \quad (3.3.9)$$

where x' and \dot{x} are the spatial and time derivatives of x [256]. The parameter κ is the string tension, which value is taken as ~ 1 GeV/fm, as usually taken to describe the tension of the strong colour field in most models .

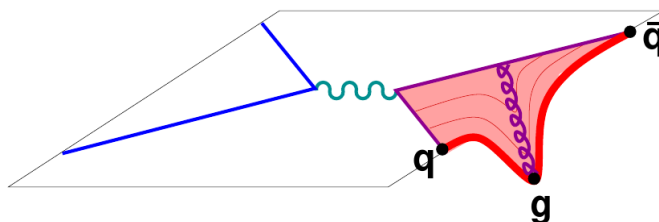


Figure 3.6: A kinky string formed by a $q\bar{q}$ pair, created after an e^+e^- annihilation, with an emitted transverse gluon [294].

In EPOS, the string is identified as a $q\bar{q}$ pair of the same flavour linked by gluons, forming thus a parton chain $q-g\dots-g-\bar{q}$. When simply formed of a $q\bar{q}$ pair, the string is a purely longitudinal object, while gluons can add a transverse dimension to it via transverse kinks. Such strings are referred to as "kinky strings", as shown in Figure 3.6 in the case of e^+e^- annihilation.

As the partons have some initial momenta, the string will be stretched as they expand, what will lead to increase its potential energy due to its tension. This mimics the linear potential of the strong interaction between quarks at relatively large distances (typically few fm). At some point, it is favorable to use this energy to produce a new $q\bar{q}$ pair, with the same flavour to not violate its conservation, rather than stretching even more the string. Thus the string will break into two segments, which will continue to evolve and fragment in turn, reducing their tension each time they will split. They will do so until they cannot break anymore: they can then be identified as hadrons, as shown in Figure 3.7. This process is often referred to as the "Schwinger mechanism" in the literature [295]. In order to account for baryon production, it is also possible to create $q_i q_j \bar{q}_i \bar{q}_j$ pairs at a breaking point, i, j being the flavour indices, with a lower probability than for a $q\bar{q}$ pair though. Although any quark flavour can compose the extremities of a string, only the light flavours u, d and s can be produced at the breaking points, for obvious kinematic reasons (the mass of a $c\bar{c}$ pair being of the order of ~ 3 GeV, compared to a $s\bar{s}$ pair with a mass of ~ 200 MeV).

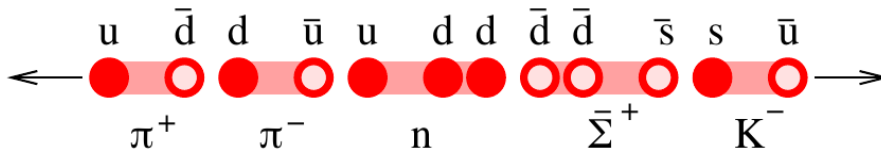


Figure 3.7: Schematic representation of the breaking of an initial $u\bar{u}$ string with the corresponding hadrons identified to the string segments obtained.

The breaking points along the string are generated following a so-called area law, based on [258]. The probability dP for a string to break at a given point (σ, τ) is similar to the exponential decay law of unstable particles:

$$dP = \lambda dA = \lambda \sqrt{(x'\dot{x})^2 - x'^2 \dot{x}^2} d\sigma d\tau, \quad (3.3.10)$$

where λ is the decay constant. Hence, the surface described by the string in the $(\vec{\sigma}, \vec{\tau})$ is randomly divided into sub-pieces of area dA , and the probability to break the string, in other words that the string along the line delimiting this area is proportional to the size of this area. In this respect, this string model is different from the Lund string model, which uses fragmentation functions [296].

The foundations of the full string model formalism used in EPOS can be found in [256], with further developments given in [297].

3.4 Generation of an event in EPOS

In this section, the complete procedure which is applied to simulate an event for a hadronic collision with EPOS 4 will be described, independently of the nature of the projectile and the target. It will therefore make the link between all the important ingredients presented previously, echoing to the general picture of HIC simulation described in figure 3.1 It will also summarise all the different features implemented step-by-step

over time in the model, as presented in section 3.2, giving so an updated picture of the event generation in EPOS.

The initial interactions between colliding hadrons are treated using the PBGR (presented in subsection 3.3.3), via the generation of a random configuration of Pomerons and the associated cross-section calculations. The cut Pomerons produce this way an initial distribution of partons, which will be used as a starting point for the event evolution. Heavy quarks are not present in the initial colliding hadrons, and can only be produced in the parton ladders at this early stage of the collision: either in space-like cascades, time-like cascades or in a Born process ($2 \rightarrow 2$ tree level diagram), as drawn in Figure 3.8. They are treated with their non-vanishing physical masses (taken as $m_c = 1.3$ GeV, $m_b = 4.2$ GeV), what will have an impact on splitting conditions in the parton ladder kinematics [291].

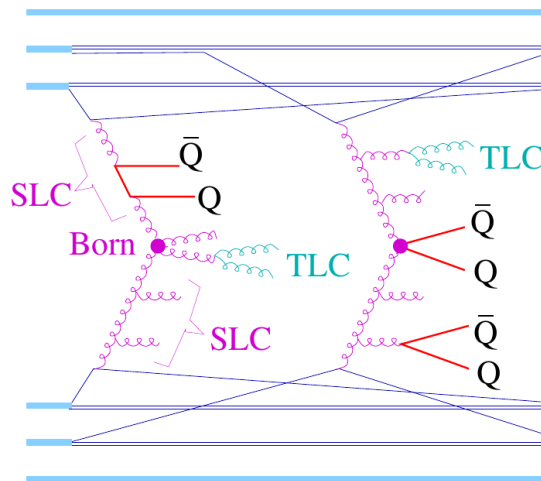


Figure 3.8: Illustration of HQs production in space-like cascade (SLC), time-like cascade (TLC) and Born process during the primary interactions of a A - A collision with EPOS. Thick blue lines represent nucleons, while thin blue lines are drawn for partons [291].

The increase of non-linear effects with the energy, *i.e.* re-interactions of ladder partons with projectile or target due to gluon saturation, is taken into account via a change of the constant Q_0 previously introduced. Each Pomeron is now getting a customised dynamical saturation scale $Q_s(x_{PE}, N_{conn})$ determining the transition from a hard to a soft treatment of the parton ladder, which depends on the Pomeron energy fraction x_{PE} and on the number of other uncut Pomerons connected to the same nucleons N_{conn} [269].

The initial partons produced in the ladders are then mapped to strings, which are always starting from (anti)quarks or (anti)diquarks from the projectile or target remnants; the kinematics of those partons provide initial conditions for the string dynamics. Also, one Pomeron corresponds to at least two strings, so that it remains a colour-neutral object. However, in A - A or even high-multiplicity p - p collisions, as multiple interactions happen at the same time, many strings can be superimposed on each other, as represented in Figure 3.9. In this situation, the strings might not be able to evolve and decay independently from each others; for that reason, a core-corona procedure is applied at some early time of the evolution τ_0 [264], which is a parameter of the model. It consists of checking, where the local string density ρ is beyond a certain critical value ρ_0 , if the

string segments have enough transverse energy to escape:

$$p_T^{new} = p_T - f_{E_{loss}} \int_{\gamma} \rho dL. \quad (3.4.1)$$

In this formula, p_T is the initial transverse momentum of the considered segment, $f_{E_{loss}}$ is a simply parametrised constant depending on p_T , and γ is the hypothetical trajectory of the segment [267]. Then, if the computed p_T^{new} value is positive, the string segment will escape and be part of the "corona", where it will continue its evolution and eventually fragment as described in subsection 3.3.4. An important feature in EPOS is the fact that target and projectile remnants are left off-shell, and will thus contribute to particle production at large rapidity as part of the corona [262].

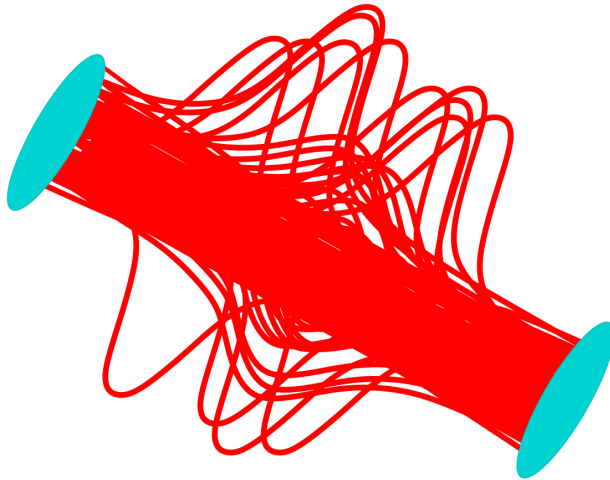


Figure 3.9: Schematic view of a collision with many strings (in red) exchanged between projectile and target remnants (in blue) : the dense part will compose the core, while the high- p_T segments will escape in the corona [294].

By opposition, if a segment doesn't have enough energy to escape, it will remain in the so-called "core". In order to reproduce the fluid-like behaviour of the QGP, the core will then evolve using viscous relativistic hydrodynamics. Such hydrodynamic treatment can be used because in this case, the mean free path of particles λ_{MFP} is small compared to the hydrodynamic lengthscale $L_{hydro} = (\partial_{\mu} u^{\mu})^{-1}$ (here the "real" particles considered are (anti)quarks). The latter can be interpreted as the length on which the system is considered homogeneous, u^{μ} being is the velocity four-vector. The energy-momentum tensor $T^{\mu\nu}$ and flavour flow vector N_q^{μ} are then determined from the string segments following the following formulae [263]:

$$T^{\mu\nu}(x) = \sum_i \frac{\delta p_i^{\mu} \delta p_i^{\nu}}{\delta p_i^0} g(x - x_i) \quad , \quad N_q^{\mu}(x) = \sum_i \frac{\delta p_i^{\mu}}{\delta p_i^0} q_i g(x - x_i), \quad (3.4.2)$$

where δp are the four-momenta of the string segments, q_i their net-flavour content (either quark flavours, or charges like B, Q and S), and $g(\dots)$ is a Gaussian smoothing kernel with a transverse width of 0.25 fm. This mapping is done by assuming a fast thermalisation of the dense medium, which is a strong assumption made in EPOS [267].

The evolution of the core is achieved event-by-event with the vHLLC code [298], which resolves the equations of relativistic viscous hydrodynamics $\partial_{\nu} T^{\mu\nu} = 0$ and $\partial_{\nu} N_q^{\mu} = 0$, using the Israel-Stewart approach [299]. This stage of the collision is what is generally

referred to as "Transport theory", as shown in figure 3.1. The equations of relativistic hydrodynamics are expressing the law of energy-momentum conservation and flavour conservation, and are general to both ideal and viscous relativistic hydrodynamics. However, in the presence of viscous effects (expressed via a non-zero value of shear viscosity $\eta/s = 0.08$), the previous tensor and vector have the expression [267]:

$$T^{\mu\nu} = \epsilon u^\mu u^\nu - (p + \Pi) \Delta^{\mu\nu} + \pi^{\mu\nu}, \quad (3.4.3)$$

$$N_q^\mu = n_q u^\mu + V_q^\mu, \quad (3.4.4)$$

where ϵ and p are respectively the energy density and the equilibrium pressure, $\pi^{\mu\nu}$ and Π the shear stress tensor and bulk pressure, V_q^μ are the quark charge diffusion currents, n_q the quark densities and $\Delta^{\mu\nu} = g^{\mu\nu} - u^\mu u^\nu$ the projector orthogonal to u^μ . In EPOS, there are two implemented choices of EoS for the hydrodynamic treatment of the core. The first one, "cross-over & 3 flavour conservation" (X3F), includes a cross-over transition between a hadron resonance gas and an ideal QGP, and is parametrised to match with lQCD calculations at vanishing chemical potentials (detailed explanations in [267]). The second one, proposed by the *Beam Energy Scan Theory* (BEST) collaboration, includes in addition of the cross-over transition at low μ_B a 1st order phase transition between hadronic gas and QGP with a CEP, which coordinates are left as free parameters [218].

Once the core has expanded, the regions which have successively been diluted down to an energy density $\epsilon_H = 0.57 \text{ GeV/fm}^3$ [270] will hadronise along given hypersurface of constant energy density. At this level, there are again two possibilities concerning the formalism chosen to achieve it. The first one is the Cooper-Frye procedure [266], also referred to as "thermal model", which amounts to generate a momentum distribution dN_i/d^3p of particles i at the hypersurface element $d\Sigma_\mu$ following the relation:

$$E \frac{dN_i}{d^3p} = \int_\Sigma d\Sigma_\mu p^\mu \times f_i(p^\mu u_\mu, T, \mu_i) \quad (3.4.5)$$

with $f_i(p^\mu u_\mu, T, \mu_i)$ the local Fermi-Dirac or Bose-Einstein distribution, depending on the nature of the considered particles i and on the local temperature and associated chemical potentials. The number of particles N_i is generated here following a Poisson distribution in the GC ensemble, as detailed in [265]. The second hadronisation process available is a microcanonical approach, in which particles are produced from the decay of fluid cells with effective volume and mass defined respectively by [294]:

$$V = \int_\Sigma u^\mu d\Sigma_\mu, \quad M = \int_\Sigma \sqrt{T^{\mu\nu} d\Sigma_\mu T_{\mu\nu} d\Sigma^\nu}. \quad (3.4.6)$$

Then, the probability to produce a n -hadrons distribution composed of n_α particles from each specie α is given, in the rest frame of the considered cell, by [271]:

$$dP = \frac{V^n}{(2\pi\hbar)^{3n}} \times \prod_{i=1}^n g_i \times \prod_\alpha \frac{1}{n_\alpha!} \times \prod_{i=1}^n d^3p_i \\ \times \delta\left(E - \sum E_i\right) \times \delta\left(\sum \|\vec{p}_i\|\right) \times \prod_A \delta\left(Q_A - \sum q_i^A\right). \quad (3.4.7)$$

The Dirac functions are here to ensure a strict conservation of energy, momentum and flavour currents (A indices referring here to conserved charges B, Q, S , with Q_A the total net-charge A of the cell and q_i^A the charge A carried by particle i). The strong point of this approach is that it converges to the GC limit for large effective masses M [271], and is therefore now the default one used in EPOS 4. Moreover, its use is of particular

importance in the frame of the study of fluctuations presented later in chapter 5, as it ensures both global and local conservation of charges.

At this stage, hadrons formed from both core and corona are still in a dense gaseous phase and can interact among each other. The hadronic cascades, or "hadronic rescatterings" from figure 3.1, are hence simulated with the *Ultra-relativistic Quantum Molecular Dynamics* (UrQMD) microscopic transport model [246, 247], where particles go through either elastic or inelastic scatterings. The cross-sections associated to each reaction available in UrQMD are coming from experimental measurements, or calculated via the *Additive Quark Model* (AQM) [300, 301]. These processes will last until the complete kinetic freeze-out of the system, when all the reactions cease, and the final-state hadrons will continue their free streaming, eventually undergoing some late weak decays. The event is then completely simulated.

When generating events with EPOS in order to compare simulations with experimental data, the analyses are generally performed directly on the list of final-state particles, without any further simulation of detector effects. The main reason is that the effort of estimating the uncertainties due to track reconstruction, particle identification and detector effects is generally made by experimentalists, as being intrinsic to their analysis procedure; such effects are taken into account in the systematic uncertainties of the presented results. This way of proceeding is generally acceptable but still shows some limitations, notably regarding the topic of centrality definition, as it will be discussed in section 4.2.

3.5 Objectives of the thesis

As a conclusion to these three chapters which settled the physical context and introduced my main working tool, I will describe in this section the main goals of this thesis. Focusing on the technical aspects related to the public release of EPOS 4 in the first place, I will then expose my research plans concerning the study of net-charge cumulants, mainly based on experimental results of the STAR collaboration from [211] and on some related investigation by the authors of [234].

3.5.1 Towards the release of EPOS 4

As already mentioned several times in this chapter, a new EPOS version has been under development in the past few years, named EPOS 4 [269, 271]. It has led to release publicly a stable version of this EG, containing all the main ingredients cited previously, including the most recent improvements on the theory and new features [268]. In this respect, an important work has been achieved on the structure of the code, its usability and connection to other tools, in order to make it easier to handle for any user.

The question of data management and analysis is of particular importance, as comparing the results of simulated events to experimental data is the fundamental purpose of EGs. It is not only essential for the developer, who has to ensure that its model can reproduce experimental observables in both qualitative and quantitative fashion, but also for the user, who needs to be able to exploit the results of the simulations with accessible tools.

Hence, having as primary objective the validation process of EPOS 4 in sight, but knowing it would be beneficial for users too once released, I have been responsible for developing an interface between EPOS and the analysis & comparison tool RIVET. Such task implied adding a new output data format to the code as a first step, and to go even further by inserting in the EPOS analysis framework a systematisation of RIVET's usage. It was obviously accompanied with the writing of corresponding documentation, concerning both user-related and internal developments, which is available online [268].

This first project will be presented in detail in chapter 4. However, the validation process of a general-purpose EG requires to compare its results to a large set of experimental data, from many different systems and energies, in order to adjust the parameters of the underlying model(s). Unfortunately, the number of analyses and corresponding data available in RIVET is limited, especially about HICs which is our main interest with EPOS.

As a consequence, I have also been responsible to check and rewrite preexisting analyses, as well as collecting more recent data and write the corresponding analyses, for the BES program energies.

The idea was to have a very complete set of analyses ready, to compare EPOS results with data from lower and lower energies, and see how reasonably can it be applied to this energy range despite the limitations of the PBGRTE discussed at the end of the subsection 3.3.3. Main results from this energy scan, using mainly conventional analyses but also the new EPOS+RIVET framework, will be presented in chapter 5.

Finally, another physics-related but rather technical problem which I have been in charge to solve has to do with some inconsistencies found in the definition list of decay branching ratios in the file `KWt/idky5.dt`. For a dozen of particles, mainly mesons for which there are not many information in [14], the sum of decay branching ratios was found to be significantly different from 1 ; more than 85% of branching ratio was even lacking for some of them in particular. These lacks of definition for decay possibilities would obviously produce, at the best, decays with inconsistent proportions of outgoing particles, but could at worst lead to unexpected behaviours of the code in the management of decays. Although the particles involved are not produced massively in collisions, it is important to keep a consistent picture on all physical aspects for a general-purpose EG. Hence, I have updated the list of decay channels for the problematic particles, considering only channels with at most five outgoing particles as EPOS is not technically designed to manage decays with more products. I have especially taken into account the Clebsch-Gordan coefficients in the calculation of branching ratios for charge symmetric channels. For quarkonia with lacks of information in [14], I have followed the Pythia method by completing the ratios up to 1 via $X \rightarrow gg$ decay channels, replacing gluons by $q\bar{q}$ pairs as EPOS does not have any routine to hadronise gluons in the final state. I used this occasion to reorganise completely the file by sorting it in ascending order of particle IDs, for readability, and correct some double declarations discovered during the operation.

3.5.2 Towards the study of net-charge cumulants

Using the events we generated for the BES energies as part of the validation process of EPOS 4, I will focus my physical study on the 2nd order cumulants of net-charges

B , Q and S and corresponding net-particles proxies p , π and K in Au-Au collisions. This work is initially based on two publications, both already introduced in subsection 2.3.3. As a reminder, the first one contains measurements of (co)variances and their ratios for particle net-cumulants made by the STAR collaboration [211]. The second one is a study on the breakdown of hadronic contribution to the net-charge cumulants, with a proposition of enhanced proxy ratios compared to the ones used by STAR [234].

The first steps of my study will consist of looking at the importance of the so-called CBWC when calculating (co)variances of net-particle number as a function of the number of N_{part} directly, as a cross-check with some previous studies.

In order to bridge a gap between the experimental results and theoretical studies led on the topic in recent years, I will use EPOS to measure the 2nd order cumulants of conserved net-charges, and of net-multiplicities for hadronic species of interest : π^\pm , K^\pm , p , \bar{p} , Λ , $\bar{\Lambda}$, Ξ^- , $\bar{\Xi}^+$, Ω^- and $\bar{\Omega}^+$. Using an event generator enables indeed to get rid of identification problems, whether for the detection neutral particles or the reconstruction of short-lived particles. Thanks to this ability, it allows to calculate directly the fluctuations of conserved charges carried by hadrons in a given kinematic region.

Hence, I will confront the results obtained with STAR proxies against the enhanced proxies from [234], presented in subsection 2.3.3. I will examine how they differ from each other, as well as their respective change with the variation of the collision energy, compared to the cumulants of corresponding net-charges.

Another strong point of working with an event generator is that one can have access to the whole history of the events simulated. With this feature, and more particularly the modular conception of EPOS, it is possible to investigate the impact of the different stages of the collision on final-state observables.

In this regard, I will try to quantify the impact of the hadronic cascades on the observables of interest as well as on some of the enhanced proxies, as motivated in subsection 2.3.3. It will be achieved by comparing their measurement from simulations, before and after this final stage of the collision, modeled via UrQMD in EPOS.

Furthermore, one of the peculiarities of EPOS is the use of a core-corona procedure when simulating the collisions, as described in section 3.4. In this picture, the core corresponds to a nearly perfect fluid which emulates the behaviour of a QGP droplet, while the corona correspond to a pure hadronic stage modeled with the string approach.

Taking advantage of this feature, I will estimate for all the observable mentioned previously the proportion of the signal originating from the core, as it is the part of the system which would go through a phase transition and thus imprint potential thermal fluctuations.

The results obtained from all the previous points will be presented and discussed in the chapter 5.

Before moving on, let still clarify already why not using the BEST equation of state containing a CEP, newly implemented in EPOS, to investigate directly the effects of criticality. The issue is that conventional relativistic viscous hydrodynamics approaches, such as the one used in EPOS [298], are all about averaged quantities at a mesoscopic scale (*i.e.* intermediary between microscopic and macroscopic). Such description is only relevant when fluctuations of the quantities in question are negligible in comparison to their average. Consequently, such frameworks are not suited to describe the rise of important thermal fluctuations caused by the presence of a CEP, and doing so would require to include stochastic terms to the dynamical evolution equations, what is currently a challenging problem in HICs simulations [222]. In fact, a first study has already been made by incorporating the BEST equation of state into EPOS, and comparing then simulations with and without a CEP. It has shown no significant differences in basic observables such as p_T spectra nor in the results of cumulant analysis, even when varying the location of the CEP, what tends to confirm the previous argument [270, 302].

Contents

4.1 RIVET	68
4.1.1 General presentation	68
4.1.2 The benefits for EPOS	71
4.2 How EPOS works in practice	72
4.2.1 Structure of the repository	72
4.2.2 Running simulations	73
4.2.3 Using on-the-run analyses	75
Writing an analysis in EPOS	75
Centrality definitions in analyses	76
4.3 Integration of RIVET into EPOS analysis framework	77
4.3.1 Producing HEPMC files	77
Structure of HEPMC event records	77
Production of HEPMC output files with EPOS	78
Content of the EPOS HEPMC output	81
4.3.2 Automating the usage of RIVET	83
Adapting the experimental data format	83
Using RIVET from the EPOS analysis system	84
4.3.3 Dealing with centrality calibration	86
4.4 Summary of the technical work	86

With the public release of any new version of an EG, comes the necessary task to fix properly all the free parameters of the underlying models. As examples, we can cite for EPOS the parameters necessary to describe the soft Pomerons amplitudes in the PB-GRT (discussed in subsection 3.3.3), or the ones used to define the saturation scale of the semi-hard Pomerons. For general-purpose EGs like EPOS, this process can however become complicated, because they generally contain many free parameters. Moreover, checking that the current parametrisation work well means running simulation for many different systems at many different energies, the aim being to see how good particle production can be reproduced, by comparing the results of simulation with several observables measured experimentally. For EPOS in particular, we talk about collisions from RHIC to LHC energies, *i.e.* from few dozens of GeV up to thousands of TeV in the center-of-mass, for all systems (p - p , p - A or A - A).

In order to help in this operation, RIVET is the ideal tool by essence, because of its purpose to automatise comparison between EGs and experimental data. Consequently, I will explain in the present chapter why and how I have adapted EPOS 4 to make it compatible with RIVET, and especially why and how I even integrated the latter in the analysis framework of EPOS to automatise its operation. To this end, I will introduce RIVET in section 4.1, describe how it works and motivate why it is useful not only for us, EG developers, but also for the users. I will give some technical explanations on the functioning of EPOS 4 in section 4.2, necessary to describe then in section 4.3 all the technical work I achieved to include RIVET in the EPOS 4 analysis system. Finally, section 4.4 will summarise the work presented beforehand by explaining how to effectively run EPOS with RIVET. Beyond the necessity to develop an analysis tool which is useful for the aforementioned tasks, this new functionality will then be useful for the study presented in chapter 5, in order to ensure that EPOS reproduces properly particle distributions in the simulated events used. It has also been shown to be useful in studying CBWE on the cumulants of net-particle multiplicities which are studied then.

4.1 RIVET

Robust Independent Validation of Experiments and Theory (RIVET) is a toolkit made of a collection of libraries, developed for over a decade now for MC event generators validation and tuning [303]. The main philosophy behind RIVET is to offer an easy-to-handle, automatic and standardised tool for analysis and data comparison. Initially created to study mainly SM physics and PDFs in e^+e^- and p - p collisions, it has developed over a wide variety of applications since. Recently, new features have notably been implemented in order to facilitate the use of heavy-ion analyses [304], expanding thus its range of applicability. Being the main thematic of research for EPOS, I will hence explain in this section the motives of using RIVET, after a brief presentation of its structure and actual functioning.

4.1.1 General presentation

RIVET is principally based on C++ libraries and Python programming and command interfaces. It comes with a collection of pre-encoded and functional analyses, each analysis corresponding to one given publication. Effectively, the user has to provide the data to analyse (generally from EG simulations) in specific files written in the standard of *High-energy physics Monte-Carlo* (HEPMC) package. In such files, the history of each event is recorded under text format, with information on beam and projectile, vertices and particles produced, etc. (more details will be given in subsection 4.3.1). The user can

then run the analysis of their choice on it, what will reproduce the distributions shown in the corresponding publication, but based on the provided data. Finally, the user can display the results in plots, where they will be compared to the actual experimental data from the publication, as the binning used in the analyses is based on the latter ones.

Hence, each analysis package comes with 4 different files, all named the same way (*e.g.* "**ANALYSIS_NAME**") but with different extensions:

- **ANALYSIS_NAME.cc** contains the analysis itself to be run on EG data, written in C++ with the help of RIVET dedicated libraries;
- **ANALYSIS_NAME.yoda** contains the experimental data from the figures shown in the publication (for simplicity, this file is synchronised with the HEPData website¹ when data are available on it);
- **ANALYSIS_NAME.plot** contains the information of the plots from which experimental data plans to be compared to (axes labels and scales, title and more if necessary);
- **ANALYSIS_NAME.info** contains general information on the RIVET analysis, such as its author(s), the publication of reference, etc.

One of the strengths of RIVET is its ease of use : very few commands are necessary to run analyses and display the results, as will be presented in the following paragraphs. The aim is not to give complete and exhaustive explanations on how to run RIVET, but to show concretely the few commands that will be useful in the automation of RIVET use, described in subsection 4.3.2. To find more documentation, reference publications, a list of available analyses or even tutorials, one can visit the RIVET website².

In the standard case of a previously available analysis "**ANALYSIS_NAME**", the user can simply run it on the events recorded from simulations (stored in a file which will be called **DATA.hepmc**), specifying if necessary a name for the output file with the flag "-o" (for this example **ANALYSIS_EG.yoda**):

```
$> rivet DATA.hepmc -a ANALYSIS_NAME -o ANALYSIS_EG.yoda
```

The results of the analysis are stored in a **.yoda** extension file, *Yet more Objects for Data Analysis* (YODA) being a package of classes delivered with RIVET, used to manage histogramming. Then, in order to display the results, the user can run the following command :

```
$> rivet-mkhtml ANALYSIS_EG.yoda -o ANALYSIS
```

which will produce one data file for each histogram of the analysis, and display the plots with the results of the analysis compared to the corresponding experimental results under PDF and PNG formats. It will, in addition, generate a plot web page which gather all these plots. The data files thus created (with **.dat** extensions) contain results as (x, y) values, plus the associated uncertainties, unlike the YODA file resulting from the analyses, which contain the complete information on the filling of histograms (more details will be given in subsection 4.3.2).

When dealing with substantial numbers of events (basically millions, when trying to have similar statistics than for experimental results), the user might want to run

¹<https://www.hepdata.net/>

²<https://rivet.hepforge.org/>

the analysis in parallel on several HEPMC files. There is, in this case, one additional command to merge the multiple files obtained from the same analysis (and, by extension, the results they contain for different sets of events) into a unique file :

```
$> rivet-merge ANALYSIS_EG-1.yoda ANALYSIS_EG-2.yoda [...]
-o ANALYSIS_EG.yoda
```

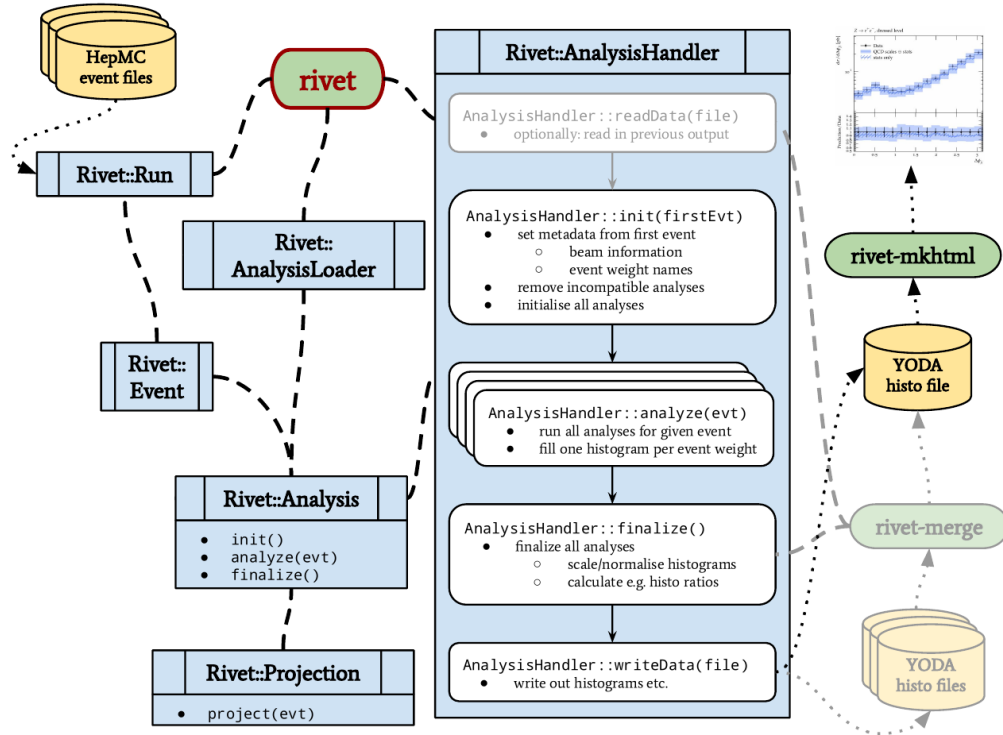


Figure 4.1: Schematic representation of the principal components of RIVET acting in the data flow from event record to results of the analysis, with the links between classes (in blue), files (in yellow) and the different commands (in green) used to execute it [303].

A summary of how RIVET works, linking commands and files from the different steps cited previously with the corresponding classes, is shown in Figure 4.1.

Last but not least important point, for a user interested into heavy-ion analyses, is the necessity to provide a centrality calibration in order to make the analysis run successfully (as for some p - p analyses dealing with high-multiplicity events). The user thus has to run the calibration analysis on the events, and to provide the resulting distributions (stored in a file called **CALIB.yoda** for this example) as an input for the desired heavy-ion analysis, preceded by a "-p" flag:

```
$> rivet DATA.hepmc -a ANALYSIS_NAME:cent=GEN
-p CALIB.yoda -o ANALYSIS_EG.yoda
```

One shall notice there the complementary instruction indicated after the analysis name, *i.e.* ":cent=GEN". This instruction indicates in which way the calibration has to be done:

- "cent=EXP" to define centrality classes based on provided experimental multiplicity distribution (when available), as described in section 2.2;
- "cent=GEN" to define centrality classes based on generated multiplicity distribution;
- "cent=IMP" to define centrality classes based on the generated impact parameter distribution.

In light of these explanations, one might now understand the crucial role that is playing RIVET in the physics of colliders, by offering a dedicated comparison tool. It is indeed of interest for the theoretical community and especially EG developers, as already discussed, because it propose a simple way to compare the results of their simulations to experimental data for the validation of the models. It can also be used as a way to dialog with experimental collaborations in need of predictions for their publications, as it is customary when publishing new measurements results. The collaborations could for instance provide a functional RIVET analysis to developers of the EGs they want predictions from. While binning is usually automatically based on the experimental data distributions, RIVET offers the possibility to define a customised binning for histograms used in analyses what allows in such situations to deliver the analysis without the experimental data to be published, hence preserving their confidentiality. On a purely experimental level, and additionally to the powerful toolkit it offers to perform analyses, RIVET even offers for experimental collaborations a good alternative to save, and maintain the usability of their analyses.

Finally, RIVET is being developed by a dedicated team of scientists from various fields of HEP, who know the different needs proper to each field. Being easily reachable via the RIVET GitLab project ³, they are open to any suggestions to improve the toolkit and broaden its possibilities. However, they highly rely on contributions from outside people to carry out the tedious task of expanding the analysis catalogue. RIVET is thus a tool developed for the HEP community, but which also needs contributions from community to keep growing and to offer features answering its needs.

4.1.2 The benefits for EPOS

Although EPOS contains its own event-by-event analysis system integrated in the code itself, which will be introduced in subsection 4.2.3, there are several advantages to adapt it for RIVET's use.

First of all, there are clear benefits for us, EPOS developers. By offering a large catalogue of analyses, it can be used to test our EG during the validation phase as said before. But more importantly, it frees us from having to write the analyses by ourselves, especially the elaborated ones like flow analyses. Even though such things can be done in EPOS analysis framework, we ensure that the analysis is made exactly as it should when using RIVET. We don't have to take care then about all tiny details on the methods and kinematic cuts applied, which are not always clearly explicit in the publications.

There are also multiple benefits of adapting EPOS to RIVET for users. Primarily, it offers an easy way to compare the simulated events to experimental data without having to handle EPOS analysis framework or ROOT, for which EPOS can also produce compatible event records. RIVET enable users either to run some available analyses, or to write their own analyses quite easily. Secondly, the new output format necessary for such compatibility, the HEPMC files, is in a simple text format which is easily readable. It could even be used directly to make quick analyses via simple scripts, in whatever language, for pedagogical purposes. Finally, we hope that proposing such compatibility will encourage experimentalists to systematically submit their analyses to RIVET when publishing new results, for all the reasons exposed at the end of the last section.

³<https://gitlab.com/hepcedar/rivet>

Nevertheless, RIVET suffers from limitations because of its dependency on contributions from user to submit analyses. For instance, the fact that heavy-ion dedicated tools were developed only recently can be seen by the small number of heavy-ion analyses available, compared to analyses for p - p collisions. Moreover, the different experimental collaborations are not all equal regarding the coverage of their analyses in RIVET. One can see in Figure 4.2 that the coverage percentage vary from experiments to experiments. The number of available analyses is especially low for RHIC experiments in particular, which explains why we had to use EPOS analysis system to check the validity of EPOS 4 in the energy range of the BES program.

Key	ALICE	ATLAS	CMS	LHCb	Forward	RHIC	SPS
Rivet wanted (total):	278	334	447	269	17	469	64
Rivet REALLY wanted:	36	37	89	8	0	1	0
Rivet provided:	26/304 = 9%	189/523 = 36%	103/550 = 19%	17/286 = 6%	8/25 = 32%	8/477 = 2%	4/68 = 6%

Figure 4.2: RIVET analysis coverage compared to the total number of publications for LHC, SPS and RHIC experiments [305].

4.2 How EPOS works in practice

Having motivated the reasons that led to integrate RIVET in EPOS analysis framework, I will now introduce some technical elements about EPOS operation and the structure of the code. These explanations are provided to apprehend how EPOS works, and therefore to understand how RIVET has been integrated, as I will present in section 4.3. They might also be useful to the reader when the implementation of the net-cumulants analysis necessary to the main study of this thesis will be discussed in appendix C. Nevertheless, only the pieces of the code that matters for the following discussions will be introduced, hence not all details of the structure and functioning of EPOS will be mentioned.

4.2.1 Structure of the repository

I will introduce step by step the different pieces of the code structure, as displayed in Figure 4.3. As a consequence, I will not repeat each time the complete path of the file I will be citing, considering this Figure as a reference for the reader. Let me however notice that the structure of the repository, as I will describe it here, can be subject to changes after potential future developments of EPOS 4.

The main directory, that I will call **EPOS/** here, contains multiple folders and, among others, the script **epos** which is called to execute the program. The **EPOS/src/** folder is of particular importance since it contains the source code, and in particular the file **main.cpp** which is the spinal column of the program, as it calls all the main

functions and subroutines of the program. The **EPOS/src/KW/** folder contains several Fortran files with the subroutines composing the rest of the skeleton of the code. In **EPOS/src/KWb/** are principally stored C++ files in which are defined the functions used to manage the record of the events in the ROOT format, and consequently where I will store the equivalent functions to produce the HEPMC output files (see subsection 4.3.1). In the **EPOS/src/KWt/** folder are tabulated important informations about physics: the list of defined particles and their properties in **idky5.dt**, the definitions of all decay channels for each particle in **idt.dt** (discussed with more details in appendix ??). Among other things, it also contains all the centrality calibration information for each system at each simulated energy, in files called **iclSYSeng.optns**, where "**SYS**" refers to the system simulated and "**eng**" the energy (*e.g.* **iclAuAu200.optns**). I will come back on the content of those files in subsection 4.2.2, when discussing the way we deal with centrality in HIC simulations.

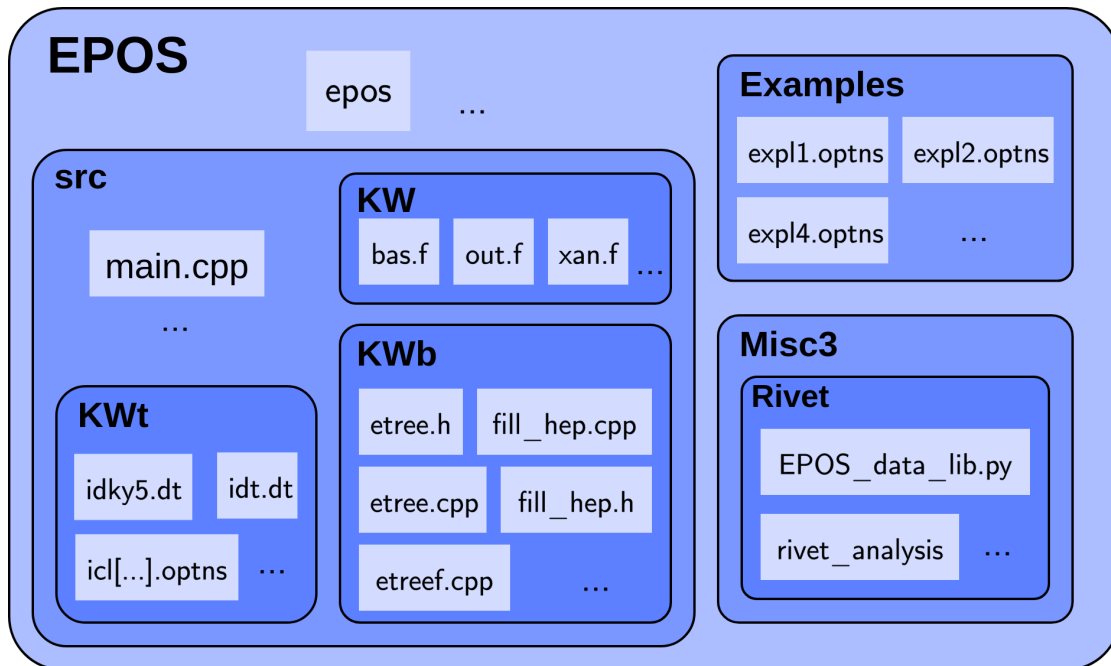


Figure 4.3: Non-exhaustive structure of the directories containing the EPOS code.

4.2.2 Running simulations

In order to run simulations with EPOS, one has to define the parameters of the collision in a file with a **.optns** extension. Some examples of such files can be found in the **EPOS/Misc2/** repository, under the names **expl[...].optns**. I will discuss here a basic example of a file defining simulations of Au-Au collisions at an energy of $\sqrt{s_{NN}} = 200$ GeV, thus called **AuAu200.optns**.

The very first thing to do is to define the type of system to collide, as EPOS can simulate any type of hadronic systems but also e^+e^- and $e-p$ collisions as well (see last paragraph of subsection 3.1.1). Once having defined the nuclei to collide, the energy is set in GeV, in the center-of-mass of a nucleon pair. Even though for hadronic systems the particles collided are traditionally nuclei, EPOS really offers the possibility to collide any hadron like pions, kaons, etc. In the same way, EPOS can not only simulate e^+e^- collisions but also $\mu^+\mu^-$ ones. An example is displayed in figure 4.4.

```

application hadron    ! hadron-hadron / hadron-nucleus / nucleus-nucleus
set laproj   79      ! projectile atomic number
set maproj   197     ! projectile mass number
set latarg   79      ! target atomic number
set matarg   197     ! target mass number
set ecms     200     ! sqrt(s_NN)

core         off     ! core/corona activated (full) or not (off)
hydro        off     ! hydro activated (hllc) or not (off)
eos          x3ff    ! choice of EoS (x3ff / best)
hacas        off     ! hadronic cascade activated (full) or not (off)
set nfull    1       ! number of events
set nfreeze  1       ! number of freeze out events per hydro event

xinput KwT/iclAuAu200.optns ! centrality classes definition
set centrality 0           ! 0=min bias

nodecays 110 20 end ! suppressed decays

fillTree4(C1)          ! to record events in ROOT Tree output

```

Figure 4.4: Example of instructions used in a `.optns` file to define a simulation for Au-Au collisions.

One can choose to activate or not the different features of EPOS presented in section 3.4, *i.e.* the core-corona separation with hydrodynamical evolution of the core, and the hadronic re-scatterings simulated with UrQMD. In case the hydrodynamics is activated, one can choose which EoS to use for the simulation, between the two introduced in section 3.4.

To define the number of events simulated in the run, one has to set `"nfull"` and `"nfreeze"` so that the total number of event generated will be equal to `nfull` \times `nfreeze`. The `"nfull"` value corresponds to the number of different initial conditions simulated, and `"nfreeze"` to the number of hadronisation and subsequent evolution of the system for each initial evolution simulated. This feature is notably used in the case of simulations using hydrodynamics, which can be extremely time-consuming in term of computing resources. It is thus customary to set for instance `"nfull"` to 4 and `"nfreeze"` to 5 for Au-Au collisions simulated with hydrodynamics at $\sqrt{s_{NN}} = 200$ GeV, meaning that 5 complete events are generated out of each of the 4 different prior hydrodynamic simulations. For simulations without hydrodynamics, `"nfreeze"` is generally left to 1 though.

There is also a possibility to specify some particles for which the decay will be blocked, and that will then be considered as final-state (FS) particles if produced during the collision, using the `"nodecays"` instruction. Such possibility allows to apply a perfect feed-down correction to specific hadronic species suffering from weak decays, or to keep track of short-lived particles of interest such as quarkonia. Note that the numbering scheme for particle IDs in EPOS is different than the usual Particle Data Group (PDG) numbering scheme [14]. Even though the philosophy is the same, the main difference is that up quark comes with $ID_{EPOS} = 1$ and down quark with $ID_{EPOS} = 2$, while being the contrary in the PDG numbering scheme. Hence, in the previous example, particles for which the decay is blocked are π^0 ($ID_{EPOS} = 110$) and K_s^0 ($ID_{EPOS} = 20$, as 230 is being used for K^0).

In order to manage the centrality for HIC simulations, one can set the value of the "centrality" variable in the `.optns` file to -1 to have a random generation of the value of the impact parameter b . If set to 0, the random value of b will be generated ensuring at least one hadronic interaction in the collision (minimum bias). Otherwise, one can at last assign it to a value from 1 to 20, corresponding to 5% based centrality classes going increasingly from the most central collisions ("centrality 1" for 0-5% collisions) to the most peripheral ones ("centrality 20" for 95-100% collisions). These centrality classes are based on the impact parameter distribution, and are defined in `EPOS/src/KWt/icl[...].optns` files, which are read via the "xinput" command

One can finally run simulations by calling the `epos` script, and providing as an argument the name of any `.optns` file (without the extension though), like:

```
$> epos -root AuAu200
```

The "-root" flag is optional and indicates to save the ROOT file in which the events are recorded, as the "fillTree4()" instructions is only used to activate the recording.

4.2.3 Using on-the-run analyses

As mentioned in the previous section, EPOS comes with an "on-the-run" event-by-event analysis system, mainly defined in Fortran subroutines written in `EPOS/src/KW/xan.f`. It allows to run analyses on the simulated events without necessarily having to store those events in any output file, which is fast and really convenient for developers when performing tests with the model. Nevertheless, there is still a possibility to run these analyses on events pre-recorded in ROOT files, as it can be useful to perform analyses on some events for a second time (*e.g.* for centrality calibration, discussed earlier).

Writing an analysis in EPOS

To use this tool, the analyses have to be written directly in the `.optns` file, after the settings of the events simulated. A simple analysis is shown here in figure 4.5, used to reproduce a p_T distribution like the ones which will be presented in chapter 5. Some other examples are also available in the `expl[...].optns` files of the `EPOS/Misc2/` folder.

```
beginhisto
  histogram pt numpt1 212 0 12 60
  idcode 120
  noweak
  trigger absrap 0 0.1
  set hisfac 5
  trigger bimevt bim00 bim05
endhisto
beginwrite
  openhisto name AuAu-pt-yield-00to05-pip
  [[histoweight writearray 3]]
  closehisto plot 0
endwrite
```

Figure 4.5: Example of an analysis defined in a `.optns` file to get a p_T distribution of π^+ .

Between the "**beginhisto**" and "**endhisto**" shall be specified all the characteristics of the analysis. In first place, after the "**histogram**" word, has to be defined what kind of distribution is desired : successively x and y variables. Next are defined normalisation number (details in **expl4.optns**), the lowest and greatest abscissa values, and the number of bins wanted. Here, the normalisation value "**212**" means that each bin of the histogram will be normalised by $1/2\pi x$, its own width and by the number of events triggered for this analysis. The "**idcode 120**" instruction means that only particles with $ID_{EPOS} = 120$, *i.e.* π^+ , will be considered; "**noweak**" indicates to ignore all the particles coming from weak decays (acting as a perfect feed-down correction). Next come the triggers, here applied on the absolute value of rapidity of the particles of interest, and on the centrality of the event. The "**hisfac**" is just a normalisation factor, accounting here for the $1/dy$ normalisation. Finally, the "**bimevt**" instruction indicates to consider only events in a certain centrality class, which lower and higher bounds are specified by the two next variables "**bim00**" and "**bim05**". To summarise, in light of the previous explanations, this example will create a p_T distribution ($d^2N_{\pi^+}/2\pi p_T dp_T dy$) of exclusive π^+ within $|y| < 0.1$, for events within centrality class 0-5% based on impact parameter calibration, distributed in 60 bins between $p_T = 0$ and $p_T = 12$ GeV.

Everything written between "**beginwrite**" and "**endwrite**" will then be registered as is in the **.histo** output file produced, except the instructions within the brackets. Those instructions indicate to write the results of the analysis as a 3-column array, and then the weight associated to the current histogram. While the two first columns always contain x and y values of the bins, the content of the third column and of the weight depends on if the result of the analysis is an histogram (simple distribution for a given x variable) or a profile histogram (averaged y -values for each x):

- for histograms, the "**histoweight**" correspond to the number of events triggered by the analysis, and the third column of the results array contains the absolute statistics uncertainty y/\sqrt{N} (N being the number of entries in the considered bin);
- for profile histograms, the "**histoweight**" is set to 0 and the third column of the results array contains the number of entries in the current bin.

Those differences are due to the fact these different types of histograms are added with each other, as the analyses are run event-by-event. They are especially important for the explanations on the integration of RIVET in the EPOS analysis framework, discussed in the next subsection.

In the end, all the results obtained from the analyses are stored in one **.histo** file, as mentioned in the previous paragraph. Using a dedicated script based on the HIGZ package from the CERN tool *Physics Analysis Workstation* (PAW) [306], we can display the results of all the distributions stored in such files, easily comparable with experimental data (stored in other dedicated **.histo** files) by adding few instructions. This a really fast tool which stores all the plot under a unique PostScript file, which is convenient when one wants to have a quick overview of results for a large panels of observables, so is really useful for developers.

Centrality definitions in analyses

Coming back to the analysis itself, one could however wonder why using b -based centrality definitions to run an analysis that is intended to be compared with experimental results. Indeed, in experiments, centrality is always defined after a given distribution measured in a given kinematic region (explained in subsection 2.2.1). Nevertheless,

because not all experiments use the same distributions to determine centrality classes (sometimes done using mid-rapidity particles multiplicity [136], some other times using forward and backward particle multiplicity [307]), we use b -based centrality classes such that these definition are the same whatever data we compare our results with.

Independently from experimental results, a b -based centrality definition is also useful when one wants to compare the effect of using hydrodynamics or not in our simulations, or in other words to compare a pure string model with a core-corona approach to model HICs. As a matter of fact, using an hydrodynamical expansion of the core will lead to produce less particles in the FS, for the same initial conditions, than with a pure string model. This is due to the fact that, with a flowing medium, part of the energy is consumed by the expansion of the fluid. Therefore, in order to ensure to compare the same events between them, it is mandatory to use b -based centrality classes for studying such effects.

4.3 Integration of RIVET into EPOS analysis framework

In the current section, I will start by explaining how EPOS was upgraded in order to produce event records under HEPMC format, enabling thus to perform RIVET analyses on EPOS events. Moreover, motivated by the fact that RIVET provides a constantly growing library of analyses with their corresponding experimental data, I will detail then how it has been integrated to the analysis framework of EPOS. By "*integrated*", I do not mean that RIVET's code has been merged and comes naturally with EPOS when installing the latter. The goal was to find a way to get results from RIVET's analyses directly after a run, in the same `.histo` file in which we get results from EPOS analyses, without having to save the HEPMC output file and run RIVET afterward. This way, results from RIVET's analyses can be displayed in the same PostScript file containing result from all other analyses, as explained in subsection 4.2.3.

4.3.1 Producing HEPMC files

The first step to make EPOS compatible with RIVET is of course to produce files under HEPMC format, to store the records of simulated events. To do so, I have taken as a basis a previous attempt to produce such files by Maria Stefaniak during her PhD [270]. Nevertheless, before explaining how I achieved this, I will briefly describe the content of the HEPMC files in order to present what information has to be provided, and how they are structured.

Structure of HEPMC event records

The HEPMC files contain event records under text format, and are structured following lines. Each line starts with a certain character, indicating to what are related the information stored after. Here is a summary of the most important ones, with some of their content (descriptions are not exhaustive, see [308] for more details):

- "E" lines define the events, with information on the event number, the number of vertices recorded in the event, the barcodes of colliding particles, etc.;
- "C" lines contain information on the cross-section of the reaction (in picobarn);
- "H" lines contain information necessary for HICs such as the number of participants for projectile and target ($N_{part}^{targ/proj}$), the number of proton & neutron spectators

$(N_{spec}^{p/n})$, the number of nucleon-nucleon collisions (N_{coll}), or the impact parameter b ;

- "V" lines contain information on vertices, successively their barcode, ID, (x, y, z, c, τ) coordinates, the number of orphan incoming particles and the number of outgoing particles;
- "P" lines contain information on particles, *i.e.* their barcode, ID_{PDG}, (p_x, p_y, p_z, E) coordinates, mass, status (whether the particle is a beam particle, a stable FS particle or will decay), and the barcode of any vertex which can have the considered particle as an input.

An example of the content of such file is shown in figure 4.6, coming from a file produced with EPOS for a peripheral Pb-Pb collision ($b = 13.45$ fm) at 2.76 GeV/A. The event contain 154 vertices, with colliding particles having barcodes 10001 and 10002 (as it is customary). From the original vertex, located at $(0, 0, 0, 0)$, are going out 2181 particles, while taking two particles in. Those two particles are of course the particles 10001 and 10002, as indicated by the vertex barcode -1 at the end of their lines, and by their status number, "4", which corresponds to beam particles.

After each vertex are listed all the particles going out from it, with a status 1 for particles considered as stable FS particle. The hadrons or leptons which later decay through Standard Model processes are labeled with a status 2 and with the barcode of their decay vertex, which are written afterward, followed at their turn by the corresponding outgoing particles. Here, we can see that the colliding lead nuclei (with their atomic and mass numbers explicated in their ID_{PDG} = 1000822080) are followed by FS protons and neutrons with no transverse momentum ($p_x = p_y = 0$) which are spectator nucleons from the colliding ions.

```

E 1 -1 -1.000e+00 -1.000e+00 -1.000e+00 0 -1 154 10001 10002 0 0
U GEV MM
C 8.4970962524414062e+10 0.000e+00
H 0 11 16 44 235 154 0 0 0 1.3447725296020508e+01 0 0 0
V -1 0 0 0 0 0 2 2181 0
P 10001 1000822080 0 0 -2.870399e+05 2.8704e+05 1.93729e+02 4 0 0 -1 0
P 10002 1000822080 0 0 2.870399e+05 2.8704e+05 1.93729e+02 4 0 0 -1 0
P 10003 2212 0 0 1.3799996e+03 1.3799999e+03 9.3827e-01 1 0 0 0 0
P 10004 2112 0 0 1.3799996e+03 1.3799999e+03 9.3965e-01 1 0 0 0 0
P 10005 2112 0 0 1.3799996e+03 1.3799999e+03 9.3965e-01 1 0 0 0 0
...

```

Figure 4.6: Example of the content of a HEPMC file for a Pb-Pb collision at 2.76 GeV/A.

Production of HEPMC output files with EPOS

In order to produce the HEPMC output files, I started from the functions written previously by Maria Stefaniak in `EPOS/src/KWb/fill_hep.cpp` (and its associated header `fill_hep.h`), based on HEPMC version 2.06.09 [308]. These files had of course to be added in the list of compiled files in order to be part of the EPOS compilation.

To call the functions creating the HEPMC file and writing in, I followed the same path in the EPOS code as for the production of ROOT files. Thus, I added the call of "open_hepmc()" and "fillhepmc()" functions in the "treestore()" subroutine and of "closehepmc" function in the "treeclose" subroutine (both written in **out.f**). Those two subroutines are called by "eposevent" (**bas.f**), if the "fillTree4()" function is called in the **.optns** file (see subsection 4.2.2), when simulating events. The same thing had to be done in the subroutine "getCevtCpt1" (in **out.f**), which is called when reading events recorded in ROOT files for re-analysis (by using the flag "-cproot" when calling **epos**).

Further modifications were also necessary on the content of the ROOT files at this point, because some general information on the events necessary for the HEPMC files ($N_{part}^{targ/proj}$, $N_{spec}^{p/n}$) were not saved so far. When reading events stored in those files for re-analysis, it was not possible then to pass the information to the HEPMC records, while it was possible when simulating the events. Therefore, I modified the structure of the TTree objects used to store events under ROOT format in the files **etree.cpp**, **etree.h** and **etreef.cpp**, adding new branches to store those information.

Because we don't want the HEPMC output file to be systematically created nor saved when recording or reading ROOT files, as they are called in the same subroutines, I created a similar scheme to activate the recording as for the ROOT files production. I defined a new variable "ihepmc" used to indicate if the HEPMC file has to be created and filled, and thus made the call of the functions used to do so (discussed in previous paragraphs) depend on its value. Then, I had of course to make the bridge with the **.optns** file instructions, *i.e.* allowing the user to control the value of this variable from there. To do so, I modified the subroutines "aset()" and "aread" (in **bas.f**), used to read and interpret the content of **.optns** files, to activate the HEPMC file writing via the instruction:

```
set ihepmc 1
```

In the same manner as for the ROOT files, I also modified the **epos** script to create a "-hepmc" flag which indicates to save the HEPMC output file created once the run is finished.

Finally, the most important task in this work was to re-write the main C++ function "fillhepmc()", used to create the event structure and write it in the output file. The first reason for that, which I already mentioned, was to complete the general information provided about the events, compared to the original version written by Maria Stefaniak.

The second important reason behind this rewriting was that, in the original version, only the FS particles of the collision were recorded in the events stored in HEPMC files. This was problematic in the case of feed-down corrections in analyses, or studies of exclusive particle spectra for instance. Such analyses were not achievable then as no information on the particle's parents were accessible, making impossible to know if particles were produced from hadronisation or from secondary decays. It could also be problematic for the study of short-lived particles like quarkonia, as the only way to have them recorded in the HEPMC from EPOS would then be to use the "nodecays" feature in the **.optns** files. It would then have been impossible to know how such particles decay afterward, what is essential when comparing to experimental data as they are generally reconstructed through specific decay channels. However, the solution was not to jump to

the other extreme by recording the complete history of each event in our HEPMC output files. As it can be seen in the extract of such file shown in the first part of this subsection, a peripheral Pb-Pb collision at LHC usually produces more than two thousands particles in the final state. Recording the entirety of such events would then take an incredible amount of disk space, knowing for instance that the event in question (recorded with only FS particles) is already weighing 0.5 MB. To overcome this problem, I added a second possibility for the recording procedure which saves FS particles plus their parents (and potentially grand-parents) in certain cases; the details on what is saved exactly will be given in the next and last part of the subsection. I even added a third possibility to record particles before hadronic cascades for each event, with the help of Axel Le Béguéc, a Master student whom I supervised for his last year internship. This allowed the usage of RIVET to look at the impact of hadronic cascade on cumulants of particle net-multiplicities, in order to cross-check the results obtained with the EPOS analysis framework which are presented in chapter 5. In the end, it is possible to switch between to three versions of the recording procedure by changing the value of the "which_table" variable in `fill_hep.cpp`, being nevertheless set on the second version by default.

Another modification achieved on the HEPMC recording procedure was to change the way the energy of particles is calculated. The kinematic information on particles provided by EPOS to the "fillhepmc()" function are their momentum vector coordinates and mass, while in the HEPMC format the energy is provided for each particle recorded. Initially using the energy-momentum relation $E = \sqrt{p^2 + m^2}$ to calculate their energy, we observed non-physical results of $|\vec{p}| > E$ for some particles with a large value of momentum in one direction compared to the other ones (*e.g.* very forward particles with $|p_z| > 10^3$ GeV while $|p_{x,y}| < 10^{-2}$). This issue being the results of a rounding error due to the limited precision of numerical variables, we decided to use another formula to determine the energy, starting from the definition of the rapidity y :

$$\begin{aligned}
 y = \frac{1}{2} \ln \left(\frac{E + p_z}{E - p_z} \right) &\longleftrightarrow e^{2y} = \frac{E + p_z}{E - p_z}, \\
 &\longleftrightarrow e^{2y}(E - p_z) = E + p_z, \\
 &\longleftrightarrow p_z (1 + e^{2y}) = E (e^{2y} - 1), \\
 &\longleftrightarrow p_z (e^y + e^{-y}) = E (e^y - e^{-y}), \\
 &\longleftrightarrow p_z = E \times \tanh(y).
 \end{aligned} \tag{4.3.1}$$

Then, using the fact that $E^2 = m^2 + p^2 = m_T^2 + p_z^2$ with equation 4.3.1, one gets:

$$\begin{aligned}
 m_T^2 &= E^2 - p_z^2, \\
 &= E^2 (1 - \tanh^2(y)), \\
 &= E^2 \frac{1}{\cosh^2(y)}, \\
 \implies E &= m_T \times \cosh(y).
 \end{aligned} \tag{4.3.2}$$

Hence, as the only accessible particles information provided are the mass and momentum

coordinates, one can obtain rapidity starting from equation 4.3.1 again:

$$\begin{aligned}
 p_z (e^y + e^{-y}) = E (e^y - e^{-y}) &\longleftrightarrow p_z^2 (e^y + e^{-y})^2 = (m_T^2 + p_z^2) (e^y - e^{-y})^2, \\
 &\longleftrightarrow p_z^2 \left[(e^y + e^{-y})^2 - (e^y - e^{-y})^2 \right] = m_T^2 (e^y - e^{-y})^2, \\
 &\longleftrightarrow p_z^2 \times 4 = m_T^2 (e^y - e^{-y})^2, \\
 &\longleftrightarrow p_z = m_T \cdot \sinh(y), \\
 &\longleftrightarrow y = \operatorname{arcsinh} \left(\frac{p_z}{m_T} \right)
 \end{aligned} \tag{4.3.3}$$

which gives finally, when using equation 4.3.3 in equation 4.3.2 :

$$E = m_T \times \cosh \left(\operatorname{arcsinh} \left(\frac{p_z}{m_T} \right) \right) \tag{4.3.4}$$

Using equation 4.3.4 allows finally to achieve calculation of energy with the provided information from EPOS without encountering any calculation issue like the one exposed before.

The last major modification was to include the possibility to apply a rapidity boost to the whole frame of the particles from any event. This feature is mandatory to produce HEPMC files for asymmetric systems like p-Pb collisions at LHC, as EPOS always simulate collisions in the center-of-mass frame while this one is boosted compared to the laboratory frame in these collisions. Fortunately, as this boost is purely longitudinal, one can easily calculate the coordinates (p'_x, p'_y, p'_z, E') in the laboratory frame from the ones in the center-of-mass (p_x, p_y, p_z, E) with the simple Lorentz transformation:

$$\begin{pmatrix} p'_x \\ p'_y \\ p'_z \\ E' \end{pmatrix} = \begin{pmatrix} 1 & 0 & 0 & 0 \\ 0 & 1 & 0 & 0 \\ 0 & 0 & \cosh(y) & -\sinh(y) \\ 0 & 0 & -\sinh(y) & \cosh(y) \end{pmatrix} \begin{pmatrix} p_x \\ p_y \\ p_z \\ E \end{pmatrix}, \tag{4.3.5}$$

using the fact that $\gamma = \cosh(y)$ and that $\gamma\beta = \sinh(y)$, with y being the rapidity boost between the two frames. Using this transformation, I just needed to add in "`fillhepmc()`" the recalculation of E and p_z from the center-of-mass to the lab frame, using the value of rapidity boost indicated in the `.optns` file in such case, and stored in the "`rapcms`" variable. In addition, a variable "`ihepframe`" has been created to indicate if rapidity boost should be applied to the particles, following the same philosophy as for the "`ihepmc`" variable.

Content of the EPOS HEPMC output

To conclude this subsection, here is a summary of the physical information which are provided or not in the events recorded in the HEPMC output files produced with EPOS. The first important point is the cross-section information, whose value provided for p - A and A - A events is the corresponding p - p cross-section value.

Towards the heavy-ion information provided, the number of hard scatterings is not provided as it is not stored in EPOS, even though the number of Pomerons exchanged during the collision is known. The number of spectator protons and neutrons (N_{spec}^p and N_{spec}^n respectively) are provided from the real values of the simulations, to match with the spectating particles recorded at the beginning of the event (including the diffractive states). However, the number of participants from projectile and targets (N_{part}^{proj} and

N_{part}^{targ} respectively) as well as the number of binary collisions (N_{coll}) are not taken from the actual simulations, but from Glauber calculations [138]. The reason is that experimental collaboration use this model to estimate such observables when displaying results as a function of them, as already explained in subsection 2.2.1. By doing so, we ensure to perform apples-to-apples comparison when comparing those values provided in EPOS HEPMC files to experimental data.

In the default version of the HEPMC recording, mentioned in the previous part, all particles with a lifetime $\tau > 10^{-19}$ s are recorded, as well as the complete sequence of following decays, until the FS particles. To apply this condition, used mainly to give the possibility to achieve feed-down correction from weak decays (see again discussion in previous part), I added a list of exceptions for shorter-lived particles which has to be recorded anyway. This feature allows to study the production of specific hadronic species, and contain for the moment the EPOS IDs of commonly studied quarkonia: J/ψ , $\psi(2S)$, $\Psi(3770)$ and the $\Upsilon(1/2/3/4S)$ family. To complete this list, one would just need to add the ID_{EPOS} of the particle(s) of interest to the "excpn_list" in the "fillhepmc()" function. An example of a particle decay chain recorded in a HEPMC file is shown in figure 4.7, where a D^+ meson (particle n°10487) decays into a K^+ (n°10488) and a ρ^+ (n°10489), the latter decaying in turn into a π^+ (n°11222) and a π^0 (n°11223). Here, K^+ , π^+ and π^0 are considered as stable because they have been specified as so in the .optns file with the "nodecays" instruction, as explained in subsection 4.2.2.

```

...
P 10487 411 -1.79e+00 3.86e-01 -2.43e+00 3.58e+00 1.86e+00 2 0 0 -11 0
...
V -11 0 -6.12e+11 1.31e+11 -8.29e+11 1.21e+12 0 2 0
P 10488 130 -5.55e-02 -6.01e-02 -1.09e+00 1.20e+00 4.97e-01 1 0 0 0 0
P 10489 213 -1.74e+00 4.46e-01 -1.34e+00 2.37e+00 7.75e-01 2 0 0 -77 0
...
V -77 0 -6.12e+11 1.31e+11 -8.29e+11 1.21e+12 0 2 0
P 11222 211 -1.12e+00 1.64e-01 -4.15e-01 1.21e+00 1.39e-01 1 0 0 0 0
P 11223 111 -6.19e-01 2.82e-01 -9.26e-01 1.15e+00 1.34e-01 1 0 0 0 0
...

```

Figure 4.7: Example of the record of a decay chain of a particle in a HEPMC file for a Pb-Pb collision at 2.76 GeV/A, from the same event displayed in figure 4.6. Note that the precision on numerical values have been truncated for the purpose of the figure.

Finally, in order to prevent for potential problems in the event recording, I have defined a specific status for non-FS particles for which daughter particles can not be found. This status code has been taken as 12 (as not used in HEPMC standards), because such particles seem to be FS particle (status 1) while it is actually not (status 2), what is verified using the EPOS particle status.

To summarise, I have brought several improvements to the content of the HEPMC formatted files produced with EPOS 4, compared to the first version included by Maria Stefaniak [270]. The first major change was to add more flexibility in its use. One can now allow to take into account rapidity shifts of the center-of-mass of the system in case of asymmetric collisions, or by letting the choice of recording either only FS particles, or also their parents to enable weak decays reconstruction. Moreover, the user can now

activate HEPMC files production but without having to record it in the end, in order to enable the use of RIVET without saving files uselessly. Another important change was to add more information to the records, by passing more input variables, like the number of participants or spectators from each collisions for instance. Finally, I have modified the way kinematic variables stored in HEPMC are calculated from the information provided by EPOS, by using more robust formulae to avoid numerical errors in the calculations.

4.3.2 Automating the usage of RIVET

The production of HEPMC output files with EPOS allows now to perform RIVET analyses on the results of its simulations. However, as explained in the introduction of this section, we have decided to go further with EPOS by using RIVET as a data and analysis library. To this end, I included the possibility to call it via the EPOS analysis system, and to store the results in our own output **.histo** files. All the scripts I have created for the purposes described in this section can be found in the EPOS repository in **EPOS/Misc3/Rivet/**.

Adapting the experimental data format

In order to use RIVET as a data library for the EPOS analysis framework, it was necessary to adapt the format of the data provided via YODA files in RIVET. As a matter of fact, EPOS has its own analysis language (presented in subsection 4.2.3), and data has to be stored in a specific way to be called with it, using the same structure as for the results of analyses. An example of the content of such file once transcribed will be shown further.

To achieve this task, I decided to write everything in Python, which is a really convenient tool for such operation, added to the fact that it benefits from a very good documentation on the internet. Hence, I created a fully automated program called **RIVET_to_histo.py** embedded with a user interface, to offer several possibilities of use. After asking for technical information (the path to RIVET and the address of a directory where to store the created files), the program asks the user for 3 different ways to process. They can choose whether they want to convert all experimental data provided with RIVET, only a selection of them which names match a list of entered keywords ("selection mode"), or all of them excepted some which names match a list of entered keywords ("exception mode"). Finally, the user can decide if all of these data has to be written in one file, which they can name, or to write in several files depending on the different experiments, with a limit on the size of each file written.

The resulting **.histo** files will contain, for each different publication corresponding to a set of data, a header with information on the publication (taken from the associated **.info** file in RIVET). Each data table is then stored with a plot header, giving information on its content, *i.e.* title and axes labels (taken from the associated **.plot** file in RIVET). If no information are provided in the **.plot** file, which is the case for some analyses submitted to RIVET, the plot headers are simply left empty. Finally, the name given to each data table is simply composed of the name of the analysis it belongs to, with a series of 3 numbers based on the YODA numbering: "d.-x.-y..". An example of the content from a **.histo** file is provided in the next page, based on a STAR publication for which I have written myself the RIVET analysis. The results obtained with EPOS with this analysis will be shown, among other, in chapter 5.

By writing the aforementioned program, I realised that it would be useful to structure it in a modular way, so that part of the code with a specific purpose could be used in other

contexts. The YODA format being now a standard format proposed to download data from HEPData, the part responsible for reading YODA files and storing their content (data tables) could be useful for other tasks. With this in mind, I wrote a kind of *library* file called `EPOS_DATA_lib.py`, in which I wrote different functions such as the one evoked in the last sentence to store data from a YODA file, "`Read_yoda_file()`". With the same logic, I also wrote a function called "`Write_histo()`" which writes `.histo` files from provided data tables, in the same format as the example displayed in Fig. 4.8. These two functions has notably been useful when I had to write analyses using the EPOS dedicated system, to compare EPOS simulations with experimental data for which no analyses were available in RIVET. An example of how to use "`Read_yoda_file()`" and "`Write_histo()`" to convert data tables from YODA to `.histo` format is available in `EPOS/Misc3/Rivet/Simple_templates.py`, with corresponding explanatory notes.

```
#####
! STAR Data:
!"Bulk properties of identified hadrons in the Au Au medium
! from the RHIC beam-energy scan "
! Reference(s) :
! - 'Phys.Rev. C96 (2017) no.4, 044904'
! - 'DOI: 10.1103/PhysRevC.96.044904'
! - 'arXiv:1701.07065'
! Run Info :
!   Minimum bias AuAu events at various collision energies.
! Beam(s): Au/Au
! Energie(s): 7.7, 11.5, 19.6, 27.0, 39.0 (GeV or GeV/A)
#####

!-----
! Figure 02.01.01
! Title :  $\pi^-$  (Au+Au 7.7 GeV)
! X :  $p_T$  (GeV/c)
! Y :  $\frac{1}{2\pi} \frac{dN}{d^3p_T d^3p_T} [(GeV/c)^{-2}]$ 
!
! x   xerr-   xerr+   y   yerr-   yerr+
!-----
openhisto name STAR_2017_I1510593-02-01-01
array 6
[... ..]
endarray
closehisto
```

Figure 4.8: Example of an analysis defined in a `.optns` file to get a p_T distribution of π^+ .

Using RIVET from the EPOS analysis system

Having stored the experimental data to compare our simulation results with in the right format, I had to find a way to make the link between EPOS and RIVET. As the HEPMC files need to be filled before running any RIVET analysis on it, the first step was to add a new kind of output file, containing the information on which analysis to perform once EPOS run ends. These new output files, with a `.dataR` extension, are created when the "`rivet`" instruction is written in the `.optns` file, followed with

the name of the analysis to perform and by which plots to save in the `.histo` file. As an example, the following instruction will create a `.dataR` file with the information "ALICE_2010_S8625980 d03:log/d06" inside:

```
rivet ALICE_2010_S8625980 d03:log/d06
```

The first instruction refers to the required RIVET analysis, and then the plot numbers which can be provided only partially, so that all the plots matching the partial numbering will be saved in the `.histo` file in the end. It is also possible to specify what scale to use for the y axis when displaying the plot, as this information is not always provided in RIVET and the default linear scale is not always appropriate. It of course possible to call several RIVET analyses, by writing one line for each analysis in the `.optns` file.

In order to execute RIVET, I wrote a Python script, `rivet_analysis`, which is called in the `epos` script once EPOS has run. It takes the `.dataR` file as an input, reads and store the information written inside. Then, it runs each analysis, reports any error message potentially encountered during the run, and calls another program to save the results from plots selected by the user into the `.histo` file (by default, all plots are saved).

This program, `RIVET_to_histo_analysis.py`, is called once per analysis and is also written in a modular way, based on functions defined in `EPOS_DATA_lib.py`. The first one, `Read_yoda_analysis()`, will read and store the results of the analysis from the plots selected by the user, as its name indicates. It will then get the plotting information from the RIVET `.plot` file using the `Read_plot_file()` function, and finally write all the results of the plots stored in the `.histo` file. It will write as well the instruction to call the corresponding experimental data stored to compare with, from the `.histo` files created as described in the previous part. In the end, the intermediary YODA file is deleted, as well as the `HepMC` file if the `"-hepmc"` flag has not been used when executing `epos`.

As the YODA files resulting from analyses do not provide directly the y -values for each bin, but the complete information on its filling (sum of weights, number of entries, etc.), the function `Read_yoda_analysis()` has to calculate these y -values. This calculation will vary depending on the nature of the distribution, whether it is a classical histogram or a profile histogram. As explained in subsection 4.2.3, the value of the `"histoweight"` and the content of the third column will depend on the type of histogram. This is of important when adding the results of different runs for the same histogram, *i.e.* when merging different `.histo` files. To ensure the information are provided correctly for the different types of histogram, I conducted a test :

- running twice an analysis on two different set of events, obtaining thus two files `Test1a.yoda` and `Test1b.yoda` which I saved and merged using RIVET, and then transcribed into `Test1.histo`;
- repeating the same operation, but transcribing the results of the plots directly into `.histo` files `Test2a.histo` and `Test2b.histo`, and merge them into `Test2.histo` using a dedicated script created by my supervisor.

Comparing the results of `Test1.histo` and `Test2.histo` show then almost no differences, or only tiny ones of the order of the sixth decimal digit due to numerical precision, proving that the information were correctly provided.

4.3.3 Dealing with centrality calibration

The use of heavy-ion analyses, and also some analyses regarding high-multiplicity p - p events, requires to run calibration analyses in RIVET as presented in subsection 4.1.1. Nevertheless, executing such analysis for each EPOS run to use the results for the analyses of the same run is not a proper solution. Each run contain only a fraction (generally small) of the total number of events simulated for the corresponding system, so the calibration distributions are not representative of the whole ensemble, and would even vary from a run to another. In the end, each run would give results based on different calibration, completely distorting the results of the concerned analyses.

To avoid this problem, we proceed like for the management of centrality calibration in the EPOS analysis framework (see subsection 4.2.3). We start by creating, for each system, a file called `icl[...]._rvt.optns` containing definitions of centrality classes based on impact parameter and multiplicity, stored in `EPOS/KWt/` with the regular `icl[...].optns` files. We also store in this same directory the original YODA file from the corresponding RIVET calibration analysis used to get these definitions. Then, we run simulations where we call the RIVET calibration analyses, using a specific instruction in the `.optns` file which is slightly modified compared to the one used for regular analysis :

```
rivet calib_run STAR_BES_CALIB[mult/imp]
```

This will save the resulting YODA file, recalculate the different centrality classes based on the new distribution and compare them to the one stored in the `icl[...]._rvt.optns` files. This calculation is done either with the multiplicity or impact parameter distribution, depending on the parameter specified between brackets ("`mult`" being the default case if nothing is indicated). As for the analyses requiring a centrality calibration as an input, we provide the distribution from the YODA file obtained with a prior simulation, stored in `EPOS/KWt/`.

If the centrality definitions of the new simulations differ too much from the ones stored in `icl[...]._rvt.optns`, we change the latter ones by the new ones, and replace the old YODA reference file in `EPOS/KWt/` by the newly obtained one. In such situation, we need to run again the analysis on the same set of events, to benefit this time of an updated definition of centrality classes corresponding to these events. This cross-check and update of centrality calibration distribution is however only necessary for developers when operating changes in the parameters from one EPOS version to another. The users will, of course, not have to perform such procedure, as the `icl[...]._rvt.optns` provided with the incoming public version will be based on events obtained with this same version.

Note finally that, as there are sometimes different centrality calibration analyses for one kind of collision, because each experiment has its own way to perform it, we record the information for each different analysis.

4.4 Summary of the technical work

I have explained in this chapter how I added the possibility to create a new output file with EPOS, to record the events simulated in the HEPMC standard format, making it compatible with RIVET. In order to go even further, I have then developed a code architecture to handle the use of RIVET via the EPOS analysis system, taking into account

the necessity of centrality calibrations.

To sum it up, I will recall the different steps to follow in order to use these new features. To make the most complete description possible, I will use as an example the call of an analysis from the ATLAS collaboration dedicated to the study of η density distribution of charged particles for p-Pb collisions at 5.02 TeV/A.

The first step is of course to configure **pPb5T.optns**, in order to produce the **HepMC** output file and to take into account the rapidity shift of the center-of-mass compared to the lab frame. Then, one has of course to call the desired analysis, here "**ATLAS_2015_I1386475**". The associated calibration analysis is called too, to ensure that the pre-recorded distribution, stored in **EPOS/KWt/iclpPb5T_rvt.optns** and used in the call of "**ATLAS_2015_I1386475**", is compatible with the analysed set of events. Hence, the file **pPb5T.optns** should contain what is indicated in figure 4.9.

```

set ihepmc 1          ! Activate HepMC production

set rapcms -0.465    ! CoM rapidity shift
set ihepframe 1      ! To apply shift on particle coordinates in HepMC

! Centrality calibration(s)
rivet calib_run ATLAS_pPb_Calib[mult]

! Pseudorapidity density for charged particles
rivet ATLAS_2015_I1386475 d02 calib:ATLAS_pPb_Calib

```

Figure 4.9: Example of the instructions to write in a **.optns** file to run RIVET.

Then, one simply has to run EPOS (here with the flag to save the produced HepMC file with the events recorded, not mandatory though):

```
$> epos -hepmc pPb5T
```

Note that the path to RIVET is expected to be defined as an environment variable, and so does not need to be written anywhere.

In order to clarify the functioning of the machinery introduced in detail in the previous section, and triggered when using such instructions, an illustration is given in the figure 4.10. There, the files in black/white are permanent files, except for **pPb5T.hepmc** which can be saved or not following user's will, and files in grey are temporary files. Straight lines represent processes achieved by EPOS, while dashed lines show processes achieved by **rivet_analysis**. Finally, the dotted lines account for the processes which are achieved by **RIVET_to_histo_analysis.py**.

Even though the use of RIVET through the EPOS analysis system is now fully functional, some potential improvements can still be made. On RIVET's side, the main limit for the developers is of course the lack of analyses for HICs, which I already mentioned. We cannot rely exclusively on it to perform our comparison with experimental data yet: we need thus more contributions from the experimental collaborations to make of RIVET the perfect tool it has the potential to be, in the exchanges between theoretical and experimental communities. On EPOS' side, one minor technical issue still remains in the

recording of e^+e^- collisions (or for other leptonic system) with HEPMC, as the information on colliding particles are not recorded correctly. Beyond this, the use of RIVET could be improved, by allowing the user to save the YODA file produced so that they can display the results directly using the "`rivet-mkhtml`" command. Another improvement would be to enable to perform the call of RIVET's analyses with a First-In, First-Out (FIFO) pipe, so that events stored by EPOS under HEPMC format would be read in continuous flow as soon as they are recorded. Letting the user getting rid of the HEPMC files once the analyses are performed, if they do not need it, allows to save memory space over runs, nevertheless it still takes space for the time of the run, which could be limiting when reading a large number of events in one run.

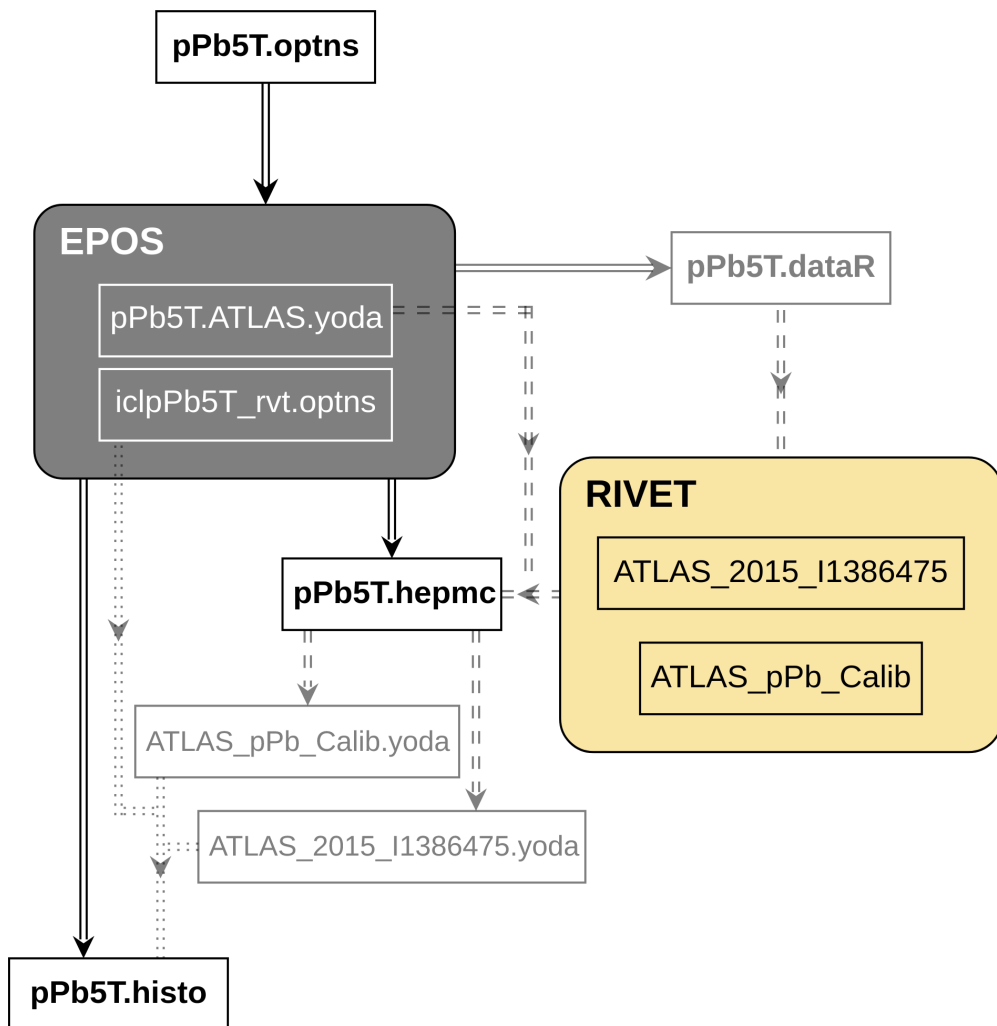


Figure 4.10: Functional diagram of data & processes flow when calling RIVET through the EPOS analysis system.

Despite the aforementioned flaws, which will most probably be fixed in future versions of EPOS 4, this new feature is functional and can be useful for both users or developers. It is particularly true for developers, as will be shown in the next chapter, where I will present the results of EPOS 4 for several observables in Au-Au collisions, at many energies of the BES program. Although most of the results are obtained via the conventional EPOS analysis framework, the few ones coming from RIVET will thus demonstrate the proper functioning of this new tool.

CHAPTER 5

BEAM ENERGY SCAN & STUDY OF CUMULANTS WITH EPOS

Contents

5.1 Basic spectra for the BES energies	91
5.1.1 Pseudorapidity densities of charged hadrons	91
5.1.2 Transverse momentum spectra of identified hadrons	93
Light hadrons	93
Strange baryons	95
5.2 Study of the 2nd order cumulants of conserved charges	99
5.2.1 Results for STAR proxies: variances, covariances and their ratios	99
5.2.2 Comparison with enhanced proxies and conserved charges cu- mulants	102
5.2.3 Impact of hadronic cascades on the 2 nd order cumulants	106
5.3 Summary of results on 2nd order cumulants study	111

In this last chapter, I will present the main physical results obtained thanks to the work achieved during the three years of my PhD thesis, issued from one of the latest versions of EPOS 4 and compared with experimental measurements. As explained in the previous chapters, my work focuses on Au-Au collisions performed in the energy range of the BES achieved at RHIC, for $7.7 \leq \sqrt{s_{NN}} \leq 200$ GeV. Therefore, all the experimental results which will be used in this chapter are coming from experiments presented in the subsection 2.2.2.

The section 5.1 will be centered on basic observables that are η distributions of charged hadrons and p_T spectra of identified particles. There are two goals: first of all ensuring that particle production is well reproduced by EPOS in the kinematic range of interest for the study of cumulants, and also using this occasion to display first physical results from EPOS 4. Thus, I will especially concentrate on the central ($|\eta| < 0.5$) and low- p_T ($p_T < 2$ GeV) region of the phase space, where the particles used in the cumulants analyses are coming from. It will also be the occasion to check until when can EPOS offer a good description of the physics of HICs, while going down in energy. Following the simple reasoning exposed in subsection 3.3.3, the PBGR model used to describe the initial interactions is not expected to be relevant anymore below ~ 20 GeV/A in HICs, what the results displayed here will enable to verify.

In section 5.2, I will expose all the results obtained for the study of 2nd order cumulants of net-charges and their proxies. Let me recall briefly the main objectives, motivated by the publications presented in subsection 2.3.3 and exposed in section 3.5:

- to compare the proxies used by STAR in [211], and the enhanced proxies proposed in [234], to the cumulants of associated conserved charges B , Q and S ;
- to quantify the impact of the hadronic cascades on those observables ;
- to estimate the proportion of the signal originating from the core, the part mimicking the fluid behaviour of QGP in EPOS simulations.

All the results from EPOS used from now on in this chapter are obtained from simulations run with one of the last and most advanced EPOS 4 beta versions, EPOS 3.451, unless specified otherwise. They have all been performed with the core-corona procedure activated, and the subsequent relativistic fluid dynamical evolution of the core using the X3F equation of state. Moreover, hadronisation of the core is achieved via the micro-canonical procedure, which ensures both local and global conservation of the conserved charges, described with the other features in section 3.4. Because the version used is quite recent, and the simulation of such collisions is very demanding in terms of computing resources (even when using a dedicated computing centre¹), the statistics available for each collision energy is very limited. As shown in table 5.1, results from EPOS are based on ~ 250 k events per energy, compared to the several millions generally used in experimental analyses [177].

$\sqrt{s_{NN}}$ (GeV)	7.7	11.5	14.5	19.6	27	39	62.4	200
N_{evts}	240k	240k	240k	240k	300k	300k	270k	240k

Table 5.1: Number of events simulated with EPOS 3.451 per collision energy.

¹IN2P3 Computing Centre

5.1 Basic spectra for the BES energies

The generic results presented in this section will be divided into two parts, one for each of the two reviewed observables, which have been both introduced in subsection 2.2.1. Thus, the first subsection will deal with the spatial distribution of produced charged hadrons, via the measurement of pseudorapidity (η) particle density. The second part will then cover the transverse momentum distributions of identified particles, starting with the lightest ones (π^\pm , K^\pm and p/\bar{p}) to then expose the strange heavier ones (Λ , $\bar{\Lambda}$, Ξ^- , Ξ^+ , Ω^- and $\bar{\Omega}^+$). This way, I will check that the production of all the particles used later in the study of cumulants is relatively well reproduced by the set of simulated events used.

Because experimental data are not available at all energies for every observables in Au-Au collisions, or simply because of readability when it's the case, I will not show results for the eight different energies for each observable. When the choice is possible among all collision energies (or almost) though, I will try to have the widest and most regular energy scan possible. Concerning the collision centrality, all results displayed in this section have been obtained by using the impact parameter distribution to determine the centrality classes, for the reasons explained in the end of subsection 4.2.3.

All the analyses whose results are shown in this chapter have been written by myself, and performed using the EPOS "on-the-run" analysis framework, described in subsection 4.2.3. They represent an important amount of work, as each of them require to understand properly how the analysis has been achieved on the experimental side, especially regarding the correction of feed-down from weak decays. The reason, already mentioned, for still using this system is that only few analyses for HICs are available so far in RIVET, and a very small number for the energy range of the BES program especially. The only exceptions are the p_T spectra of light hadrons for $\sqrt{s_{NN}} \leq 39$ GeV, obtained from a RIVET analysis² (mainly written and submitted by myself) by using the new framework described in section 4.3.

5.1.1 Pseudorapidity densities of charged hadrons

In order to ensure that the spatial distribution of charged particles is correctly reproduced by EPOS, we study their pseudorapidity densities, *i.e.* the number of charged particles per pseudorapidity unit $dN_{ch}/d\eta$ as a function of η . In figure 5.1 are shown the results from EPOS 3.451 compared with data from the PHOBOS experiment for Au-Au collisions at 19.6, 62.4 and 200 GeV/A [309].

The experimental results have been obtained using the PHOBOS detector covering almost the whole azimuths in the region $-5.4 < \eta < 5.4$, with centrality determined thanks to the energy deposited in detectors covering $3 < |\eta| < 4.5$, independents from the ones used for the measure. The charged particle distribution are corrected from all kinds of background contamination, and specifically from the feed-down of charged particles originating from weak decays (like K_s^0 , Λ , Ξ and Ω decays) [309]. Hence, I also corrected for feed-down of weak decays in the analyses of the simulated events. Monte Carlo simulations have also been used to correct the distributions for missing hadrons which are not detected at very low p_T ; the data are thus considering the whole p_T range ($0 \rightarrow \infty$ GeV).

²RIVET analysis: STAR_2017_I1510593

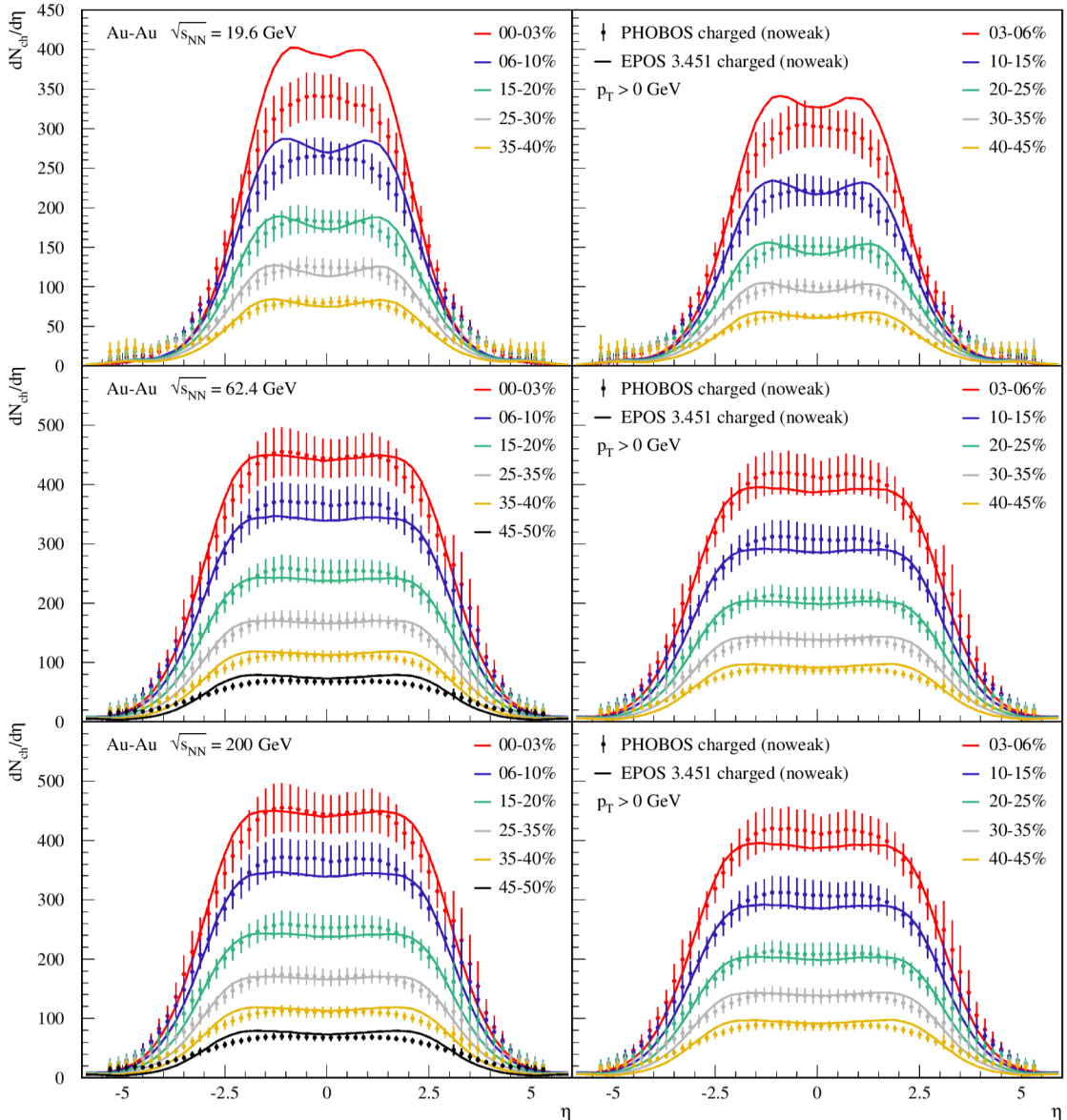


Figure 5.1: Pseudorapidity densities of charged particles for Au-Au collisions at $\sqrt{s_{NN}} = 19.6, 62.4$ and 200 GeV, in different centrality classes within 0-50%. Results from EPOS 3.451 are compared with data from PHOBOS, results from different centrality classes being displayed alternatively in two plots per energy for visibility [309].

One observes for all energies a typical structure with two bumps at forward and backward rapidity regions, which are caused by corona particles coming from the fragmentation of excited remnants after the initial interactions [290]. In the central region, the vast majority of particles are coming from the core, or the "central plateau" in the picture depicted by Björken (introduced in subsection 2.1.1). Hence, the bumps are more separated when beam energy increases, because the rapidity of colliding nuclei (and so the one of their remnants) increases. In the central region $|\eta| < 0.5$ which is of most interest for us because of the study presented in section 5.2, EPOS simulations are in agreement with experimental data for all results presented, even though generally on the lower side within the error bars. The only exception is for very central (0-3%) collisions at 19.6 GeV/A, where the remnants play an important role as they are closer to each other, and seem to overproduce charged particles and thus contaminate the central η region. Note nevertheless that, compared to EPOS 3.444, an earlier beta versions of

EPOS 4 [283], the simulations are in better agreement with data at 200 GeV/A thanks to an improvement of the treatment of remnants fragmentation.

5.1.2 Transverse momentum spectra of identified hadrons

The p_T spectra displayed in this subsection, combined with the previous pseudorapidity densities, are essentials to legitimate the events simulated with EPOS 3.451, at least for particle production in the kinematic range considered in section 5.2. Due to the fact that the runs of Au-Au collisions at different energies at RHIC has not been all performed in a short time, there is no single systematic analysis of p_T spectra for all hadronic species at all energies. Instead, the several sets of data used here are coming from different experiments, and thus with different kinematic ranges. In order to have an similar view across the different energies and identified hadrons checked, I will only display results in the range $0 \leq p_T \leq 2$ GeV, even when experimental results are available for a larger p_T range.

Light hadrons

Let first start with the light hadrons (*i.e.* π^\pm , K^\pm and p/\bar{p}), for which simulations will be compared to experimental data for $\sqrt{s_{NN}} = 7.7, 14.5, 27, 62.4$ and 200 GeV, although results are available at all energies simulated. The reason for having chosen these particular energies is that each of these steps corresponds approximately to the double of the energy of the previous one, and spans hence the whole range of the BES energies.

Starting from the highest energy, the first results to which I've compared EPOS simulations with data coming from the PHENIX experiment [310]. The p_T spectra have been obtained using the mid-rapidity range of $|\eta| < 0.35$, and corrected to account for the incomplete azimuthal coverage of the detector with the help of simulations. The events analysed have been divided into five centrality classes: 0-10%, 10-20%, 20-40%, 40-60% and 60-92%. The feed-down from weak decays have been corrected with Monte Carlo methods for all light hadron species. The results, plotted in figure 5.2, show a pretty good agreement between EPOS 3.451 and experimental data, except for a slight overestimation in peripheral events.

For Au-Au collisions at 62.4 GeV/A, the only available data of identified hadrons p_T spectra are coming from the PHOBOS collaboration [311]. Because this analysis was achieved using the spectrometer arms which cover a restrained phase space, the measurement have been made for $y = 0.8$ only and with a limited azimuthal coverage, which has been extrapolated then to account for the $1/2\pi$ normalisation. The events used have been divided into three centrality classes corresponding to 0-15%, 15-30% and 30-50% of the total cross-section. Feed-down corrections have only been applied to (anti)protons distribution, by selecting only the ones with a distance of closest approach (DCA) < 0.35 cm from the interaction vertex. Such method rejects naturally all the secondary protons originating from the weak decays of strange baryons like Λ ($c\tau = 7.89$ cm) or Σ^+ ($c\tau = 2.40$ cm). However, it was estimated to reject only $\sim 25\%$ of the total feed-down protons, thus the correction was mainly achieved thanks to estimations obtained by simulations. The π^\pm and K^\pm spectra, in turn, have not been corrected from any feed-down. The comparison between EPOS 3.451 simulations and experimental data for this energy, displayed in figure 5.3, show again an excellent agreement. The only deviation observed for the proton spectra might come from a small protons overproduction from EPOS, but the feed-down correction method applied by PHOBOS should not be

neglected neither to explain this difference, as it only considered two possible sources of feed-down.

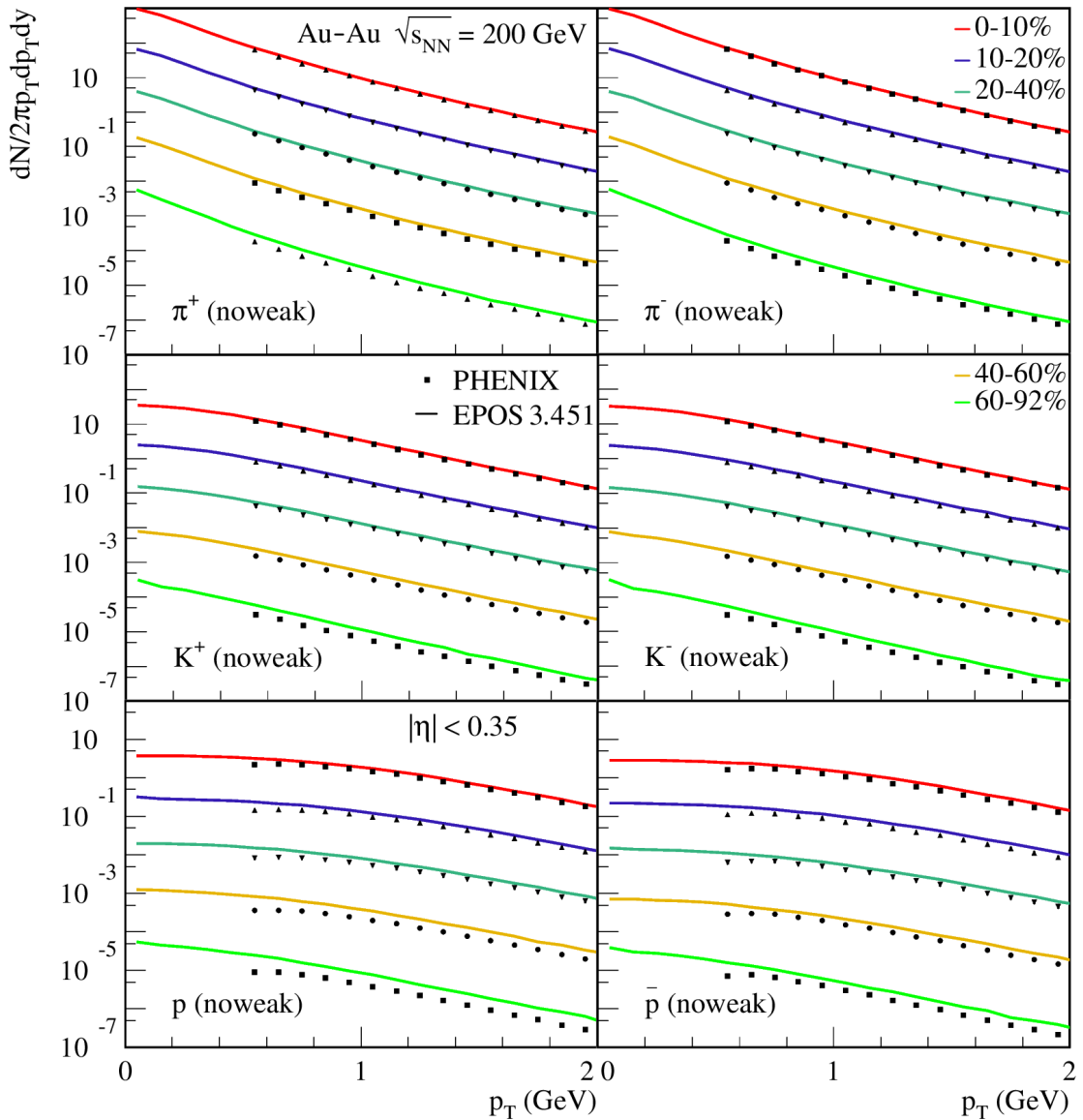


Figure 5.2: Transverse momentum spectra of π^\pm , K^\pm and p/\bar{p} within $|\eta| < 0.35$, for different centrality classes in Au-Au events at $\sqrt{s_{NN}} = 200$ GeV. Spectra for the most central events are at real scale, while the others are scaled by factors 10^{-x} ($x = \{1, 2, 3, 4\}$) (data from [310]).

The most detailed analyses of light identified hadrons p_T spectra has been delivered by the STAR collaboration, in [177] for Au-Au collisions at 7.7, 11.5, 19.6, 27 and 39 GeV/A, and in [312] for the ones at 14.5 GeV/A. They used particles detected within $|y| < 0.1$ in a full 2π azimuthal coverage, and divided events into nine centrality classes, *i.e.* 0-5%, 5-10% and 10%-large classes from 10 to 80%. The feed-down correction consists of a $DCA < 3\text{cm}$ selection, which works effectively well for π^\pm but not for p/\bar{p} , considered then as not corrected. Results for K^\pm being almost not affected whether this selection is applied or not, I decided nevertheless to correct them from the feed-down contamination. Because of the numerous centrality classes used in this analysis, I have splitted the spectra for each light hadron into 2 plots for readability ; therefore, results for $\sqrt{s_{NN}} = 7.7, 14.5$ and 27 GeV are to be found in appendix A. Again, results

from EPOS 3.451 are in very good quantitative agreement with experimental data for 27 GeV/A, displayed in figures A.1 and A.2, whatever specie considered. At 14.5 GeV/A, for which results can be seen in figures A.3 and A.4, π^\pm and K^\pm spectra are also very well reproduced, but the ones for p and \bar{p} are found to get slightly steeper slopes than data. Finally, the same observation can be made at 7.7 GeV/A, but this time for all species and even more accentuated, as shown in figures A.5 and A.6. There, the sudden drop of some EPOS curves are simply due to a lack of observed particles in the considered bins, because of the relatively small number of simulated events used in the analyses.

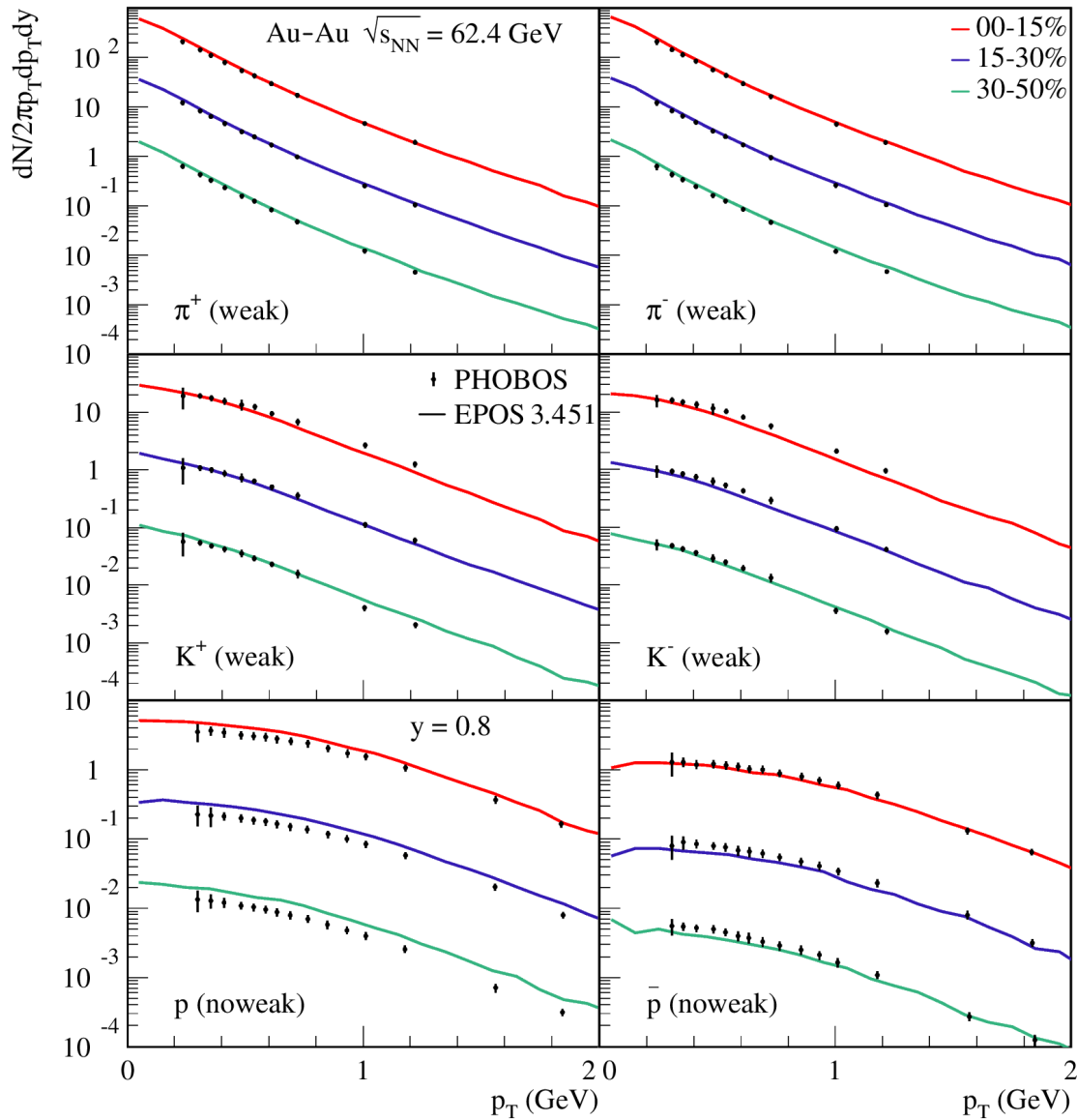


Figure 5.3: Transverse momentum spectra of π^\pm , K^\pm and p/\bar{p} at $y = 0.8$, for different centrality classes in Au-Au events at $\sqrt{s_{NN}} = 62.4$ GeV. Spectra for the most central events are at real scale, while the others are scaled by factors 10^{-1} (15-30%) and 10^{-2} (30-50%) (data from [311]).

Strange baryons

I will now expose the different results of EPOS 3.451 for the production of the hyperons Λ , Ξ^- , Ω^- and their respective antiparticles, still for the range $0 \leq p_T \leq 2$ GeV. As there are no experimental results at 14.5 and 62.4 GeV/A comparable to the ones

from last section, I will review in this case Au-Au collisions for $\sqrt{s_{NN}} = 7.7, 27$ and 200 GeV, proceeding in the same way by going down in energy.

The results at 200 GeV/A are coming from a STAR publication using five different centrality classes: 0-5%, 10-20%, 20-40%, 40-60% and 60-80% [313]. The Λ and $\bar{\Lambda}$ have been measured within $|y| < 1$, reconstructed via the specific topology of their weak decays $\Lambda \rightarrow p\pi^- / \bar{\Lambda} \rightarrow \bar{p}\pi^+$ by selecting (anti)protons with a DCA > 0.9cm and pions with a DCA > 2.85cm [314]. Moreover, they have been corrected from the feed-down of Ξ and Ω hyperons, what has consequently been done in EPOS results as well, with a strict feed-down correction from all weak decays. The latter ones are measured within $|y| < 0.75$, reconstructed via the processes $\Xi \rightarrow \Lambda\pi$ and $\Omega \rightarrow \Lambda K$ respectively, and did not require any specific feed-down correction. In order to increase the statistics, both Ω^- and $\bar{\Omega}^+$ are combined in the same distributions.

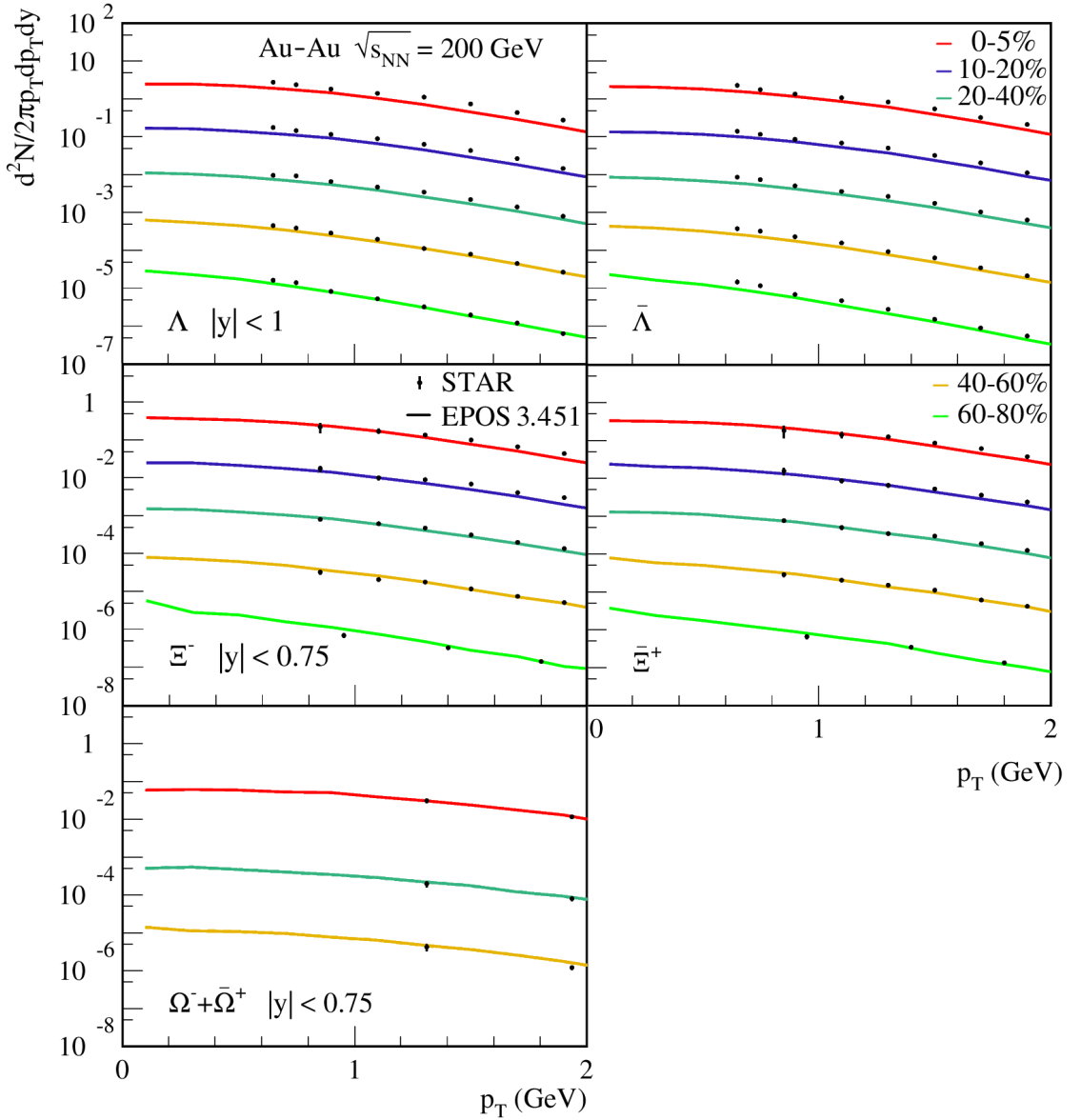


Figure 5.4: Transverse momentum spectra of Λ , $\bar{\Lambda}$, Ξ^- , Ξ^+ and $\Omega^- + \bar{\Omega}^+$ for different centrality classes in Au-Au events at $\sqrt{s_{NN}} = 200$ GeV. Spectra for the most central events are at real scale, while the others are scaled by factors 10^{-x} ($x = \{1, 2, 3, 4\}$) (data from [313]).

The second publication on which my study of hyperons production is based is also from the STAR collaboration, treating, like in the case of light hadrons, collisions for 7.7, 11.5, 19.6, 27 and 39 GeV/A [315]. The spectra have been distributed, for Λ and Ξ baryons, into the centrality classes 0-5%, 5-10%, 10-20%, 20-30%, 30-40%, 40-60% and 60-80% for all energies, while this repartition varies with energy for Ω baryons due to statistics. Again, Λ and $\bar{\Lambda}$ are corrected from the feed-down of heavier hyperons ; they are nevertheless contaminated by the electromagnetic feed-down of Σ^0 , as they can not be distinguished due to their very short lifetime ($\sim 10^{-19}$ s). For EPOS results, the same procedure have been applied, with a strict feed-down correction on weak decays but no corrections from Σ^0 decays. Contrary to the reconstruction method used for the results at 200 GeV/A, all strange baryons discussed here are measured within $|y| < 0.5$.

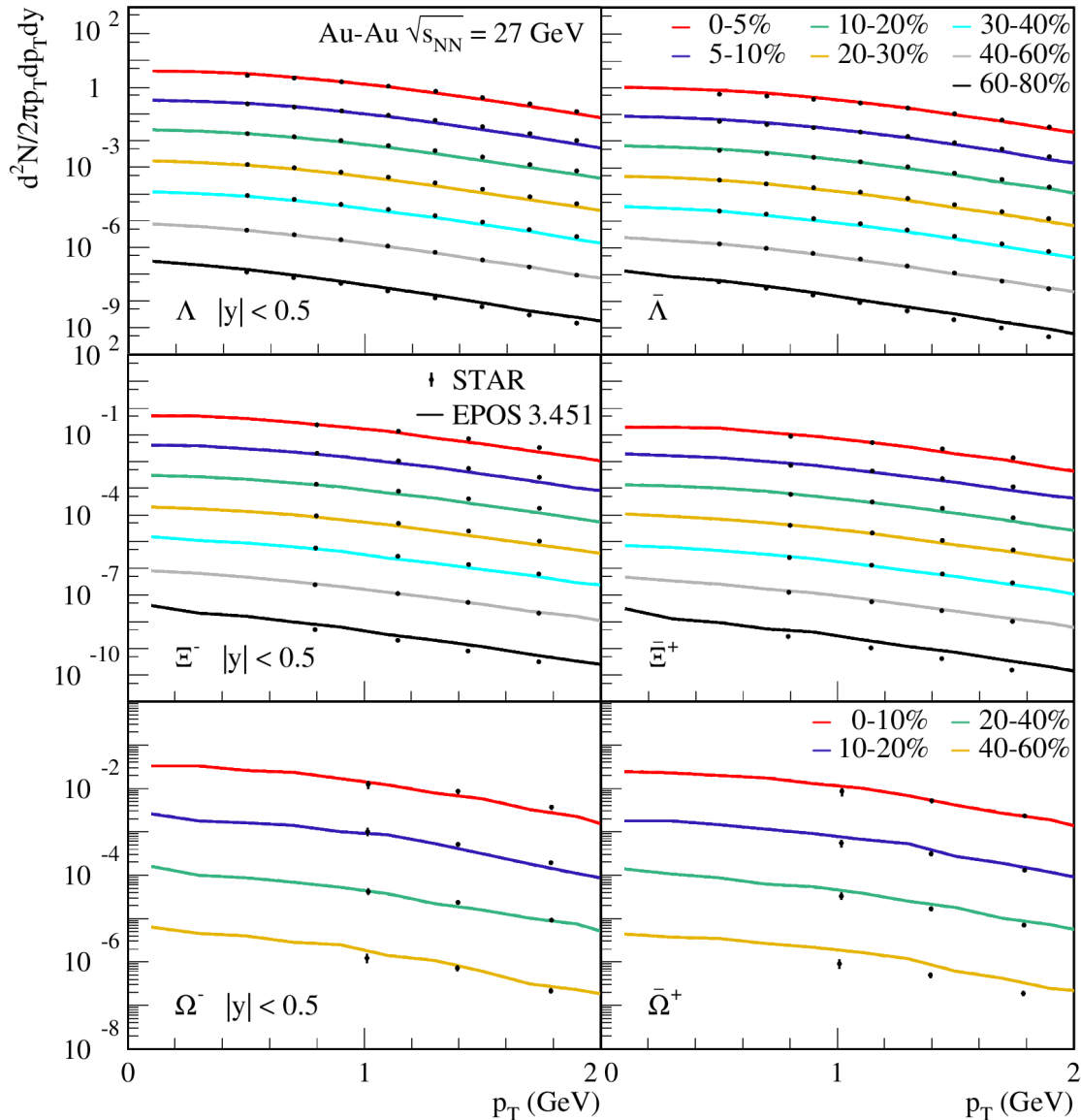


Figure 5.5: Transverse momentum spectra of Λ , $\bar{\Lambda}$, Ξ^- , Ξ^+ , Ω^- and $\bar{\Omega}^+$ for different centrality classes in Au-Au events at $\sqrt{s_{NN}} = 27$ GeV. Spectra for the most central events are at real scale, while the others are scaled by factors 10^{-x} ($x = \{1, 2, 3, 4, 5, 6\}$) (data from [315]).

The results are displayed in figures 5.5 and 5.6 for 27 and 7.7 GeV/A respectively, in addition to the ones from 200 GeV/A in figure 5.4. Reviewing all these results seems

to lead to a similar conclusion as for the light identified hadrons: EPOS reproduces perfectly the experimental data at both 27 and 200 GeV/A, but show discrepancies at 7.7 GeV/A. When taking into account the results from other energies with available data from [315], EPOS starts to show deviations from the experimental measurements starting from 19.6 GeV/A. The results for the latter collision energy are displayed in figure A.7.

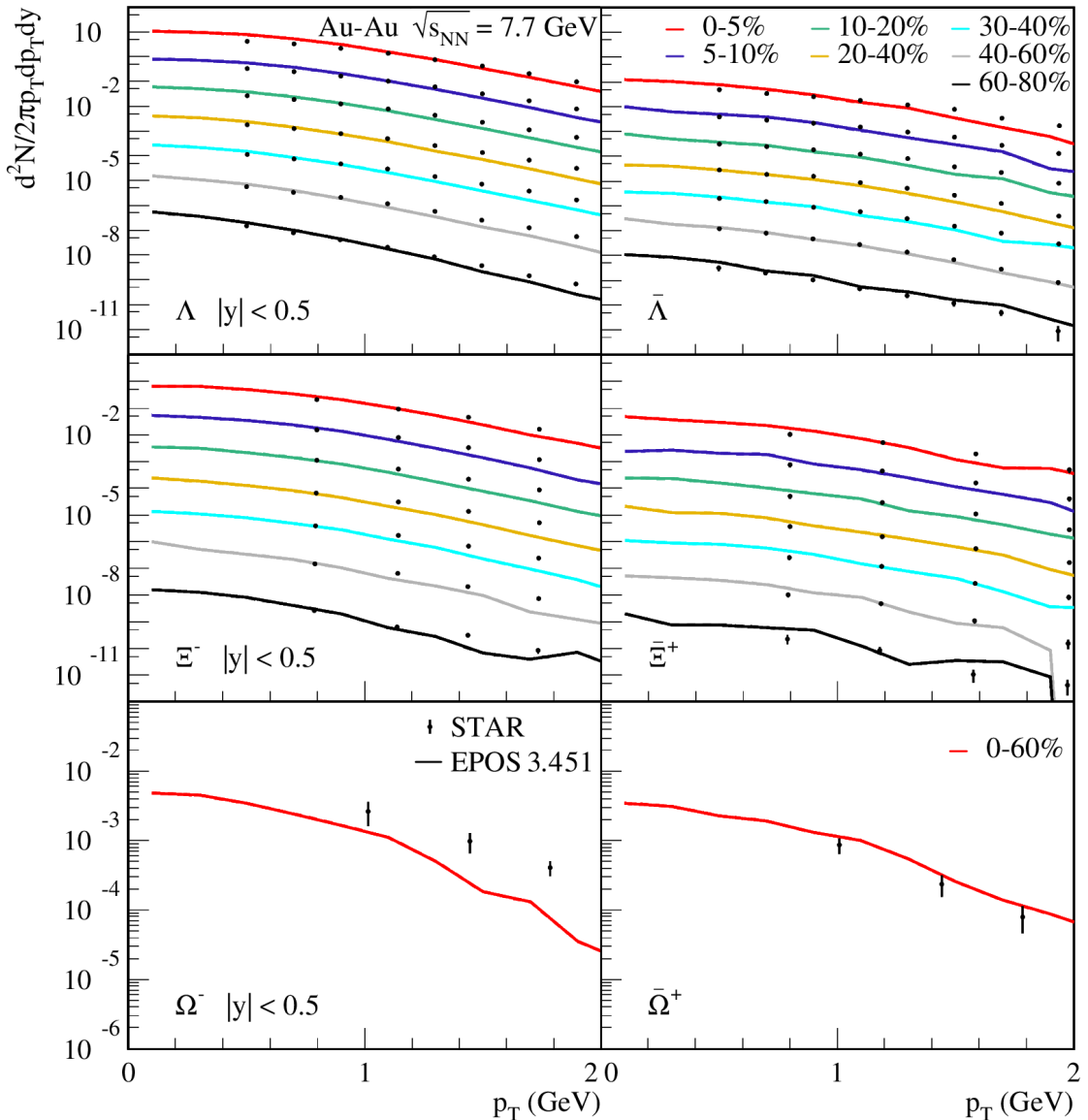


Figure 5.6: Transverse momentum spectra of Λ , $\bar{\Lambda}$, Ξ^- , $\bar{\Xi}^+$, Ω^- and $\bar{\Omega}^+$ for different centrality classes in Au-Au events at $\sqrt{s_{NN}} = 7.7$ GeV. Spectra for the most central events are at real scale, while the others are scaled by factors 10^{-x} ($x = \{1, 2, 3, 4, 5, 6\}$) (data from [315]).

Overall, the results for both light hadrons and hyperons confirm that EPOS is able to reproduce pretty well the production of these particles at mid-rapidity and low- p_T , for the whole range of the BES, on a quantitative level in particular for $\sqrt{s_{NN}} > 20$ GeV. This systematic study tends thus to confirm that EPOS is not really suited to simulate HICs at low energies (*i.e.* below 20 GeV/A), as expected. It starts, from these energies, to show significant differences with data, even though not completely off the mark. In particular, the softening of the p_T spectra compared to the experimental results at low energies might result from the instantaneousness assumption of the primary

interactions, equivalent to assume very thin colliding nuclei, a limitation discussed already in subsection 3.3.3. However, because of a smaller Lorentz boost, the nuclei has a thicker longitudinal extension at low energies. Hence, the particles produced early at mid-rapidity might lose more energy as they could be slowed down by the colliding nuclei. This would result into a shift of particles towards lower p_T values, as EPOS simulations show. Meanwhile, in a more realistic picture taking into account the finite extension of colliding nuclei, the particles could be produced later as the nuclei get through each other. Those particles would thus lose less energy by escaping the interaction region, as they would face less of the remaining nuclei matter on their way. This, on the contrary, would result into a less steep slope of the p_T spectra, as observed experimentally.

5.2 Study of the 2nd order cumulants of conserved charges

The results from the previous section revealed that EPOS 3.451 seems essentially able to reproduce properly the production of light hadrons and hyperons down to ~ 20 GeV/A, as expected, in the kinematic range $0 < p_T < 2$ GeV at mid-rapidity. Below this energy, the results from simulation show increasing deviations regarding experimental data as energy decreases, but stay relatively close to it down to 7.7 GeV/A still. Hence, EPOS 3.451 appears to be adequate for the study of 2nd order cumulants which has been motivated in subsection 2.3.3, and should be able to reproduce the variances and covariances measured by STAR in [211].

Therefore, I will start by showing in the first subsection the results from EPOS simulations for the (co)variances of net- π , net- K and net- p , as well as the related ratios C_{Qp} , C_{QK} and C_{pK} defined by the formulae (2.3.18). The objective is, in fact, to compare them with the results from STAR, in order to check if those results are correctly reproduced. Then, in subsection 5.2.2, I will display the comparison between these proxies and the enhanced ones suggested in [234] calculated from EPOS simulated events, and the exact 2nd order cumulants ratios of B , Q and S . In this way I can verify, with dynamical simulations of HICs, if the proposed enhanced proxy ratios enable to better reproduce the results from exact conserved charges. Finally, in subsection 5.2.3, I will expose the results of the estimation of the impact of the late stages of the collision on those observables, made possible by the modular conception of EPOS. I will show as well how much of the signal before hadronic cascades is originating from the core, which plays the role of QGP in EPOS simulations and is thus the part which goes through a phase transition. Indeed, if there were to be fluctuations emerging from the presence of criticality in the evolution of the system, it would be carried by the particles produced from the core.

In this section, I will exclusively focus on the results and their physical interpretation. Thus, all the details about the analysis employed to get those results from EPOS simulations are given in the appendix C. There, the analysis routine is detailed, and some information about its technical implementation are also provided, as well as an example of how to run it via the EPOS analysis framework. While results at all energies will be used for plots as a function of $\sqrt{s_{NN}}$, results as a function of the centrality (displayed by N_{part}) will be provided only for 7.7, 14.5, 27, 62.4 and 200 GeV/A for readability.

5.2.1 Results for STAR proxies: variances, covariances and their ratios

The first step, basic but very important, is to verify if EPOS can reproduce approximately well the experimental distributions of (co)variances of net- π , net- K and net- p and related ratios from [211]. As a reminder, all those particles are measured within

$|\eta| < 0.5$, have $0.4 < p_T < 1.6$ GeV and a DCA < 1 cm from the interaction vertex in the experiment, so the same cuts have been applied in the analysis of simulated events. Note that, from these (co)variances, the ratios C_{Qp} and C_{QK} from equation (2.3.18) are obtained via the relations (for both STAR and EPOS results):

$$C_{Qp} = \frac{\sigma_{Qp}^{11}}{\sigma_p^2} = \frac{\sigma_{\pi p}^{11} + \sigma_{pK}^{11} + \sigma_p^2}{\sigma_p^2} = \frac{\sigma_{\pi p}^{11}}{\sigma_p^2} + \frac{\sigma_{pK}^{11}}{\sigma_p^2} + 1 \quad (5.2.1)$$

$$C_{QK} = \frac{\sigma_{QK}^{11}}{\sigma_K^2} = \frac{\sigma_{\pi K}^{11} + \sigma_{pK}^{11} + \sigma_K^2}{\sigma_K^2} = \frac{\sigma_{\pi K}^{11}}{\sigma_K^2} + \frac{\sigma_{pK}^{11}}{\sigma_K^2} + 1 \quad (5.2.2)$$

I have decided to calculate the displayed cumulants as a function of N_{part} directly, instead of applying the CBWC introduced in subsection 2.3.2. The first reason is that EPOS enables this feature, as one can access this quantity on an event-by-event basis in the simulations. In order to really compare apples to apples, I used the Glauber estimated N_{part} values, and not the one provided by the PBGRT, as STAR uses the Glauber model for centrality determination. Secondly, it allows to have clearer results, and are simpler to calculate as they do not require intermediary calculation. Moreover, a study of the impact of the size of centrality classes already shown that for 2nd order cumulants, there are no effects visible whether correcting or not from the CBWE [224]. In order to ensure it, a graduate student I have supervised for an internship has performed the analysis using both N_{part} directly, and the CBWC for the same centrality classes as the ones used by STAR. He has notably used RIVET to code the analysis, taking advantage of the new possibility offered by the system I have elaborated and presented previously in chapter 4. Using 40 bins in N_{part} , he found absolutely no difference between the direct method and the CBWC method, the points obtained with the latter one matching perfectly with the curved obtained with the former one. Those results are shown for Au+Au at $\sqrt{s_{NN}} = 200$ GeV in figures B.1 and B.2. Besides confirming the results from [224], it was also expected as using 40 bins is roughly equivalent to considering 2.5% centrality classes, what largely reduces volume fluctuations compared to the 10% centrality classes of STAR.

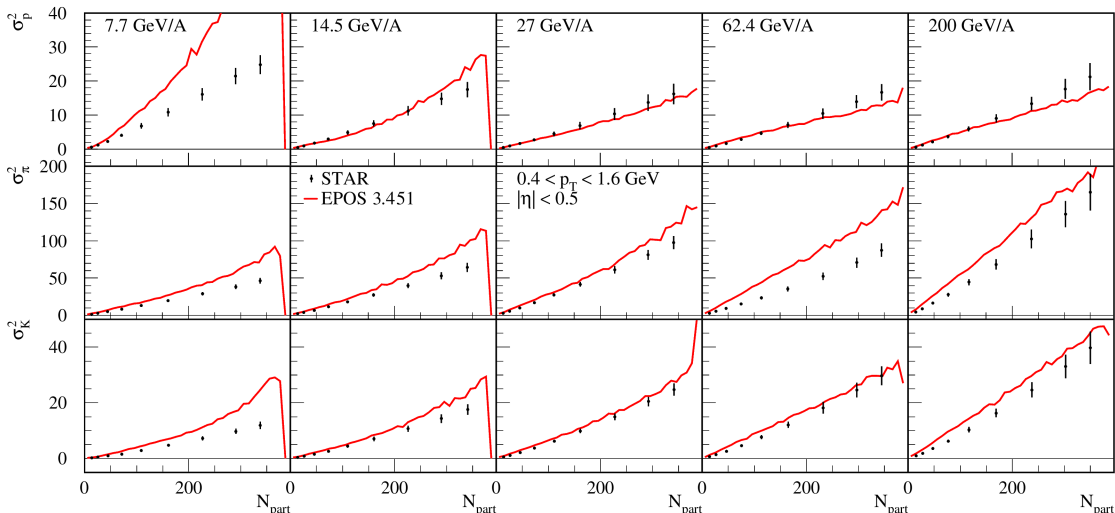


Figure 5.7: Net- p , net- K and net- π multiplicity variances vs. N_{part} for different energies, obtained from EPOS 3.451 simulations (red lines) and compared with STAR results (dots) [211].

The results for the variances are displayed in figure 5.7, compared with the data from STAR presented in 2.3.3. Above ~ 20 GeV/A, EPOS results are qualitatively good as

they show a linear increase with decreasing centrality of the collision (\leftrightarrow increasing of N_{part}) as expected. Still in this energy range, the results are globally good on a quantitative level, except for the net- π variance at 62.4 and 200 GeV/A which are very slightly overestimated. Such deviations from data are usually caused by either global overproduction of both π^+ and π^- , for this precise case, or an imbalance in their production with more π^+ than π^- produced, compared to data. Indeed, looking at equation (2.3.14) I repeat here:

$$\sigma_\alpha^2 = \langle \delta N_\alpha^2 \rangle - \langle \delta N_\alpha \rangle^2 ,$$

one understands that a modification of δN_α by a factor c_α , caused by any of the previously mentioned reasons, would account for a change of σ_α^2 by a factor c_α^2 . Physically speaking, it can be understood by the fact that when the global multiplicity of a system is higher, there are more different configurations (or micro-states) possible and then the variance of the distribution increases as fluctuations are more important from one event to another. Thus, although the production of charged pions seemed to be perfectly reproduced by EPOS in the results exposed in the previous section for 62.4 and 200 GeV/A, variances are pretty sensitive to multiplicity variation. Moreover, the results in question for p_T spectra of charged pions at those two energies are compared to data from different experiments than STAR, *i.e.* PHOBOS and PHENIX, what could also play a role. Below ~ 20 GeV/A however, the results from EPOS deviate from a linear increase, even further as the energy decreases. This is no surprise considering the conclusion from last section, which showed that in this range, EPOS do not reproduce very well particle production. In particular, the huge overshooting of σ_p^2 for central collisions at 7.7 GeV/A can be directly connected to the results in figure A.6, where proton production exceeds data for the whole displayed p_T range while antiproton production is globally underestimated. Despite this failure at low energy, the slope variation of the variances for the whole scrutinised energy range is nonetheless well reproduced, even though not always in the right proportion.

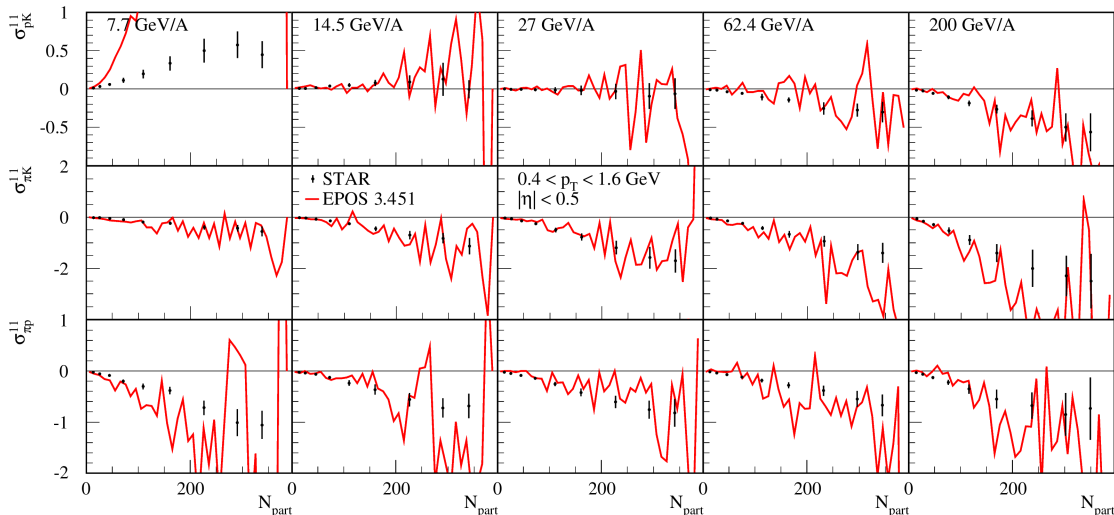


Figure 5.8: Net- p , net- K and net- π multiplicity covariances vs. N_{part} for different energies, obtained from EPOS 3.451 simulations (red lines) and compared with STAR results (dots) [211].

The results for the covariances are shown in figure 5.8. Here, statistical fluctuations are far more important because of the relatively small number of events analysed for each energy (see table 5.1). Still, the tendencies show by results obtained with EPOS manage to reproduce well the experimental measurements on average. The only clear

discrepancy with data is seen for σ_{pK}^{11} at 7.7 GeV/A, but EPOS is still able to reproduce the particular change of sign of this observable around 20 GeV/A, as measured by STAR. This is all the more notable as UrQMD alone, whose results are shown in comparison with the data in the STAR publication [211], obtains a signal compatible with zero at high energy for this covariance.

Finally, the obtained ratios C_{pK} , C_{Qp} and C_{QK} are presented in figure 5.9. Differences between EPOS results and STAR data are obviously visible at 7.7 GeV/A, due to the deviations of (co)variances discussed precedingly. Nevertheless, the agreement is good among the other energies for all three ratios within statistical fluctuations. A slight centrality dependence is potentially visible for C_{Qp} and C_{QK} at the two top energies though, while STAR data are centrality independent. As a first conclusion, the results of this subsection tend to indicate that EPOS is appropriate to lead a study, both qualitative and quantitative, on the experimental proxies of 2nd order susceptibilities of B , Q and S . The results below ~ 20 GeV/A need however to be taken carefully, as EPOS show here some limits of applicability.

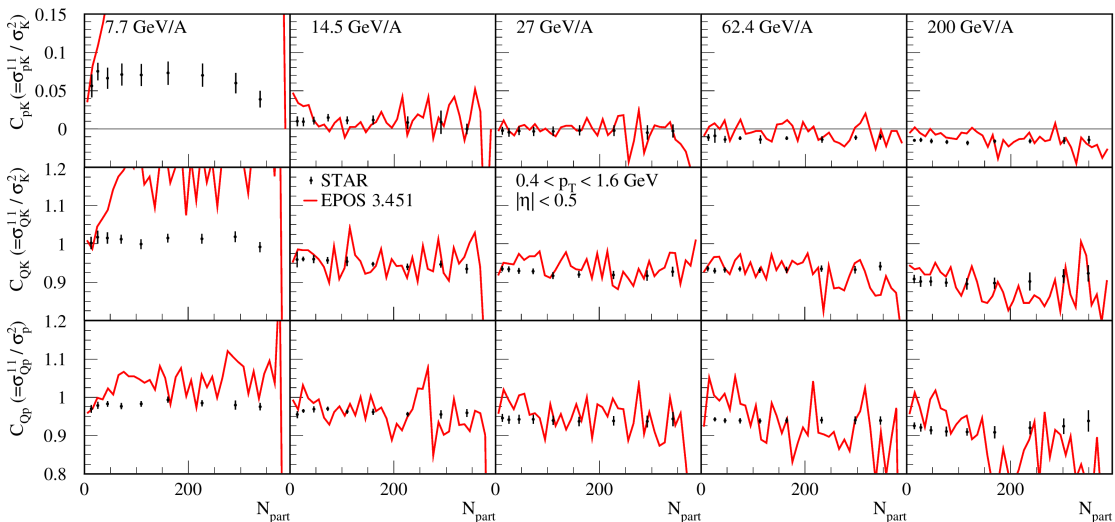


Figure 5.9: Ratios of net- p , net- K and net- π multiplicity (co)variances vs. N_{part} for different energies, obtained from EPOS 3.451 simulations (red lines) and compared with STAR results (dots) [211].

5.2.2 Comparison with enhanced proxies and conserved charges cumulants

Taking advantage of the fact that EPOS offers the possibility to get access to all particles produced in heavy-ion collisions, I could calculate the ratios of exact 2nd order cumulants of conserved charges using the analysis described in appendix C. It has been motivated by the objective, explained in section 3.5, to compare them with the enhanced proxies proposed in [234] and the one measured by STAR, studied in the previous subsection. This way, I can test if the proposed enhanced proxies, resulting from a theoretical study, are effectively better at reproducing cumulants of conserved charges than the ones used by STAR, via dynamical simulations which recreates the conditions of the experiment.

The ratios of conserved charge (co)variances studied here are the following ones:

$$C_{QB} = \frac{\sigma_{QB}^{11}}{\sigma_B^2} \left(\equiv \frac{\chi_{11}^{QB}}{\chi_2^B} \right), \quad C_{QS} = \frac{\sigma_{QS}^{11}}{\sigma_S^2} \left(\equiv \frac{\chi_{11}^{QS}}{\chi_2^S} \right), \quad C_{BS} = \frac{-\sigma_{BS}^{11}}{\sigma_S^2} \left(\equiv \frac{\chi_{11}^{BS}}{\chi_2^S} \right). \quad (5.2.3)$$

The minus sign in the definition of C_{BS} comes from the fact that, when measuring these conserved charges from net-hadron multiplicities, positive baryonic number is associated to a negative strangeness as strange baryons carry s quarks which have $S = -1$ by convention. These ratios are, so far, approximated experimentally with net- π , net- K and net- p (co)variances ratios measured by STAR, recalled here from equation (2.3.18):

$$C_{Qp} = \frac{\sigma_{Qp}^{11}}{\sigma_p^2} \left(\cong \frac{\chi_{11}^{QB}}{\chi_2^B} \right), \quad C_{QK} = \frac{\sigma_{QK}^{11}}{\sigma_K^2} \left(\cong \frac{\chi_{11}^{QS}}{\chi_2^S} \right), \quad C_{pK} = \frac{\sigma_{pK}^{11}}{\sigma_K^2} \left(\cong \frac{\chi_{11}^{BS}}{\chi_2^S} \right).$$

The enhanced proxies related to the two strangeness-related ratios, presented in subsection 2.3.3 and based on variances of net- K , Λ , Ξ and Ω , are also recalled here from equations (2.3.25) and (2.3.26):

$$\tilde{C}_{QS} = \frac{1}{2} \cdot \frac{\sigma_K^2}{\sigma_K^2 + \sigma_\Lambda^2} \left(\cong \frac{\chi_{11}^{QS}}{\chi_2^S} \right),$$

$$\tilde{C}_{BS} = \frac{\sigma_\Lambda^2}{\sigma_K^2 + \sigma_\Lambda^2} \quad \text{or} \quad \tilde{C}'_{BS} = \frac{\sigma_\Lambda^2 + 2\sigma_\Xi^2 + 3\sigma_\Omega^2}{\sigma_\Lambda^2 + 4\sigma_\Xi^2 + 9\sigma_\Omega^2 + \sigma_K^2} \left(\cong \frac{-\chi_{11}^{BS}}{\chi_2^S} \right).$$

However, no enhanced proxy ratio has been proposed for the QB correlation (χ_{QB}^{11}/χ_2^B) in [234], whereas it has been measured by the STAR collaboration via C_{Qp} . Hence, I propose to study the following proxy ratio:

$$\tilde{C}_{QB} = \frac{\sigma_{\pi p}^{11} + \sigma_p^2}{2\sigma_p^2 + \sigma_\Lambda^2} \left(\cong \frac{\chi_{11}^{QB}}{\chi_2^B} \right). \quad (5.2.4)$$

This proposition is based on the breakdown of hadronic contribution to χ_{11}^{BQ} and χ_2^B , shown in figure 5.10. It follows the argument from the authors saying that, to build a good proxy ratio, it is important to use (co)variance proxies that are equally good for both numerator and denominator. However, when looking at those figures, one can realise that $\sigma_p^2 + \sigma_{\pi p}^{11}$ contribute to a bigger fraction (< 1) of χ_{11}^{BQ} than $2\sigma_p^2 + \sigma_\Lambda^2$ contributes to χ_2^B . I could have proposed to use only σ_p^2 as a proxy for χ_{11}^{BQ} , to keep almost equal contribution proportions. I still propose to use $\sigma_{\pi p}^{11}$ in addition to σ_p^2 though, in order to follow the authors' claim that isospin randomisation prevents from building proxies with fluctuations of net- p only [234]. Because of isospin randomisation, protons represent approximately half of the nucleons in the system, what justifies then the factor 2 in front of σ_p^2 for the χ_2^B proxy.

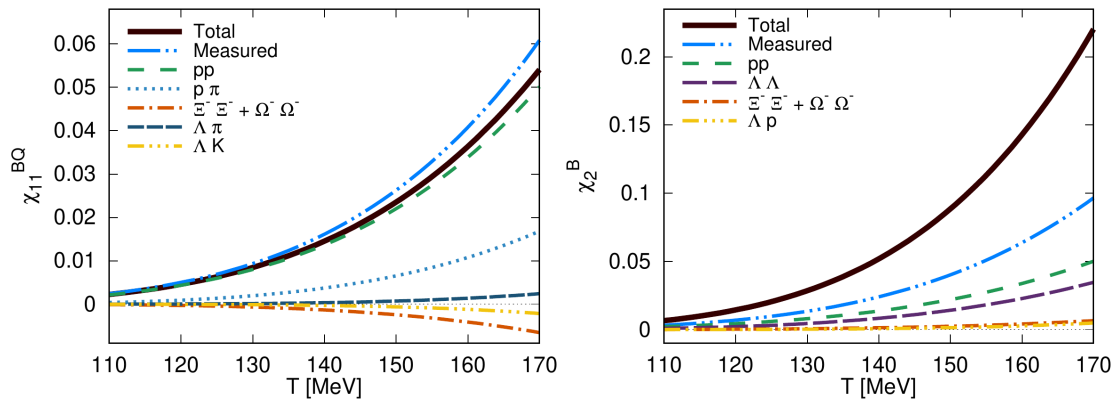


Figure 5.10: Breakdown of hadronic contribution to χ_{QB}^{11} and χ_2^B as a function of T , obtained with HRG model calculations [234].

Hence, all these ratios have been calculated from particles still measured within $|\eta| < 0.5$ and with $0.4 < p_T < 1.6$ GeV, to match with the measurement of the STAR proxies. The results as a function of N_{part} are displayed in figure 5.11, for the five same energies from which results of the previous subsection have been shown. The first important conclusion from these results is that the enhanced proxies, proposed in [234] and denoted \tilde{C}_{XY} (in blue/cyan in the plots), are effectively way better at reproducing the ratios of conserved charges (co)variances (in green) than the one used by STAR (in red).

In particular, the C_{BS} ratios deserves a special attention here. As discussed already in subsection 2.3.3, its proxy C_{pK} measured by STAR show a certain centrality dependence below 19.6 GeV/A which is not present for higher collision energies, where it also changes its global sign. For what can be observed here, the ratio C_{BS} for exact charges has absolutely no centrality dependence except for 7.7 GeV where it operates a clear change of behaviour. Its value decreases from ultra-peripheral to peripheral events, and then remains at an overall value consistent with 0, while it remains at 0.2 whatever the centrality for all energies above. The results at $\sqrt{s_{NN}} = 7.7$ GeV/A are also the only ones for which the enhanced ratio \tilde{C}_{BS} does not reproduce better the ratio of conserved charges than C_{pK} . However, results from the previous sections shown that EPOS 3.451 simulations are not really consistent with experimental data at such low energies of the BES program, so it is hard to make any interpretation of these results specifically.

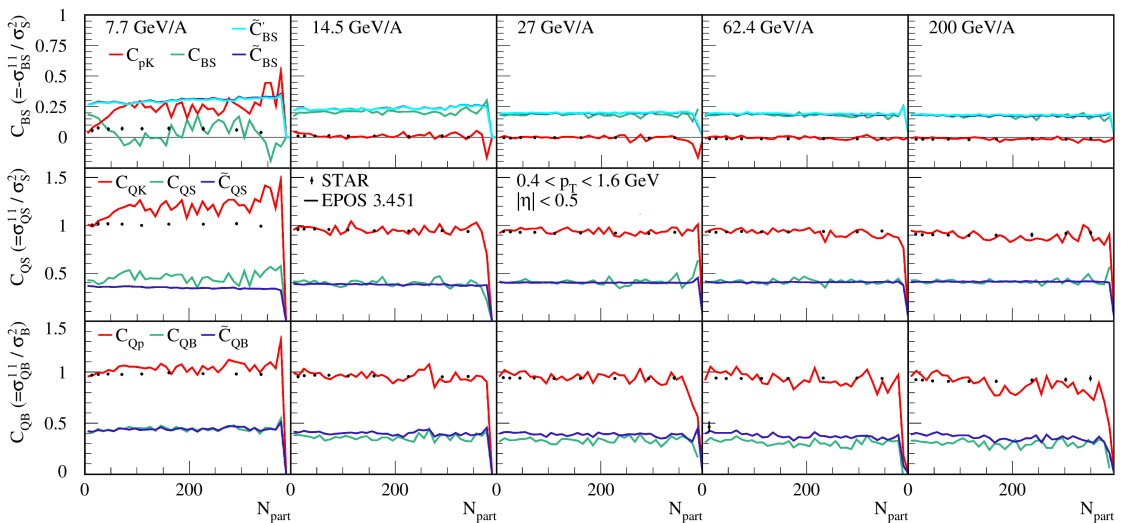


Figure 5.11: Ratios of exact B , Q and S conserved charges (co)variances and their proxies displayed as a function of N_{part} for different energies, obtained from EPOS 3.451 simulations (lines) and compared with STAR data (dots) as an indication [211].

On a different level, it is worth noticing that no difference is visible between the two enhanced proxies \tilde{C}_{BS} (involving only net- K and net- Λ variances) and \tilde{C}'_{BS} (involving in addition net- Ξ and net- Ω). This observation is very interesting as it means that using only net- Λ variance in addition to the ones already measured by STAR improves significantly the proxies. This is true for the study of C_{BS} in particular, but also more generally for all 2nd order cumulants of conserved charges, as the baryon-strangeness correlator is the only one where using Ξ and Ω has been proposed. Hence, the \tilde{C}'_{BS} ratio is not really useful as it does not bring anything more than the \tilde{C}_{BS} one. Consequently, \tilde{C}_{BS} will be the only enhanced proxy of C_{BS} considered for the rest of my work, while \tilde{C}'_{BS} will not be used anymore.

The only enhanced ratio based on a covariance is the \tilde{C}_{QB} proxy ratio proposed by myself, using $\sigma_{\pi p}^{11}$. One could even do without though, as its amplitude is negligible compared to the one of σ_p^2 with which it is combined at the numerator, as seen from figures 5.7 and 5.8. An important thing to notify then is the fact that the enhanced proxies, which show a remarkable good agreement with ratios of conserved charges, contain only variances. This allows to reduce drastically the statistical fluctuations of obtained ratios, which are mainly originating from covariances in the STAR proxies as can be seen in the previous subsection.

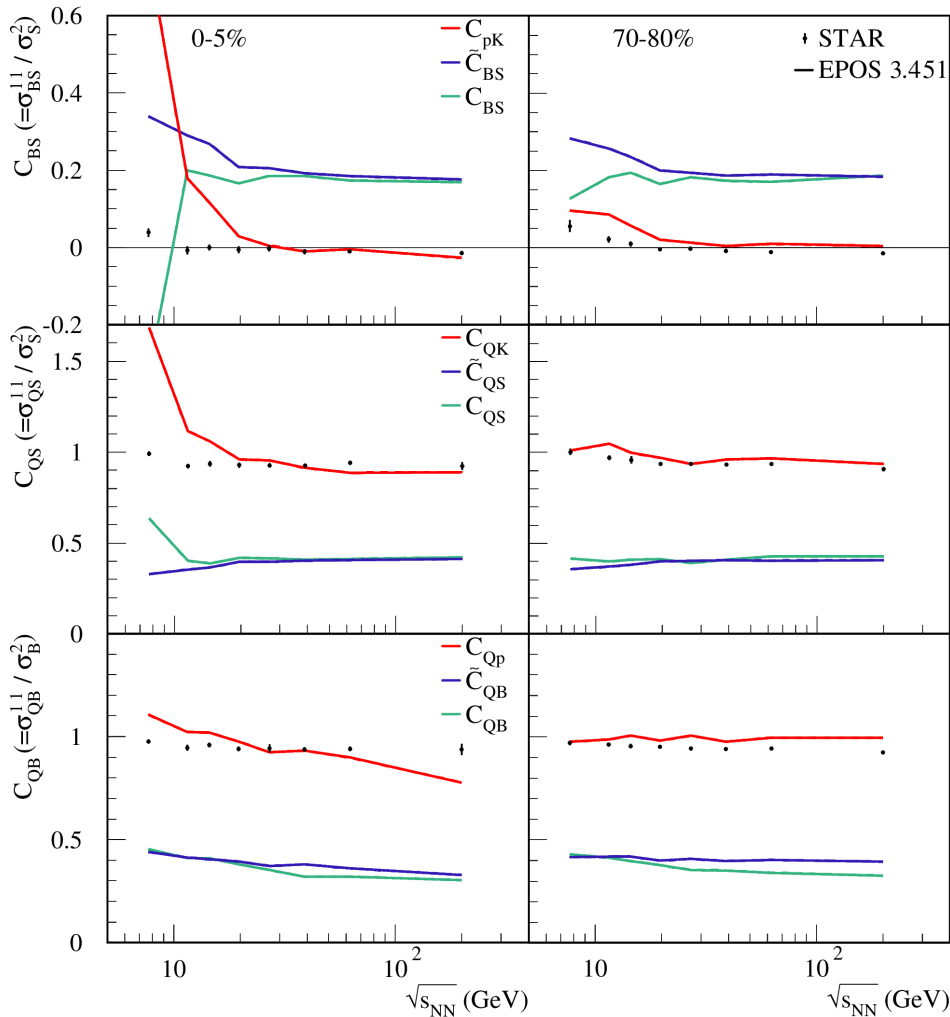


Figure 5.12: Ratios of exact B , Q and S conserved charges (co)variances and their proxies displayed as a function of $\sqrt{s_{NN}}$ for central (left) and peripheral (right) collisions. Results from EPOS 3.451 simulations (lines), compared with STAR data (dots) as an indication [211].

The comparison between the ratios of 2nd order cumulants of B , Q and S , their STAR proxies and proposed enhanced proxies, all of them calculated from EPOS 3.451 simulations, is summarised in figure 5.12. All the ratios are displayed there as a function of the collision energy, for the most central (0-5%) and most peripheral (70-80%) collisions as considered in the analysis made by STAR in [211]. As already stated, the fact that the enhanced proxies reproduces almost perfectly the conserved charges ratios is clearly visible there. I recall that experimental data from STAR are only displayed to compare with STAR proxies calculated from simulated events, but that the main purpose is to see which proxies, between the STAR ones and the enhanced ones, are the most similar to cumulants of conserved charges. The quantitative variations of these ratios as a function

of the energy are nevertheless pretty identical from 19.6 GeV/A up to higher energies, and using either enhanced proxies or STAR proxies does not make any difference. Below 19.6 GeV/A, where significant variations of C_{BS} and C_{QS} are observed, the enhanced proxies seem to show less pronounced changes than the STAR ones. However, once again the results from EPOS in this energy range are found to diverge substantially from the experimental data, what prevents to draw any conclusion.

5.2.3 Impact of hadronic cascades on the 2nd order cumulants

The last part of my work concerns the impact of the hadronic phase at the end of HICs on the observables studied previously. During these last stages, the hadrons formed from the bulk matter will re-interact with each other in successive collisions, both elastic and inelastic, what changes both the chemistry of the system and the kinematic distributions, until the freeze-outs happen. Hence, as I explained already in section 3.5, my objective is to study how the fluctuations of conserved charges imprinted in the distribution of particles formed at hadronisation survive these hadronic cascades. In particular, I have intended to quantify these changes, in order to support the experimental efforts to probe those fluctuations through the measurement of net-multiplicity cumulants. To do so, I can take advantage of the modular conception of EPOS, which allows to access the distribution of particles before they enter the UrQMD afterburner simulating these hadronic re-interactions.

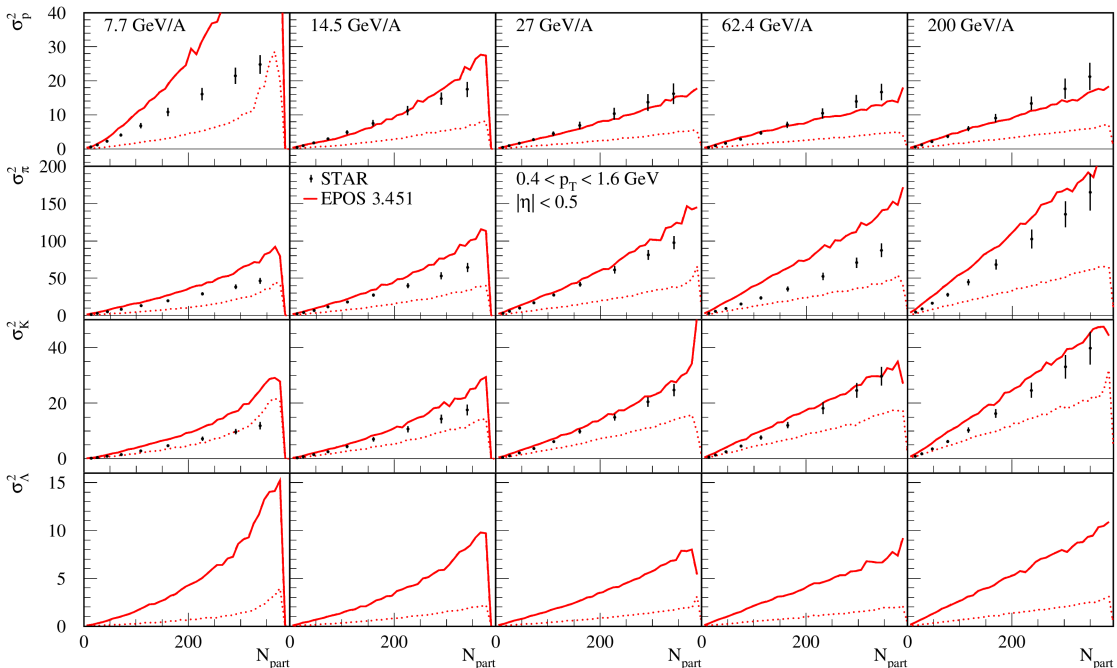


Figure 5.13: Net- p , net- π , net- K and net- Λ multiplicity variances vs. N_{part} for different energies, obtained from EPOS 3.451 simulations and compared with STAR results (dots) [211]. The results calculated from full events are represented by full lines, while results calculated before hadronic cascades are represented by dotted lines.

I started by looking at the impact of hadronic cascades on the (co)variances of net-multiplicity cumulants used to form the ratios of interest. In figure 5.13 are displayed σ_p^2 , σ_π^2 , σ_K^2 and σ_Λ^2 calculated for particles at the end of complete event simulations (referred to as "full" events) and before the hadronic cascades (designated by "no hacas" in the plots). These variances are of interest as they are used in both STAR proxies and the

proposed enhanced proxies, introduced in subsection 2.3.3 and discussed in the previous subsection. In both cases, before hadronic cascades and at the end of the events, they are calculated in the same conditions than the STAR measurements, *i.e.* for $0.4 < p_T < 1.6$ GeV and within $|\eta| < 0.5$.

The principal conclusion coming from figure 5.13 is the fact that hadronic cascades are shown to have a strong impact on variances of net-particle multiplicities. They increase greatly the signal, from doubling to even tripling it, with different magnitudes depending on the hadronic species though. The increase of variances of mesons (charged π and K) due to hadronic cascades tends to grow with energy. Meanwhile, the proportion of signal for baryons (p and Λ) due to hadronic cascades decreases from 7.7 GeV/A to 27 GeV/A while increases again when going up to 200 GeV/A. The same conclusion is also visible for the covariances, shown in figure 5.14 for full events and before hadronic cascades as well. Here again, a great part of the signal seem to originate from the hadronic phase for all three covariances studied. In fact, for all covariances results shown here, hadronic cascades are responsible for most of the covariance amplitude, if not all of it, as seen despite the important statistical fluctuations.

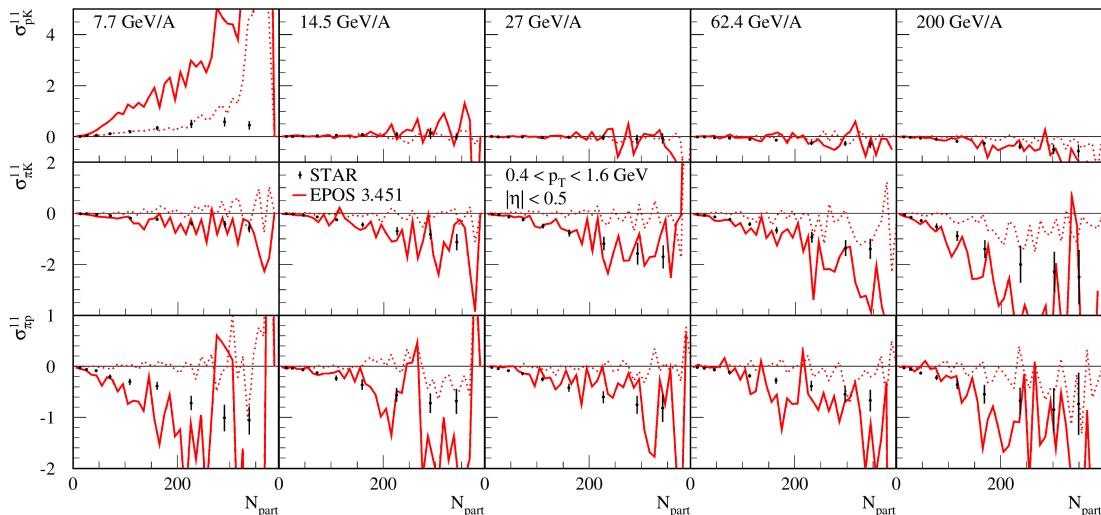


Figure 5.14: Covariances of net- p , net- π and net- K multiplicity distribution vs. N_{part} for different energies, obtained from EPOS 3.451 simulations and compared with STAR results (dots) [211]. The results calculated from full events are represented by full lines, while results calculated before hadronic cascades are represented by dotted lines.

The increase of the variances and covariances can be explained by the fact that, during the hadronic cascades, the numerous inelastic scatterings that occur produces many more of the involved hadronic species, coupled to the successive decays of heavy resonances produced at hadronisation. Hence, the successive decays and inelastic scatterings, producing simultaneously several of the hadronic species of interest, lead unavoidably to the amplification the correlations carried by (co)variances, blurring this way the real amplitude of the thermal fluctuations of interest. Another effect which might play a role here is the kinematic spreading, or the fact that particles carrying conserved charges might contaminate the phase space considered in the analysis while not originating from there originally. Towards contamination of the η window studied, we can naively postulate that the number of conserved charges (carried by hadrons) entering the considered window, during the hadronic cascades, is counterbalanced by the same charges going out during this same phase. The statement made from the results exposed here supports strongly

the results from a study led with a hybrid version of UrQMD, which has been coupled to a fluid dynamical simulation of bulk matter [231]. They investigated the time-evolution of the correlation of distributions of hadron families carrying conserved charges, with regard to these same distribution at hadronisation time. The conclusion was that the final distribution of hadrons observed by experiments is not really related anymore to the one obtained after hadronisation, which is containing the potential critical signal from phase transition. In other words, any information encoded in the kinematic distribution of hadrons at hadronisation time is not reflected in the distribution at the very end of the collision, because hadronic rescatterings decorrelate significantly these distributions.

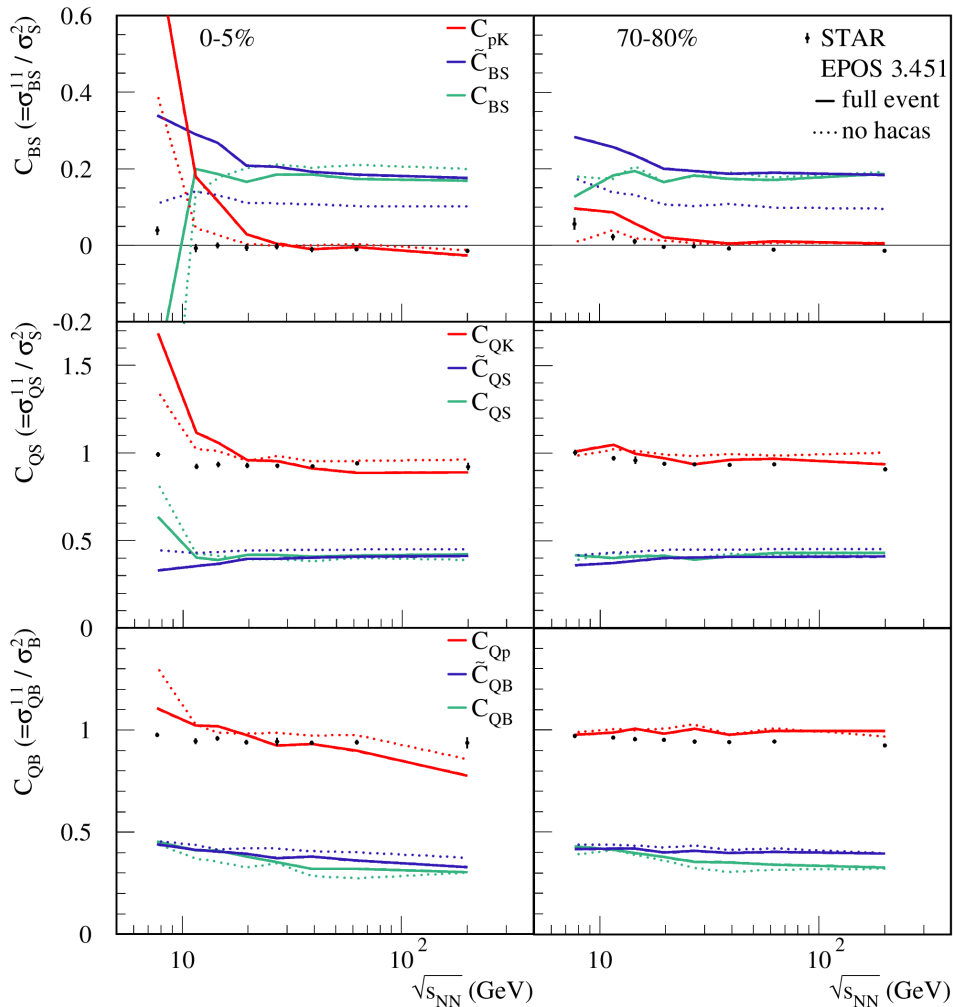


Figure 5.15: Ratios of exact B , Q and S conserved charges (co)variances and their proxies plotted as a function of $\sqrt{s_{NN}}$ for central (left) and peripheral (right) collisions. Results are displayed for full event calculation (full lines) and calculation before hadronic cascades (dotted lines) from EPOS 3.451 simulations. STAR data (dots) are shown as an indication [211].

The second step being to have a look at the proxy ratios, I show in figure 5.15 the results obtained for conserved charges and both STAR and enhanced proxies as a function of $\sqrt{s_{NN}}$, for full events and before hadronic cascades. Here, almost all ratios show a very small variation between before and after hadronic cascades, except \tilde{C}_{BS} which value is approximately doubled by hadronic cascades for both central and peripheral centrality classes. It confirms thus, with what can be observed from the variances and covariances used to build these proxy ratios, that the apparent small modification due to the hadronic phase do not mean that it has a negligible impact. On the contrary, the

results on other ratios just reflect incidentally the fact that proxies used in numerator and denominator are modified in the same proportions during hadronic cascades. For exact conserved charges however, the small modifications of ratios are truly due to small modifications of the conserved charges (co)variances caused by hadronic cascades, thanks to the precautions taken in the analysis which is exposed in appendix C. The impact of hadronic cascades on variances and covariances of conserved charges for the simulated events used in this work can be seen in figures D.1 and D.2, respectively.

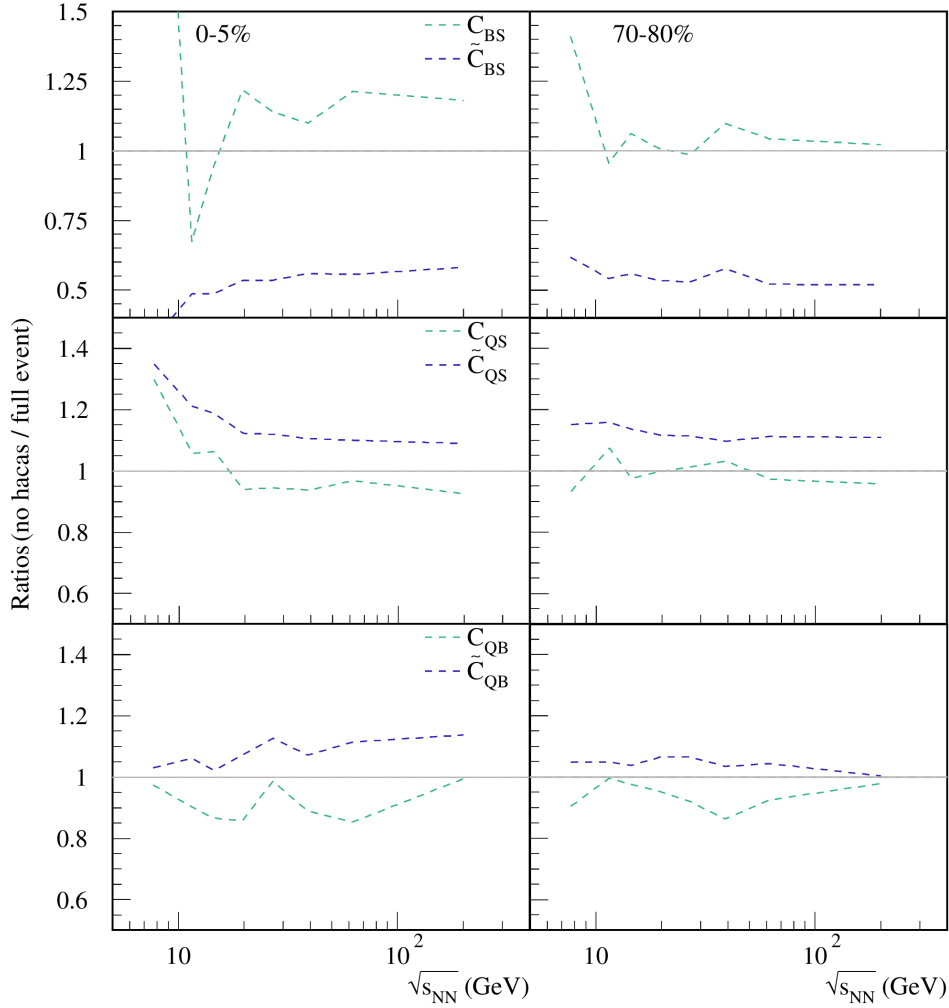


Figure 5.16: Ratios of C_{XY} and enhanced proxies \tilde{C}_{XY} calculated before hadronic cascades over full event calculations, plotted as a function of $\sqrt{s_{NN}}$ for central (left) and peripheral collisions (right).

Although it is difficult, as it stands, to quantify the impact of hadronic cascades on STAR proxy ratios due to the large statistical fluctuations of covariances (see figure 5.14), I can still legitimately try to quantify it on enhanced proxies and conserved charge ratios. Consequently, the ratios of C_{XY} and associated proxies \tilde{C}_{XY} before hadronic cascades over the values for full events are shown in figure 5.16. Note that even though I am talking about quantifying the impact of hadronic cascades, I do represent here, via these ratios, the proportion of the signal measured in the end of the collision which effectively originates from hadronisation. The most important modification of the signal is obtained for the \tilde{C}_{BS} proxy, as mentioned in the discussion of the previous figure. Only 50 to 60% of the final measured proxy is effectively coming from before hadronic cascade. Contrary to this proxy, the corresponding exact ratio C_{BS} has a proportion of signal from hadro-

nisation varying from ~ 1.2 in central collisions to ~ 1 in peripheral ones. At low energy, it even shows strong variations, which can however hardly be interpreted as discussed several time already. For the two other correlators related to Q , an interesting point to notice is that even though their modification factors due to hadronic cascades do not have the same amplitude, they have approximately similar variations with energy. Those proportion of signal originating from before the hadronic cascades are roughly varying between ~ 0.8 and ~ 1 for exact ratios C_{QS} and C_{QB} , while varying between ~ 1 and ~ 1.2 for enhanced proxies \tilde{C}_{QS} and \tilde{C}_{QB} .

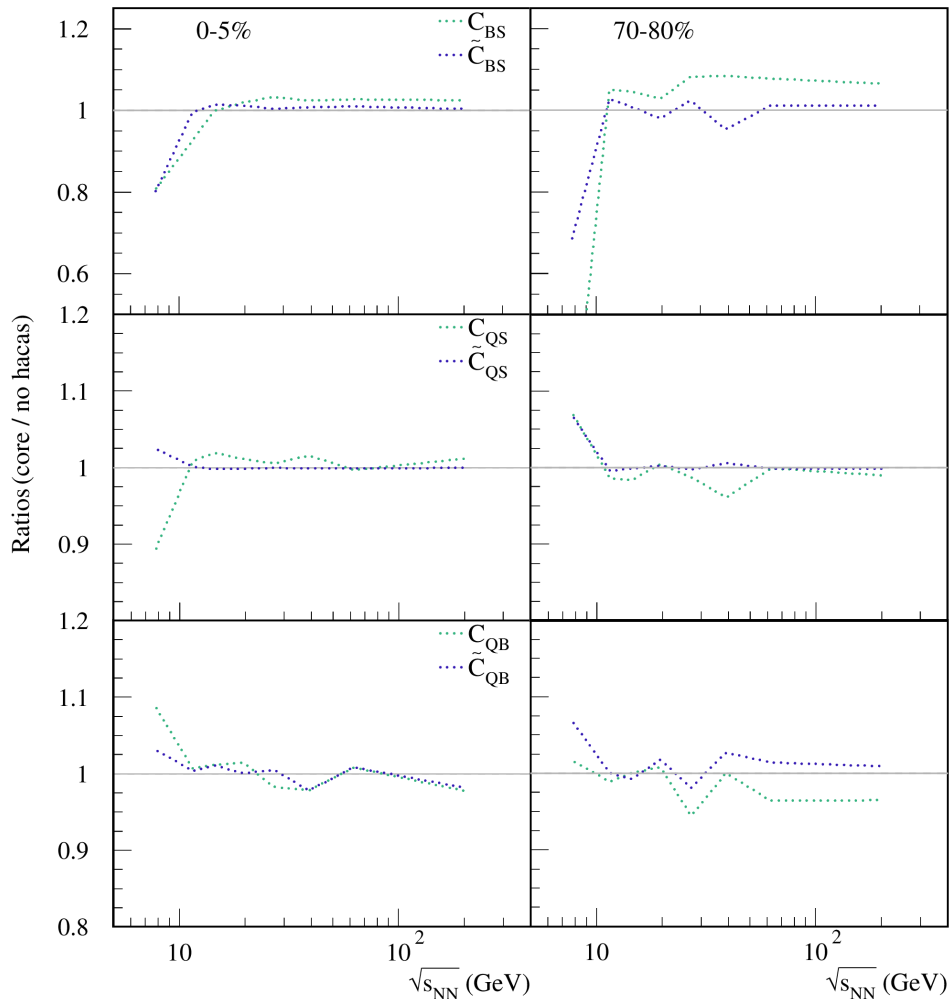


Figure 5.17: Core proportion of C_{XY} and enhanced proxies \tilde{C}_{XY} ratios over the total value calculated before hadronic cascades, plotted as a function of $\sqrt{s_{NN}}$ for central (left) and peripheral collisions (right).

At last, it is important to see how much of the signal before hadronic cascades is really coming from the fluid itself, identified by the core in EPOS framework. Hence, figure 5.17 show the ratio between proxy and conserved charges ratios originating from the core, over their total values before hadronic cascades. These ratio are all very close to 1 above ~ 15 GeV/A, but diverge from this value at low collision energies. This result was expected, as a previous study conducted with EPOS on the origin of produced particles, made via p_T distribution for BES Au-Au collisions, has shown that the vast majority of low- p_T hadrons are originating from the core [290]. For low energy however, the core is supposed to represent a smaller part of the system, as it is harder to reach the critical energy density to form it, what explains the observed deviation to 1.

5.3 Summary of results on 2nd order cumulants study

Before moving on to the general conclusion of the thesis, I will summarise the results obtained in this chapter, based on the objectives outlined in section 3.5. As a reminder, all the work presented here is related to Au-Au collisions performed in the energy range of the BES program, *i.e.* $\sqrt{s_{NN}} = 7.7, 11.5, 14.5, 19.6, 27, 39, 62.4$ and 200 GeV here in particular.

In the first section, I have exposed some results concerning particle production of commonly measured hadronic species from simulations obtained with EPOS 3.451, one of the latest versions of the EG. To obtain them, an important work has been necessary to collect the experimental data to compare with, and to write the corresponding analyses using the EPOS analysis framework. The new machinery I have developed by integrating the use of RIVET in this analysis framework, presented in chapter 4, could only be used for one of these analyses. Even if we could have used RIVET to write the analyses we wanted to apply on our simulations which were not available yet, the system natively available in EPOS is more convenient to use as most of the classical distributions usually measured are already encoded into routines. Although we were limited in employing RIVET, because of the small number of analyses for Au-Au collisions available for the BES so far, it shown that this new feature has been successfully integrated and is now functional. The results for particle production consist of charged particles pseudorapidity distributions for a large acceptance, and p_T spectra in the low momentum range ($0 < p_T < 2$ GeV) for identified light hadrons ($\pi^\pm, K^\pm, p/\bar{p}$) and strange baryons ($\Lambda/\bar{\Lambda}, \Xi^-/\bar{\Xi}^+, \Omega^-/\bar{\Omega}^+$).

In the phase space of interest for my next study, *i.e.* for $p_T < 2$ GeV and at central pseudorapidity $|\eta| < 0.5$, EPOS has been shown to reproduce very well particle production in overall. It is especially the case for collisions energies above 20 GeV/A, while under this scale, the results show more and more important discrepancies with the experimental measurements as collision energy decreases.

This result was nevertheless expected, because of the important assumption on which relies the Parton-Based Gribov-Regge Theory used in EPOS, that initial interactions happens all instantaneously. By exploring this energy range, we are in fact testing the limits of EPOS applicability, as it was originally designed to be mainly applied to the physics of the LHC.

As it has been proven to reproduce properly experimental data in general, I have then employed EPOS 3.451 to study the 2nd order cumulants of conserved charges B, Q, S and its proxies used in experiments in the second section. I started by comparing the results on variances and covariances of net-multiplicity distributions for protons, pions and kaons to the data from the STAR collaboration.

Results for (co)variances of net- p , net- π , net- K and their ratios from EPOS simulations are in good qualitative agreement, and even quantitative globally, with STAR measurements for collisions energies above ~ 20 GeV/A. For low energies however, EPOS results show a slightly different qualitative behaviour, reflecting its difficulties to reproduce properly particle production, pointed out in the previous paragraphs.

I have then measured from EPOS simulations some enhanced proxy ratios based on variances of net- Λ , net- Ξ and net- Ω in addition, proposed by the authors of [234] and myself, who have been inspired by their study. Both proxy ratios, with the ones measured by STAR, were compared to the (co)variances ratios of exact conserved charges, to evaluate how effective are the former ones to approximate the latter ones.

It appears that proxy ratios \tilde{C}_{QS} and \tilde{C}_{BS} , proposed in [234], and \tilde{C}_{QB} proposed by myself thanks to this cited work, are way better at reproducing the conserved charge ratios than the STAR proxies. In particular, the only use of net- Λ variance, in addition to the usual net- p , net- π and net- K variances, improve already greatly the efficiency of the proxies to reproduces the exact ratios. Moreover, using only variances appears to be sufficient to build good proxies, as protons, kaons and lambdas carry each of them two different conserved charges, what reduces greatly the statistical fluctuations on the ratios.

Another measure of both proxy and exact ratios just after hadronisation of the simulated system, made possible by the modular conception of EPOS, have allowed me to quantify the impact of hadronic cascades on these observables.

Supporting the conclusion from previous studies, it appears that the hadronic re-scattering stage of the collision modifies importantly the signal of net-multiplicity fluctuations. Although hadronic cascades have a large influence on the amplitude of the net-multiplicity (co)variances, the proxy ratios built out of them seem to be little affected by hadronic cascades. \tilde{C}_{QS} and \tilde{C}_{QB} in particular suffer very small quantitative modifications due to the hadronic stage, so they can be used as good proxies to probe their corresponding conserved charges ratios. The \tilde{C}_{BS} proxy ratio, though, do not share this property and makes a bad proxy in that sense.

Finally, I could estimate the proportion of fluctuations originating from the core itself before hadronisation, for ratios of conserved charges and proxies. I expected that most of the signal should come from the core, which evolves like an almost perfect fluid in EPOS to mimic the behaviour of QGP. Precedent work had in fact demonstrated that as the vast majority of low- p_T particles at mid-rapidity are produced by the hadronisation of this bulk matter.

My results confirmed that the fluctuations measured after hadronisation in the phase space considered ($0.4 < p_T < 1.6$ GeV for $|\eta| < 0.5$) are almost exclusively originating from the core, except at the lowest energies considered where the bulk matter represent a smaller fraction of the system created.

CONCLUSION & OUTLOOK

The main goal of my research, presented in this thesis, was to study the impact of hadronic cascades on the 2nd order cumulants of net-multiplicity distributions (also called variances and covariances), for different proxies of conserved charges B , Q and S . The main motivations for this work have been exposed in the end of chapter 2, following a detailed description of the context discussed in the previous paragraphs, after having depicted in chapter 1 the main background in which it takes place, *i.e.* the SM of particle physics. It is based in particular on the measurement of net- π , net- K and net- p (co)variances by the STAR collaboration [211], and the proposition of enhanced proxies employing additionally net- Λ , net- Ξ and net- Ω variances from a study combining lattice quantum chromodynamics and HRG model calculations [234]. To conduct this research, I have used the EPOS general purpose event generator, principally dedicated to the study of HICs. It allows to study properly the event-by-event fluctuations of conserved charges by simulating, one by one, the complete dynamics of collisions, reproducing the conditions of the experiments. It features notably, among many other characteristics introduced in chapter 3, a core-corona separation of matter, with the densest part (core) treated as a near-perfect fluid to mimic the expected behaviour of the evolution of QGP. This specificity makes it very successful to reproduce many results from the experiments toward the study of the QGP. The modular conception of EPOS provides access to the particles distributions just after hadronisation, what makes it a tool of choice for my work. Moreover, the core-corona feature enables to identify which hadrons originate from the core, hence which part of the fluctuations of conserved charges they carry really comes effectively from QGP.

This study takes place in the process of validation for EPOS 4, a new version of the event generator released publicly recently [268]. Whereas it was initially developed mainly to study the physics of the LHC, in the range of the TeV/A in collision energy, some new changes in the models it uses makes it now legitimately applicable to the BES program, down to a certain given energy [269]. This limit of applicability, inherent to the main theoretical piece on which EPOS relies, is expected around ~ 20 GeV/A, but one needs in any case to test it by comparing simulation results with experimental data. In order to help in this process, I have adapted EPOS to make it compatible with RIVET, an analysis toolkit built to systematise the comparison between experimental data and EG simulations, as detailed in chapter 4. This new feature is of course useful to all potential future users, as it will allow to compare easily and directly the simulations from EPOS to data for which the analysis is available. But it also brings a significant help to the developers of EGs, as it offers an experimental data library delivered with the associated analysis: for this reason, I have developed an ensemble of codes to include the possibility to call RIVET directly from EPOS' own analysis framework. Nevertheless,

despite being fully functional, this upgrade is limited by the available analyses in RIVET regarding HICs, and more precisely for the BES which is the energy range of interest for my work. For this reason, I had to write many analyses and collect the corresponding data to test EPOS 3.451, one of the last and most advanced beta-version of EPOS 4, against experimental measurements. Although the new feature with RIVET feature has not been much used for the next study, it still helped into checking particle production for the simulated collisions of interest, as well as checking the validity of my analysis method.

The first step of my work exposed in chapter 5 has been to check particle production in the phase space of interest for the measurement of cumulants. Having looked at p_T spectra for light hadrons π^\pm , K^\pm , p/\bar{p} and (anti)hyperons Λ , Ξ^- and Ω^- , in addition to the pseudorapidity distribution of charged particles, it appears that EPOS simulations are overall in very good agreement with experimental data for Au-Au collisions down to ~ 20 GeV/A. Below these energies, as expected, the p_T spectra start to deviate from the measurements, by getting steeper slopes as a consequence of the hypothesis of simultaneous initial interactions of the PBGR. Even though the discrepancies are not dramatic, and EPOS displayed results remains reasonably close to the data in the scrutinised kinematic range ($p_T < 2$ GeV at $|\eta| < 0.5$), this clearly confirms our expectations and establishes in some way a limit of application for the EG.

In the second part of chapter 5, I have displayed first of all the results from EPOS compared with STAR measurements of net- p , net- π and net- K (co)variances and their ratios. Despite the pretty important statistical fluctuations of my results for the covariances, due to insufficient simulations statistics, EPOS is able to properly reproduce the experimental data in both qualitative and quantitative ways, above ~ 20 GeV/A. At lower energies, the shape of EPOS results deviates from the expected linear increasing with decreasing centrality, what simply reflects the limits observed in particle production. Then, I have compared the ratios of (co)variances of conserved charges with the corresponding STAR proxy ratios and the proposed enhanced proxy ratios. These comparisons demonstrate that, for particle distribution in the final state, the proposed enhanced proxy ratios do effectively reproduce much better the results for exact conserved charges than the ones employed by STAR, in the range where EPOS reproduces correctly particle production. As a matter of fact, it shows that the additional use of net- Λ variances alone improves drastically the quality of the proxies. This is a very encouraging finding, as the STAR collaboration has recently published results for the measurement of cumulants for net- Λ distributions at several different orders [212], meaning that they could measure these enhanced proxy ratios:

$$\tilde{C}_{QS} = \frac{1}{2} \cdot \frac{\sigma_K^2}{\sigma_K^2 + \sigma_\Lambda^2} \quad , \quad \tilde{C}_{BS} = \frac{\sigma_\Lambda^2}{\sigma_K^2 + \sigma_\Lambda^2} \quad , \quad \tilde{C}_{QB} = \frac{\sigma_{\pi p}^{11} + \sigma_p^2}{2\sigma_p^2 + \sigma_\Lambda^2} .$$

Another important takeaway message in addition is the fact that the use of covariances is absolutely not necessary to build good proxy ratios. At the exception of the \tilde{C}_{QB} proxy ratio proposed by myself, which employs $\sigma_{\pi p}^{11}$ (even though its impact on the ratio is almost negligible compared to σ_p^2), variances are enough. Indeed, many hadronic species carry two conserved charges at once, like p for B and Q or Λ for B and S , what makes them alone very good probes for correlations between different charges.

Then, I have shown the impact of the hadronic cascades on the (co)variances studied, by calculating them from the particle distributions just after hadronisation. For conserved charges, the ratios are left unchanged before and after hadronic cascades, as the (co)variances of B, Q, S are almost not impacted by this re-interaction phase. Even if it

was expected from charges which are supposed to be conserved, it proves at least that kinematic spreading or feed-down from heavier resonances (for S in particular) do not play an important role. On the contrary, the (co)variances of net-particle distribution are highly impacted by the hadronic stage, which amplifies their signal by factors 2 to 4 compared to the measurements after hadronisation. Nevertheless, most of the proxy ratios are little modified by the hadronic cascades, as both their numerators and denominators seem to be impacted in the same way, except for the enhanced proxy \tilde{C}_{BS} . Although the latter is in very good agreement with the conserved charges ratio C_{BS} for complete events, it does not reproduce quantitatively well C_{BS} before hadronic cascades, even if quantitatively closer to it than the STAR proxy C_{pK} . However, to form a good proxy, a ratio should not be too much impacted by the hadronic cascades, to reflect as much as possible its value before after hadronisation. Finally, I have estimated the proportion of the signal originating from the core, for both ratios of conserved charge (co)variances and corresponding enhanced proxies. At low- p_T and central (pseudo)rapidity, the majority of particles is produced from the core (or, in a more physical picture, the QGP). Thus, the signal of fluctuations from net-charges and their proxies being measured in this kinematic range comes almost exclusively from the core. Only for the low energies, this proportion deviates from one, as the dense matter represents a smaller part of the system created in the collision. This is an important results which means that, in the phase space where the fluctuations of net-particles are probed, there is very few contamination from the hadrons which are not originating from bulk matter, and which consequently did not carry any mark of the potential critical fluctuations.

The conclusions from this work are very important as they shed light on significant effects on the experimental observables used to probe the presence of a CEP. Moreover, using EG simulations allows to quantify how the last stages of the collisions modify the signal of interest, as fluctuations of several natures emerge from different sources in the complex evolution of systems created in HICs. Nevertheless, this work could be led even further. As a first simple step, the statistical fluctuations of the covariances in particular could be reduced by simulating a more consequent number of events. Then, it could also be good to try to find, for C_{BS} , a proxy which would reproduce it quantitatively both after hadronisation and in the final state, as the \tilde{C}_{BS} one does only fulfill its mission in the last case. Eventually, and most importantly, this study could also be applied to higher order cumulants of net-particle multiplicity, which are also measured experimentally [212, 214, 220, 316]. As they are expected to be even more sensitive to the presence of criticality than the 2nd order ones, it would be very interesting to see if the enhanced proxy ratios discussed in this thesis reproduce as well their corresponding ratios of conserved charges at higher orders.

APPENDIX A

TRANSVERSE MOMENTUM SPECTRA FOR IDENTIFIED
HADRONS

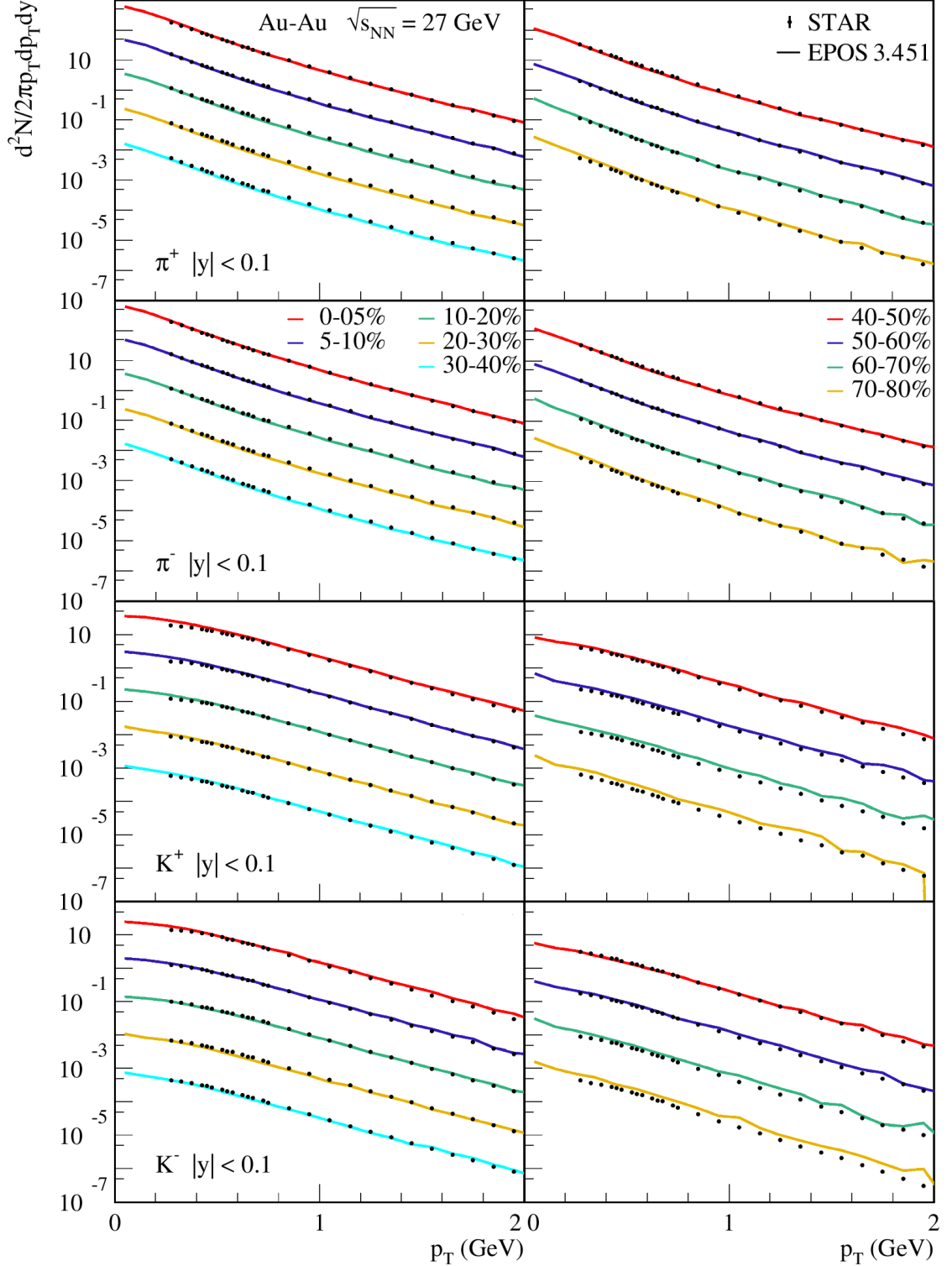


Figure A.1: Transverse momentum spectra of respectively line by line π^+ , π^- , K^+ and K^- , at $|y| < 0.1$, for centrality classes from 0% to 40% (left) and 40% to 80% (right) in Au-Au events at $\sqrt{s_{NN}} = 27$ GeV. In each plot, spectra for the most central events are at real scale, while the others are scaled by factors 10^{-x} ($x = \{1, 2, 3, 4\}$) (data from [177]).

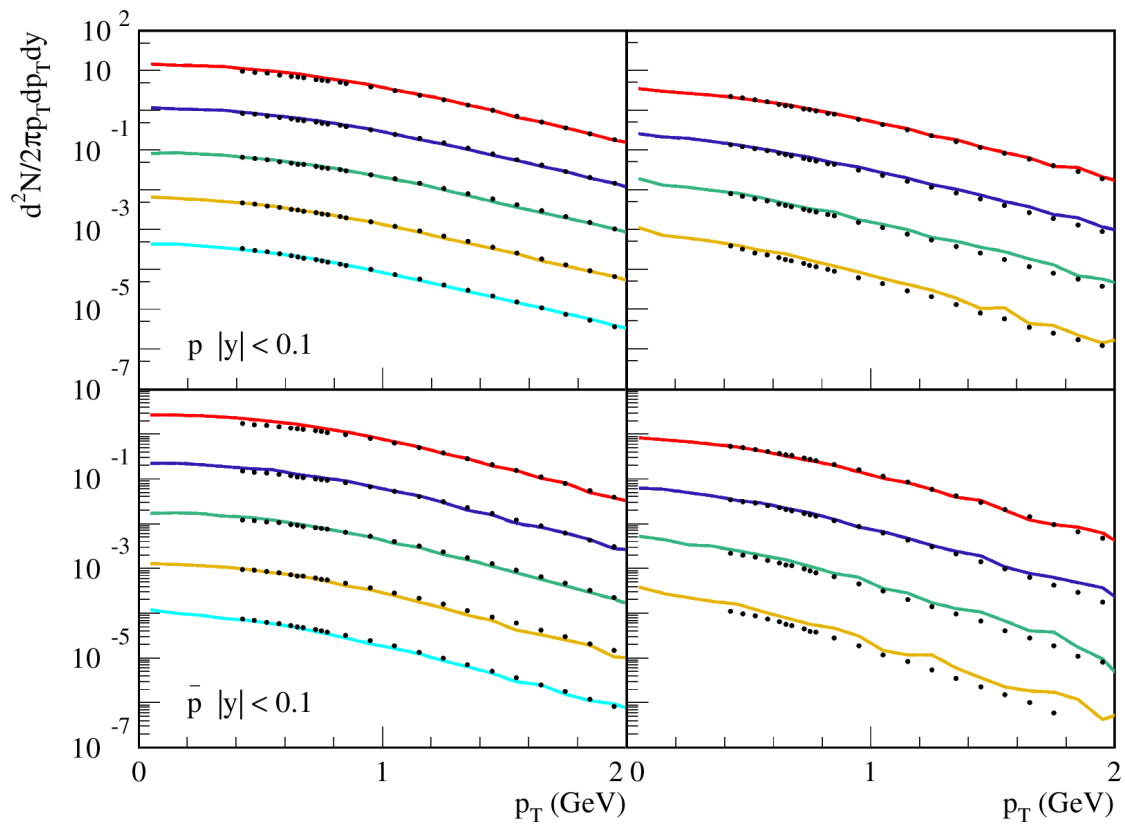


Figure A.2: Same than previous figure but for p and \bar{p} .

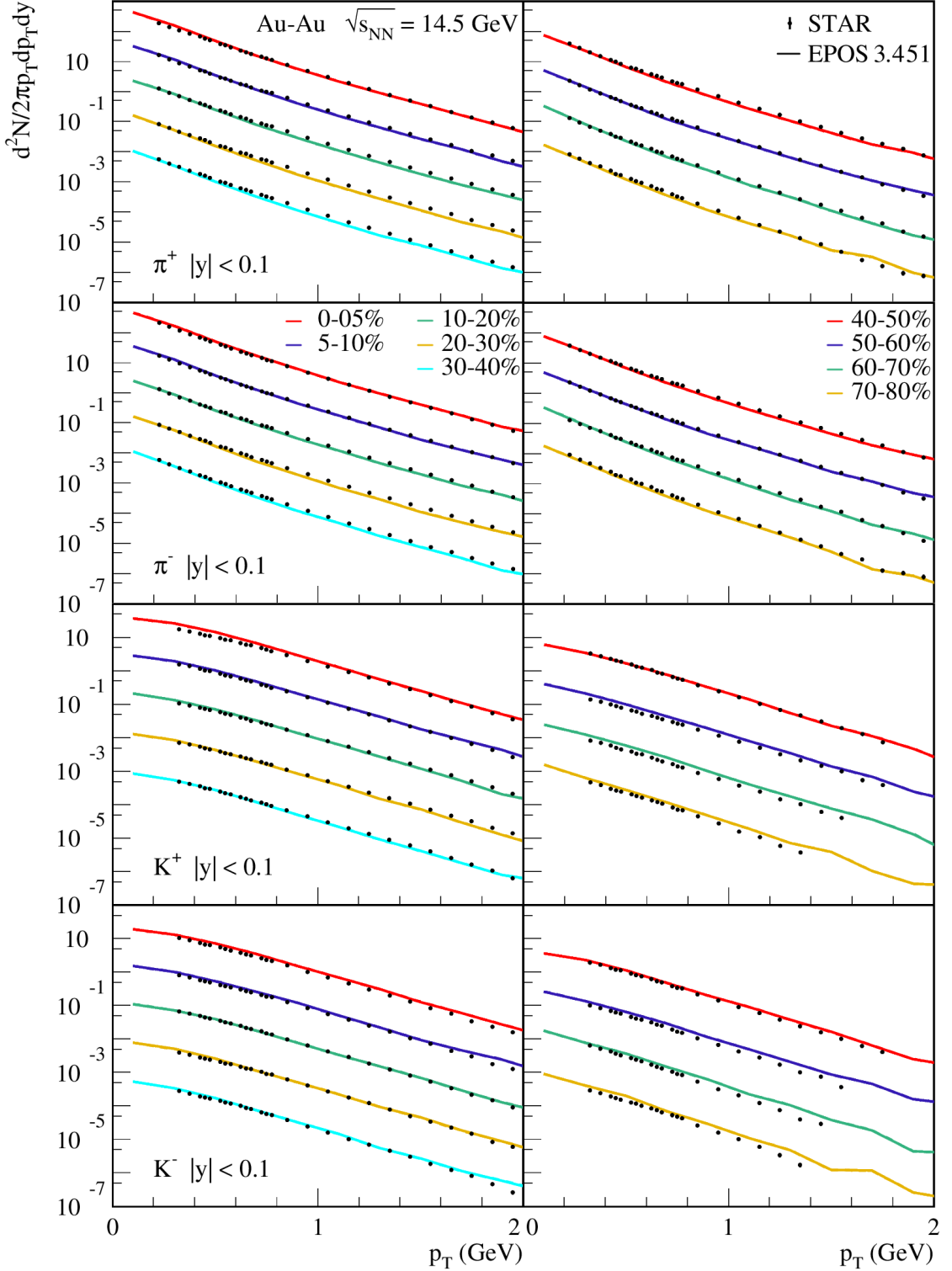


Figure A.3: Transverse momentum spectra of respectively line by line π^+ , π^- , K^+ and K^- , at $|y| < 0.1$, for centrality classes from 0% to 40% (left) and 40% to 80% (right) in Au-Au events at $\sqrt{s_{NN}} = 14.5$ GeV. In each plot, spectra for the most central events are at real scale, while the others are scaled by factors 10^{-x} ($x = \{1, 2, 3, 4\}$) (data from [177]).

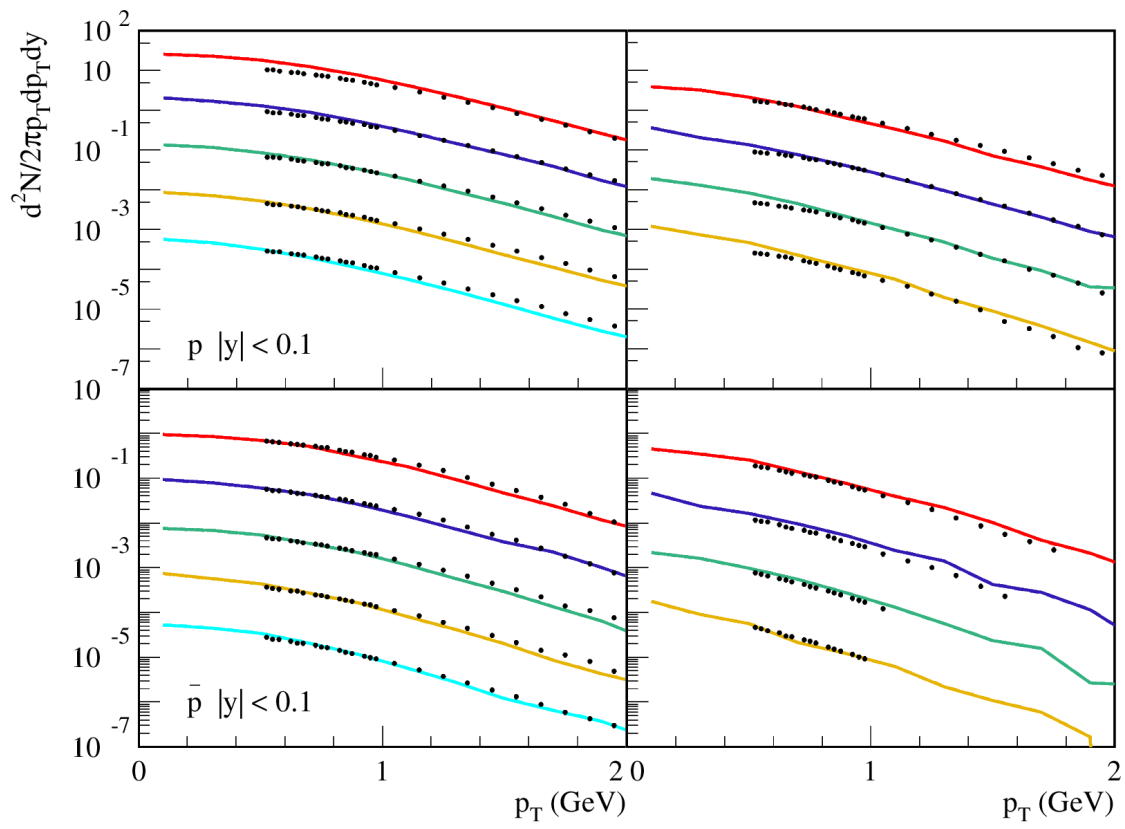


Figure A.4: Same than previous figure but for p and \bar{p} .

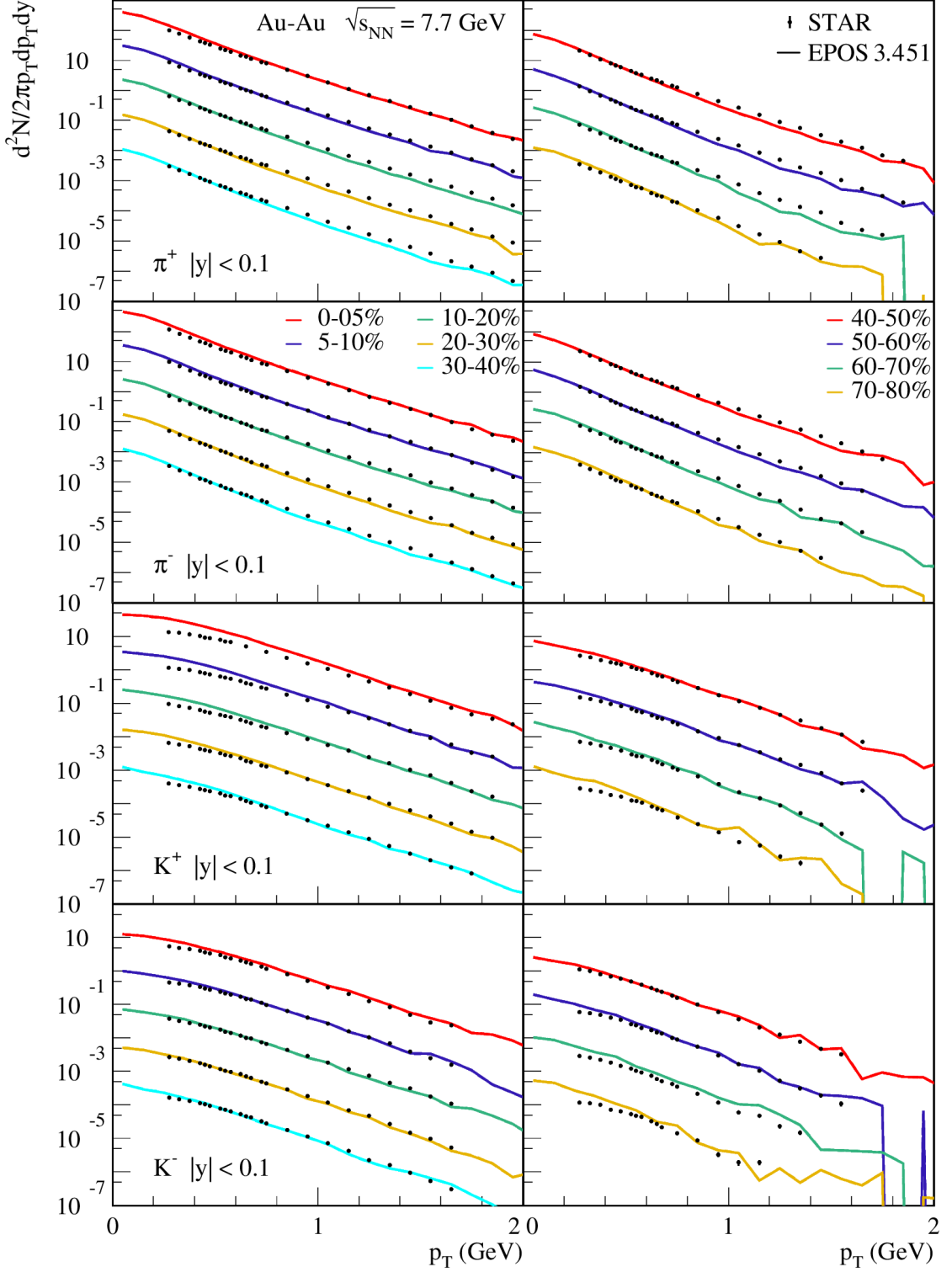


Figure A.5: Transverse momentum spectra of respectively line by line π^+ , π^- , K^+ and K^- , at $|y| < 0.1$, for centrality classes from 0% to 40% (left) and 40% to 80% (right) in Au-Au events at $\sqrt{s_{NN}} = 7.7$ GeV. In each plot, spectra for the most central events are at real scale, while the others are scaled by factors 10^{-x} ($x = \{1, 2, 3, 4\}$) (data from [177]).

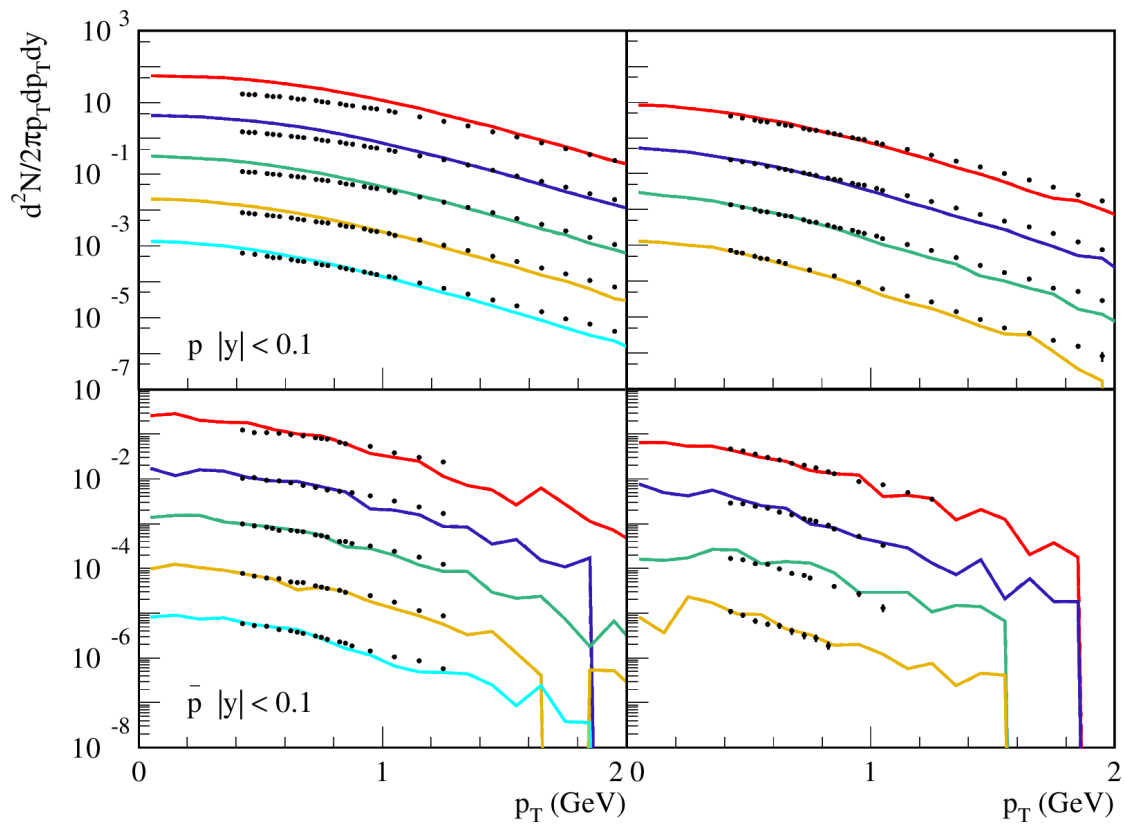


Figure A.6: Same than previous figure but for p and \bar{p} .

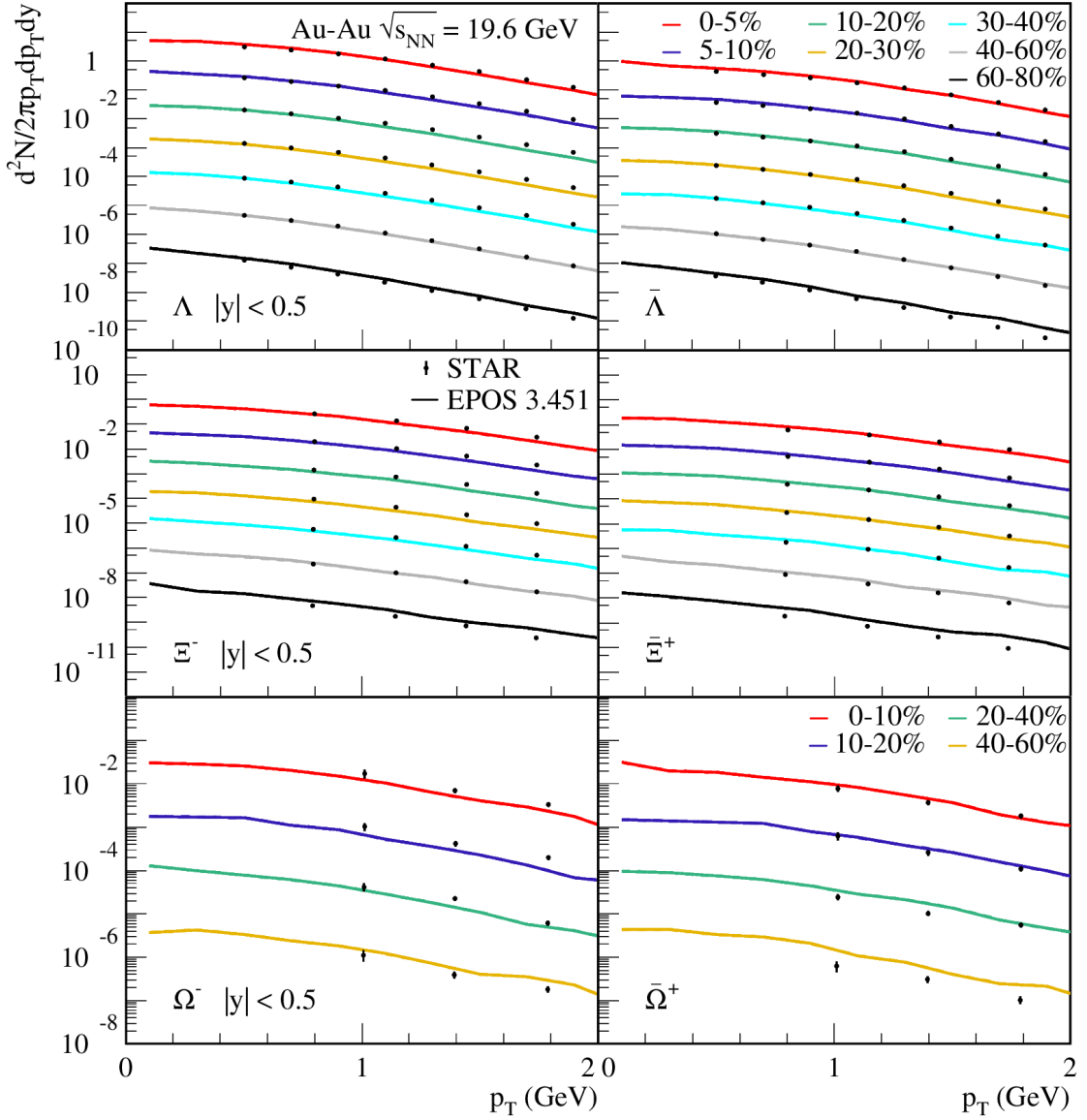


Figure A.7: Transverse momentum spectra of Λ , $\bar{\Lambda}$, Ξ^- , Ξ^+ , Ω^- and $\bar{\Omega}^+$ for different centrality classes in Au-Au events at $\sqrt{s_{NN}} = 19.6$ GeV. Spectra for the most central events are at real scale, while the others are scaled by factors 10^{-x} ($x = \{1, 2, 3, 4, 5, 6\}$) (data from [315]).

APPENDIX B

CENTRALITY-BIN WIDTH CORRECTION

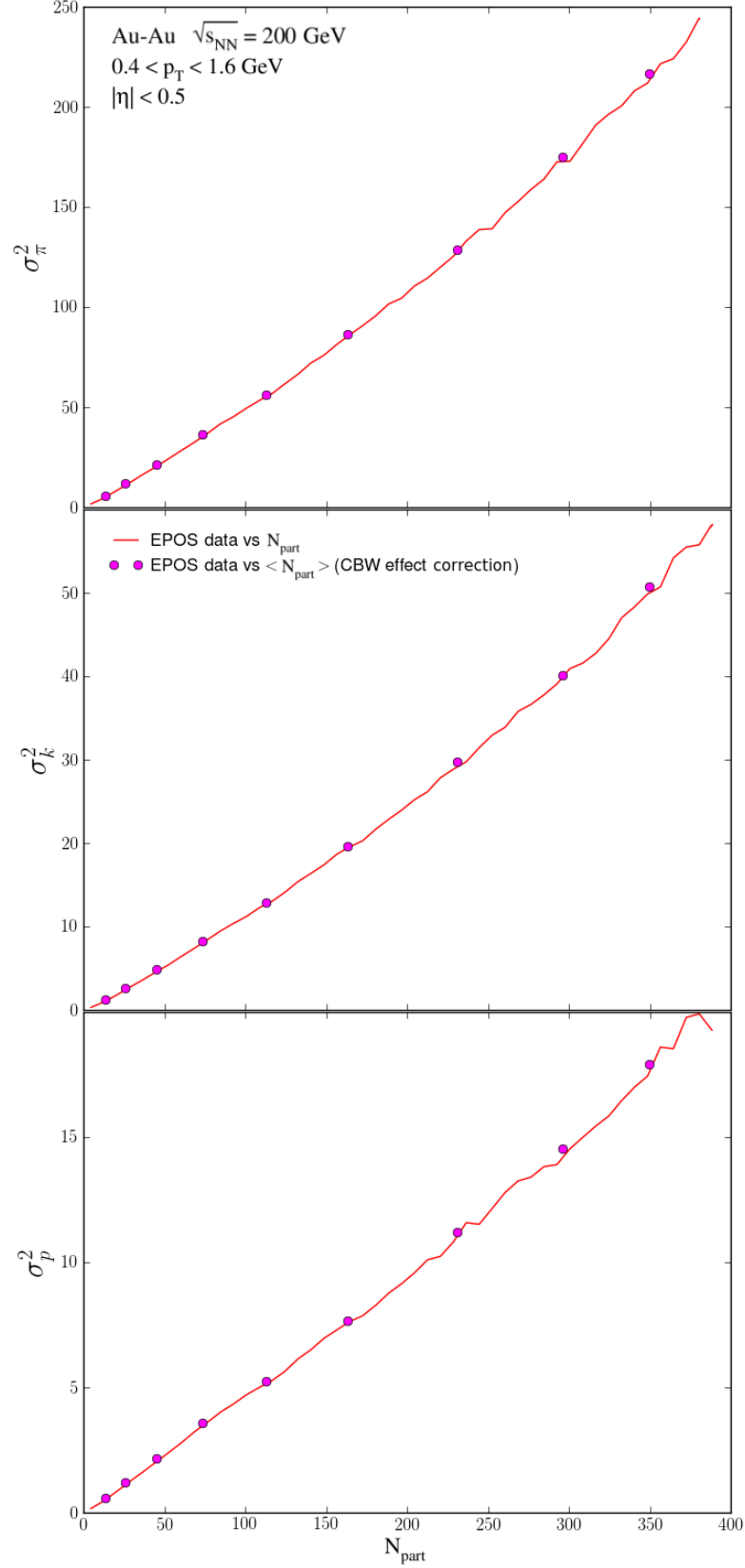


Figure B.1: Centrality dependence of net- p , net- K and net- π multiplicity variances for Au+Au collisions at $\sqrt{s_{NN}} = 200$ GeV, obtained from EPOS 3.451 simulations. The lines represent cumulant calculations as a function of the N_{part} variable directly, while the point represent cumulants calculated for usual STAR centrality classes (*i.e.* 0-5%, 5-10%, 10-20%...70-80%) [211].

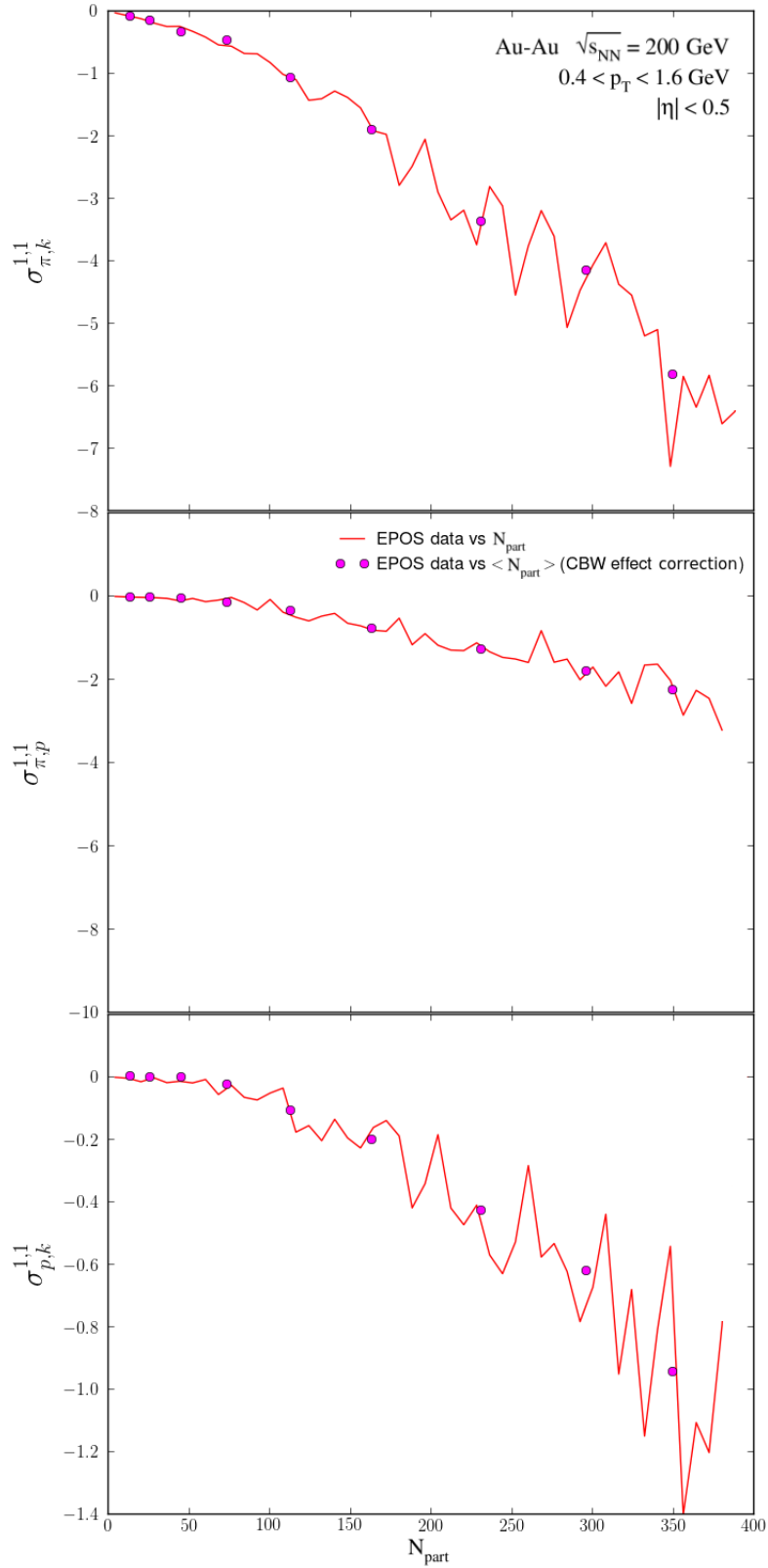


Figure B.2: Centrality dependence of net- p , net- K and net- π multiplicity covariances for Au+Au collisions at $\sqrt{s_{NN}} = 200$ GeV, obtained from EPOS 3.451 simulations. The lines represent cumulant calculations as a function of the N_{part} variable directly, while the point represent cumulants calculated for usual STAR centrality classes (*i.e.* 0-5%, 5-10%, 10-20%...70-80%) [211].

APPENDIX C

NET-MULTIPLICITY CUMULANTS ANALYSIS IN EPOS

Contents

C.1	Technical implementation of the analysis	129
C.2	Structure of the analysis routine	130
C.3	Writing a net-multiplicity cumulant analysis	132

In this appendix, I will explain briefly how the analysis for calculating cumulants of net-multiplicity distributions, from 1st to 4th order, have been implemented in EPOS, before to list all the different parameters and detail its functioning. In a second time, I will display a simple example of the instructions necessary to calculate a net-multiplicity 2nd order cumulant with the EPOS analysis framework. These analyses are the one which have been used to obtain the results shown in section 5.2.

C.1 Technical implementation of the analysis

The code necessary to calculate the moments of net-multiplicity distribution, used in the calculation of cumulants, have been incorporated in the pre-existent analysis framework of EPOS presented in subsection 4.2.3. All these implementations have been made in the file `$EPO/KW/xan.f`.

I started with enabling the `"xtrans()"` subroutine, responsible for the reading of `.optns` files and interpretation of the instructions written within, to understand the new variable created to call the cumulants analysis. This new variable, which I have named `"ncum-evt"`, can be used as a function of any event variable like the collision energy, the number of participants N_{part} , or the charged multiplicity for instance. I have defined the subroutine responsible for the cumulants calculation, `"mupurp_susc()"`, as a multi-purpose analysis one, *i.e.* a subroutine taking input parameters in addition to all the generic ones introduced in subsection 4.2.3. Hence, I had to adapt the corresponding subroutine `"mupurp()"` by adding a new identifier, 1006, which calls `"mupurp_susc()"` when used with `"xpara()"`, the function storing the additional input parameters.

Finally, once the code of the analysis subroutine itself had been implemented, I just needed to ensure that the results were properly transmitted, via the `"ypara()"` function storing them, to the `.histo` file. To do so, I added the appropriate instructions in the `"xval()"` subroutine, in charge of assigning to the histogram bins the value of the corresponding observable calculated over the event.

C.2 Structure of the analysis routine

The bases of the analysis are of course the input parameters, that I will detail in first. As explained previously, they are provided to the "mupurp_susc()" subroutine via the "xpara()" function, whose different elements are expected to contain the following information ("n" simple refers here to the histogram number). The expected parameter to be used and their possible values are summed up in the table C.1.

	Parameter value(s)	Parameter correspondence
xpara(1, n)	1006	indicates to call "mupurp_susc()"
xpara(2, n)	$[0, \infty] \in \mathbb{R}$	lowest p_T value of particles to consider
xpara(3, n)	$[0, \infty] \in \mathbb{R}$	highest p_T value of particles to consider
xpara(4, n)	0	cut applied in rapidity y
	1	cut applied in pseudorapidity η
xpara(5, n)	$[0, \infty] \in \mathbb{R}$	maximum $ y/\eta $ of particles to consider
xpara(6, n)	0	no feed-down correction
	1	geometrical cut (DCA < 1cm)
	2	strict feed-down correction (\equiv "noweak")
xpara(7, n)	0	considers only FS particles + parents
	1	considers particles before hadronic cascade
xpara(8, n)	0	considers all particles
	1	considers particle from the core only
	2	considers particle from the corona only
xpara(9, n)	a	indicates to calculate δN_a^1
	ab	indicates to calculate δN_{ab}^2
	abc	indicates to calculate δN_{abc}^3
	$abcd$	indicates to calculate δN_{abcd}^4

Table C.1: Input parameters of the "mupurp_susc()" subroutine to perform a calculation of moments from 1st to 4th order of net-multiplicity distribution.

The last parameter will indicate, by its length, the order of the moment to be calculated, and the charges or particles to consider by the digits it is made of. The correspondence between the digits and the associated net-charge or net-particle number is given in table C.2.

a, b, c, d	1	2	3	4	5	6	7	8	9
Charge/particle	B	Q	S	π	K	p	Λ	Ξ	Ω

Table C.2: Correspondence between digits and associated charge or particle for xpara(9, n).

Although the study presented in this thesis focus on the 2nd order cumulants, which require both 1st and 2nd order moments of net-multiplicity distribution to be calculated, I have developed the subroutine with the ability to calculate moments up to the 4th order. Moreover, it was conceived in a way that only few modifications are necessary to enable it to calculate even higher order moments.

After having treated properly the input parameters, the subroutine will perform a loop over the particles of the event analysed, and select only the particles fulfilling the criteria established. That is to say, it will consider either FS particles and their parents or particles before hadronic cascades, apply either a strict feed-down correction, a DCA criteria or no correction at all, and consider either all particles or particles coming exclusively from the core or corona part. The calculation of the moment of net-charge/particle will then vary, following which charge or particle has been chosen.

In the case of baryonic number B or electric charge Q , as the goal would be to compare these net-charge cumulants with the net-particle cumulants used as proxies by the experiment, the analysis has to be as close as possible to the net-particle case. Hence, as in the latter case the DCA cut is often used, the net-charges considered will be calculated at the primary particle level (i.e. before decays of particles), and not at the FS level. It could legitimately be done at the FS level, as Q and B are conserved in weak decays. However, we ensure by doing so to consider the net-charge of the phase space of interest (PSOI) without any loss or gain due to kinematic spreading, i.e. the loss of a charge due to daughter particles going out of the PSOI while their parents were in. It prevents equally, on the contrary, from counting the charge of daughter particles which are in the PSOI, while their parents were out. In order to avoid double-counting, the particles having the required status will only have their B or Q charge accounted if their parents does not have the required status, as the charge of the latter would have been counted already otherwise. For net- B calculation, the difference between quarks and antiquarks $\delta q_i = n_{q_i} - n_{\bar{q}_i}$ is checked for each particle i , and the net- B value is added to the total one $\delta B_{(0,N_{ptl})}$:

$$\delta B_{(0,i)} = \delta B_{(0,i-1)} + \delta q_i \div 3, \quad (\text{C.2.1})$$

with \div symbolising the quotient of euclidean division. Thus $\delta q_i \div 3 = \pm 1$ for (anti)baryons, and is null for mesons (no tetra/pentaquarks defined in EPOS). For net- Q calculation, the charge Q_i is checked for each particle i and simply added to the total net- Q value $\delta Q_{(0,N_{ptl})}$:

$$\delta Q_{(0,i)} = \delta Q_{(0,i-1)} + Q_i. \quad (\text{C.2.2})$$

In addition to the problem of kinematic spreading described for net- B and net- Q calculations, stable FS particles cannot be considered alone for net- S calculation, as strangeness is not conserved by the weak interaction. Consequently, it would be washed out by successive weak decays, unless using the "noddecay" instruction for the weak decaying particles like Λ , Σ , Ξ , Ω or K_s^0 . However, the aim of this analysis is to avoid such constraints as much as possible. The simple strategy I used to limit this problem consists of ignoring all particles for which the parent matches the required status, without any kinematic consideration. In other words, only the first particles with the required status within the PSOI are accounted and their daughter ignored, similarly to the net- B/Q case, in order to avoid double counting, kinematic spreading but also potential contamination from c/b weak feed-down. In the end, in order to calculate net- S , the net-number of strange quarks $\delta s_i = n_{s_i} - n_{\bar{s}_i}$ composing each particle i is subtracted to the total net- S value $\delta S_{(0,N_{ptl})}$:

$$\delta S_{(0,i)} = \delta S_{(0,i-1)} - \delta s_i, \quad (\text{C.2.3})$$

as positive strangeness is associated to \bar{s} quarks by convention, so $\delta s_i = -S_i$.

Finally, to calculate the net-number of identified particles X_{ID} , the only ingredient to take into account in addition to the status and origin of particles, like for the conserved charges, is the feed-down correction. Depending on the user's choice, the feed-down contribution can be corrected either following the DCA selection method (DCA < 1cm here, to match with STAR definition), or with a strict rejection of all particles coming from weak decays. In the latter case, which corresponds to "noweak" in the EPOS analysis language, the particles from which all daughter particles are ignored are the K_s^0 , Λ , $\Sigma^{-/0/+}$, $\Xi^{-/0}$ and Ω^- , and the associated anti-particles. Straight-forwardly, the total net- X_{ID} value $\Delta X_{(0,i)}$ is calculated by adding +1 for particles (or positively charged mesons, by convention) and -1 for anti-particles (negatively charged mesons):

$$\Delta X_{(0,i)} = \Delta X_{(0,i-1)} \pm 1 . \quad (\text{C.2.4})$$

At last, once the loop over particles is achieved, the different net-charge/particle numbers are multiplied with each other in the case of a moment of order > 1, and the result is stored in the "ypara()" function. The operation is then repeated for each event analysed.

C.3 Writing a net-multiplicity cumulant analysis

In this last subsection, I will show explicitly the instructions to write in an `.optns` file to calculate the variance of net-proton σ_p^2 as a function of N_{part} , as an example. The first step is of course to calculate δN_p and δN_p^2 , respectively 1st and 2nd order moments of the net- p multiplicity distribution.

```

beginhisto
  histogram npnevt ncum-evt 4 0 400 40
  xparas 9 1006 0.4 1.6 1 0.5 1 0 0 6
  trigger bimevt bim00 bim80
endhisto
beginwrite
  openhisto name Npart-ncum-p
  [[histoweight writearray 3]]
  closehisto
endwrite
    
```

The "npnevt" refers here to N_{part} , and "ncum-evt" to the analysis for cumulants described in the last section. The normalisation factor "4" indicates to average the observable over the events analysed, and the following numbers that it will be divided into 40 bins between $N_{part} = 0$ and $N_{part} = 400$. The number "9" after "xparas" is just here to specify that there will be nine input parameters, which correspond to the ones described in table C.1. Hence, the analysis written here will calculate $\langle \delta N_p \rangle$ for FS (anti)protons from all origins, with $0.4 < p_T < 1.6$ GeV and within $|\eta| < 0.5$. The distribution is corrected from feed-down by selecting the (anti)protons with a DCA < 1cm, and calculated as a function of N_{part} from 0 to 400 with bins of width $\Delta N_{part} = 10$ for events in the centrality range 0-80%. With the following instructions, one can then calculate $\langle \delta N_p^2 \rangle$ for the exact same selection criteria.

```

beginhisto
  histogram npnevt ncum-evt 4 0.5 400.5 40
  xparas 9 1006 0.4 1.6 1 0.5 1 0 0 66
  trigger bimevt bim00 bim80
endhisto
beginwrite
  openhisto name Npart-ncum-pp
  [[histoweight writearray 3]]
  closehisto
endwrite

```

Finally, in order to obtain the variance, one simply needs to apply the formula (2.3.14), done with the commands displayed in the next frame. The histogram obtained is also complemented with instructions for the plotting, *i.e.* axes labels (N_{part} and σ_p^2 for x and y axes respectively, in the PAW language). The first operation achieved with "calc" calculates $\langle \delta N_p \rangle^2$, and the second gives $\sigma_p^2 = \langle \delta N_p^2 \rangle - \langle \delta N_p \rangle^2$.

```

beginwrite
  openhisto name Npart-variance-pp htyp lin
  txt ""xaxis N?part!""
  txt ""yaxis green: [s]?B!&^2!""
  calc Npart-ncum-p * Npart-ncum-p ; -> 1
  calc Npart-ncum-pp - $1 ;
  closehisto plot 0
endwrite

```


APPENDIX D

CUMULANTS OF CONSERVED CHARGES BEFORE & AFTER HADRONIC CASCADES

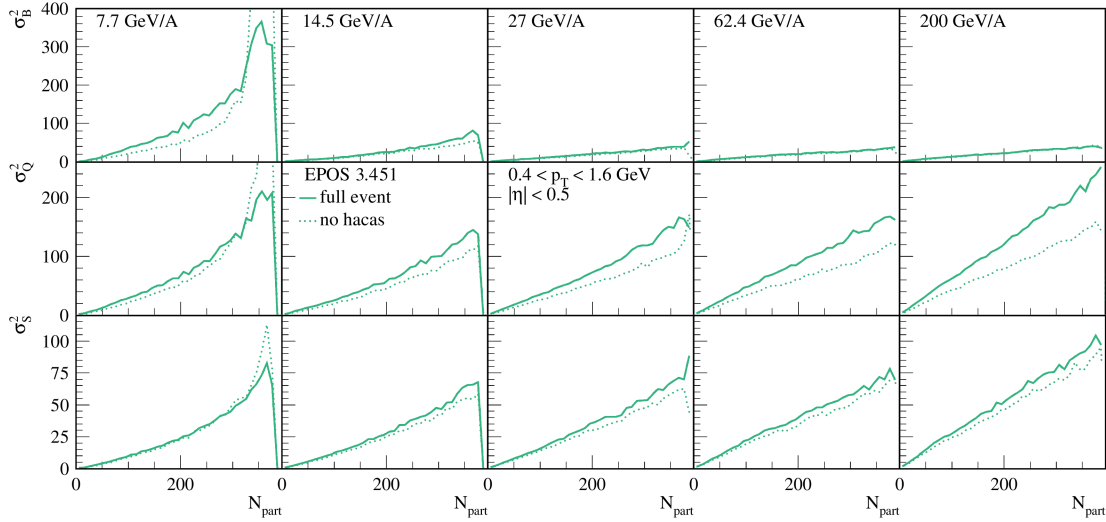


Figure D.1: Variances of B , Q and S vs. N_{part} for different Au-Au collisions energies, obtained from EPOS 3.451 simulations. The results calculated from full events are represented by full lines, while results calculated before hadronic cascades are represented by dotted lines.

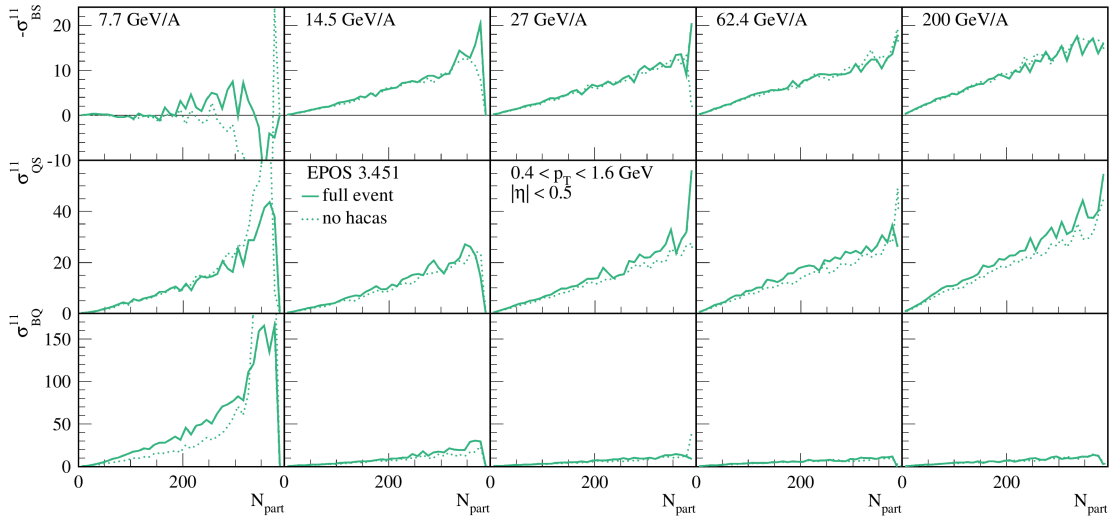


Figure D.2: Covariances of B , Q and S vs. N_{part} for different Au-Au collision energies, obtained from EPOS 3.451 simulations. The results calculated from full events are represented by full lines, while results calculated before hadronic cascades are represented by dotted lines.

Contents

E.1	Contexte et motivations	137
E.2	Motivations et objectifs de la thèse	141
E.3	Développements techniques pour EPOS 4	143
E.4	Résultats sur l'étude des cumulants de charges conservées	145

Cette dernière annexe résume, en français, les travaux présentés précédemment dans ce manuscrit. Dans un premier temps sera rappelé, dans la section [E.1](#), le contexte de ces travaux, suivi d'une présentation du générateur d'événements EPOS qui en fut l'outil principal, couvrant ainsi le contenu des chapitres [1](#), [2](#) et [3](#). Les motivations et objectifs ayant guidé ces travaux, énoncés dans la section [3.5](#), seront alors présentés dans la section [E.2](#). Les développements techniques effectués sur EPOS 4 dans le cadre de cette thèse, discutés dans le chapitre [4](#), seront décrits dans la section [E.3](#). L'étude exposée dans le chapitre [5](#) sera ensuite abordée dans la section [E.4](#), se clôturant sur une discussion des potentielles perspectives envisageables afin de poursuivre ces travaux.

E.1 Contexte et motivations

Les travaux présentés dans cette thèse s'inscrivent dans l'étude du Modèle Standard (MS) de la physique des particules. Cette théorie décrit comment les particules élémentaires composant la matière interagissent par l'intermédiaire des forces électromagnétique, faible et forte. La figure [1.1](#) représente ainsi les différentes particules le composant, séparées en deux grandes familles : les fermions, particules de matière, et les bosons, médiateurs d'interaction. L'interaction forte, exprimée sous la forme d'une théorie quantique des champs portant le nom de chromodynamique quantique (CDQ), à cause de la charge dite de couleur qui lui est propre, agit sur les quarks et est transmise par l'échange de gluons. Une des caractéristiques majeures de la CDQ, le "confinement de couleur", se traduit par le fait qu'aucune particule portant une charge de couleur ne peut être observée seule en conditions normales de densité et température. Ainsi, les quarks sont toujours regroupés afin de former des objets neutres en terme de charge de couleur, appelés hadrons. Par trois (qqq), ils forment les baryons, tels que les nucléons composant le noyau de l'atome, ou par paire de quark-antiquark ($q\bar{q}$) des mésons, tels que les pions ou kaons.

Il a cependant été prédit que sous des conditions extrêmes de très haute température et/ou densité, un gaz de hadrons devrait transitionner vers un nouvel état de matière où les quarks et gluons sont déconfinés, et apparaissent comme libres vis-à-vis de l'interaction forte : le plasma de quarks et gluons (PQG). James Björken proposa alors que cette phase, dans laquelle l'Univers se serait trouvé quelques micro-secondes après le Big-Bang, pourrait être recréée dans des collisions d'ions lourds (CIL) aux énergies ultra-relativistes. La figure 2.1 illustre l'évolution du système créé dans de telles collisions sur un diagramme d'espace-temps, où le PQG est supposé exister le temps d'une dizaine de fm/c, soit $\sim 10^{-22}$ s. L'étude du diagramme de phase de la matière nucléaire motiva alors une communauté grandissante de chercheurs à mettre en place des expériences pour étudier ces CIL, ce qui poussa à la création d'accélérateurs de particules tels que le SPS et le LHC au CERN, ou bien le RHIC au BNL. Il fut finalement annoncé en 2005 que la création du PQG dans des collisions Au-Au avait été observée conjointement par les expériences du RHIC, bien qu'il fut publié *a posteriori* qu'un tel état de matière avait déjà été créé auparavant dans des collisions Pb-Pb réalisées au SPS.

Sur le plan théorique, l'étude du diagramme de phase est cependant rendue difficile par une seconde propriété importante de la CDQ : le fait que sa constante de couplage α_s , mesurant l'intensité de son interaction, ne soit en réalité pas constante. Cette dernière varie en fonction de l'échelle d'énergie Q^2 impliquée dans l'interaction considérée, comme illustré dans la figure 1.3. À basse énergie, la relativement grande valeur de $\alpha_s(Q^2)$ entrave l'utilisation de méthodes perturbatives, qui ne peuvent être appliquées qu'à haute énergie où son intensité décroît asymptotiquement. Il est ainsi impossible de résoudre analytiquement la théorie à faible température T et potentiel chimique baryonique μ_B , et donc d'établir directement une équation d'état couvrant cette région du diagramme. Une approche non-perturbative de la CDQ, consistant à discrétiser l'espace-temps en un réseau où les quarks sont placés sur les sommets et les gluons sur les arêtes, permet néanmoins de calculer des grandeurs thermodynamiques à partir des premiers principes. Bien que restreinte initialement au domaine où $\mu_B \approx 0$, l'utilisation de la CDQ sur réseau donna lieu à la prédiction d'une transition de phase continue (dite *crossover*) entre les phases de gaz hadronique et le PQG, à petites valeurs de μ_B . Cela semble aujourd'hui confirmé par les résultats de CIL effectuées à très haute énergie au LHC depuis 2011, explorant cette région spécifique du diagramme de phase. Plusieurs autres modèles, basés sur des premiers principes de la CDQ, ont quant à eux émis l'hypothèse de l'existence d'une transition de phase de 1^{er} ordre entre la matière hadronique et le PQG à faible T et à μ_B fini. Cette transition de phase impliquerait alors la présence d'un point critique (PC) à la jonction de cette transition avec le *crossover*. La recherche de ce PC est donc la motivation principale du travail présenté dans cette thèse, basé sur les motivations qui seront détaillées à la fin de cette section.

Une vision schématique du diagramme de phase de la matière nucléaire, résumant l'ensemble des points mentionnés précédemment, est présentée dans la figure 2.3. L'existence d'une phase de superconductivité de couleur, analogue à la théorie de la supraconductivité électromagnétique pour des charges de couleur, fut également conjecturée dans la région de basse température et de haut potentiel chimique baryonique.

Dans la recherche du point critique, les susceptibilités thermodynamiques des charges conservées (nombre baryonique B , charge électrique Q et étrangeté S) sont des quantités théoriques très largement utilisées. Elles quantifient l'amplitude des changements dans la fonction de partition thermodynamique du système, dues aux variations de potentiels chimiques des charges conservées, autrement dit les fluctuations desdites charges. Or, ces

fluctuations sont supposées diverger dans un système subissant des phénomènes critiques, *i.e.* dont les conditions s'approchent de celles du PC, ce qui en font donc des outils de choix. Les susceptibilités sont également reliées aux différents moments statistiques des distributions de valeurs nettes des charges conservées. En particulier, les susceptibilités du 2nd ordre sont reliées aux (co)variances des distributions de charges correspondantes (voir équations (2.3.12) et (2.3.13)). Du point de vue expérimental, la recherche du PC est un des objectifs majeurs du programme BES, via un scan du diagramme de phase en étudiant des collisions Au-Au à différentes énergies. En effet, alors que le système créé dans des collisions avec une énergie $\sqrt{s_{NN}} > 100$ GeV/A décrit une trajectoire très proche de $\mu_B \approx 0$ dans le diagramme de phase, diminuer l'énergie de la collision augmente les valeurs de μ_B atteintes par le système. Mesurer les fluctuations de charges conservées pour des collisions à différentes énergies devrait donc permettre d'identifier quel système expérimente des effets critiques, en cas de divergences de ces observables comparées à des références établies en l'absence de criticalité.

Cependant, de nombreux éléments rendent cette étude complexe, de par les différences fondamentales entre le cadre théorique dans lequel les prédictions sont réalisées, et le cadre expérimental dans lequel les observables correspondantes sont mesurées. Il est notamment impossible de mesurer expérimentalement les charges conservées, puisqu'elles sont portées par différentes espèces hadroniques qui ne sont pas toutes identifiables par les détecteurs utilisés. L'utilisation de familles de particules de procreation (ou *proxies*) pour mesurer les distributions de B , Q et S dans les CIL est donc indispensable, mais il est alors nécessaire de comprendre à quel point ces *proxies* reflètent effectivement le comportement des charges qu'elles sont censées représenter. De plus, de nombreux phénomènes dans les CIL sont sources de fluctuations, et il est important d'essayer de démêler les fluctuations dites "thermales", qui portent la trace d'une potentielle criticalité, des autres sources de fluctuations telles que les fluctuations de l'état initial, ou bien les fluctuations dues au processus statistique d'hadronisation.

Dans le contexte du programme BES, la collaboration STAR a récemment publié le résultat des mesures de (co)variances de distributions nettes de pions, kaons et protons à pseudorapidité centrale ($\Delta\eta < 0.5$) et à bas p_T ($0.4 < p_T < 1.6$ GeV), dans des collisions Au-Au à $\sqrt{s_{NN}} = 7.7, 11.5, 14.5, 19.6, 27, 39, 62.4$ et 200 GeV [211]. Dans cette publication, les (co)variances sont notamment étudiées en fonction de la centralité des collisions (représentée par le nombre de nucléons participants $\langle N_{part} \rangle$), comme montré dans la figure 2.9. Ces variances et covariances sont utilisées pour construire des ratios de *proxies* comparables aux ratios de susceptibilités, exprimés dans l'équation (2.3.18). Ils sont étudiés en fonction leur dépendance à la centralité et à l'énergie de collision, comme montré dans la figure 2.10, afin de chercher un quelconque signe de criticalité. Parallèlement à cela, les auteurs de [234] ont mené une étude sur la décomposition des contributions de différentes espèces hadroniques aux susceptibilités totales. Ils ont pour cela utilisé le gaz de résonances de hadrons (GRH), un modèle statistique dans lequel un gaz de hadrons interagissant dans leur état fondamental est représenté par un gaz de hadrons et leurs résonances sans interactions. En comparant ensuite dans quelle proportion chaque espèce hadronique contribue aux susceptibilités totales obtenues par calculs de CDQ sur réseau (voir figure 2.11), ils ont pu proposer des nouveaux *proxies* pour les ratios $C_{QS} = \chi_{11}^{QS}/\chi_2^S$ et $C_{BS} = \chi_{11}^{BS}/\chi_2^S$, alternatifs à ceux utilisés par la collaboration STAR. Ces *proxies* alternatifs sont explicités dans les équations (2.3.25) et (2.3.26), et furent sélectionnés à partir de leur proximité aux ratios exacts de susceptibilités tels que présenté dans la figure 2.12.

Basé sur les résultats des deux publications citées précédemment, l'idée principale de mon étude est alors d'utiliser le générateur d'événements (GE) EPOS afin de comparer les *proxies* mesurés par STAR avec les *proxies* alternatifs résultants de l'étude menée avec le modèle du GRH. EPOS est un GE dit "générique", dans le sens où il permet de générer différents types de collisions dans leur intégralité, qu'il s'agisse d'annihilation e^+e^- , ou bien de collisions $p-p$, $p-A$ ou $A-A$. Ayant été avant tout développé pour l'étude de collisions hadroniques, EPOS repose sur une structure modulaire classique de générateurs d'événements dédiés aux CIL. Toutes les étapes y sont simulées successivement dans un ordre chronologique, comme illustré sur la figure 3.1.

Une des principales caractéristiques distinctive et unique d'EPOS réside en la PB-GRT, utilisée pour générer les conditions initiales des collisions hadroniques. Elle résulte de l'union du modèle des partons, utilisé pour calculer des processus inclusifs dits durs (où $Q^2 > 1$ GeV), avec la théorie de Gribov-Regge (GRT), une théorie d'interactions partoniques multiples basée sur le formalisme de la matrice de diffusion S . Dans ce modèle, les interactions entre les partons qui constituent les projectiles sont représentées par des objets mathématiques appelés Pomerons. Ces objets représentent physiquement des échelles de partons, et peuvent avoir différentes structures possibles (représentées schématiquement dans la figure 3.4) selon la nature et l'énergie des partons à leurs extrémités. Ces caractéristiques déterminent alors le formalisme employé pour simuler l'évolution de la cascade partonique, afin de calculer les sections efficaces qui sont alors factorisées comme explicité dans l'équation (3.3.8). Les effets non-linéaires dus à la saturation des gluons, dont la fréquence augmente à haute énergie, sont pris en compte via une échelle de saturation individuelle pour chaque Pomeron. Chaque Pomeron est soit entier, contribuant alors avec un terme d'interférence dans le calcul de section efficace totale d'interaction, ou soit coupé et participe alors à la production de particule (voir figure 3.5). Une fois générées, les distributions de partons sont alors modélisées par des cordes, des chaînes de gluons ayant pour début et fin une paire $q\bar{q}$ ($q-g-\dots-g-\bar{q}$), qui possèdent une tension égale à ~ 1 GeV/fm et se fragmentent par création de paires de (di)quarks $q\bar{q}$ / $qq\bar{q}\bar{q}$. Ces cordes, principalement longitudinales et dont la dimension transverse est causée par des "kinks" de gluons, évoluent alors suivant la dynamique d'un lagrangien invariant de Lorentz. Dans le cas de collisions impliquant de nombreux échanges de Pomerons, tel que les collisions $A-A$ ou bien même certaines collisions $p-p$ de haute multiplicité, la densité de cordes devient tellement importante qu'elles ne peuvent alors plus fragmenter indépendamment les unes des autres, comme représenté dans la figure 3.9. Dans ce cas, le système est séparé en deux parties distinctes, dans une procédure appelée *core-corona*. Dans la *corona*, région moins dense, les segments de cordes ayant une impulsion transverse suffisante pour échapper au *core* évoluent suivant la procédure standard décrite précédemment. L'évolution du *core*, la région de haute densité d'énergie, est simulée à l'aide d'équations d'hydrodynamique relativiste visqueuse, afin de reproduire le comportement fluide du PQG. Pour cela, il est possible de choisir entre deux équations d'état différentes : dans cette étude, les simulations réalisées utilisent une équation d'état contenant uniquement un *crossover* entre la phase hadronique et le PQG. Lorsque la densité d'énergie repasse sous une valeur critique, chaque cellule est alors hadronisée selon un processus microcanonique d'après une densité de probabilité décrite dans l'équation (3.4.7). Une fois le système complètement hadronisé, les ré-interactions entre particules formées sont simulées à l'aide du modèle de transport microscopique UrQMD. Cette phase hadronique autrement appelé "cascade hadronique", affecte à la fois la chimie du système mais aussi la distribution cinématique des particules, et joue un rôle important dans l'étude des cumulants présentée en section E.4.

E.2 Motivations et objectifs de la thèse

Suivant le développement d'EPOS 4 durant les quelques dernières années, un des objectifs de ma thèse était d'aider à la préparation de sa diffusion publique. Cela requiert en particulier de s'assurer que la paramétrisation de l'ensemble des éléments du GE permet de reproduire correctement la production de particules pour un maximum de systèmes et d'énergies différentes, afin d'évaluer ses limites d'application. La question de la gestion des données et de leur analyse revêt notamment un aspect important pour le développeur dans ce processus de validation, autant que pour les potentiels futurs utilisateurs d'EPOS. S'il possède déjà un système d'analyse d'événements "à la volée" qui lui est propre, et qui permet de reproduire la plupart des analyses expérimentales, il ne s'agit pas d'un outil standardisé.

Ainsi, une de mes tâches consiste à développer un interface entre EPOS et l'outil d'analyses et de comparaison RIVET. Cela implique d'ajouter un nouveau format d'enregistrement des données d'événements simulés dans un premier temps, puis de développer l'architecture nécessaire pour pouvoir faire appel à RIVET systématiquement lors de l'utilisation d'EPOS. Ce travail s'accompagne de la rédaction d'une documentation associée, tant pour l'utilisateur que pour les développeurs, via des notes internes.

Après une présentation rapide de RIVET, le développement de cette nouvelle interface sera ainsi résumé en section E.3. Avec comme visée finale le processus de validation d'EPOS 4, le premier objectif est d'utiliser cette nouvelle interface afin d'employer RIVET pour comparer les résultats de simulations obtenues avec EPOS, aux résultats expérimentaux de collisions Au-Au aux énergies du programme BES. Cependant, peu d'analyses sont actuellement disponibles dans RIVET à ces énergies.

Par conséquent, je suis chargé de récolter des données expérimentales, ainsi que d'écrire les analyses correspondantes dans le système d'analyse "à la volée" d'EPOS, afin de pouvoir procéder à la validation d'EPOS 4 pour les CIL aux énergies du programme BES.

Ainsi, le début de la section E.4 portera sur les résultats distributions en pseudorapidité η et les spectres en p_T de particules. Les collisions Au-Au simulées à cette occasion pourront alors être utilisées afin de réaliser l'étude des *proxies* de cumulants des charges B , Q et S , introduite à la fin de la section E.1.

Mon premier objectif à ce sujet est de reproduire l'analyse réalisée par l'expérience STAR sur la mesure des (co)variances de distributions nettes de π^\pm , K^\pm et $p(\bar{p})$, après une rapide étude de l'effet de largeur de bins en centralité sur ces (co)variances lorsque mesurées en fonction de la centralité.

Afin de combler le fossé entre les études théoriques menées sur les cumulants de charges conservées, et le *proxies* mesurés expérimentalement, je prévois ensuite de mesurer additionnellement les (co)variances des multiplicités nettes de Λ , Ξ^- et Ω^- , afin de pouvoir construire les nouveaux *proxies* alternatifs.

Dans un second temps, l'idée est de confronter à la fois les *proxies* utilisés par STAR ainsi que ces *proxies* alternatifs, aux ratios de (co)variances de charges B , Q et S elles-mêmes, tous mesurés à partir de simulations réalisées avec EPOS. L'objectif étant alors d'évaluer à quel point les *proxies* alternatifs et ceux utilisés par STAR diffèrent les uns des autres, et notamment de regarder leurs évolutions respectives en fonction de l'énergie de collision. Cela permettra ainsi de vérifier si les *proxies* alternatifs sont effectivement plus efficaces pour reproduire les cumulants de charges conservées que les *proxies* utilisés par STAR.

Puisqu'un GE permet d'avoir accès à la liste complète des particules créées lors d'une collision simulée, il est possible de comparer ces *proxies* aux réels cumulants des charges B , Q et S correspondantes, en utilisant toutes les particules issues de la simulation portant ces charges. De plus, la construction modulaire d'EPOS permet d'avoir accès aux distributions de particules avant les cascades hadroniques, et donc d'étudier à quel point la phase hadronique modifie le signal des cumulants de multiplicités nettes de particules.

La suite de l'étude consiste donc à quantifier l'impact des cascades hadroniques sur les (co)variances de charges conservées et leurs *proxies*, en mesurant ces derniers avant et après la phase hadronique simulée à l'aide d'UrQMD.

Enfin, la procédure de *core-corona* utilisée dans les simulations d'EPOS permet de distinguer si les particules produites proviennent ou non du *core*, qui est censé représenter le PQG créé dans les CIL.

Il est donc possible d'estimer, pour les (co)variances de distributions de particules, quelle proportion du signal trouve son origine dans le *core*, et porte donc effectivement la trace de potentielles fluctuations critiques.

La version d'EPOS utilisée pour cette étude est EPOS 3.451, une version *beta* d'EPOS 4 ; tous les résultats physiques présentés en section E.4 sont donc obtenus à partir de simulations réalisées avec cette version. À noter que l'objectif de ce travail n'est pas d'étudier le signal du point critique en tant que tel, mais bien de se concentrer sur les observables expérimentales utilisées pour le sonder. En particulier, l'objectif est de déterminer à quel point les *proxies* utilisés sont fidèles aux ratios de cumulants de charges nettes conservées correspondantes. Il aurait été possible d'employer, dans les simulations d'événements utilisées, la deuxième équation d'état disponible pour l'évolution du *core* dans EPOS 4, contenant une transition de 1^{er} ordre et un PC en plus du *crossover*. Cependant, le formalisme utilisé pour simuler l'évolution hydrodynamique du *core* ne permet pas la propagation de fluctuations thermales telles que celles générées par des phénomènes critiques. Ce sujet fait actuellement l'objet de recherches actives, et bien que certaines approches permettraient depuis peu de le faire, elles n'ont pas encore été implémentées dans EPOS. Le lecteur doit donc garder à l'esprit que les résultats montrés ci-après n'exhibent en aucun cas des comportements dus à une quelconque criticalité du diagramme de phase de la matière nucléaire.

E.3 Développements techniques pour EPOS 4

Comme expliqué précédemment, le processus de validation d'un GE est une étape cruciale afin de fixer tous les paramètres physiques des différents modèles sous-jacents. Ce processus nécessitant cependant un travail long et fastidieux d'analyse de données simulées et de comparaison aux résultats expérimentaux, il est avantageux de pouvoir systématiser cette étape autant que possible. Or, l'outil RIVET a justement été développé dans ce but. Il s'agit d'un code composé d'un ensemble de bibliothèques, contenant de très nombreuses analyses recensées par publications, et dont la philosophie est d'offrir un outil automatique, standardisé et facile à prendre en main pour comparer les données expérimentales aux résultats de simulations de GE. Bien qu'à l'origine principalement utilisé pour l'étude de la physique du MS et des fonctions de distributions partoniques dans les collisions e^+e^- et $p-p$, RIVET a connu de nombreuses améliorations ces dernières années afin de faciliter l'utilisation d'analyses dédiées aux CIL. Pour cette raison, il est apparu naturel de vouloir associer RIVET à EPOS 4 afin d'assister dans le processus de validation. De plus, avec en vue l'objectif d'une diffusion publique d'EPOS 4, il est primordial d'offrir une compatibilité aussi large que possible aux différents outils utiles à l'utilisateur, et RIVET remplit également ce critère de par sa facilité d'utilisation.

Dans RIVET, chaque analyse consiste en un ensemble de quatre fichiers : un fichier C++ dans lequel est codée l'analyse correspondante à la publication associée, un fichier au format YODA contenant les données expérimentales à comparer, un fichier contenant les informations générales sur l'analyse, et un fichier contenant les détails sur l'affichage des graphes. En effet, YODA est un ensemble de bibliothèques dédié à l'affichage des données, en plus d'être un format standard dans lequel les données expérimentales disponibles en libre accès peuvent être téléchargées. La facilité d'utilisation de RIVET réside dans le fait qu'il ne suffit que de quelques lignes de commande pour l'exécuter. Il suffit d'avoir à disposition un fichier au format HEPMC, un format standard pour stocker les informations de collisions simulées, et une seule ligne de commande permet d'exécuter l'analyse de son choix sur les événements stockés dans ce fichier. En sortie, un fichier contenant les résultats d'analyse au format YODA également est créé. Les résultats d'analyse y sont ordonnés de la même manière que dans le fichier YODA contenant les données expérimentales de référence. De cette façon, une seule autre ligne de commande est suffisante pour générer les graphes des comparaisons entre données expérimentales et résultats d'analyse sur les événements simulés. Enfin, dans le cadre d'analyses de CIL, il est nécessaire de rajouter une étape pour calibrer la centralité des événements avant d'utiliser la plupart des analyses dédiées. Il faut en effet dans ce cas appliquer une analyse de calibration en centralité dans un premier temps, afin de générer une première distribution qui sert de référence pour définir les différentes classes en centralité. Cette distribution sera alors utilisée comme prérequis pour n'importe quelle analyse nécessitant une telle calibration, qui saura alors dans quelle classe en centralité placer chaque événement analysé. Ces commandes sont explicitées dans la sous-section 4.1.1.

La première étape afin d'adapter EPOS à l'utilisation de RIVET est bien sûr d'ajouter la possibilité d'enregistrer les événements simulés au format HEPMC, qui est le seul format lu par RIVET, ce qui est décrit dans la sous-section 4.3.1. Pour cela, je suis reparti du travail entamé par Maria Stefaniak, en complétant tout d'abord les informations physiques qui sont enregistrées au format HEPMC pour chaque événement. J'ai notamment ajouté les informations concernant la section efficace d'interaction, le nombre de nucléons participants à la collision N_{part} , le nombre de nucléons spectateurs N_{spec} . Alors qu'il n'était initialement pas possible d'enregistrer que les particules dans l'état final, j'ai rajouté la possibilité d'enregistrer les désintégrations faibles dans chaque événement.

Cela permet de corriger de la contamination par les désintégration faibles lors d'analyses de spectres exclusifs, qui ne considèrent que les particules primaires d'une certaine espèce hadronique. Un exemple de cascade de désintégrations faibles enregistrée au format HEPMC est illustré en figure 4.7. J'ai également modifié la manière de calculer l'énergie des particules pour le format HEPMC à partir des informations fournies par EPOS, afin de résoudre des problèmes de précision numérique menant à des résultats physiquement incorrects (notamment des particules avec une valeur d'impulsion supérieure à leur énergie). La formule désormais utilisée est explicitée dans l'équation (4.3.4). J'ai rajouté la possibilité d'appliquer une translation en rapidité au référentiel de la collision simulée, suivant la transformation donnée dans l'équation (4.3.5), puisque les collisions sont toujours simulées dans le référentiel du centre de masse par EPOS. Or, expérimentalement, les référentiels du centre de masse et du laboratoire pour les systèmes asymétriques tels que les collisions p - A ne pas confondus, et les analyses RIVET sont alors définies dans le référentiel du laboratoire. Cette fonction permet donc de s'assurer que les coordonnées des particules enregistrées au format HEPMC sont bien définies dans le bon référentiel. Il a finalement été nécessaire de modifier le code d'EPOS afin de donner le choix à l'utilisateur de générer ou non les fichiers contenant l'enregistrement de collisions simulées au format HEPMC, ainsi que la possibilité d'ajouter ou non une translation en rapidité au système simulé comme décrit précédemment.

EPOS étant désormais compatible avec RIVET, la deuxième partie du travail a alors consisté à intégrer l'utilisation de RIVET dans le système d'analyse "à la volée" d'EPOS. Ce système analyse chaque événement un à un après leur simulation, afin de ne garder que le résultat des analyses de ces simulations sans avoir nécessairement besoin d'enregistrer et stocker les événements en question. En l'état, un utilisateur aurait besoin d'exécuter EPOS dans un premier temps afin de générer un fichier au format HEPMC contenant les listes de particules des événements simulés, pour ensuite devoir exécuter RIVET dans un second temps, autant de fois que le nombre d'analyses qu'il souhaiterait appliquer sur ces événements. L'idée d'intégrer RIVET au système d'analyse d'EPOS permettrait alors de réduire le nombre d'étapes intermédiaires et donc de simplifier le processus de comparaison entre les simulations d'EPOS et les données expérimentales disponibles dans RIVET. De plus, cela permettrait d'économiser de l'espace-disque, puisqu'il ne serait alors plus nécessaire de stocker tous les événements que l'utilisateur souhaite analyser au format HEPMC, mais uniquement certains événements de manière temporaire, les uns après les autres.

Le processus, résumé de manière schématique dans la figure 4.10, consiste à transmettre dans un premier temps à un script Python développé pour l'occasion les instructions définies dans un fichier d'options classique d'EPOS, via un fichier temporaire d'extension **".dataR"**. Le script lit alors la liste des analyses requises par l'utilisateur. Une fois que le fichier HEPMC contenant l'enregistrement des collisions simulées est produit, RIVET est successivement exécuté pour chacune des analyses requises. Le fichier YODA contenant les résultats d'analyse obtenu est alors lu par le script Python puis supprimé, pour transcrire les résultats dans le format utilisé par le système d'analyse d'EPOS (**".histo"**), afin de centraliser tous les résultats d'analyses (obtenus via RIVET ou bien directement EPOS). La raison pour cela est que le nombre d'analyses disponibles dans RIVET varie d'une expérience à une autre, et repose sur la bonne volonté de collaborations de soumettre leurs analyses à RIVET. Ainsi, dans de nombreux cas, et notamment pour les collisions Au-Au aux énergies du programme BES, le nombre d'analyses disponibles via RIVET est insuffisant pour le processus de validation d'EPOS 4, et nécessite d'utiliser simultanément le système d'analyse d'EPOS pour compléter.

Le cas des analyses de CIL rajoute à ce fonctionnement quelques subtilités. Parce qu'il est nécessaire de posséder une distribution en centralité sur l'ensemble des événements analysés au préalable, il n'est pas possible d'exécuter la calibration sur un sous-ensemble d'événements pour utiliser cela comme référence pour les analyses suivantes. Ainsi, les résultats de ces analyses de calibration sont stockés dans le répertoire du code d'EPOS. Ainsi, à chaque fois qu'une analyse RIVET nécessitant une calibration en centralité est appelée, elle utilise comme référence une distribution en centralité obtenue préalablement sur un très grand nombre d'événements. Cela permet de s'assurer que le relativement petit nombre d'événements analysés à chaque simulation soit correctement classifié en terme de centralité.

Il est ainsi possible de trouver, en figure 4.9, un extrait de fichier d'option d'EPOS. Y sont explicitées les commandes utilisées afin d'activer la production de fichier au format HEPMC, d'appliquer une translation en rapidité au référentiel du système simulé, et d'appeler RIVET afin d'analyser les événements simulés. Bien que ce système soit opérationnel, il n'est pas parfait et est toujours sujet à de potentielles améliorations. La première consisterait à exécuter RIVET en utilisant un système de lecture de données de type FIFO, qui permettrait de ne même plus avoir à enregistrer des fichiers temporaires au format HEPMC mais de lire les événements un à un sans les garder une fois la lecture effectuée, réduisant encore l'espace disque utilisé dans le processus. Le fait de laisser à l'utilisateur la possibilité de conserver les fichiers YODA d'analyse obtenu par l'exécution de RIVET permettrait également de ne pas reposer sur le système d'affichage des graphes propre à EPOS, mais de pouvoir utiliser les libraires YODA développées à cet effet.

E.4 Résultats sur l'étude des cumulants de charges conservées

Une fois l'architecture d'analyse nécessaire au processus de validation développée, il est alors possible de réaliser une comparaison systématique des résultats de simulations d'EPOS 3.451 aux données expérimentales, et ainsi de réaliser l'étude sur les cumulants motivée précédemment. Je rappelle que je me suis ici intéressé aux collisions Au-Au dans un domaine en énergie de collision de $7.7 \leq \sqrt{s_{NN}} \leq 200$ GeV du programme BES. Parce que les simulations d'EPOS sont coûteuses en temps de calcul, à cause de l'évolution hydrodynamique du *core* en particulier, et qu'il est nécessaire de simuler des collisions à de nombreuses énergies, le nombre d'événements disponible à chaque énergie est relativement limité, comme illustré dans le tableau 5.1. Les énergies de collisions auxquelles j'ai choisi de comparer les simulations aux données expérimentales ci-après dépendent, avant tout, de la disponibilité de données expérimentales. Aussi, pour des raisons de lisibilité des résultats, je n'ai parfois sélectionné que certaines de toutes les énergies de collisions disponibles, tout en gardant à l'esprit de scanner au plus large possible en terme de valeurs d'énergie.

La production de particules à toutes les énergies simulées a été comparée aux résultats expérimentaux, en portant un intérêt particulier à la région cinématique des particules utilisées pour construire les cumulants, *i.e.* $|\eta| < 0.5$ et $0 < p_T < 2$ GeV. Pour commencer, les distributions en pseudorapidité de particules chargées ont été comparées aux données expérimentales à 19.6, 62.4 et 200 GeV/A, telles que montrées dans la figure 5.1. Ici, EPOS se révèle être capable de reproduire correctement ces distributions excepté à 19.6 GeV/A pour les collisions les plus centrales. Ces résultats sont cependant très large-

ment satisfaisants dans l'ensemble. Les spectres en p_T ont ensuite été étudiés pour les hadrons légers (π^\pm , K^\pm et p/\bar{p}), illustrés dans les figures 5.2, 5.3 et A.1 à A.6, ainsi que pour les baryons étranges ($\Lambda/\bar{\Lambda}$, $\Xi^-/\bar{\Xi}^+$ et $\Omega^-/\bar{\Omega}^+$), présentés dans les figures 5.4 à 5.6 et A.7. Ces figures montrent ainsi que les spectres p_T obtenus à partir des événements simulés avec EPOS 3.451 sont en très bon accord avec les données expérimentales aux énergies de collision supérieures à 20 GeV/A, puis s'en écartent de plus en plus à mesure que l'énergie de collision décroît sous $\sqrt{s_{NN}} \approx 20$ GeV/A.

Les résultats obtenus pour la production de particules dans l'intervalle cinématique d'intérêt pour l'étude des cumulants montre qu'EPOS 3.451 obtient des résultats en bon accord quantitatif avec les données expérimentales, au moins au-dessus de $\sqrt{s_{NN}} \sim 20$ GeV. Au-dessous de cette valeur, les résultats de simulations divergent peu à peu des données expérimentales à mesure que l'énergie de collision décroît, bien qu'en conservant une allure encore relativement proche. On constate notamment un adoucissement progressif des spectres en p_T , c'est-à-dire une modification des spectres avec une production trop importante dans les plus basses valeurs de p_T , et pas assez importante à plus haut p_T , comparé aux données expérimentales.

Ces résultats ne sont pas inattendus, puisqu'une des hypothèses importantes de la PBGRT, utilisée pour simuler les conditions initiales dans EPOS, est que toutes les interactions doivent avoir lieu simultanément. Or, à plus basse énergie, la contraction de Lorentz dans la direction longitudinale des noyaux collisionnants est moins importante, et ces noyaux vont alors mettre plus de temps à se traverser. Ainsi, de rapides calculs permettent d'estimer qu'au-dessous d'une énergie de collision d'environ une vingtaine de GeV/A, l'épaisseur de ces noyaux entraînerait un temps d'interaction suffisamment long pour que les partons du projectile aient le temps de réinteragir avec ceux de la cible. Dans ce cas-ci, la PBGRT employée dans EPOS n'offrirait alors plus un formalisme adapté pour étudier ce genre de collisions. Cependant, ces calculs n'étant qu'approximatifs, puisque reposant sur une hypothèse purement qualitative quant à l'épaisseur nécessaire pour permettre plusieurs interactions successives entre partons, il est difficile d'en tirer une valeur d'énergie de collision limite stricte pour pouvoir utiliser EPOS.

Afin de calculer les (co)variances de distributions nettes de π^\pm , K^\pm et $p(\bar{p})$ dans les simulations d'EPOS 3.451, j'ai reproduit l'analyse effectuée par l'expérience STAR. Je me suis pour cela servi du système d'analyse d'EPOS, et ai donc dû développer les routines d'analyse nécessaires. Je les ai développées en donnant la possibilité de calculer les cumulants d'ordre 1 à 4, pour les charges conservées B , Q et S ainsi que les distributions nettes de π^\pm , K^\pm , $p(\bar{p})$, $\Lambda(\bar{\Lambda})$, $\Xi^-(\bar{\Xi}^+)$ et $\Omega^-(\bar{\Omega}^+)$ avant ou après les cascades hadroniques. J'y ai de plus ajouté la possibilité de corriger ces distributions des contributions dues aux désintégrations faibles, pour le cas d'espèces hadroniques identifiées. Dans le cas de charges conservées, le calcul se fait systématiquement à partir des particules primordiales, puisque l'étrangeté S n'est pas conservée par l'interaction faible. Enfin, ces routines ont été développées de manière à être facilement étendues à d'autres espèces de particules, ou bien même à des ordres de cumulants supérieurs. Les détails concernant le fonctionnement et l'intégration de cette analyse sont donnés dans l'annexe C.

Les résultats de (co)variances des distributions de π^\pm , K^\pm et $p(\bar{p})$, représentées en fonction de N_{part} , sont exposés dans les figures 5.7 et 5.8. On constate que les résultats d'EPOS sont en accord à la fois qualitatif, mais aussi quantitatif dans l'ensemble, avec les données de STAR. Cela est vrai pour des énergies de collisions supérieures à ~ 20 GeV/A en particulier, alors que ces résultats présentent des divergences de plus en plus importantes avec les données expérimentales avec la décroissance de l'énergie de collision, reflétant les difficultés d'EPOS à reproduire correctement les distributions de particules à ces énergies.

Les ratios de *proxies* formés par ces (co)variances, exposés dans la figure 5.9, exhibent alors logiquement le même comportement vis-à-vis des résultats expérimentaux. Aucune claire dépendance à la centralité n'est observée dans les fluctuations statistiques, qui sont assez importantes à cause du nombre relativement faible d'événements simulés pour chaque énergie.

L'étape suivante de l'étude consiste alors à comparer les résultats de *proxies* de STAR aux *proxies* alternatifs \tilde{C}_{QS} et $\tilde{C}_{BS}/\tilde{C}'_{BS}$ explicités dans les équations (2.3.25) et (2.3.26), respectivement. Aucun *proxy* n'ayant été proposé pour le ratio $C_{BQ} = \chi_{11}^{QB}/\chi_2^B$, je me suis inspiré de l'étude basée sur le modèle du GRH pour proposer un *proxy* alternatif \tilde{C}_{QB} explicité dans l'équation (5.2.4). Je me suis pour cela basé sur la décomposition des contributions hadroniques aux susceptibilités χ_{11}^{QB} et χ_2^B , présentée dans la figure 5.10, en utilisant les mêmes arguments que les auteurs afin de construire ce ratio. Le résultat des comparaisons entre ratios de (co)variances de charges conservées, et de leurs différents *proxies* associés, est présenté dans la figure 5.11 pour 5 différentes énergies, en fonction de la centralité de la collision. Les mêmes résultats sont présentés en fonction de l'énergie de collision dans la figure 5.12 pour les collisions les plus centrales et les plus périphériques. Dans les deux cas, les résultats expérimentaux de STAR sont uniquement montrés à titre indicatif, pour comparer aux résultats de *proxies* correspondants avec EPOS 3.451. Les *proxies* alternatifs \tilde{C}_{QS} , \tilde{C}_{BS} et \tilde{C}_{QB} (en bleu) se révèlent être de bien meilleurs *proxies* des ratios de (co)variances de charges conservées (en vert) que les *proxies* de STAR (en rouge). On observe en effet qu'ils se situent toujours très proches quantitativement des ratios de charges correspondants, là où les *proxies* de STAR en sont plus éloignés, au dessus de $\sqrt{s_{NN}} \approx 20$ GeV/A. Au-dessous de cette énergie, les difficultés d'EPOS 3.451 à reproduire correctement la production de particules rendent non pertinente toute interprétation du comportement de ces ratios.

Ainsi, dans la recherche d'un potentiel PC du diagramme de phase de la matière nucléaire, les quantités suivant sont de meilleurs *proxies* que ceux utilisés jusque-là par la collaboration STAR:

$$\tilde{C}_{QS} = \frac{1}{2} \cdot \frac{\sigma_K^2}{\sigma_K^2 + \sigma_\Lambda^2} \quad , \quad \tilde{C}_{BS} = \frac{\sigma_\Lambda^2}{\sigma_K^2 + \sigma_\Lambda^2} \quad , \quad \tilde{C}_{QB} = \frac{\sigma_{\pi p}^{11} + \sigma_p^2}{2\sigma_p^2 + \sigma_\Lambda^2}$$

Il est intéressant de noter que l'utilisation presque exclusive de variances, ainsi que le seul ajout de la variance de distribution nette de Λ en plus des (co)variances déjà mesurées par STAR, sont suffisants pour construire des *proxies* quantitativement plus proches des ratios de cumulants de charges conservées.

Profitant de la construction modulaire d'EPOS, j'ai ensuite pu mesurer l'impact des cascades hadroniques sur les (co)variances de charges et de distributions de particules, ainsi que des ratios et *proxies* correspondants. Pour cela, j'ai comparé la valeur de ces observables calculées à partir des particules obtenues juste après hadronisation, avec leur valeur calculée à partir des particules à la fin de l'évolution de la collision. Les résultats montrent que les variances et covariances de distributions nettes de particules, montrées respectivement dans les figures 5.13 et 5.14, sont très fortement impactées par la phase hadronique, contrairement aux (co)variances de charges conservées exposés dans les figures D.1 et D.2. Ainsi, l'amplitude du signal est généralement multipliée par un facteur 2 à 3 durant cette phase, principalement à cause des désintégrations de résonances et réactions inélastiques successives y ayant lieu. Cependant, les ratios obtenus à partir de ces (co)variances sont quant à eux très peu modifiés.

\tilde{C}_{QS} et \tilde{C}_{QB} s'avèrent ainsi être de très bons *proxies* des ratios de cumulants de charges conservées correspondants, puisque leur amplitude n'est que très peu modifiée par la phase hadronique, comme quantifié dans la figure 5.16. Ainsi, l'amplitude d'un potentiel signal critique porté par ces observables survivrait aux cascades hadroniques et pourrait être mesurée expérimentalement, reflétant alors de manière fidèle le signal produit après hadronisation du système. Seul \tilde{C}_{BS} forme un *proxy* peu adapté, dans le sens où son amplitude est modifiée d'un facteur 2 par la phase hadronique, et ne reflète donc pas à la fin de la collision le signal obtenu après hadronisation.

La dernière étape de mon étude a consisté à calculer quelle proportion des ratios de cumulants de charges conservées, et des *proxies* alternatifs associés, provient effectivement du *core*, correspondant à l'image physique du PQG dans les simulations d'EPOS 3.451. Les résultats, montrés dans la figure 5.17, indiquent que l'intensité du signal des cumulants de charges conservées et de leurs *proxies* provient quasi exclusivement du "core" pour les particules considérées dans cette analyse, dans les collisions d'énergie supérieure à 10 GeV/A.

Ainsi les fluctuations de distributions de particules mesurées après hadronisation, reflétées de manière relativement fidèle à la fin de la collision comme montré précédemment, sont portées presque exclusivement par des particules issues de l'hadronisation du "core", pour des particules considérées avec $|\eta| < 0.5$ et $0 < p_T < 2$ GeV. Au-dessous de $\sqrt{s_{NN}}$, cette proportion diminue, simplement dû au fait que la proportion du "core" est moins importante pour les systèmes de basse énergie.

En conclusion, cette étude apporte des résultats très importants en terme d'observables expérimentales employées pour sonder la présence d'un signal, dû à un potentiel PC, dans le diagramme de phase de la matière nucléaire. Une poursuite de ce travail pourrait notamment consister à chercher un potentiel *proxy* alternatif pour C_{BS} qui survivrait aux cascades hadroniques sans voir l'amplitude de son signal modifié. Cette étude pourrait également être étendue aux cumulants d'ordre supérieurs, d'autant plus intéressants qu'ils sont plus sensibles à la criticalité, et donc largement étudiés aujourd'hui.

- AGK** Abramovsky-Gribov-Kancheli.
- AGS** *Alternating Gradient Synchrotron.*
- ALICE** *A Large Ion Collider Experiment.*
- AMOR** *Artru-Mennessier Off-shell Resonance.*
- AMPT** *A Multiphase Transport Model.*
- AQM** *Additive Quark Model.*
- ATLAS** *A Toroidal LHC ApparatuS.*
- BES** *Beam Energy Scan.*
- BEST** *Beam Energy Scan Theory.*
- BNL** *Brookhaven National Laboratory.*
- BRAHMS** *Broad RAnge Hadron Magnetic Spectrometers.*
- BSM** beyond the Standard Model.
- CBM** *Compact Baryonic Matter.*
- CBWC** centrality bin-width corrections.
- CBWE** centrality bin-width effect.
- CDF** *Collider Detector at Fermilab.*
- CDQ** chromodynamique quantique.
- CEP** critical endpoint.
- CERN** *European Organization for Nuclear Research, or "Conseil Européen pour la Recherche Nucléaire".*
- CGC** Color-Glass Condensate.
- CIL** collisions d'ions lourds.
- CKM** Cabibbo-Kobayashi-Maskawa.

- CLT** Central Limit Theorem.
- CMS** *Compact Muon Solenoid*.
- CORSIKA** *COsmic Ray Simulations for KAscade*.
- DCA** distance of closest approach.
- DGLAP** Dokshitzer-Gribov-Lipatov-Altarelli-Parisi.
- DIS** deep inelastic scattering.
- DREENA** *Dynamical Radiative and Elastic ENergy loss Approach*.
- EAS** extensive air-shower.
- EFT** effective field theory.
- EG** event generator.
- EM** electromagnetic.
- EoS** equation of state.
- EPOS** *Energy conserving quantum mechanical approach based on Partons, parton ladders, strings, Off-shell remnants and Saturation of parton ladders*.
- EPOS-HQ** EPOS *Heavy Quarks*.
- EW** electroweak.
- FAIR** *Facility for Antiproton and Ion Research*.
- FCC** *Future Circular Collider*.
- FIFO** First-In, First-Out.
- FS** final-state.
- GC** grand-canonical.
- GE** générateur d'événements.
- GRH** gaz de résonances de hadrons.
- GRT** Gribov-Regge theory.
- HEPMC** *High-energy physics Monte-Carlo*.
- HEP** high-energy physics.
- HIC** heavy-ion collision.
- HIJING** *Heavy Ion Jet INteraction Generator*.
- HL-LHC** *High-Luminosity Large Hadron Collider*.
- HQ** heavy quark.
- HRG** Hadron Resonance Gas.

- ISR** *Intersecting Storage Rings.*
- JETSCAPE** *Jet Energy-loss Tomography with a Statistically and Computationally Advanced Program Envelope.*
- JEWEL** *Jet Evolution With Energy Loss.*
- J-PARC** *Japanese Proton Accelerator Research Complex.*
- LBNL** *Lawrence Berkeley National Laboratory.*
- LHC** *Large Hadron Collider.*
- LHCb** *Large Hadron Collider beauty.*
- IQCD** lattice quantum chromodynamics.
- MC** Monte Carlo.
- MPD** *Multi-Purpose Detector.*
- MPI** multiple parton interactions.
- MS** *Modèle Standard.*
- NICA** *Nuclotron-based Ion Collider fAcility.*
- PAW** *Physics Analysis Workstation.*
- PBGRT** Parton-Based Gribov-Regge Theory.
- PC** point critique.
- PDF** parton distribution function.
- PDG** Particle Data Group.
- PHENIX** *Pioneering High Energy Nuclear Interaction eXperiment.*
- PHSD** *Parton-Hadron String Dynamics.*
- PMNS** Pontecorvo-Maki-Nakagawa-Sakata.
- PNJL** Poliakov-Nambu-Jona-Lasinio.
- pQCD** perturbative quantum chromodynamics.
- PQG** plasma de quarks et gluons.
- PSOI** phase space of interest.
- QCD** quantum chromodynamics.
- QED** quantum electrodynamics.
- QFT** quantum field theory.
- QGP** quark-gluon plasma.
- QGSJet** *Quark-Gluon String Jet.*

RIVET *Robust Independent Validation of Experiments and Theory.*

RHIC *Relativistic Heavy Ion Collider.*

SAM subensemble acceptance method.

SBM Statistical Bootstrap Model.

SHINE *SPS Heavy Ion and Neutrino Experiment.*

SLAC *Stanford Linear Accelerator Center.*

SM Standard Model.

SMASH *Simulating Many Accelerated Strongly-interacting Hadrons.*

SPS *Super Proton Synchrotron.*

STAR *Solenoidal Tracker At RHIC.*

SUSY Supersymmetry.

UHECR ultra-high energy cosmic-ray.

UrQMD *Ultra-relativistic Quantum Molecular Dynamics.*

VENUS *Very Energetic Nuclear Scattering.*

X3F "cross-over & 3 flavour conservation".

YODA *Yet more Objects for Data Analysis.*

ZDC *Zero Degree Calorimeter.*

1.1	Components of the Standard Model listed with their main properties (mass, spin and electric charge) [15] taken from the <i>Particle Data Group</i> 2022 [14].	13
1.2	Illustration of the $J = 0$ and $J = 1/2$ octets as representations of the SU(3) group.	17
1.3	The intensity of the running coupling constant α_s as a function of the virtuality Q of the process considered. Analytical prediction based on the renormalisation scale of the order of M_Z , and values extracted from different processes are also displayed [14].	19
2.1	Description of the evolution of the system created in HICs, in a space-time diagram, following the Björken scenario. The t and z coordinates are in Euclidean space-time, while the $\tau = \sqrt{t^2 - z^2}$ is in Milne coordinate [99].	23
2.2	Timeline of the different experiments which took place at the CERN SPS, with the different ion beams used to collide on various targets, with the main topics of interest specified on top of the corresponding boxes [100].	24
2.3	The semi-hypothetical phase diagram of nuclear matter sketched as a function of temperature T and baryonic chemical potential μ_B . Exact position of phase transitions and critical point are approximate, just displayed to illustrate roughly the main structures [117].	26
2.4	Distribution of the total inelastic cross-section as a function of the number of charged particles N_{ch} produced by a collision within the $ \eta < 1$ region. A correspondence with the integrated percentage of the total cross-section, used to determine the centrality percentage, is added. Values used on both axes are arbitrary and purely indicative [138].	28
2.5	Phase diagram of nuclear matter, with representations of the trajectories described by several collisions systems of the BES program. Positions of phase transitions and critical point are purely illustrative [151].	30
2.6	K/π ratios measured within $ y < 1$ in 0-5% Au-Au collisions as a function of the collision energy [177].	33
2.7	3D representation of the behaviour of χ_2^B as a function of T and μ_B , for an equation of state containing a CEP at coordinates $T_{CEP} = 143$ MeV and $\mu_B^{CEP} = 350$ MeV. The divergence of χ_2^B around this location is indicated [218].	37

2.8	Left: cumulant ratio $C_4/C_2(= \kappa\sigma^2)$ for net-protons, measured by STAR as a function of energy for central (0-5%) Au-Au collisions, compared to the linear Poisson baseline in the lower panel [214]. Right: expected behaviour of $C_4/C_1(= \omega_4)$ for net-protons, in the case of a freeze-out line passing through the critical region near the CEP (modified from [151]).	39
2.9	Centrality dependence of the covariances of p , K and π net-multiplicity distributions, for Au-Au collisions at several indicated energies of the BES program, within $ \eta < 0.5$ and $0.4 < p_T < 1.6$ GeV. Results from STAR, with systematic errors indicated by the boxes, are compared to CLT expectations and UrQMD simulations results [211].	42
2.10	Energy dependence of the cumulants ratios C_{pK} , C_{QK} for central (0-5%) and peripheral (70-80%) Au-Au collisions, within $ \eta < 0.5$ and $0.4 < p_T < 1.6$ GeV. Results from STAR have systematic errors indicated by the boxes and statistical ones by bars. Poisson baseline, UrQMD simulations results and calculations using HRG model including the PDG16+ [236] particles set are displayed for comparison [211].	43
2.11	Breakdown of hadronic contribution to χ_{11}^{QS} and χ_2^S as a function of T , obtained with HRG model calculations [234].	45
2.12	Comparison of several proxy ratios for QS and BS correlations obtained via HRG model calculations. Both are plotted as a function of T , with their related ratio of exact susceptibilities calculated with lQCD [234].	46
3.1	Schematised general structure of an event simulated with HIC event generators.	50
3.2	Timeline of the different versions of VENUS, NEXUS, EPOS and side-projects, based on the publication date of the first papers mentioning them. (<i>N.B. : EPOS-LHC [272] was released as a stable version, no longer developed after then</i>)	53
3.3	Diagram of a $A-A$ collision viewed by the PBGR formalism (original figure from [284])	55
3.4	The five different structures of Pomerons considered in the PBGR, corresponding respectively to (from left to right): G_{soft} , $G_{val-val}$, $G_{sea-sea}$, $G_{val-sea}$ and $G_{sea-val}$ [284].	56
3.5	Schematic view of a cut Pomeron as a cut parton ladder, used to model particle production in the PBGR. The blue lines are the initial interacting partons, the curly lines are gluons and straight lines quarks [290, 291]	57
3.6	A kinky string formed by a $q-\bar{q}$ pair, created after an e^+e^- annihilation, with an emitted transverse gluon [294].	58
3.7	Schematic representation of the breaking of an initial $u-\bar{u}$ string with the corresponding hadrons identified to the string segments obtained.	59
3.8	Illustration of HQs production in space-like cascade (SLC), time-like cascade (TLC) and Born process during the primary interactions of a $A-A$ collision with EPOS. Thick blue lines represent nucleons, while thin blue lines are drawn for partons [291].	60
3.9	Schematic view of a collision with many strings (in red) exchanged between projectile and target remnants (in blue) : the dense part will compose the core, while the high- p_T segments will escape in the corona [294].	61
4.1	Schematic representation of the principal components of RIVET acting in the data flow from event record to results of the analysis, with the links between classes (in blue), files (in yellow) and the different commands (in green) used to execute it [303].	70

4.2	RIVET analysis coverage compared to the total number of publications for LHC, SPS and RHIC experiments [305].	72
4.3	Non-exhaustive structure of the directories containing the EPOS code.	73
4.4	Example of instructions used in a <code>.optns</code> file to define a simulation for Au-Au collisions.	74
4.5	Example of an analysis defined in a <code>.optns</code> file to get a p_T distribution of π^+	75
4.6	Example of the content of a HEPMC file for a Pb-Pb collision at 2.76 GeV/A.	78
4.7	Example of the record of a decay chain of a particle in a HEPMC file for a Pb-Pb collision at 2.76 GeV/A, from the same event displayed in figure 4.6. Note that the precision on numerical values have been truncated for the purpose of the figure.	82
4.8	Example of an analysis defined in a <code>.optns</code> file to get a p_T distribution of π^+	84
4.9	Example of the instructions to write in a <code>.optns</code> file to run RIVET.	87
4.10	Functional diagram of data & processes flow when calling RIVET through the EPOS analysis system.	88
5.1	Pseudorapidity densities of charged particles for Au-Au collisions at $\sqrt{s_{NN}} = 19.6, 62.4$ and 200 GeV, in different centrality classes within 0-50%. Results from EPOS 3.451 are compared with data from PHOBOS, results from different centrality classes being displayed alternatively in two plots per energy for visibility [309].	92
5.2	Transverse momentum spectra of π^\pm, K^\pm and p/\bar{p} within $ \eta < 0.35$, for different centrality classes in Au-Au events at $\sqrt{s_{NN}} = 200$ GeV. Spectra for the most central events are at real scale, while the others are scaled by factors 10^{-x} ($x = \{1, 2, 3, 4\}$) (data from [310]).	94
5.3	Transverse momentum spectra of π^\pm, K^\pm and p/\bar{p} at $y = 0.8$, for different centrality classes in Au-Au events at $\sqrt{s_{NN}} = 62.4$ GeV. Spectra for the most central events are at real scale, while the others are scaled by factors 10^{-1} (15-30%) and 10^{-2} (30-50%) (data from [311]).	95
5.4	Transverse momentum spectra of $\Lambda, \bar{\Lambda}, \Xi^-, \bar{\Xi}^+$ and $\Omega^- + \bar{\Omega}^+$ for different centrality classes in Au-Au events at $\sqrt{s_{NN}} = 200$ GeV. Spectra for the most central events are at real scale, while the others are scaled by factors 10^{-x} ($x = \{1, 2, 3, 4\}$) (data from [313]).	96
5.5	Transverse momentum spectra of $\Lambda, \bar{\Lambda}, \Xi^-, \bar{\Xi}^+, \Omega^-$ and $\bar{\Omega}^+$ for different centrality classes in Au-Au events at $\sqrt{s_{NN}} = 27$ GeV. Spectra for the most central events are at real scale, while the others are scaled by factors 10^{-x} ($x = \{1, 2, 3, 4, 5, 6\}$) (data from [315]).	97
5.6	Transverse momentum spectra of $\Lambda, \bar{\Lambda}, \Xi^-, \bar{\Xi}^+, \Omega^-$ and $\bar{\Omega}^+$ for different centrality classes in Au-Au events at $\sqrt{s_{NN}} = 7.7$ GeV. Spectra for the most central events are at real scale, while the others are scaled by factors 10^{-x} ($x = \{1, 2, 3, 4, 5, 6\}$) (data from [315]).	98
5.7	Net- p , net- K and net- π multiplicity variances vs. N_{part} for different energies, obtained from EPOS 3.451 simulations (red lines) and compared with STAR results (dots) [211].	100
5.8	Net- p , net- K and net- π multiplicity covariances vs. N_{part} for different energies, obtained from EPOS 3.451 simulations (red lines) and compared with STAR results (dots) [211].	101

5.9	Ratios of net- p , net- K and net- π multiplicity (co)variances vs. N_{part} for different energies, obtained from EPOS 3.451 simulations (red lines) and compared with STAR results (dots) [211].	102
5.10	Breakdown of hadronic contribution to χ_{QB}^{11} and χ_B^2 as a function of T , obtained with HRG model calculations [234].	103
5.11	Ratios of exact B , Q and S conserved charges (co)variances and their proxies displayed as a function of N_{part} for different energies, obtained from EPOS 3.451 simulations (lines) and compared with STAR data (dots) as an indication [211].	104
5.12	Ratios of exact B , Q and S conserved charges (co)variances and their proxies displayed as a function of $\sqrt{s_{NN}}$ for central (left) and peripheral (right) collisions. Results from EPOS 3.451 simulations (lines), compared with STAR data (dots) as an indication [211].	105
5.13	Net- p , net- π , net- K and net- Λ multiplicity variances vs. N_{part} for different energies, obtained from EPOS 3.451 simulations and compared with STAR results (dots) [211]. The results calculated from full events are represented by full lines, while results calculated before hadronic cascades are represented by dotted lines.	106
5.14	Covariances of net- p , net- π and net- K multiplicity distribution vs. N_{part} for different energies, obtained from EPOS 3.451 simulations and compared with STAR results (dots) [211]. The results calculated from full events are represented by full lines, while results calculated before hadronic cascades are represented by dotted lines.	107
5.15	Ratios of exact B , Q and S conserved charges (co)variances and their proxies plotted as a function of $\sqrt{s_{NN}}$ for central (left) and peripheral (right) collisions. Results are displayed for full event calculation (full lines) and calculation before hadronic cascades (dotted lines) from EPOS 3.451 simulations. STAR data (dots) are shown as an indication [211].	108
5.16	Ratios of C_{XY} and enhanced proxies \tilde{C}_{XY} calculated before hadronic cascades over full event calculations, plotted as a function of $\sqrt{s_{NN}}$ for central (left) and peripheral collisions (right).	109
5.17	Core proportion of C_{XY} and enhanced proxies \tilde{C}_{XY} ratios over the total value calculated before hadronic cascades, plotted as a function of $\sqrt{s_{NN}}$ for central (left) and peripheral collisions (right).	110
A.1	Transverse momentum spectra of respectively line by line π^+ , π^- , K^+ and K^- , at $ y < 0.1$, for centrality classes from 0% to 40% (left) and 40% to 80% (right) in Au-Au events at $\sqrt{s_{NN}} = 27$ GeV. In each plot, spectra for the most central events are at real scale, while the others are scaled by factors 10^{-x} ($x = \{1, 2, 3, 4\}$) (data from [177]).	118
A.2	Same than previous figure but for p and \bar{p}	119
A.3	Transverse momentum spectra of respectively line by line π^+ , π^- , K^+ and K^- , at $ y < 0.1$, for centrality classes from 0% to 40% (left) and 40% to 80% (right) in Au-Au events at $\sqrt{s_{NN}} = 14.5$ GeV. In each plot, spectra for the most central events are at real scale, while the others are scaled by factors 10^{-x} ($x = \{1, 2, 3, 4\}$) (data from [177]).	120
A.4	Same than previous figure but for p and \bar{p}	121
A.5	Transverse momentum spectra of respectively line by line π^+ , π^- , K^+ and K^- , at $ y < 0.1$, for centrality classes from 0% to 40% (left) and 40% to 80% (right) in Au-Au events at $\sqrt{s_{NN}} = 7.7$ GeV. In each plot, spectra for the most central events are at real scale, while the others are scaled by factors 10^{-x} ($x = \{1, 2, 3, 4\}$) (data from [177]).	122

A.6	Same than previous figure but for p and \bar{p}	123
A.7	Transverse momentum spectra of Λ , $\bar{\Lambda}$, Ξ^- , Ξ^+ , Ω^- and $\bar{\Omega}^+$ for different centrality classes in Au-Au events at $\sqrt{s_{NN}} = 19.6$ GeV. Spectra for the most central events are at real scale, while the others are scaled by factors 10^{-x} ($x = \{1, 2, 3, 4, 5, 6\}$) (data from [315]).	124
B.1	Centrality dependence of net- p , net- K and net- π multiplicity variances for Au+Au collisions at $\sqrt{s_{NN}} = 200$ GeV, obtained from EPOS 3.451 simulations. The lines represent cumulant calculations as a function of the N_{part} variable directly, while the point represent cumulants calculated for usual STAR centrality classes (<i>i.e.</i> 0-5%, 5-10%, 10-20%...70-80%) [211].	126
B.2	Centrality dependence of net- p , net- K and net- π multiplicity covariances for Au+Au collisions at $\sqrt{s_{NN}} = 200$ GeV, obtained from EPOS 3.451 simulations. The lines represent cumulant calculations as a function of the N_{part} variable directly, while the point represent cumulants calculated for usual STAR centrality classes (<i>i.e.</i> 0-5%, 5-10%, 10-20%...70-80%) [211].	127
D.1	Variances of B , Q and S vs. N_{part} for different Au-Au collisions energies, obtained from EPOS 3.451 simulations. The results calculated from full events are represented by full lines, while results calculated before hadronic cascades are represented by dotted lines.	135
D.2	Covariances of B , Q and S vs. N_{part} for different Au-Au collisions energies, obtained from EPOS 3.451 simulations. The results calculated from full events are represented by full lines, while results calculated before hadronic cascades are represented by dotted lines.	136

LIST OF TABLES

5.1	Number of events simulated with EPOS 3.451 per collision energy.	90
C.1	Input parameters of the "mupurp_susc()" subroutine to perform a calculation of moments from 1 st to 4 th order of net-multiplicity distribution. . .	130
C.2	Correspondence between digits and associated charge or particle for xpara (9,n).	130

- [1] J.J. Thomson. “**Cathode Rays**”. In: *The London, Edinburgh, and Dublin Philosophical Magazine and Journal of Science* 44.269 (1897), pp. 293–316. DOI: [10.1080/14786449708621070](https://doi.org/10.1080/14786449708621070).
- [2] H. Geiger and E. Marsden. “**On a Diffuse Reflection of the α -Particles**”. In: *Proceedings of the Royal Society of London Series A* 82.557 (July 1909), pp. 495–500. DOI: [10.1098/rspa.1909.0054](https://doi.org/10.1098/rspa.1909.0054).
- [3] E. Rutherford. “**The scattering of α and β particles by matter and the structure of the atom**”. In: *Phil. Mag. Ser. 6* 21 (1911), pp. 669–688. DOI: [10.1080/14786440508637080](https://doi.org/10.1080/14786440508637080).
- [4] Max Planck. “**Ueber das Gesetz der Energieverteilung im Normalspectrum**”. In: *Annalen der Physik* 309.3 (Jan. 1901), pp. 553–563. DOI: [10.1002/andp.19013090310](https://doi.org/10.1002/andp.19013090310).
- [5] A. Einstein. “**Über einen die Erzeugung und Verwandlung des Lichtes betreffenden heuristischen Gesichtspunkt**”. In: *Annalen der Physik* 322.6 (Jan. 1905), pp. 132–148. DOI: [10.1002/andp.19053220607](https://doi.org/10.1002/andp.19053220607).
- [6] Niels Bohr. “**I. On the constitution of atoms and molecules**”. In: *The London, Edinburgh, and Dublin Philosophical Magazine and Journal of Science* 26.151 (1913), pp. 1–25. DOI: [10.1080/14786441308634955](https://doi.org/10.1080/14786441308634955).
- [7] Niels Bohr. “**XXXVII. On the constitution of atoms and molecules**”. In: *The London, Edinburgh, and Dublin Philosophical Magazine and Journal of Science* 26.153 (1913), pp. 476–502. DOI: [10.1080/14786441308634993](https://doi.org/10.1080/14786441308634993).
- [8] Niels Bohr. “**LXXIII. On the constitution of atoms and molecules**”. In: *The London, Edinburgh, and Dublin Philosophical Magazine and Journal of Science* 26.155 (1913), pp. 857–875. DOI: [10.1080/14786441308635031](https://doi.org/10.1080/14786441308635031).
- [9] Wolfgang Pauli. “**Pauli letter collection: letter to Lise Meitner**”. URL: <https://cds.cern.ch/record/83282>.
- [10] Enrico Fermi. “**Tentativo di una teoria dell’emissione dei raggi beta**”. In: *Ric. Sci.* 4 (1933), pp. 491–495.
- [11] J. Chadwick. “**Possible Existence of a Neutron**”. In: *Nature* 129 (1932), p. 312. DOI: [10.1038/129312a0](https://doi.org/10.1038/129312a0).
- [12] Otto Hahn and Fritz Strassmann. “**Nachweis der Entstehung aktiver Bariumisotope aus Uran und Thorium durch Neutronenbestrahlung; Nachweis weiterer aktiver Bruchstücke bei der Uranspaltung**”. In: *Naturwissenschaften* 27.6 (Feb. 1939), pp. 89–95. DOI: [10.1007/BF01488988](https://doi.org/10.1007/BF01488988).

- [13] Lise Meitner. “**New Products of the Fission of the Thorium Nucleus**”. In: *Nature* 143.3624 (Apr. 1939), p. 637. DOI: [10.1038/143637a0](https://doi.org/10.1038/143637a0).
- [14] R. L. Workman. “**Review of Particle Physics**”. In: *PTEP* 2022 (2022), p. 083C01.
- [15] Erwann Masson. “**Mesure de la production de photons isolés dans les collisions proton-proton et proton-plomb au LHC avec l’expérience ALICE**”. PhD thesis. Ecole nationale supérieure Mines-Télécom Atlantique, 2019. URL: <http://www.theses.fr/2019IMTA0148>.
- [16] F. J. Hasert et al. “**Observation of Neutrino Like Interactions Without Muon Or Electron in the Gargamelle Neutrino Experiment**”. In: *Phys. Lett. B* 46 (1973), pp. 138–140. DOI: [10.1016/0370-2693\(73\)90499-1](https://doi.org/10.1016/0370-2693(73)90499-1).
- [17] Nicola Cabibbo. “**Unitary Symmetry and Leptonic Decays**”. In: *Phys. Rev. Lett.* 10 (1963), pp. 531–533. DOI: [10.1103/PhysRevLett.10.531](https://doi.org/10.1103/PhysRevLett.10.531).
- [18] Makoto Kobayashi and Toshihide Maskawa. “**CP Violation in the Renormalizable Theory of Weak Interaction**”. In: *Prog. Theor. Phys.* 49 (1973), pp. 652–657. DOI: [10.1143/PTP.49.652](https://doi.org/10.1143/PTP.49.652).
- [19] Sheldon L. Glashow. “**The renormalizability of vector meson interactions**”. In: *Nucl. Phys.* 10 (1959), pp. 107–117. DOI: [10.1016/0029-5582\(59\)90196-8](https://doi.org/10.1016/0029-5582(59)90196-8).
- [20] Abdus Salam and John Clive Ward. “**Weak and electromagnetic interactions**”. In: *Nuovo Cim.* 11 (1959), pp. 568–577. DOI: [10.1007/BF02726525](https://doi.org/10.1007/BF02726525).
- [21] Steven Weinberg. “**A Model of Leptons**”. In: *Phys. Rev. Lett.* 19 (1967), pp. 1264–1266. DOI: [10.1103/PhysRevLett.19.1264](https://doi.org/10.1103/PhysRevLett.19.1264).
- [22] F. Englert and R. Brout. “**Broken Symmetry and the Mass of Gauge Vector Mesons**”. In: *Phys. Rev. Lett.* 13 (1964). Ed. by J. C. Taylor, pp. 321–323. DOI: [10.1103/PhysRevLett.13.321](https://doi.org/10.1103/PhysRevLett.13.321).
- [23] Peter W. Higgs. “**Broken Symmetries and the Masses of Gauge Bosons**”. In: *Phys. Rev. Lett.* 13 (1964). Ed. by J. C. Taylor, pp. 508–509. DOI: [10.1103/PhysRevLett.13.508](https://doi.org/10.1103/PhysRevLett.13.508).
- [24] G. S. Guralnik, C. R. Hagen, and T. W. B. Kibble. “**Global Conservation Laws and Massless Particles**”. In: *Phys. Rev. Lett.* 13 (1964). Ed. by J. C. Taylor, pp. 585–587. DOI: [10.1103/PhysRevLett.13.585](https://doi.org/10.1103/PhysRevLett.13.585).
- [25] Kimberly K. Boddy et al. “**Snowmass2021 theory frontier white paper: Astrophysical and cosmological probes of dark matter**”. In: *JHEAp* 35 (2022), pp. 112–138. DOI: [10.1016/j.jheap.2022.06.005](https://doi.org/10.1016/j.jheap.2022.06.005). arXiv: [2203.06380](https://arxiv.org/abs/2203.06380) [hep-ph].
- [26] Vera C. Rubin and Jr. Ford W. Kent. “**Rotation of the Andromeda Nebula from a Spectroscopic Survey of Emission Regions**”. In: *Astrophys. J.* 159 (Feb. 1970), p. 379. DOI: [10.1086/150317](https://doi.org/10.1086/150317).
- [27] M. S. Roberts and R. N. Whitehurst. “**The rotation curve and geometry of M31 at large galactocentric distances**”. In: *Astrophys. J.* 201 (Oct. 1975), pp. 327–346. DOI: [10.1086/153889](https://doi.org/10.1086/153889).
- [28] Volker Springel, Carlos S. Frenk, and Simon D. M. White. “**The large-scale structure of the Universe**”. In: *Nature* 440 (2006), p. 1137. DOI: [10.1038/nature04805](https://doi.org/10.1038/nature04805). arXiv: [astro-ph/0604561](https://arxiv.org/abs/astro-ph/0604561).
- [29] N. Aghanim et al. “**Planck 2018 results. VI. Cosmological parameters**”. In: *Astron. Astrophys.* 641 (2020). [Erratum: *Astron. Astrophys.* 652, C4 (2021)], A6. DOI: [10.1051/0004-6361/201833910](https://doi.org/10.1051/0004-6361/201833910). arXiv: [1807.06209](https://arxiv.org/abs/1807.06209) [astro-ph.CO].

- [30] Andrei Smilga. *Digestible Quantum Field Theory*. Springer, 2017. ISBN: 978-3-319-59920-5. DOI: [10.1007/978-3-319-59922-9](https://doi.org/10.1007/978-3-319-59922-9).
- [31] Gilly Elor et al. “**New Ideas in Baryogenesis: A Snowmass White Paper**”. In: *2022 Snowmass Summer Study*. Mar. 2022. arXiv: [2203.05010](https://arxiv.org/abs/2203.05010) [hep-ph].
- [32] Y. Fukuda et al. “**Evidence for oscillation of atmospheric neutrinos**”. In: *Phys. Rev. Lett.* 81 (1998), pp. 1562–1567. DOI: [10.1103/PhysRevLett.81.1562](https://doi.org/10.1103/PhysRevLett.81.1562). arXiv: [hep-ex/9807003](https://arxiv.org/abs/hep-ex/9807003).
- [33] Fumihiko Suekane. *Neutrino Oscillations: A Practical Guide to Basics and Applications*. Vol. 898. 2015. ISBN: 978-4-431-55461-5. DOI: [10.1007/978-4-431-55462-2](https://doi.org/10.1007/978-4-431-55462-2).
- [34] Paul A. M. Dirac. “**The quantum theory of the electron**”. In: *Proc. Roy. Soc. Lond. A* 117 (1928), pp. 610–624. DOI: [10.1098/rspa.1928.0023](https://doi.org/10.1098/rspa.1928.0023).
- [35] Julian S. Schwinger. “**On Quantum electrodynamics and the magnetic moment of the electron**”. In: *Phys. Rev.* 73 (1948), pp. 416–417. DOI: [10.1103/PhysRev.73.416](https://doi.org/10.1103/PhysRev.73.416).
- [36] B. Abi et al. “**Measurement of the Positive Muon Anomalous Magnetic Moment to 0.46 ppm**”. In: *Phys. Rev. Lett.* 126.14 (2021), p. 141801. DOI: [10.1103/PhysRevLett.126.141801](https://doi.org/10.1103/PhysRevLett.126.141801). arXiv: [2104.03281](https://arxiv.org/abs/2104.03281) [hep-ex].
- [37] G. W. Bennett et al. “**Final Report of the Muon E821 Anomalous Magnetic Moment Measurement at BNL**”. In: *Phys. Rev. D* 73 (2006), p. 072003. DOI: [10.1103/PhysRevD.73.072003](https://doi.org/10.1103/PhysRevD.73.072003). arXiv: [hep-ex/0602035](https://arxiv.org/abs/hep-ex/0602035).
- [38] J. P. Lees et al. “**Evidence for an excess of $\bar{B} \rightarrow D^{(*)}\tau^{-}\bar{\nu}_{\tau}$ decays**”. In: *Phys. Rev. Lett.* 109 (2012), p. 101802. DOI: [10.1103/PhysRevLett.109.101802](https://doi.org/10.1103/PhysRevLett.109.101802). arXiv: [1205.5442](https://arxiv.org/abs/1205.5442) [hep-ex].
- [39] Roel Aaij et al. “**Test of lepton universality in beauty-quark decays**”. In: *Nature Phys.* 18.3 (2022), pp. 277–282. DOI: [10.1038/s41567-021-01478-8](https://doi.org/10.1038/s41567-021-01478-8). arXiv: [2103.11769](https://arxiv.org/abs/2103.11769) [hep-ex].
- [40] Bernat Capdevila et al. “**Patterns of New Physics in $b \rightarrow s\ell^{+}\ell^{-}$ transitions in the light of recent data**”. In: *JHEP* 01 (2018), p. 093. DOI: [10.1007/JHEP01\(2018\)093](https://doi.org/10.1007/JHEP01(2018)093). arXiv: [1704.05340](https://arxiv.org/abs/1704.05340) [hep-ph].
- [41] T. Aaltonen et al. “**High-precision measurement of the W boson mass with the CDF II detector**”. In: *Science* 376.6589 (2022), pp. 170–176. DOI: [10.1126/science.abk1781](https://doi.org/10.1126/science.abk1781).
- [42] S. W. Hawking. “**Particle Creation by Black Holes**”. In: *Commun. Math. Phys.* 43 (1975). Ed. by G. W. Gibbons and S. W. Hawking. [Erratum: *Commun.Math.Phys.* 46, 206 (1976)], pp. 199–220. DOI: [10.1007/BF02345020](https://doi.org/10.1007/BF02345020).
- [43] S. W. Hawking. “**Breakdown of Predictability in Gravitational Collapse**”. In: *Phys. Rev. D* 14 (1976), pp. 2460–2473. DOI: [10.1103/PhysRevD.14.2460](https://doi.org/10.1103/PhysRevD.14.2460).
- [44] B. Greene. *The Elegant Universe: Superstrings, Hidden Dimensions, and the Quest for the Ultimate Theory*. Vintage Series. Vintage Books, 2000. ISBN: 9780375708114. URL: <https://books.google.fr/books?id=8QYs7n3klvYC>.
- [45] Stephen P. Martin. “**A Supersymmetry primer**”. In: *Adv. Ser. Direct. High Energy Phys.* 18 (1998). Ed. by Gordon L. Kane, pp. 1–98. DOI: [10.1142/9789812839657_0001](https://doi.org/10.1142/9789812839657_0001). arXiv: [hep-ph/9709356](https://arxiv.org/abs/hep-ph/9709356).

- [46] M. A. Boussejra, F. Mahmoudi, and G. Uhlich. “**Flavor anomalies in supersymmetric scenarios with nonminimal flavor violation**”. In: *Phys. Rev. D* 106.1 (2022), p. 015018. DOI: [10.1103/PhysRevD.106.015018](https://doi.org/10.1103/PhysRevD.106.015018). arXiv: [2201.04659](https://arxiv.org/abs/2201.04659) [[hep-ph](#)].
- [47] D. R. Tovey. “**Searches for supersymmetry at the LHC**”. In: *4th International Workshop on the Identification of Dark Matter*. Sept. 2002, pp. 138–143.
- [48] V. Barger et al. “**Report of the SUGRA Working Group for run II of the Tevatron**”. In: (Mar. 2000). arXiv: [hep-ph/0003154](https://arxiv.org/abs/hep-ph/0003154).
- [49] Deborah Pinna. “**Searches for dark matter at ATLAS and CMS**”. In: *54th Rencontres de Moriond on QCD and High Energy Interactions*. ARISF, 2019, pp. 141–144.
- [50] Marc Schumann. “**Direct Detection of WIMP Dark Matter: Concepts and Status**”. In: *J. Phys. G* 46.10 (2019), p. 103003. DOI: [10.1088/1361-6471/ab2ea5](https://doi.org/10.1088/1361-6471/ab2ea5). arXiv: [1903.03026](https://arxiv.org/abs/1903.03026) [[astro-ph.CO](#)].
- [51] M. A. Acero et al. “**White Paper on Light Sterile Neutrino Searches and Related Phenomenology**”. In: (Mar. 2022). arXiv: [2203.07323](https://arxiv.org/abs/2203.07323) [[hep-ex](#)].
- [52] M. Zito. *Dans le tourbillon des particules*. Belin, 2015. ISBN: 978-2-7011-9277-2.
- [53] Hideki Yukawa. “**On the Interaction of Elementary Particles**”. In: *Proc. Phys. Math. Soc. Jap.* 17 (1935), pp. 48–57. DOI: [10.1143/PTPS.1.1](https://doi.org/10.1143/PTPS.1.1).
- [54] A. Pais. “**On the Baryon-meson-photon System***”. In: *Progress of Theoretical Physics* 10.4 (Oct. 1953), pp. 457–469. DOI: [10.1143/PTP.10.457](https://doi.org/10.1143/PTP.10.457). URL: <https://doi.org/10.1143/PTP.10.457>.
- [55] A. Pais. “**Some Remarks on the V-Particles**”. In: *Phys. Rev.* 86 (5 June 1952), pp. 663–672. DOI: [10.1103/PhysRev.86.663](https://doi.org/10.1103/PhysRev.86.663).
- [56] M. Gell-Mann. “**Isotopic Spin and New Unstable Particles**”. In: *Phys. Rev.* 92 (1953), pp. 833–834. DOI: [10.1103/PhysRev.92.833](https://doi.org/10.1103/PhysRev.92.833).
- [57] T. Nakano and K. Nishijima. “**Charge Independence for V-particles**”. In: *Prog. Theor. Phys.* 10 (1953), pp. 581–582. DOI: [10.1143/PTP.10.581](https://doi.org/10.1143/PTP.10.581).
- [58] Murray Gell-Mann. “**The Eightfold Way: A Theory of strong interaction symmetry**”. In: (Mar. 1961). DOI: [10.2172/4008239](https://doi.org/10.2172/4008239).
- [59] Yuval Ne’eman. “**Derivation of strong interactions from a gauge invariance**”. In: *Nucl. Phys.* 26 (1961), pp. 222–229. DOI: [10.1016/0029-5582\(61\)90134-1](https://doi.org/10.1016/0029-5582(61)90134-1).
- [60] A. Pevsner et al. “**Evidence for a Three Pion Resonance Near 550 MeV**”. In: *Phys. Rev. Lett.* 7 (1961), pp. 421–423. DOI: [10.1103/PhysRevLett.7.421](https://doi.org/10.1103/PhysRevLett.7.421).
- [61] Murray Gell-Mann. “**A Schematic Model of Baryons and Mesons**”. In: *Phys. Lett.* 8 (1964), pp. 214–215. DOI: [10.1016/S0031-9163\(64\)92001-3](https://doi.org/10.1016/S0031-9163(64)92001-3).
- [62] G Zweig. “**An SU₃ model for strong interaction symmetry and its breaking**”. In: CERN-TH-412 (Feb. 1964), 80 p. URL: [%5Curl%7Bhttp://cds.cern.ch/record/570209%7D](https://cds.cern.ch/record/570209?d=record).
- [63] O. W. Greenberg. “**Spin and Unitary Spin Independence in a Paraquark Model of Baryons and Mesons**”. In: *Phys. Rev. Lett.* 13 (1964), pp. 598–602. DOI: [10.1103/PhysRevLett.13.598](https://doi.org/10.1103/PhysRevLett.13.598).
- [64] M. Y. Han and Yoichiro Nambu. “**Three Triplet Model with Double SU(3) Symmetry**”. In: *Phys. Rev.* 139 (1965). Ed. by T. Eguchi, B1006–B1010. DOI: [10.1103/PhysRev.139.B1006](https://doi.org/10.1103/PhysRev.139.B1006).

- [65] E. A. Paschos J. D. Björken. “**Inelastic Electron-Proton and γ -Proton Scattering and the Structure of the Nucleon**”. In: *Physical Review* 185 (Apr. 1969).
- [66] Richard P. Feynman. “**The behavior of hadron collisions at extreme energies**”. In: *Third Conference on High-Energy Collisions*. Sept. 1969.
- [67] Francis Halzen. Alan D. Martin. “**Quarks & Leptons : An Introductory Course in Modern Particle Physics**”. In: John Wiley & Sons, Inc., 1984. Chap. 1, 8, 9.
- [68] R. P. Feynman. *Photon-hadron interactions*. 1973. ISBN: 9780429493331.
- [69] David J. Gross and Frank Wilczek. “**Ultraviolet Behavior of Non-Abelian Gauge Theories**”. In: *Phys. Rev. Lett.* 30 (26 June 1973), pp. 1343–1346. DOI: [10.1103/PhysRevLett.30.1343](https://doi.org/10.1103/PhysRevLett.30.1343). URL: [%5Curl%7Bhttps://link.aps.org/doi/10.1103/PhysRevLett.30.1343%7D](https://link.aps.org/doi/10.1103/PhysRevLett.30.1343).
- [70] H. David Politzer. “**Reliable Perturbative Results for Strong Interactions ?**” In: *Phys. Rev. Lett.* 30 (26 June 1973), pp. 1346–1349. DOI: [10.1103/PhysRevLett.30.1346](https://doi.org/10.1103/PhysRevLett.30.1346). URL: [%5Curl%7Bhttps://link.aps.org/doi/10.1103/PhysRevLett.30.1346%7D](https://link.aps.org/doi/10.1103/PhysRevLett.30.1346).
- [71] H. Fritzsch, Murray Gell-Mann, and H. Leutwyler. “**Advantages of the Color Octet Gluon Picture**”. In: *Phys. Lett.* 47B (1973), pp. 365–368. DOI: [10.1016/0370-2693\(73\)90625-4](https://doi.org/10.1016/0370-2693(73)90625-4).
- [72] G. Hanson et al. “**Evidence for Jet Structure in Hadron Production by $e^+ e^-$ Annihilation**”. In: *Phys. Rev. Lett.* 35 (1975). Ed. by Martha C. Zipf, pp. 1609–1612. DOI: [10.1103/PhysRevLett.35.1609](https://doi.org/10.1103/PhysRevLett.35.1609).
- [73] R. Schwitters et al. “**Azimuthal Asymmetry in Inclusive Hadron Production by $e^+ e^-$ Annihilation**”. In: *Phys. Rev. Lett.* 35 (1975), p. 1320. DOI: [10.1103/PhysRevLett.35.1320](https://doi.org/10.1103/PhysRevLett.35.1320).
- [74] J. D. Bjorken and Stanley J. Brodsky. “**Statistical Model for electron-Positron Annihilation Into Hadrons**”. In: *Phys. Rev. D* 1 (1970), pp. 1416–1420. DOI: [10.1103/PhysRevD.1.1416](https://doi.org/10.1103/PhysRevD.1.1416).
- [75] S. D. Drell, Donald J. Levy, and Tung-Mow Yan. “**A Theory of Deep Inelastic Lepton-Nucleon Scattering and Lepton Pair Annihilation Processes. 3. Deep Inelastic electron-Positron Annihilation**”. In: *Phys. Rev. D* 1 (1970), pp. 1617–1639. DOI: [10.1103/PhysRevD.1.1617](https://doi.org/10.1103/PhysRevD.1.1617).
- [76] Christoph Berger et al. “**Experimental search for Υ decay into 3 gluons**”. In: *1979 EPS High-Energy Physics Conference*. Vol. 1. Geneva, Switzerland: CERN, 1979, pp. 338–342. DOI: [10.3204/PUBDB-2017-12813](https://doi.org/10.3204/PUBDB-2017-12813).
- [77] Kenneth G. Wilson. “**Confinement of Quarks**”. In: *Phys. Rev. D* 10 (1974). Ed. by J. C. Taylor, pp. 2445–2459. DOI: [10.1103/PhysRevD.10.2445](https://doi.org/10.1103/PhysRevD.10.2445).
- [78] S. Durr et al. “**Ab-Initio Determination of Light Hadron Masses**”. In: *Science* 322 (2008), pp. 1224–1227. DOI: [10.1126/science.1163233](https://doi.org/10.1126/science.1163233). arXiv: [0906.3599 \[hep-lat\]](https://arxiv.org/abs/0906.3599).
- [79] S. Durr et al. “**Lattice QCD at the physical point: light quark masses**”. In: *Phys. Lett. B* 701 (2011), pp. 265–268. DOI: [10.1016/j.physletb.2011.05.053](https://doi.org/10.1016/j.physletb.2011.05.053). arXiv: [1011.2403 \[hep-lat\]](https://arxiv.org/abs/1011.2403).
- [80] T. Blum et al. “**Domain wall QCD with physical quark masses**”. In: *Phys. Rev. D* 93.7 (2016), p. 074505. DOI: [10.1103/PhysRevD.93.074505](https://doi.org/10.1103/PhysRevD.93.074505). arXiv: [1411.7017 \[hep-lat\]](https://arxiv.org/abs/1411.7017).

- [81] G. Aarts et al. “**Heavy-flavor production and medium properties in high-energy nuclear collisions - What next?**” In: *Eur. Phys. J. A* 53.5 (2017), p. 93. DOI: [10.1140/epja/i2017-12282-9](https://doi.org/10.1140/epja/i2017-12282-9). arXiv: [1612.08032](https://arxiv.org/abs/1612.08032) [[nucl-th](#)].
- [82] John C. Collins and M. J. Perry. “**Superdense Matter: Neutrons Or Asymptotically Free Quarks?**” In: *Phys. Rev. Lett.* 34 (1975), p. 1353. DOI: [10.1103/PhysRevLett.34.1353](https://doi.org/10.1103/PhysRevLett.34.1353).
- [83] Andrei D. Linde. “**Phase Transitions in Gauge Theories and Cosmology**”. In: *Rept. Prog. Phys.* 42 (1979), p. 389. DOI: [10.1088/0034-4885/42/3/001](https://doi.org/10.1088/0034-4885/42/3/001).
- [84] Ulrich W. Heinz. “**Towards the Little Bang Standard Model**”. In: *J. Phys. Conf. Ser.* 455 (2013). Ed. by Jean Cleymans, p. 012044. DOI: [10.1088/1742-6596/455/1/012044](https://doi.org/10.1088/1742-6596/455/1/012044). arXiv: [1304.3634](https://arxiv.org/abs/1304.3634) [[nucl-th](#)].
- [85] Alessandro Lovato et al. “**Long Range Plan: Dense matter theory for heavy-ion collisions and neutron stars**”. In: (Nov. 2022). arXiv: [2211.02224](https://arxiv.org/abs/2211.02224) [[nucl-th](#)].
- [86] R. Hagedorn. “**Statistical thermodynamics of strong interactions at high-energies**”. In: *Nuovo Cim. Suppl.* 3 (1965), pp. 147–186.
- [87] Rolf Hagedorn. “**Multiplicities, p_T Distributions and the Expected Hadron \rightarrow Quark - Gluon Phase Transition**”. In: *Riv. Nuovo Cim.* 6N10 (1983), pp. 1–50. DOI: [10.1007/BF02740917](https://doi.org/10.1007/BF02740917).
- [88] Johann Rafelski and Torleif Ericson. In: *Melting Hadrons, Boiling Quarks - From Hagedorn Temperature to Ultra-Relativistic Heavy-Ion Collisions at CERN*. Ed. by Johann Rafelski. Springer, 2016. Chap. 6. ISBN: 978-3-319-17545-4. DOI: [10.1007/978-3-319-17545-4](https://doi.org/10.1007/978-3-319-17545-4).
- [89] I. Ya. Pomeranchuk. “**On the theory of multiple particle production in a single collision**”. In: *Dokl. Akad. Nauk SSSR* 78.5 (1951), pp. 889–891. DOI: [10.1142/9789812815941_0009](https://doi.org/10.1142/9789812815941_0009).
- [90] Krzysztof Redlich and Helmut Satz. In: *Melting Hadrons, Boiling Quarks - From Hagedorn Temperature to Ultra-Relativistic Heavy-Ion Collisions at CERN*. Ed. by Johann Rafelski. Springer, 2016. Chap. 7. ISBN: 978-3-319-17545-4. DOI: [10.1007/978-3-319-17545-4](https://doi.org/10.1007/978-3-319-17545-4).
- [91] T. D. Lee and G. C. Wick. “**Vacuum Stability and Vacuum Excitation in a Spin 0 Field Theory**”. In: *Phys. Rev. D* 9 (1974), pp. 2291–2316. DOI: [10.1103/PhysRevD.9.2291](https://doi.org/10.1103/PhysRevD.9.2291).
- [92] H. Stöcker et al. “**Shock waves in nuclear matter - proof by circumstantial evidence**”. In: *Progress in Particle and Nuclear Physics* 4 (1980), pp. 133–195. ISSN: 0146-6410. DOI: [https://doi.org/10.1016/0146-6410\(80\)90006-X](https://doi.org/10.1016/0146-6410(80)90006-X). URL: <https://www.sciencedirect.com/science/article/pii/014664108090006X>.
- [93] G. F. Chapline and A. K. Kerman. *On the Possibility of Making Quark Matter in Nuclear Collisions*. Report MIT-CTP-695 (1978).
- [94] E J Lofgren. “**Accelerator Division - Annual Reports: 1 Jul. 1972 - 31 Dec. 1974**”. In: (Oct. 1975). DOI: [10.2172/937059](https://doi.org/10.2172/937059). URL: <https://www.osti.gov/biblio/937059>.
- [95] Kjell Johnsen. “**CERN Intersecting Storage Rings (ISR)**”. In: *Proc. Nat. Acad. Sci.* 70 (1973), pp. 619–626. DOI: [10.1073/pnas.70.2.619](https://doi.org/10.1073/pnas.70.2.619).
- [96] R. Hagedorn and Johann Rafelski. “**From Hadron Gas to Quark Matter**”. In: *International Conference on Nuclear Physics*. Sept. 1980, pp. 237–251.
- [97] A. Chodos et al. “**A New Extended Model of Hadrons**”. In: *Phys. Rev. D* 9 (1974), pp. 3471–3495. DOI: [10.1103/PhysRevD.9.3471](https://doi.org/10.1103/PhysRevD.9.3471).

- [98] N. Cabibbo and G. Parisi. “**Exponential Hadronic Spectrum and Quark Liberation**”. In: *Phys. Lett. B* 59 (1975), pp. 67–69. DOI: [10.1016/0370-2693\(75\)90158-6](https://doi.org/10.1016/0370-2693(75)90158-6).
- [99] J. D. Bjorken. “**Highly Relativistic Nucleus-Nucleus Collisions: The Central Rapidity Region**”. In: *Phys. Rev. D* 27 (1983), pp. 140–151. DOI: [10.1103/PhysRevD.27.140](https://doi.org/10.1103/PhysRevD.27.140).
- [100] Johann Rafelski. “**Melting Hadrons, Boiling Quarks**”. In: *Eur. Phys. J. A* 51.9 (2015), p. 114. DOI: [10.1140/epja/i2015-15114-0](https://doi.org/10.1140/epja/i2015-15114-0). arXiv: [1508.03260](https://arxiv.org/abs/1508.03260) [nucl-th].
- [101] Grazyna Odyniec. In: *Melting Hadrons, Boiling Quarks - From Hagedorn Temperature to Ultra-Relativistic Heavy-Ion Collisions at CERN*. Ed. by Johann Rafelski. Springer, 2016. Chap. 12. ISBN: 978-3-319-17545-4. DOI: [10.1007/978-3-319-17545-4](https://doi.org/10.1007/978-3-319-17545-4).
- [102] Willem Cornelis Middelkoop. “**Remarks on the possible use of the SPS for ^{16}O ion beams**”. In: (1982). URL: <https://cds.cern.ch/record/601487>.
- [103] M. G. Albrow. “**Experiments with nuclear beams and targets**”. In: *CERN Yellow Rep. Conf. Proc.* 2 (1983), pp. 462–476. DOI: [10.5170/CERN-1983-002-V-2.462](https://doi.org/10.5170/CERN-1983-002-V-2.462).
- [104] T. Ludlam. “**RHIC And Quark Matter: A Proposed Heavy Ion Collider At Brookhaven National Laboratory**”. In: (June 1984). DOI: [10.2172/1118855](https://doi.org/10.2172/1118855). URL: <https://www.osti.gov/biblio/1118855>.
- [105] Ulrich W. Heinz and Maurice Jacob. “**Evidence for a new state of matter: An Assessment of the results from the CERN lead beam program**”. In: (Jan. 2000). arXiv: [nuc1-th/0002042](https://arxiv.org/abs/nuc1-th/0002042).
- [106] B. B. Back et al. “**The PHOBOS perspective on discoveries at RHIC**”. In: *Nucl. Phys. A* 757 (2005), pp. 28–101. DOI: [10.1016/j.nuclphysa.2005.03.084](https://doi.org/10.1016/j.nuclphysa.2005.03.084). arXiv: [nuc1-ex/0410022](https://arxiv.org/abs/nuc1-ex/0410022).
- [107] I. Arsene et al. “**Quark gluon plasma and color glass condensate at RHIC? The Perspective from the BRAHMS experiment**”. In: *Nucl. Phys. A* 757 (2005), pp. 1–27. DOI: [10.1016/j.nuclphysa.2005.02.130](https://doi.org/10.1016/j.nuclphysa.2005.02.130). arXiv: [nuc1-ex/0410020](https://arxiv.org/abs/nuc1-ex/0410020).
- [108] K. Adcox et al. “**Formation of dense partonic matter in relativistic nucleus-nucleus collisions at RHIC: Experimental evaluation by the PHENIX collaboration**”. In: *Nucl. Phys. A* 757 (2005), pp. 184–283. DOI: [10.1016/j.nuclphysa.2005.03.086](https://doi.org/10.1016/j.nuclphysa.2005.03.086). arXiv: [nuc1-ex/0410003](https://arxiv.org/abs/nuc1-ex/0410003).
- [109] John Adams et al. “**Experimental and theoretical challenges in the search for the quark gluon plasma: The STAR Collaboration’s critical assessment of the evidence from RHIC collisions**”. In: *Nucl. Phys. A* 757 (2005), pp. 102–183. DOI: [10.1016/j.nuclphysa.2005.03.085](https://doi.org/10.1016/j.nuclphysa.2005.03.085). arXiv: [nuc1-ex/0501009](https://arxiv.org/abs/nuc1-ex/0501009).
- [110] *‘Perfect’ Liquid Hot Enough to be Quark Soup (Protons, neutrons melt to produce ‘quark-gluon plasma’ at RHIC)*. RHIC press release. Feb. 2010.
- [111] R.K. Pathria and P.D. Beale. *Statistical Mechanics*. Elsevier Science, 2011. ISBN: 9780123821898. URL: [%5Curl%7Bhttps://books.google.fr/books?id=KdbJJAXQ-RsC%7D](https://books.google.fr/books?id=KdbJJAXQ-RsC%7D).
- [112] M. Asakawa and K. Yazaki. “**Chiral Restoration at Finite Density and Temperature**”. In: *Nucl. Phys. A* 504 (1989), pp. 668–684. DOI: [10.1016/0375-9474\(89\)90002-X](https://doi.org/10.1016/0375-9474(89)90002-X).

- [113] A. Barducci et al. “**Chiral Symmetry Breaking in QCD at Finite Temperature and Density**”. In: *Phys. Lett. B* 231 (1989), pp. 463–470. DOI: [10.1016/0370-2693\(89\)90695-3](https://doi.org/10.1016/0370-2693(89)90695-3).
- [114] Frank R. Brown et al. “**On the existence of a phase transition for QCD with three light quarks**”. In: *Phys. Rev. Lett.* 65 (1990), pp. 2491–2494. DOI: [10.1103/PhysRevLett.65.2491](https://doi.org/10.1103/PhysRevLett.65.2491).
- [115] T. Niida and Y. Miake. “**Signatures of QGP at RHIC and the LHC**”. In: *AAPPS Bull.* 31.1 (2021), p. 12. DOI: [10.1007/s43673-021-00014-3](https://doi.org/10.1007/s43673-021-00014-3). arXiv: [2104.11406](https://arxiv.org/abs/2104.11406) [nucl-ex].
- [116] Szabolcs Borsanyi et al. “**QCD Crossover at Finite Chemical Potential from Lattice Simulations**”. In: *Phys. Rev. Lett.* 125.5 (2020), p. 052001. DOI: [10.1103/PhysRevLett.125.052001](https://doi.org/10.1103/PhysRevLett.125.052001). arXiv: [2002.02821](https://arxiv.org/abs/2002.02821) [hep-lat].
- [117] Mikhail Stephanov. “**QCD phase diagram: an overview**”. In: *Proceedings of XXIVth International Symposium on Lattice Field Theory — PoS(LAT2006)*. Vol. 032. 2006, p. 024. DOI: [10.22323/1.032.0024](https://doi.org/10.22323/1.032.0024).
- [118] Christian S. Fischer, Jan Luecker, and Christian A. Welzbacher. “**Phase structure of three and four flavor QCD**”. In: *Phys. Rev. D* 90.3 (2014), p. 034022. DOI: [10.1103/PhysRevD.90.034022](https://doi.org/10.1103/PhysRevD.90.034022). arXiv: [1405.4762](https://arxiv.org/abs/1405.4762) [hep-ph].
- [119] David Fuseau, Thorsten Steinert, and Joerg Aichelin. “**Phase diagram of the Polyakov–Nambu–Jona-Lasinio approach for finite chemical potentials**”. In: *Phys. Rev. C* 101.6 (2020), p. 065203. DOI: [10.1103/PhysRevC.101.065203](https://doi.org/10.1103/PhysRevC.101.065203). arXiv: [1908.08122](https://arxiv.org/abs/1908.08122) [hep-ph].
- [120] Wei-jie Fu, Jan M. Pawłowski, and Fabian Rennecke. “**QCD phase structure at finite temperature and density**”. In: *Phys. Rev. D* 101.5 (2020), p. 054032. DOI: [10.1103/PhysRevD.101.054032](https://doi.org/10.1103/PhysRevD.101.054032). arXiv: [1909.02991](https://arxiv.org/abs/1909.02991) [hep-ph].
- [121] Matthias Troyer and Uwe-Jens Wiese. “**Computational complexity and fundamental limitations to fermionic quantum Monte Carlo simulations**”. In: *Phys. Rev. Lett.* 94 (2005), p. 170201. DOI: [10.1103/PhysRevLett.94.170201](https://doi.org/10.1103/PhysRevLett.94.170201). arXiv: [cond-mat/0408370](https://arxiv.org/abs/cond-mat/0408370).
- [122] R. Bellwied et al. “**The QCD phase diagram from analytic continuation**”. In: *Phys. Lett. B* 751 (2015), pp. 559–564. DOI: [10.1016/j.physletb.2015.11.011](https://doi.org/10.1016/j.physletb.2015.11.011). arXiv: [1507.07510](https://arxiv.org/abs/1507.07510) [hep-lat].
- [123] A. Bazavov et al. “**Chiral crossover in QCD at zero and non-zero chemical potentials**”. In: *Phys. Lett. B* 795 (2019), pp. 15–21. DOI: [10.1016/j.physletb.2019.05.013](https://doi.org/10.1016/j.physletb.2019.05.013). arXiv: [1812.08235](https://arxiv.org/abs/1812.08235) [hep-lat].
- [124] J. M. Lattimer and M. Prakash. “**The physics of neutron stars**”. In: *Science* 304 (2004), pp. 536–542. DOI: [10.1126/science.1090720](https://doi.org/10.1126/science.1090720). arXiv: [astro-ph/0405262](https://arxiv.org/abs/astro-ph/0405262).
- [125] Mark G. Alford et al. “**Color superconductivity in dense quark matter**”. In: *Rev. Mod. Phys.* 80 (2008), pp. 1455–1515. DOI: [10.1103/RevModPhys.80.1455](https://doi.org/10.1103/RevModPhys.80.1455).
- [126] R. Rapp et al. “**Diquark Bose condensates in high density matter and instantons**”. In: *Phys. Rev. Lett.* 81 (1998), pp. 53–56. DOI: [10.1103/PhysRevLett.81.53](https://doi.org/10.1103/PhysRevLett.81.53). arXiv: [hep-ph/9711396](https://arxiv.org/abs/hep-ph/9711396).
- [127] B. P. Abbott et al. “**GW170817: Observation of Gravitational Waves from a Binary Neutron Star Inspiral**”. In: *Phys. Rev. Lett.* 119.16 (2017), p. 161101. DOI: [10.1103/PhysRevLett.119.161101](https://doi.org/10.1103/PhysRevLett.119.161101). arXiv: [1710.05832](https://arxiv.org/abs/1710.05832) [gr-qc].

- [128] Andreas Bauswein et al. “**Identifying a first-order phase transition in neutron star mergers through gravitational waves**”. In: *Phys. Rev. Lett.* 122.6 (2019), p. 061102. DOI: [10.1103/PhysRevLett.122.061102](https://doi.org/10.1103/PhysRevLett.122.061102). arXiv: [1809.01116](https://arxiv.org/abs/1809.01116) [astro-ph.HE].
- [129] Eemeli Annala et al. “**Evidence for quark-matter cores in massive neutron stars**”. In: *Nature Phys.* 16.9 (2020), pp. 907–910. DOI: [10.1038/s41567-020-0914-9](https://doi.org/10.1038/s41567-020-0914-9). arXiv: [1903.09121](https://arxiv.org/abs/1903.09121) [astro-ph.HE].
- [130] Tyler Gorda, Oleg Komoltsev, and Aleksi Kurkela. “**Ab-initio QCD calculations impact the inference of the neutron-star-matter equation of state**”. In: (Apr. 2022). arXiv: [2204.11877](https://arxiv.org/abs/2204.11877) [nucl-th].
- [131] Emanuel V. Chibanski et al. “**Bayesian Inference of Phenomenological EoS of Neutron Stars with Recent Observations**”. In: (May 2022). arXiv: [2205.01174](https://arxiv.org/abs/2205.01174) [nucl-th].
- [132] Oleksii Ivanytskyi and David Blaschke. “**A new class of hybrid EoS with multiple critical endpoints for simulations of supernovae, neutron stars and their mergers**”. In: (May 2022). arXiv: [2205.03455](https://arxiv.org/abs/2205.03455) [nucl-th].
- [133] Elias R. Most et al. “**Probing neutron-star matter in the lab: connecting binary mergers to heavy-ion collisions**”. In: (Jan. 2022). arXiv: [2201.13150](https://arxiv.org/abs/2201.13150) [nucl-th].
- [134] S. Mandelstam. “**Determination of the Pion-Nucleon Scattering Amplitude from Dispersion Relations and Unitarity. General Theory**”. In: *Phys. Rev.* 112 (4 Nov. 1958), pp. 1344–1360. DOI: [10.1103/PhysRev.112.1344](https://doi.org/10.1103/PhysRev.112.1344). URL: <https://link.aps.org/doi/10.1103/PhysRev.112.1344>.
- [135] Wit Busza. “**Review of Experimental Data on Hadron-Nucleus Collisions at High-Energies**”. In: *Acta Phys. Polon. B* 8 (1977), p. 333.
- [136] B. I. Abelev et al. “**Systematic Measurements of Identified Particle Spectra in pp, d^+ Au and Au+Au Collisions from STAR**”. In: *Phys. Rev. C* 79 (2009), p. 034909. DOI: [10.1103/PhysRevC.79.034909](https://doi.org/10.1103/PhysRevC.79.034909). arXiv: [0808.2041](https://arxiv.org/abs/0808.2041) [nucl-ex].
- [137] E. Abbas et al. “**Performance of the ALICE VZERO system**”. In: *JINST* 8 (2013), P10016. DOI: [10.1088/1748-0221/8/10/P10016](https://doi.org/10.1088/1748-0221/8/10/P10016). arXiv: [1306.3130](https://arxiv.org/abs/1306.3130) [nucl-ex].
- [138] Michael L. Miller et al. “**Glauber Modeling in High-Energy Nuclear Collisions**”. In: *Annual Review of Nuclear and Particle Science* 57.1 (Nov. 2007), pp. 205–243. DOI: [10.1146/annurev.nucl.57.090506.123020](https://doi.org/10.1146/annurev.nucl.57.090506.123020). URL: <https://doi.org/10.1146/annurev.nucl.57.090506.123020>.
- [139] R. J. Glauber. “**Cross Sections in Deuterium at High Energies**”. In: *Phys. Rev.* 100 (1 Oct. 1955), pp. 242–248. DOI: [10.1103/PhysRev.100.242](https://doi.org/10.1103/PhysRev.100.242). URL: <https://link.aps.org/doi/10.1103/PhysRev.100.242>.
- [140] M. Harrison, T. Ludlam, and S. Ozaki. “**RHIC project overview**”. In: *Nucl. Instrum. Meth. A* 499 (2003), pp. 235–244. DOI: [10.1016/S0168-9002\(02\)01937-X](https://doi.org/10.1016/S0168-9002(02)01937-X).
- [141] Clemens Adler et al. “**The RHIC zero degree calorimeter**”. In: *Nucl. Instrum. Meth. A* 470 (2001), pp. 488–499. DOI: [10.1016/S0168-9002\(01\)00627-1](https://doi.org/10.1016/S0168-9002(01)00627-1). arXiv: [nuc1-ex/0008005](https://arxiv.org/abs/nuc1-ex/0008005).
- [142] M Adamczyk et al. “**The BRAHMS experiment at RHIC**”. In: *Nucl. Instrum. Meth. A* 499 (2003), pp. 437–468. DOI: [10.1016/S0168-9002\(02\)01949-6](https://doi.org/10.1016/S0168-9002(02)01949-6).

- [143] B. B Back et al. “**The PHOBOS detector at RHIC**”. In: *Nucl. Instrum. Meth. A* 499 (2003), pp. 603–623. DOI: [10.1016/S0168-9002\(02\)01959-9](https://doi.org/10.1016/S0168-9002(02)01959-9).
- [144] Shoji Nagamiya et al. “**PHENIX Conceptual Design Report**”. In: (Jan. 1993). DOI: [10.2172/6370496](https://doi.org/10.2172/6370496). URL: <https://www.osti.gov/biblio/6370496>.
- [145] A. Adare et al. “**An Upgrade Proposal from the PHENIX Collaboration**”. In: (Jan. 2015). arXiv: [1501.06197](https://arxiv.org/abs/1501.06197) [nucl-ex].
- [146] K. H. Ackermann et al. “**STAR detector overview**”. In: *Nucl. Instrum. Meth. A* 499 (2003), pp. 624–632. DOI: [10.1016/S0168-9002\(02\)01960-5](https://doi.org/10.1016/S0168-9002(02)01960-5).
- [147] F. Pilat et al. “**Operations and Performance of RHIC as a Cu-Cu Collider**”. In: *Proceedings of the 2005 Particle Accelerator Conference*. 2005, pp. 4281–4283. DOI: [10.1109/PAC.2005.1591791](https://doi.org/10.1109/PAC.2005.1591791).
- [148] Yadav Pandit. “**Anisotropy results from 193 GeV U+U collisions at RHIC**”. In: *49th Rencontres de Moriond on QCD and High Energy Interactions*. 2014, pp. 345–348. arXiv: [1405.5510](https://arxiv.org/abs/1405.5510) [nucl-ex].
- [149] Wolfram Fischer. *Run Overview of the RHIC*. Consulted on 8th Aug., 2022. URL: https://www.agsrhichome.bnl.gov/RHIC/Runs/index.html#RHIC_Runs.
- [150] STAR collaboration. “**Studying the Phase Diagram of QCD Matter at RHIC**”. STAR Note **0598** (2014).
- [151] Adam Bzdak et al. “**Mapping the Phases of Quantum Chromodynamics with Beam Energy Scan**”. In: *Phys. Rept.* 853 (2020), pp. 1–87. DOI: [10.1016/j.physrep.2020.01.005](https://doi.org/10.1016/j.physrep.2020.01.005). arXiv: [1906.00936](https://arxiv.org/abs/1906.00936) [nucl-th].
- [152] Kathryn C. Meehan. “**Fixed Target Collisions at STAR**”. In: *Nucl. Phys. A* 956 (2016). Ed. by Y. Akiba et al., pp. 878–881. DOI: [10.1016/j.nuclphysa.2016.04.016](https://doi.org/10.1016/j.nuclphysa.2016.04.016).
- [153] N. Antoniou et al. “**Study of hadron production in hadron nucleus and nucleus nucleus collisions at the CERN SPS**”. In: (Nov. 2006).
- [154] C. Alt et al. “**Pion and kaon production in central Pb + Pb collisions at 20-A and 30-A-GeV: Evidence for the onset of deconfinement**”. In: *Phys. Rev. C* 77 (2008), p. 024903. DOI: [10.1103/PhysRevC.77.024903](https://doi.org/10.1103/PhysRevC.77.024903). arXiv: [0710.0118](https://arxiv.org/abs/0710.0118) [nucl-ex].
- [155] Marek Gazdzicki. “**Ion Program of NA61/Shine at the CERN SPS**”. In: *J. Phys. G* 36 (2009). Ed. by Feng Liu, Zhigang Xiao, and Pengfei Zhuang, p. 064039. DOI: [10.1088/0954-3899/36/6/064039](https://doi.org/10.1088/0954-3899/36/6/064039). arXiv: [0812.4415](https://arxiv.org/abs/0812.4415) [nucl-ex].
- [156] Wojciech Bryliński. “**News from the strong interactions program of NA61/SHINE**”. In: *EPJ Web Conf.* 258 (2022), p. 05007. DOI: [10.1051/epjconf/202225805007](https://doi.org/10.1051/epjconf/202225805007).
- [157] CERN News. *The third run of the Large Hadron Collider has successfully started*. 5 July 2022. URL: <https://home.cern/news/news/cern/third-run-large-hadron-collider-has-successfully-started>.
- [158] S. Acharya et al. “**Anisotropic flow in Xe-Xe collisions at $\sqrt{s_{NN}} = 5.44$ TeV**”. In: *Phys. Lett. B* 784 (2018), pp. 82–95. DOI: [10.1016/j.physletb.2018.06.059](https://doi.org/10.1016/j.physletb.2018.06.059). arXiv: [1805.01832](https://arxiv.org/abs/1805.01832) [nucl-ex].
- [159] Shreyasi Acharya et al. “**Centrality and pseudorapidity dependence of the charged-particle multiplicity density in Xe–Xe collisions at $\sqrt{s_{NN}} = 5.44$ TeV**”. In: *Phys. Lett. B* 790 (2019), pp. 35–48. DOI: [10.1016/j.physletb.2018.12.048](https://doi.org/10.1016/j.physletb.2018.12.048). arXiv: [1805.04432](https://arxiv.org/abs/1805.04432) [nucl-ex].

- [160] Jaroslav Adam et al. “**Centrality dependence of the charged-particle multiplicity density at midrapidity in Pb-Pb collisions at $\sqrt{s_{NN}} = 5.02$ TeV**”. In: *Phys. Rev. Lett.* 116.22 (2016), p. 222302. DOI: [10.1103/PhysRevLett.116.222302](https://doi.org/10.1103/PhysRevLett.116.222302). arXiv: [1512.06104](https://arxiv.org/abs/1512.06104) [nucl-ex].
- [161] Shreyasi Acharya et al. “**Production of charged pions, kaons, and (anti-)protons in Pb-Pb and inelastic pp collisions at $\sqrt{s_{NN}} = 5.02$ TeV**”. In: *Phys. Rev. C* 101.4 (2020), p. 044907. DOI: [10.1103/PhysRevC.101.044907](https://doi.org/10.1103/PhysRevC.101.044907). arXiv: [1910.07678](https://arxiv.org/abs/1910.07678) [nucl-ex].
- [162] Néstor Armesto. “**Small collision systems: Theory overview on cold nuclear matter effects**”. In: *EPJ Web Conf.* 171 (2018). Ed. by A. Mischke and P. Kuijser, p. 11001. DOI: [10.1051/epjconf/201817111001](https://doi.org/10.1051/epjconf/201817111001).
- [163] K. Aamodt et al. “**The ALICE experiment at the CERN LHC**”. In: *JINST* 3 (2008), S08002. DOI: [10.1088/1748-0221/3/08/S08002](https://doi.org/10.1088/1748-0221/3/08/S08002).
- [164] N. Grau. “**Heavy Ion Physics Prospects with the ATLAS Detector at the LHC**”. In: *J. Phys. G* 35 (2008). Ed. by Jan-e Alam et al., p. 104040. DOI: [10.1088/0954-3899/35/10/104040](https://doi.org/10.1088/0954-3899/35/10/104040). arXiv: [0805.4656](https://arxiv.org/abs/0805.4656) [nucl-ex].
- [165] G. L. Bayatian et al. “**CMS physics technical design report: Addendum on high density QCD with heavy ions**”. In: *J. Phys. G* 34 (2007). Ed. by David G. d’Enterria et al., pp. 2307–2455. DOI: [10.1088/0954-3899/34/11/008](https://doi.org/10.1088/0954-3899/34/11/008).
- [166] Albert Bursche et al. “**Physics opportunities with the fixed-target program of the LHCb experiment using an unpolarized gas target**”. In: (2018).
- [167] M. Durante et al. “**All the fun of the FAIR: fundamental physics at the facility for antiproton and ion research**”. In: *Phys. Scripta* 94.3 (2019), p. 033001. DOI: [10.1088/1402-4896/aaf93f](https://doi.org/10.1088/1402-4896/aaf93f). arXiv: [1903.05693](https://arxiv.org/abs/1903.05693) [nucl-th].
- [168] Kshitij Agarwal. “**Status of the Compressed Baryonic Matter (CBM) Experiment at FAIR**”. In: (July 2022). arXiv: [2207.14585](https://arxiv.org/abs/2207.14585) [hep-ex].
- [169] V. D. Kekelidze et al. “**Three stages of the NICA accelerator complex**”. In: *Eur. Phys. J. A* 52.8 (2016), p. 211. DOI: [10.1140/epja/i2016-16211-2](https://doi.org/10.1140/epja/i2016-16211-2).
- [170] V. Abgaryan et al. “**Status and initial physics performance studies of the MPD experiment at NICA**”. In: *Eur. Phys. J. A* 58.7 (2022), p. 140. DOI: [10.1140/epja/s10050-022-00750-6](https://doi.org/10.1140/epja/s10050-022-00750-6). arXiv: [2202.08970](https://arxiv.org/abs/2202.08970) [physics.ins-det].
- [171] Takao Sakaguchi. “**High density matter physics at J-PARC-HI**”. In: *PoS CORFU2018* (2019). Ed. by Konstantinos Anagnostopoulos et al., p. 189. DOI: [10.22323/1.347.0189](https://doi.org/10.22323/1.347.0189). arXiv: [1904.12821](https://arxiv.org/abs/1904.12821) [nucl-ex].
- [172] A. Abada et al. “**FCC-hh: The Hadron Collider - Future Circular Collider Conceptual Design Report Volume 3**”. In: *Eur. Phys. J. ST* 228.4 (2019), pp. 755–1107. DOI: [10.1140/epjst/e2019-900087-0](https://doi.org/10.1140/epjst/e2019-900087-0).
- [173] Larry D. McLerran and T. Toimela. “**Photon and Dilepton Emission from the Quark - Gluon Plasma: Some General Considerations**”. In: *Phys. Rev. D* 31 (1985), p. 545. DOI: [10.1103/PhysRevD.31.545](https://doi.org/10.1103/PhysRevD.31.545).
- [174] Simon Turbide, Ralf Rapp, and Charles Gale. “**Hadronic production of thermal photons**”. In: *Phys. Rev. C* 69 (1 Jan. 2004), p. 014903. DOI: [10.1103/PhysRevC.69.014903](https://doi.org/10.1103/PhysRevC.69.014903). URL: [%5Curl%7Bhttps://link.aps.org/doi/10.1103/PhysRevC.69.014903%7D](https://link.aps.org/doi/10.1103/PhysRevC.69.014903%7D).
- [175] A. Adare et al. “**Enhanced production of direct photons in Au+Au collisions at $\sqrt{s_{NN}} = 200$ GeV and implications for the initial temperature**”. In: *Phys. Rev. Lett.* 104 (2010), p. 132301. DOI: [10.1103/PhysRevLett.104.132301](https://doi.org/10.1103/PhysRevLett.104.132301). arXiv: [0804.4168](https://arxiv.org/abs/0804.4168) [nucl-ex].

- [176] Jaroslav Adam et al. “**Direct photon production in Pb-Pb collisions at $\sqrt{s_{NN}} = 2.76$ TeV**”. In: *Phys. Lett. B* 754 (2016), pp. 235–248. DOI: [10.1016/j.physletb.2016.01.020](https://doi.org/10.1016/j.physletb.2016.01.020). arXiv: [1509.07324 \[nucl-ex\]](https://arxiv.org/abs/1509.07324).
- [177] L. Adamczyk et al. “**Bulk Properties of the Medium Produced in Relativistic Heavy-Ion Collisions from the Beam Energy Scan Program**”. In: *Phys. Rev. C* 96.4 (2017), p. 044904. DOI: [10.1103/PhysRevC.96.044904](https://doi.org/10.1103/PhysRevC.96.044904). arXiv: [1701.07065](https://arxiv.org/abs/1701.07065).
- [178] S. Wheaton and J. Cleymans. “**THERMUS: A Thermal model package for ROOT**”. In: *Comput. Phys. Commun.* 180 (2009), pp. 84–106. DOI: [10.1016/j.cpc.2008.08.001](https://doi.org/10.1016/j.cpc.2008.08.001). arXiv: [hep-ph/0407174](https://arxiv.org/abs/hep-ph/0407174).
- [179] Ekkard Schnedermann, Josef Sollfrank, and Ulrich W. Heinz. “**Thermal phenomenology of hadrons from 200-A/GeV S+S collisions**”. In: *Phys. Rev. C* 48 (1993), pp. 2462–2475. DOI: [10.1103/PhysRevC.48.2462](https://doi.org/10.1103/PhysRevC.48.2462). arXiv: [nuc1-th/9307020](https://arxiv.org/abs/nuc1-th/9307020).
- [180] Johann Rafelski and Berndt Muller. “**Strangeness Production in the Quark-Gluon Plasma**”. In: *Phys. Rev. Lett.* 48 (1982). [Erratum: *Phys.Rev.Lett.* 56, 2334 (1986)], p. 1066. DOI: [10.1103/PhysRevLett.48.1066](https://doi.org/10.1103/PhysRevLett.48.1066).
- [181] P. Koch, Berndt Muller, and Johann Rafelski. “**Strangeness in Relativistic Heavy Ion Collisions**”. In: *Phys. Rept.* 142 (1986), pp. 167–262. DOI: [10.1016/0370-1573\(86\)90096-7](https://doi.org/10.1016/0370-1573(86)90096-7).
- [182] L Ahle et al. “**An Excitation function of K- and K+ production in Au + Au reactions at the AGS**”. In: *Phys. Lett. B* 490 (2000), pp. 53–60. DOI: [10.1016/S0370-2693\(00\)00916-3](https://doi.org/10.1016/S0370-2693(00)00916-3). arXiv: [nuc1-ex/0008010](https://arxiv.org/abs/nuc1-ex/0008010).
- [183] S. V. Afanasiev et al. “**Energy dependence of pion and kaon production in central Pb + Pb collisions**”. In: *Phys. Rev. C* 66 (2002), p. 054902. DOI: [10.1103/PhysRevC.66.054902](https://doi.org/10.1103/PhysRevC.66.054902). arXiv: [nuc1-ex/0205002](https://arxiv.org/abs/nuc1-ex/0205002).
- [184] J. Adams et al. “**Multistrange baryon production in Au-Au collisions at $S(NN)^{1/2} = 130$ GeV**”. In: *Phys. Rev. Lett.* 92 (2004), p. 182301. DOI: [10.1103/PhysRevLett.92.182301](https://doi.org/10.1103/PhysRevLett.92.182301). arXiv: [nuc1-ex/0307024](https://arxiv.org/abs/nuc1-ex/0307024).
- [185] Betty Bezverkhny Abelev et al. “**Multi-strange baryon production at mid-rapidity in Pb-Pb collisions at $\sqrt{s_{NN}} = 2.76$ TeV**”. In: *Phys. Lett. B* 728 (2014). [Erratum: *Phys.Lett.B* 734, 409–410 (2014)], pp. 216–227. DOI: [10.1016/j.physletb.2014.05.052](https://doi.org/10.1016/j.physletb.2014.05.052). arXiv: [1307.5543 \[nucl-ex\]](https://arxiv.org/abs/1307.5543).
- [186] Jean-Yves Ollitrault. “**Anisotropy as a signature of transverse collective flow**”. In: *Phys. Rev. D* 46 (1992), pp. 229–245. DOI: [10.1103/PhysRevD.46.229](https://doi.org/10.1103/PhysRevD.46.229).
- [187] Raimond Snellings. “**Elliptic Flow: A Brief Review**”. In: *New J. Phys.* 13 (2011), p. 055008. DOI: [10.1088/1367-2630/13/5/055008](https://doi.org/10.1088/1367-2630/13/5/055008). arXiv: [1102.3010 \[nucl-ex\]](https://arxiv.org/abs/1102.3010).
- [188] S. Acharya et al. “**Anisotropic flow of identified particles in Pb-Pb collisions at $\sqrt{s_{NN}} = 5.02$ TeV**”. In: *JHEP* 09 (2018), p. 006. DOI: [10.1007/JHEP09\(2018\)006](https://doi.org/10.1007/JHEP09(2018)006). arXiv: [1805.04390 \[nucl-ex\]](https://arxiv.org/abs/1805.04390).
- [189] L. Adamczyk et al. “**Elliptic flow of identified hadrons in Au+Au collisions at $\sqrt{s_{NN}} = 7.7-62.4$ GeV**”. In: *Phys. Rev. C* 88 (2013), p. 014902. DOI: [10.1103/PhysRevC.88.014902](https://doi.org/10.1103/PhysRevC.88.014902). arXiv: [1301.2348 \[nucl-ex\]](https://arxiv.org/abs/1301.2348).
- [190] Chun Shen. “**Studying QGP with flow: A theory overview**”. In: *Nucl. Phys. A* 1005 (2021). Ed. by Feng Liu et al., p. 121788. DOI: [10.1016/j.nuclphysa.2020.121788](https://doi.org/10.1016/j.nuclphysa.2020.121788). arXiv: [2001.11858 \[nucl-th\]](https://arxiv.org/abs/2001.11858).

- [191] Miklos Gyulassy and Michael Plumer. “**Jet Quenching in Dense Matter**”. In: *Phys. Lett. B* 243 (1990), pp. 432–438. DOI: [10.1016/0370-2693\(90\)91409-5](https://doi.org/10.1016/0370-2693(90)91409-5).
- [192] David d’Enterria. “**Jet quenching in QCD matter: From RHIC to LHC**”. In: *Particles and nuclei. Proceedings, 18th International Conference, PANIC08, Eilat, Israel, November 9-14, 2008*. Vol. A827. 2009, pp. 356C–364C. DOI: [10.1016/j.nuclphysa.2009.05.078](https://doi.org/10.1016/j.nuclphysa.2009.05.078).
- [193] K. Adcox et al. “**Suppression of hadrons with large transverse momentum in central Au+Au collisions at $\sqrt{s_{NN}} = 130\text{-GeV}$** ”. In: *Phys. Rev. Lett.* 88 (2002), p. 022301. DOI: [10.1103/PhysRevLett.88.022301](https://doi.org/10.1103/PhysRevLett.88.022301). arXiv: [nuclex/0109003](https://arxiv.org/abs/nuclex/0109003).
- [194] C. Adler et al. “**Disappearance of back-to-back high p_T hadron correlations in central Au+Au collisions at $\sqrt{s_{NN}} = 200\text{-GeV}$** ”. In: *Phys. Rev. Lett.* 90 (2003), p. 082302. DOI: [10.1103/PhysRevLett.90.082302](https://doi.org/10.1103/PhysRevLett.90.082302). arXiv: [nuclex/0210033](https://arxiv.org/abs/nuclex/0210033).
- [195] Georges Aad et al. “**Observation of a Centrality-Dependent Dijet Asymmetry in Lead-Lead Collisions at $\sqrt{s_{NN}} = 2.77\text{ TeV}$ with the ATLAS Detector at the LHC**”. In: *Phys. Rev. Lett.* 105 (2010), p. 252303. DOI: [10.1103/PhysRevLett.105.252303](https://doi.org/10.1103/PhysRevLett.105.252303). arXiv: [1011.6182 \[hep-ex\]](https://arxiv.org/abs/1011.6182).
- [196] Serguei Chatrchyan et al. “**Observation and studies of jet quenching in PbPb collisions at nucleon-nucleon center-of-mass energy = 2.76 TeV**”. In: *Phys. Rev. C* 84 (2011), p. 024906. DOI: [10.1103/PhysRevC.84.024906](https://doi.org/10.1103/PhysRevC.84.024906). arXiv: [1102.1957 \[nucl-ex\]](https://arxiv.org/abs/1102.1957).
- [197] T. Matsui and H. Satz. “ **J/ψ Suppression by Quark-Gluon Plasma Formation**”. In: *Phys. Lett. B* 178 (1986), pp. 416–422. DOI: [10.1016/0370-2693\(86\)91404-8](https://doi.org/10.1016/0370-2693(86)91404-8).
- [198] P. Braun-Munzinger and J. Stachel. “**(Non)thermal aspects of charmonium production and a new look at J/ψ suppression**”. In: *Phys. Lett. B* 490 (2000), pp. 196–202. DOI: [10.1016/S0370-2693\(00\)00991-6](https://doi.org/10.1016/S0370-2693(00)00991-6). arXiv: [nucloth/0007059](https://arxiv.org/abs/nucloth/0007059).
- [199] Robert L. Thews, Martin Schroedter, and Johann Rafelski. “**Enhanced J/ψ production in deconfined quark matter**”. In: *Phys. Rev. C* 63 (2001), p. 054905. DOI: [10.1103/PhysRevC.63.054905](https://doi.org/10.1103/PhysRevC.63.054905). arXiv: [hep-ph/0007323](https://arxiv.org/abs/hep-ph/0007323).
- [200] A. Adare et al. “ **J/ψ Production vs Centrality, Transverse Momentum, and Rapidity in Au+Au Collisions at $\sqrt{s_{NN}} = 200\text{ GeV}$** ”. In: *Phys. Rev. Lett.* 98 (2007), p. 232301. DOI: [10.1103/PhysRevLett.98.232301](https://doi.org/10.1103/PhysRevLett.98.232301). arXiv: [nuclex/0611020](https://arxiv.org/abs/nuclex/0611020).
- [201] Serguei Chatrchyan et al. “**Suppression of non-prompt J/ψ , prompt J/ψ , and $\Upsilon(1S)$ in PbPb collisions at $\sqrt{s_{NN}} = 2.76\text{ TeV}$** ”. In: *JHEP* 05 (2012), p. 063. DOI: [10.1007/JHEP05\(2012\)063](https://doi.org/10.1007/JHEP05(2012)063). arXiv: [1201.5069 \[nucl-ex\]](https://arxiv.org/abs/1201.5069).
- [202] A. Andronic et al. “**Heavy-flavour and quarkonium production in the LHC era: from proton–proton to heavy-ion collisions**”. In: *Eur. Phys. J. C* 76.3 (2016), p. 107. DOI: [10.1140/epjc/s10052-015-3819-5](https://doi.org/10.1140/epjc/s10052-015-3819-5). arXiv: [1506.03981 \[nucl-ex\]](https://arxiv.org/abs/1506.03981).
- [203] Betty Bezverkhny Abelev et al. “**Multiplicity Dependence of Pion, Kaon, Proton and Lambda Production in p-Pb Collisions at $\sqrt{s_{NN}} = 5.02\text{ TeV}$** ”. In: *Phys. Lett. B* 728 (2014), pp. 25–38. DOI: [10.1016/j.physletb.2013.11.020](https://doi.org/10.1016/j.physletb.2013.11.020). arXiv: [1307.6796 \[nucl-ex\]](https://arxiv.org/abs/1307.6796).

- [204] Serguei Chatrchyan et al. “**Study of the Production of Charged Pions, Kaons, and Protons in pPb Collisions at $\sqrt{s_{NN}} = 5.02$ TeV**”. In: *Eur. Phys. J. C* 74.6 (2014), p. 2847. DOI: [10.1140/epjc/s10052-014-2847-x](https://doi.org/10.1140/epjc/s10052-014-2847-x). arXiv: [1307.3442](https://arxiv.org/abs/1307.3442) [hep-ex].
- [205] Vardan Khachatryan et al. “**Observation of Long-Range Near-Side Angular Correlations in Proton-Proton Collisions at the LHC**”. In: *JHEP* 09 (2010), p. 091. DOI: [10.1007/JHEP09\(2010\)091](https://doi.org/10.1007/JHEP09(2010)091). arXiv: [1009.4122](https://arxiv.org/abs/1009.4122) [hep-ex].
- [206] Jaroslav Adam et al. “**Enhanced production of multi-strange hadrons in high-multiplicity proton-proton collisions**”. In: *Nature Phys.* 13 (2017), pp. 535–539. DOI: [10.1038/nphys4111](https://doi.org/10.1038/nphys4111). arXiv: [1606.07424](https://arxiv.org/abs/1606.07424) [nucl-ex].
- [207] M. Stephanov. “**The phase diagram of QCD and the critical point**”. In: *Acta Phys. Polon. B* 35 (2004), pp. 2939–2962.
- [208] Masayuki Asakawa, Ulrich W. Heinz, and Berndt Muller. “**Fluctuation probes of quark deconfinement**”. In: *Phys. Rev. Lett.* 85 (2000), pp. 2072–2075. DOI: [10.1103/PhysRevLett.85.2072](https://doi.org/10.1103/PhysRevLett.85.2072). arXiv: [hep-ph/0003169](https://arxiv.org/abs/hep-ph/0003169).
- [209] V. Koch, A. Majumder, and J. Randrup. “**Baryon-Strangeness Correlations: A Diagnostic of Strongly Interacting Matter**”. In: *Phys. Rev. Lett.* 95 (18 Oct. 2005), p. 182301. DOI: [10.1103/PhysRevLett.95.182301](https://doi.org/10.1103/PhysRevLett.95.182301). URL: <https://link.aps.org/doi/10.1103/PhysRevLett.95.182301>.
- [210] R. V. Gavai and Sourendu Gupta. “**Fluctuations, strangeness and quasi-quarks in heavy-ion collisions from lattice QCD**”. In: *Phys. Rev. D* 73 (2006), p. 014004. DOI: [10.1103/PhysRevD.73.014004](https://doi.org/10.1103/PhysRevD.73.014004). arXiv: [hep-lat/0510044](https://arxiv.org/abs/hep-lat/0510044) [hep-lat].
- [211] Jaroslav Adam et al. “**Collision-energy dependence of second-order off-diagonal and diagonal cumulants of net-charge, net-proton, and net-kaon multiplicity distributions in Au + Au collisions**”. In: *Phys. Rev. C* 100.1 (2019). [Erratum: *Phys.Rev.C* 105, 029901 (2022)], p. 014902. DOI: [10.1103/PhysRevC.100.014902](https://doi.org/10.1103/PhysRevC.100.014902). arXiv: [1903.05370](https://arxiv.org/abs/1903.05370) [nucl-ex].
- [212] Jaroslav Adam et al. “**Beam energy dependence of net- Λ fluctuations measured by the STAR experiment at the BNL Relativistic Heavy Ion Collider**”. In: *Phys. Rev. C* 102.2 (2020), p. 024903. DOI: [10.1103/PhysRevC.102.024903](https://doi.org/10.1103/PhysRevC.102.024903). arXiv: [2001.06419](https://arxiv.org/abs/2001.06419) [nucl-ex].
- [213] J. Adam et al. “**Nonmonotonic Energy Dependence of Net-Proton Number Fluctuations**”. In: *Phys. Rev. Lett.* 126.9 (2021), p. 092301. DOI: [10.1103/PhysRevLett.126.092301](https://doi.org/10.1103/PhysRevLett.126.092301). arXiv: [2001.02852](https://arxiv.org/abs/2001.02852) [nucl-ex].
- [214] Mohamed Abdallah et al. “**Cumulants and correlation functions of net-proton, proton, and antiproton multiplicity distributions in Au+Au collisions at energies available at the BNL Relativistic Heavy Ion Collider**”. In: *Phys. Rev. C* 104.2 (2021), p. 024902. DOI: [10.1103/PhysRevC.104.024902](https://doi.org/10.1103/PhysRevC.104.024902). arXiv: [2101.12413](https://arxiv.org/abs/2101.12413) [nucl-ex].
- [215] Mohamed Abdallah et al. “**Measurement of the Sixth-Order Cumulant of Net-Proton Multiplicity Distributions in Au+Au Collisions at $\sqrt{s_{NN}} = 27, 54.4,$ and 200 GeV at RHIC**”. In: *Phys. Rev. Lett.* 127.26 (2021), p. 262301. DOI: [10.1103/PhysRevLett.127.262301](https://doi.org/10.1103/PhysRevLett.127.262301). arXiv: [2105.14698](https://arxiv.org/abs/2105.14698) [nucl-ex].
- [216] R. Bellwied et al. “**Fluctuations and correlations in high temperature QCD**”. In: *Phys. Rev. D* 92.11 (2015), p. 114505. DOI: [10.1103/PhysRevD.92.114505](https://doi.org/10.1103/PhysRevD.92.114505). arXiv: [1507.04627](https://arxiv.org/abs/1507.04627) [hep-lat].

- [217] Xiaofeng Luo and Nu Xu. “**Search for the QCD Critical Point with Fluctuations of Conserved Quantities in Relativistic Heavy-Ion Collisions at RHIC : An Overview**”. In: *Nucl. Sci. Tech.* 28.8 (2017), p. 112. DOI: [10.1007/s41365-017-0257-0](https://doi.org/10.1007/s41365-017-0257-0). arXiv: [1701.02105](https://arxiv.org/abs/1701.02105) [nucl-ex].
- [218] Paolo Parotto et al. “**QCD equation of state matched to lattice data and exhibiting a critical point singularity**”. In: *Phys. Rev. C* 101.3 (2020), p. 034901. DOI: [10.1103/PhysRevC.101.034901](https://doi.org/10.1103/PhysRevC.101.034901). arXiv: [1805.05249](https://arxiv.org/abs/1805.05249) [hep-ph].
- [219] M. A. Stephanov. “**Non-Gaussian fluctuations near the QCD critical point**”. In: *Phys. Rev. Lett.* 102 (2009), p. 032301. DOI: [10.1103/PhysRevLett.102.032301](https://doi.org/10.1103/PhysRevLett.102.032301). arXiv: [0809.3450](https://arxiv.org/abs/0809.3450) [hep-ph].
- [220] L. Adamczyk et al. “**Collision Energy Dependence of Moments of Net-Kaon Multiplicity Distributions at RHIC**”. In: *Phys. Lett. B* 785 (2018), pp. 551–560. DOI: [10.1016/j.physletb.2018.07.066](https://doi.org/10.1016/j.physletb.2018.07.066). arXiv: [1709.00773](https://arxiv.org/abs/1709.00773) [nucl-ex].
- [221] M. A. Stephanov. “**On the sign of kurtosis near the QCD critical point**”. In: *Phys. Rev. Lett.* 107 (2011), p. 052301. DOI: [10.1103/PhysRevLett.107.052301](https://doi.org/10.1103/PhysRevLett.107.052301). arXiv: [1104.1627](https://arxiv.org/abs/1104.1627) [hep-ph].
- [222] M. Bluhm et al. *Dynamics of critical fluctuations: Theory – phenomenology – heavy-ion collisions*. 2020. arXiv: [2001.08831](https://arxiv.org/abs/2001.08831) [nucl-th].
- [223] Xiaofeng Luo et al. “**Volume fluctuation and auto-correlation effects in the moment analysis of net-proton multiplicity distributions in heavy-ion collisions**”. In: *J. Phys. G* 40 (2013), p. 105104. DOI: [10.1088/0954-3899/40/10/105104](https://doi.org/10.1088/0954-3899/40/10/105104). arXiv: [1302.2332](https://arxiv.org/abs/1302.2332) [nucl-ex].
- [224] Nihar R. Sahoo, Sudipan De, and Tapan K. Nayak. “**Baseline study for higher moments of net-charge distributions at energies available at the BNL Relativistic Heavy Ion Collider**”. In: *Phys. Rev. C* 87.4 (2013), p. 044906. DOI: [10.1103/PhysRevC.87.044906](https://doi.org/10.1103/PhysRevC.87.044906). arXiv: [1210.7206](https://arxiv.org/abs/1210.7206) [nucl-ex].
- [225] Misha A. Stephanov, K. Rajagopal, and Edward V. Shuryak. “**Event-by-event fluctuations in heavy ion collisions and the QCD critical point**”. In: *Phys. Rev. D* 60 (1999), p. 114028. DOI: [10.1103/PhysRevD.60.114028](https://doi.org/10.1103/PhysRevD.60.114028). arXiv: [hep-ph/9903292](https://arxiv.org/abs/hep-ph/9903292).
- [226] Boris Berdnikov and Krishna Rajagopal. “**Slowing out-of-equilibrium near the QCD critical point**”. In: *Phys. Rev. D* 61 (2000), p. 105017. DOI: [10.1103/PhysRevD.61.105017](https://doi.org/10.1103/PhysRevD.61.105017). arXiv: [hep-ph/9912274](https://arxiv.org/abs/hep-ph/9912274).
- [227] Volodymyr Vovchenko. “**Phenomenological developments for event-by-event fluctuations of conserved charges**”. In: *International Conference on Critical Point and Onset of Deconfinement*. Oct. 2021. arXiv: [2110.02446](https://arxiv.org/abs/2110.02446) [nucl-th].
- [228] Volodymyr Vovchenko et al. “**Connecting fluctuation measurements in heavy-ion collisions with the grand-canonical susceptibilities**”. In: *Phys. Lett. B* 811 (2020), p. 135868. DOI: [10.1016/j.physletb.2020.135868](https://doi.org/10.1016/j.physletb.2020.135868). arXiv: [2003.13905](https://arxiv.org/abs/2003.13905) [hep-ph].
- [229] Bo Ling and Mikhail A. Stephanov. “**Acceptance dependence of fluctuation measures near the QCD critical point**”. In: *Phys. Rev. C* 93.3 (2016), p. 034915. DOI: [10.1103/PhysRevC.93.034915](https://doi.org/10.1103/PhysRevC.93.034915). arXiv: [1512.09125](https://arxiv.org/abs/1512.09125) [nucl-th].
- [230] Volker Koch. “**Hadronic Fluctuations and Correlations**”. In: *Relativistic Heavy Ion Physics*. Ed. by R. Stock. 2010, pp. 626–652. DOI: [10.1007/978-3-642-01539-7_20](https://doi.org/10.1007/978-3-642-01539-7_20). arXiv: [0810.2520](https://arxiv.org/abs/0810.2520) [nucl-th].

- [231] J. Steinheimer et al. “**Conserved charge fluctuations are not conserved during the hadronic phase**”. In: *Phys. Lett. B* 776 (2018), pp. 32–37. DOI: [10.1016/j.physletb.2017.11.012](https://doi.org/10.1016/j.physletb.2017.11.012). arXiv: [1608.03737](https://arxiv.org/abs/1608.03737) [nucl-th].
- [232] Masakiyo Kitazawa and Masayuki Asakawa. “**Relation between baryon number fluctuations and experimentally observed proton number fluctuations in relativistic heavy ion collisions**”. In: *Phys. Rev. C* 86 (2012). [Erratum: *Phys.Rev.C* 86, 069902 (2012)], p. 024904. DOI: [10.1103/PhysRevC.86.024904](https://doi.org/10.1103/PhysRevC.86.024904). arXiv: [1205.3292](https://arxiv.org/abs/1205.3292) [nucl-th].
- [233] Jan Hammelmann and Hannah Elfner. “**Impact of hadronic interactions and conservation laws on cumulants of conserved charges in a dynamical model**”. In: (Feb. 2022). arXiv: [2202.11417](https://arxiv.org/abs/2202.11417) [nucl-th].
- [234] Rene Bellwied et al. “**Off-diagonal correlators of conserved charges from lattice QCD and how to relate them to experiment**”. In: *Phys. Rev. D* 101.3 (2020), p. 034506. DOI: [10.1103/PhysRevD.101.034506](https://doi.org/10.1103/PhysRevD.101.034506). arXiv: [1910.14592](https://arxiv.org/abs/1910.14592) [hep-lat].
- [235] Volodymyr Vovchenko and Volker Koch. “**Efficiency corrections for factorial moments and cumulants of overlapping sets of particles**”. In: *Nucl. Phys. A* 1010 (2021), p. 122179. DOI: [10.1016/j.nuclphysa.2021.122179](https://doi.org/10.1016/j.nuclphysa.2021.122179). arXiv: [2101.02182](https://arxiv.org/abs/2101.02182) [nucl-th].
- [236] Paolo Alba et al. “**Constraining the hadronic spectrum through QCD thermodynamics on the lattice**”. In: *Phys. Rev. D* 96.3 (2017), p. 034517. DOI: [10.1103/PhysRevD.96.034517](https://doi.org/10.1103/PhysRevD.96.034517). arXiv: [1702.01113](https://arxiv.org/abs/1702.01113) [hep-lat].
- [237] R. Venugopalan and M. Prakash. “**Thermal properties of interacting hadrons**”. In: *Nucl. Phys. A* 546 (1992), pp. 718–760. DOI: [10.1016/0375-9474\(92\)90005-5](https://doi.org/10.1016/0375-9474(92)90005-5).
- [238] A. Buckley et al. “**General-purpose event generators for LHC physics**”. In: *Physics Reports* 504.5 (July 2011), pp. 145–233. DOI: [10.1016/j.physrep.2011.03.005](https://doi.org/10.1016/j.physrep.2011.03.005). URL: <https://doi.org/10.1016%5C%2Fj.physrep.2011.03.005>.
- [239] S. Agostinelli et al. “**Geant4 — A simulation toolkit**”. In: *Nuclear Instruments and Methods in Physics Research Section A: Accelerators, Spectrometers, Detectors and Associated Equipment* 506.3 (2003), pp. 250–303. ISSN: 0168-9002. DOI: [https://doi.org/10.1016/S0168-9002\(03\)01368-8](https://doi.org/10.1016/S0168-9002(03)01368-8). URL: <https://www.sciencedirect.com/science/article/pii/S0168900203013688>.
- [240] Gábor Bíró et al. “**HIJING, a Heavy Ion Jet INteraction Generator for the High-Luminosity Era of the LHC and Beyond**”. In: *MDPI Proc.* 10.1 (2019). Ed. by Javier Albacete et al., p. 4. DOI: [10.3390/proceedings2019010004](https://doi.org/10.3390/proceedings2019010004). arXiv: [1811.02131](https://arxiv.org/abs/1811.02131) [physics.comp-ph].
- [241] Christian Bierlich et al. “**The Angantyr model for Heavy-Ion Collisions in PYTHIA8**”. In: *JHEP* 10 (2018), p. 134. DOI: [10.1007/JHEP10\(2018\)134](https://doi.org/10.1007/JHEP10(2018)134). arXiv: [1806.10820](https://arxiv.org/abs/1806.10820) [hep-ph].
- [242] Francois Gelis et al. “**The Color Glass Condensate**”. In: *Ann. Rev. Nucl. Part. Sci.* 60 (2010), pp. 463–489. DOI: [10.1146/annurev.nucl.010909.083629](https://doi.org/10.1146/annurev.nucl.010909.083629). arXiv: [1002.0333](https://arxiv.org/abs/1002.0333) [hep-ph].
- [243] J. M. Campbell et al. *Event Generators for High-Energy Physics Experiments*. arXiv:2203.11110 [hep-ph]. 2022. DOI: [10.48550/ARXIV.2203.11110](https://doi.org/10.48550/ARXIV.2203.11110). URL: <https://arxiv.org/abs/2203.11110>.

- [244] W. Cassing and E. L. Bratkovskaya. “**Parton-Hadron-String Dynamics: an off-shell transport approach for relativistic energies**”. In: *Nucl. Phys. A* 831 (2009), pp. 215–242. DOI: [10.1016/j.nuclphysa.2009.09.007](https://doi.org/10.1016/j.nuclphysa.2009.09.007). arXiv: [0907.5331](https://arxiv.org/abs/0907.5331) [[nucl-th](#)].
- [245] Zi-Wei Lin et al. “**A Multi-phase transport model for relativistic heavy ion collisions**”. In: *Phys. Rev. C* 72 (2005), p. 064901. DOI: [10.1103/PhysRevC.72.064901](https://doi.org/10.1103/PhysRevC.72.064901). arXiv: [nucl-th/0411110](https://arxiv.org/abs/nucl-th/0411110).
- [246] M. Bleicher et al. “**Relativistic hadron hadron collisions in the ultrarelativistic quantum molecular dynamics model**”. In: *J. Phys.* G25 (1999), pp. 1859–1896. DOI: [10.1088/0954-3899/25/9/308](https://doi.org/10.1088/0954-3899/25/9/308). arXiv: [hep-ph/9909407](https://arxiv.org/abs/hep-ph/9909407) [[hep-ph](#)].
- [247] Hannah Petersen et al. “**A Fully Integrated Transport Approach to Heavy Ion Reactions with an Intermediate Hydrodynamic Stage**”. In: *Phys. Rev. C* 78 (2008), p. 044901. DOI: [10.1103/PhysRevC.78.044901](https://doi.org/10.1103/PhysRevC.78.044901). arXiv: [0806.1695](https://arxiv.org/abs/0806.1695) [[nucl-th](#)].
- [248] J. Weil et al. “**Particle production and equilibrium properties within a new hadron transport approach for heavy-ion collisions**”. In: *Phys. Rev. C* 94.5 (2016), p. 054905. DOI: [10.1103/PhysRevC.94.054905](https://doi.org/10.1103/PhysRevC.94.054905). arXiv: [1606.06642](https://arxiv.org/abs/1606.06642) [[nucl-th](#)].
- [249] José Guilherme Milhano and Korinna Zapp. “**Improved background subtraction and a fresh look at jet sub-structure in JEWEL**”. In: *Eur. Phys. J. C* 82.11 (2022), p. 1010. DOI: [10.1140/epjc/s10052-022-10954-1](https://doi.org/10.1140/epjc/s10052-022-10954-1). arXiv: [2207.14814](https://arxiv.org/abs/2207.14814) [[hep-ph](#)].
- [250] Dusan Zigic et al. “**DREENA-C framework: joint R_{AA} and v_2 predictions and implications to QGP tomography**”. In: *J. Phys. G* 46.8 (2019), p. 085101. DOI: [10.1088/1361-6471/ab2356](https://doi.org/10.1088/1361-6471/ab2356). arXiv: [1805.03494](https://arxiv.org/abs/1805.03494) [[nucl-th](#)].
- [251] J. H. Putschke et al. *The JETSCAPE framework*. Mar. 2019. arXiv: [1903.07706](https://arxiv.org/abs/1903.07706) [[nucl-th](#)].
- [252] Stephane Delorme. “**Theoretical description of quarkonium dynamics in the quark gluon plasma with a quantum master equation approach**”. PhD Thesis. Ecole nationale supérieure Mines-Télécom Atlantique, Oct. 2021. URL: <https://tel.archives-ouvertes.fr/tel-03664821>.
- [253] Takahiro Miura et al. “**Quantum Brownian motion of a heavy quark pair in the quark-gluon plasma**”. In: *Phys. Rev. D* 101.3 (2020), p. 034011. DOI: [10.1103/PhysRevD.101.034011](https://doi.org/10.1103/PhysRevD.101.034011). arXiv: [1908.06293](https://arxiv.org/abs/1908.06293) [[nucl-th](#)].
- [254] Denys Yen Arrebato Villar, Joerg Aichelin, and Pol Bernard Gossiaux. “**A new Microscopic Model for J/ψ Production in Heavy Ion Collisions**”. In: (June 2022). arXiv: [2206.01308](https://arxiv.org/abs/2206.01308) [[nucl-th](#)].
- [255] Hisham Ba Omar et al. “**QTRAJ 1.0: A Lindblad equation solver for heavy-quarkonium dynamics**”. In: *Comput. Phys. Commun.* 273 (2022), p. 108266. DOI: [10.1016/j.cpc.2021.108266](https://doi.org/10.1016/j.cpc.2021.108266). arXiv: [2107.06147](https://arxiv.org/abs/2107.06147) [[physics.comp-ph](#)].
- [256] K. Werner. “**Strings, pomerons and the VENUS model of hadronic interactions at ultrarelativistic energies**”. In: *Physics Report* (Sept. 1993).
- [257] V.N. Gribov. “**A Reggeon Diagram Technique**”. In: *Soviet Physics JETP* (1968).
- [258] X. Artru and G. Mennessier. “**String model and multiproduction**”. In: *Nucl. Phys. B* 70 (1974), pp. 93–115. DOI: [10.1016/0550-3213\(74\)90360-5](https://doi.org/10.1016/0550-3213(74)90360-5).

- [259] N.N. Kalmykov, S.S. Ostapchenko, and A.I. Pavlov. “**Quark-gluon-string model and EAS simulation problems at ultra-high energies**”. In: *Nuclear Physics B - Proceedings Supplements* 52.3 (1997), pp. 17–28. ISSN: 0920-5632. DOI: [https://doi.org/10.1016/S0920-5632\(96\)00846-8](https://doi.org/10.1016/S0920-5632(96)00846-8). URL: <https://www.sciencedirect.com/science/article/pii/S0920563296008468>.
- [260] H. J. Drescher et al. “**A Unified treatment of high-energy interactions**”. In: *J. Phys. G* 25 (1999), pp. L91–L96. DOI: [10.1088/0954-3899/25/10/101](https://doi.org/10.1088/0954-3899/25/10/101). arXiv: [hep-ph/9903296](https://arxiv.org/abs/hep-ph/9903296).
- [261] S. Ostapchenko. “**Hadronic Interactions at Cosmic Ray Energies**”. In: *Nucl. Phys. B Proc. Suppl.* 175-176 (2008). Ed. by Kwong Sang Cheng et al., pp. 73–80. DOI: [10.1016/j.nuclphysbps.2007.10.011](https://doi.org/10.1016/j.nuclphysbps.2007.10.011). arXiv: [hep-ph/0612068](https://arxiv.org/abs/hep-ph/0612068).
- [262] Klaus Werner, Fu-Ming Liu, and Tanguy Pierog. “**Parton ladder splitting and the rapidity dependence of transverse momentum spectra in deuteron-gold collisions at RHIC**”. In: *Phys. Rev. C* 74 (2006), p. 044902. DOI: [10.1103/PhysRevC.74.044902](https://doi.org/10.1103/PhysRevC.74.044902). arXiv: [hep-ph/0506232](https://arxiv.org/abs/hep-ph/0506232).
- [263] K. Werner et al. “**Event-by-Event Simulation of the Three-Dimensional Hydrodynamic Evolution from Flux Tube Initial Conditions in Ultra-relativistic Heavy Ion Collisions**”. In: *Phys. Rev. C* 82 (2010), p. 044904. DOI: [10.1103/PhysRevC.82.044904](https://doi.org/10.1103/PhysRevC.82.044904). arXiv: [1004.0805 \[nucl-th\]](https://arxiv.org/abs/1004.0805).
- [264] Klaus Werner. “**Core-corona separation in ultra-relativistic heavy ion collisions**”. In: *Phys. Rev. Lett.* 98 (2007), p. 152301. DOI: [10.1103/PhysRevLett.98.152301](https://doi.org/10.1103/PhysRevLett.98.152301). arXiv: [0704.1270 \[nucl-th\]](https://arxiv.org/abs/0704.1270).
- [265] Iurii Karpenko. “**Development of hydrodynamic and hydrokinetic approaches to ultrarelativistic nucleus-nucleus collisions**”. PhD Thesis. Université de Nantes & Bogolyubov Institute for Theoretical Physics - Kyiv, 2010.
- [266] F. Cooper and G. Frye. “**Single-particle distribution in the hydrodynamic and statistical thermodynamic models of multiparticle production**”. In: *Phys. Rev. D* 10 (1 July 1974), pp. 186–189. DOI: [10.1103/PhysRevD.10.186](https://doi.org/10.1103/PhysRevD.10.186). URL: <https://link.aps.org/doi/10.1103/PhysRevD.10.186>.
- [267] K. Werner et al. “**Analyzing radial flow features in p -Pb and p -p collisions at several TeV by studying identified-particle production with the event generator EPOS3**”. In: *Phys. Rev. C* 89 (6 June 2014), p. 064903. DOI: [10.1103/PhysRevC.89.064903](https://doi.org/10.1103/PhysRevC.89.064903). URL: <https://link.aps.org/doi/10.1103/PhysRevC.89.064903>.
- [268] <https://klaus.pages.in2p3.fr/epos4/>.
- [269] Klaus Werner. “**On a deep connection between factorization and saturation: new insight into modeling high-energy proton-proton and nucleus-nucleus scattering in the EPOS4 framework**”. In: (Jan. 2023). arXiv: [2301.12517 \[hep-ph\]](https://arxiv.org/abs/2301.12517).
- [270] Maria Stefaniak. “**Beam Energy Scan dependence of elliptic and triangular flow of identified hadrons in the STAR experiment and the EPOS model**”. PhD Thesis. Ecole nationale supérieure Mines-Télécom Atlantique & Uniwersytet Warszawski, Oct. 2021. URL: <https://tel.archives-ouvertes.fr/tel-03607713>.
- [271] K. Werner et al. “**Recent Developments in EPOS: Core–Corona Effects in Air Showers?**” In: *Phys. At. Nucl.* 84.6 (Dec. 2021), pp. 1026–1029. DOI: [10.1134/S106377882113041X](https://doi.org/10.1134/S106377882113041X).

- [272] T. Pierog et al. “**EPOS LHC: Test of collective hadronization with data measured at the CERN Large Hadron Collider**”. In: *Phys. Rev. C* 92.3 (2015), p. 034906. DOI: [10.1103/PhysRevC.92.034906](https://doi.org/10.1103/PhysRevC.92.034906). arXiv: [1306.0121](https://arxiv.org/abs/1306.0121) [hep-ph].
- [273] D. Heck et al. *CORSIKA: a Monte Carlo code to simulate extensive air showers*. 1998. URL: <https://ui.adsabs.harvard.edu/abs/1998cmcc.book.....H>.
- [274] L. Vermunt et al. *Influence of final-state radiation on heavy-flavour observables in pp collisions*. Oct. 2017. arXiv: [1710.09639](https://arxiv.org/abs/1710.09639) [nucl-th].
- [275] P. B. Gossiaux and J. Aichelin. “**Towards an understanding of the RHIC single electron data**”. In: *Phys. Rev. C* 78 (2008). Ed. by Jan-e Alam et al., p. 014904. DOI: [10.1103/PhysRevC.78.014904](https://doi.org/10.1103/PhysRevC.78.014904). arXiv: [0802.2525](https://arxiv.org/abs/0802.2525) [hep-ph].
- [276] Marlene Nahrgang et al. “**Toward a consistent evolution of the quark-gluon plasma and heavy quarks**”. In: *Phys. Rev. C* 93.4 (2016), p. 044909. DOI: [10.1103/PhysRevC.93.044909](https://doi.org/10.1103/PhysRevC.93.044909). arXiv: [1602.03544](https://arxiv.org/abs/1602.03544) [nucl-th].
- [277] Matteo Cacciari, Mario Greco, and Paolo Nason. “**The p_T spectrum in heavy flavor hadroproduction**”. In: *JHEP* 05 (1998), p. 007. DOI: [10.1088/1126-6708/1998/05/007](https://doi.org/10.1088/1126-6708/1998/05/007). arXiv: [hep-ph/9803400](https://arxiv.org/abs/hep-ph/9803400).
- [278] Pol Bernard Gossiaux et al. “**First results of EPOS-HQ model for open heavy flavor production in A-A collision at RHIC and LHC**”. In: *PoS HardProbes2018* (2019). Ed. by David d’Enterria, Andreas Morsch, and Philippe Crochet, p. 169. DOI: [10.22323/1.345.0169](https://doi.org/10.22323/1.345.0169). arXiv: [1901.03856](https://arxiv.org/abs/1901.03856) [hep-ph].
- [279] Denys Yen Arrebato Villar. “**Phase space coalescence model for quarkonium production in heavy ion collisions**”. PhD Thesis. Ecole nationale supérieure Mines-Télécom Atlantique, Dec. 2021. URL: <https://tel.archives-ouvertes.fr/tel-03633469>.
- [280] Martin Rohrmoser et al. “**Discrimination of effective radiative and collisional in-medium energy-loss models by their effects on angular jet structure**”. In: *24th Cracow Epiphany Conference on Advances in Heavy Flavour Physics*. Vol. 49. Jan. 2018, p. 1325. DOI: [10.5506/APhysPolB.49.1325](https://doi.org/10.5506/APhysPolB.49.1325). URL: <https://hal.archives-ouvertes.fr/hal-01815123>.
- [281] Iurii Karpenko et al. “**Jet-fluid interaction in the EPOS3-Jet framework**”. In: *Springer Proc. Phys.* 250 (2020). Ed. by Domenico Elia et al., pp. 459–463. DOI: [10.1007/978-3-030-53448-6_72](https://doi.org/10.1007/978-3-030-53448-6_72). arXiv: [1911.04155](https://arxiv.org/abs/1911.04155) [nucl-th].
- [282] Iurii Karpenko et al. “**Jet overlap in heavy ion collisions at energies available at the CERN Large Hadron Collider and its consequences for the jet shape**”. In: *Phys. Rev. C* 101.1 (2020), p. 014905. DOI: [10.1103/PhysRevC.101.014905](https://doi.org/10.1103/PhysRevC.101.014905). arXiv: [1908.00836](https://arxiv.org/abs/1908.00836) [nucl-th].
- [283] Mahbobeh Jafarpour. “**Dynamical thermalization in heavy-ion collisions**”. PhD Thesis. Nantes Université, June 2022.
- [284] H. J. Drescher et al. “**Parton based Gribov-Regge theory**”. In: *Phys. Rept.* 350 (2001), pp. 93–289. DOI: [10.1016/S0370-1573\(00\)00122-8](https://doi.org/10.1016/S0370-1573(00)00122-8). arXiv: [hep-ph/0007198](https://arxiv.org/abs/hep-ph/0007198).
- [285] V. A. Abramovsky, V. N. Gribov, and O. V. Kancheli. “**Character of Inclusive Spectra and Fluctuations Produced in Inelastic Processes by Multi-Pomeron Exchange**”. In: *Sov. J. Nucl. Phys.* 18 (1974), pp. 308–317.

- [286] Xin-Nian Wang and Miklos Gyulassy. “**A Systematic study of particle production in $p + p$ (anti- p) collisions via the HIJING model**”. In: *Phys. Rev. D* 45 (1992), pp. 844–856. DOI: [10.1103/PhysRevD.45.844](https://doi.org/10.1103/PhysRevD.45.844).
- [287] W. Heisenberg. “**Die beobachtbaren Größen in der Theorie der Elementarteilchen. II**”. In: *Zeitschrift für Physik* 120.11-12 (Nov. 1943), pp. 673–702. DOI: [10.1007/BF01336936](https://doi.org/10.1007/BF01336936).
- [288] M. A. Braun. “**Parton model for h and A - A collisions at high-energies**”. In: *Soviet Journal of Nuclear Physics* (1990).
- [289] Guido Altarelli and G. Parisi. “**Asymptotic Freedom in Parton Language**”. In: *Nucl. Phys. B* 126 (1977), pp. 298–318. DOI: [10.1016/0550-3213\(77\)90384-4](https://doi.org/10.1016/0550-3213(77)90384-4).
- [290] Gabriel Sophys. “**Formation of Quark-Gluon Plasma : Understanding the energy and system size dependance EPOS**”. PhD Thesis. Université de Nantes, 2018.
- [291] K. Werner et al. “**Charm production in high multiplicity pp events**”. In: *Proceedings, 7th International Workshop on Multiple Partonic Interactions at the LHC (MPI@LHC 2015): Miramare, Trieste, Italy, November 23-27, 2015*. 2016, pp. 66–70. arXiv: [1602.03414 \[nucl-th\]](https://arxiv.org/abs/1602.03414).
- [292] Yoichiro Nambu. “**Quark model and the factorization of the Veneziano amplitude**”. In: *International Conference on Symmetries and Quark Models, Wayne State U., Detroit*. R. Chand, 1969.
- [293] Joel Scherk. “**An Introduction to the Theory of Dual Models and Strings**”. In: *Rev. Mod. Phys.* 47 (1975), pp. 123–164. DOI: [10.1103/RevModPhys.47.123](https://doi.org/10.1103/RevModPhys.47.123).
- [294] K. Werner. “**Gribov-Regge approach and EPOS**”. Lecture, given in *KSETA Topical courses*. Germany, Apr. 2019. URL: <https://hal.archives-ouvertes.fr/hal-02434245>.
- [295] Paul H. Cox and A. Yildiz. “ **q - \bar{q} pair creation: a field theory approach**”. In: *Phys. Rev. D* 32 (1985), pp. 819–820. DOI: [10.1103/PhysRevD.32.819](https://doi.org/10.1103/PhysRevD.32.819).
- [296] B. Andersson et al. “**Parton fragmentation and string dynamics**”. In: *Physics Reports* 97.2 (1983), pp. 31–145. ISSN: 0370-1573. DOI: [https://doi.org/10.1016/0370-1573\(83\)90080-7](https://doi.org/10.1016/0370-1573(83)90080-7). URL: <https://www.sciencedirect.com/science/article/pii/0370157383900807%7D>.
- [297] H.J. Drescher. “**Les processus durs et la fragmentation dans un module unifié pour les interactions aux énergies ultra-relativistes**”. PhD Thesis. Université de Nantes, 1999. URL: <http://hal.in2p3.fr/in2p3-00021346>.
- [298] Iu. Karpenko, P. Huovinen, and M. Bleicher. “**A 3+1 dimensional viscous hydrodynamic code for relativistic heavy ion collisions**”. In: *Comput. Phys. Commun.* 185 (2014), pp. 3016–3027. DOI: [10.1016/j.cpc.2014.07.010](https://doi.org/10.1016/j.cpc.2014.07.010). arXiv: [1312.4160 \[nucl-th\]](https://arxiv.org/abs/1312.4160).
- [299] W. Israel and J. M. Stewart. “**Transient relativistic thermodynamics and kinetic theory**”. In: *Annals Phys.* 118 (1979), pp. 341–372. DOI: [10.1016/0003-4916\(79\)90130-1](https://doi.org/10.1016/0003-4916(79)90130-1).
- [300] F. E. Close. *An Introduction to Quarks and Partons*. Academic Press, 1979. ISBN: 978-0-12-175152-4.
- [301] D. H. Perkins. *Introduction to high energy physics*. Addison-Wesley, 1982. ISBN: 978-0-521-62196-0.
- [302] M. Stefaniak et al. “**The Equation of State with EPOS model**”. In: *Phys. Rev. C* (2022). To be published.

-
- [303] Christian Bierlich et al. “**Robust Independent Validation of Experiment and Theory: Rivet version 3**”. In: *SciPost Phys.* 8 (2020), p. 026. DOI: [10.21468/SciPostPhys.8.2.026](https://doi.org/10.21468/SciPostPhys.8.2.026). arXiv: [1912.05451](https://arxiv.org/abs/1912.05451) [hep-ph].
- [304] Christian Bierlich et al. “**Confronting experimental data with heavy-ion models: RIVET for heavy ions**”. In: *Eur. Phys. J. C* 80.5 (2020), p. 485. DOI: [10.1140/epjc/s10052-020-8033-4](https://doi.org/10.1140/epjc/s10052-020-8033-4). arXiv: [2001.10737](https://arxiv.org/abs/2001.10737) [hep-ph].
- [305] **RIVET’s analysis coverage**, <https://rivet.hepforge.org/rivet-coverage> (July 14th, 2022).
- [306] René Brun et al. *PAW++ : Physics Analysis Workstation : User’s Guide*. CERN Program Library Long Writeups. 1999. URL: <http://cds.cern.ch/record/2296392>.
- [307] Betty Abelev et al. “**Centrality determination of Pb-Pb collisions at $\sqrt{s_{NN}} = 2.76$ TeV with ALICE**”. In: *Phys. Rev. C* 88.4 (2013), p. 044909. DOI: [10.1103/PhysRevC.88.044909](https://doi.org/10.1103/PhysRevC.88.044909). arXiv: [1301.4361](https://arxiv.org/abs/1301.4361) [nucl-ex].
- [308] L. Garren & L. Sonnenschein M. Dobbs J.B. Hansen. *HepMC 2: A C++ event record for Monte-Carlo generators*. http://www.t2.ucsd.edu/twiki2/pub/HEPProjects/HepMCReference/HepMC2_user_manual.pdf. May 2010.
- [309] B. Alver et al. “**Phobos results on charged particle multiplicity and pseudorapidity distributions in Au+Au, Cu+Cu, d+Au, and p+p collisions at ultra-relativistic energies**”. In: *Phys. Rev. C* 83 (2011), p. 024913. DOI: [10.1103/PhysRevC.83.024913](https://doi.org/10.1103/PhysRevC.83.024913). arXiv: [1011.1940](https://arxiv.org/abs/1011.1940) [nucl-ex].
- [310] A. Adare et al. “**Spectra and ratios of identified particles in Au+Au and d+Au collisions at $\sqrt{s_{NN}} = 200$ GeV**”. In: *Phys. Rev. C* 88.2 (2013), p. 024906. DOI: [10.1103/PhysRevC.88.024906](https://doi.org/10.1103/PhysRevC.88.024906). arXiv: [1304.3410](https://arxiv.org/abs/1304.3410) [nucl-ex].
- [311] B. B. Back et al. “**Identified hadron transverse momentum spectra in Au+Au collisions at $\sqrt{s_{NN}} = 62.4$ GeV**”. In: *Phys. Rev. C* 75 (2007), p. 024910. DOI: [10.1103/PhysRevC.75.024910](https://doi.org/10.1103/PhysRevC.75.024910). arXiv: [nuc1-ex/0610001](https://arxiv.org/abs/nuc1-ex/0610001).
- [312] Jaroslav Adam et al. “**Bulk properties of the system formed in Au + Au collisions at $\sqrt{s_{NN}} = 14.5$ GeV at the BNL STAR detector**”. In: *Phys. Rev. C* 101.2 (2020), p. 024905. DOI: [10.1103/PhysRevC.101.024905](https://doi.org/10.1103/PhysRevC.101.024905). arXiv: [1908.03585](https://arxiv.org/abs/1908.03585) [nucl-ex].
- [313] J. Adams et al. “**Scaling Properties of Hyperon Production in Au+Au Collisions at $\sqrt{s_{NN}} = 200$ GeV**”. In: *Phys. Rev. Lett.* 98 (2007), p. 062301. DOI: [10.1103/PhysRevLett.98.062301](https://doi.org/10.1103/PhysRevLett.98.062301). arXiv: [nuc1-ex/0606014](https://arxiv.org/abs/nuc1-ex/0606014).
- [314] C. Adler et al. “**Midrapidity Λ and $\bar{\Lambda}$ production in Au + Au collisions at $\sqrt{s_{NN}} = 130$ GeV**”. In: *Phys. Rev. Lett.* 89 (2002), p. 092301. DOI: [10.1103/PhysRevLett.89.092301](https://doi.org/10.1103/PhysRevLett.89.092301). arXiv: [nuc1-ex/0203016](https://arxiv.org/abs/nuc1-ex/0203016).
- [315] Jaroslav Adam et al. “**Strange hadron production in Au+Au collisions at $\sqrt{s_{NN}} = 7.7, 11.5, 19.6, 27, \text{ and } 39$ GeV**”. In: *Phys. Rev. C* 102.3 (2020), p. 034909. DOI: [10.1103/PhysRevC.102.034909](https://doi.org/10.1103/PhysRevC.102.034909). arXiv: [1906.03732](https://arxiv.org/abs/1906.03732) [nucl-ex].
- [316] L. Adamczyk et al. “**Beam energy dependence of moments of the net-charge multiplicity distributions in Au+Au collisions at RHIC**”. In: *Phys. Rev. Lett.* 113 (2014), p. 092301. DOI: [10.1103/PhysRevLett.113.092301](https://doi.org/10.1103/PhysRevLett.113.092301). arXiv: [1402.1558](https://arxiv.org/abs/1402.1558) [nucl-ex].

Titre : Le *Beam Energy Scan* au travers d'EPOS 4 – Etude de l'impact des cascades hadroniques sur les cumulants d'ordre 2 des charges nettes conservées dans les collisions d'ions lourds

Mots clés : Collisions d'Ions Lourds, Plasma de Quarks & Gluons, Point Critique, Générateur d'événements EPOS, Logiciel d'Analyse RIVET

Résumé : Les collisions d'ions lourds aux énergies ultrarelativistes ont été utilisées durant les vingt dernières années afin d'étudier les propriétés du Plasma de Quarks & Gluons (PQG), un état de la matière où quarks et gluons sont déconfinés des hadrons. Un objectif de ces recherches est de cartographier le diagramme de phase de la matière nucléaire, rendu possible expérimentalement grâce au programme du *Beam Energy Scan* (BES). Il est réalisé, entre autres, afin de chercher des signatures d'une transition de 1^{er} ordre et d'un point critique entre les phases de PQG et de gaz hadronique. Les ratios de cumulants de multiplicité nette ont ainsi été proposés comme grandeurs de procuracy (*proxies*) de choix, de par leur lien avec les susceptibilités thermodynamiques. La collaboration STAR a ainsi publié récemment la mesure des cumulants d'ordre 2 de multiplicité nette des pions, kaons et protons dans les collisions Au+Au à différentes énergies du programme BES.

Cependant, les signatures d'une transition de 1^{er} ordre ou d'un point critique pourraient être modifiées par les derniers stades de la collision. Profitant de la conception modulaire du générateur d'événement EPOS, l'impact des cascades hadroniques sur ces cumulants d'ordre 2 a été étudié. Les résultats des *proxies* de STAR sont également comparés aux cumulants d'ordre 2 des charges conservées correspondantes, ainsi qu'à de meilleurs *proxies* proposés par les auteurs d'une étude basée sur des calculs de chromodynamique quantique sur réseau et l'utilisation d'un modèle de gaz de résonances hadroniques. Ce travail prend place dans le développement d'une nouvelle version d'EPOS, qui requiert de valider sa fiabilité en comparant les résultats de simulations aux données expérimentales pour un large panel de systèmes et d'énergies de faisceau. L'intégration du logiciel d'analyse RIVET, effectué afin de faciliter ce processus de validation, est également détaillée dans cette thèse.

Title : The Beam Energy Scan under the scope of EPOS 4 – Studying the impact of hadronic cascades on the 2nd order cumulants of conserved net-charges in heavy-ion collisions

Keywords : Heavy-Ion Collisions, Quark-Gluon Plasma, Critical Endpoint, EPOS Event Generator, RIVET analysis toolkit

Abstract : During the last two decades, heavy-ion collisions at ultra-relativistic energies have been used to investigate the properties of the Quark-Gluon Plasma (QGP), a state of matter in which quarks & gluons are deconfined from hadrons. One of the major goals of this research is to map the phase diagram of nuclear matter, made possible experimentally thanks to the Beam Energy Scan (BES) program. It is performed, among other objectives, to search for a 1st order phase transition and a critical endpoint between QGP and hadron gas phases. Ratios of net-multiplicities cumulants has been shown to be relevant experimental proxies for such study, due to their link with thermodynamic susceptibilities. In this regard, the STAR collaboration has recently published measurements of the 2nd order cumulants of net-multiplicities for pions, kaons and protons in Au+Au collisions at several energies of the BES program. However, signatures from a 1st

order transition or a critical point may be blurred out by the last stages of the collision. Taking advantage of the modular conception of the EPOS event generator, the impact of the hadronic cascades on these 2nd order cumulants has been studied. The STAR proxies results are also compared with the 2nd order cumulants of the corresponding conserved charges, and with enhanced proxies proposed by the authors of a study based on lattice quantum chromodynamics calculations and the use of a Hadron Resonance Gas model. This work takes place in the context of developments for a new version of EPOS, what requires to validate its reliability by comparing simulations with experimental data for a wide range of systems and beam energies. The integration of the RIVET analysis toolkit, which has been achieved to facilitate this validation process, is also presented in this thesis.